INTERFERON, VIRUSES AND DRUG DISCOVERY

Zoe O. Gage

A Thesis Submitted for the Degree of PhD
at the
University of St Andrews

2017

Interferon, Viruses and Drug Discovery.

Zoe O Gage

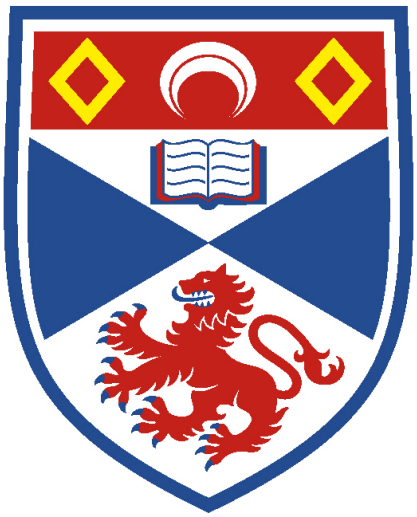

University of St Andrews

Thesis submitted for the degree of PhD

University of St Andrews

September 2016

Abstract

The interferon (IFN) response is a crucial component of cellular innate immunity, vital for controlling virus infections. Dysregulation of the IFN response however can lead to serious medical conditions including autoimmune disorders. Modulators of IFN induction and signalling could be used to treat these diseases and as tools to further understand the IFN response and viral infections. We have developed cell-based assays to identify modulators of IFN induction and signalling, based on A549 cell lines where a GFP gene is under the control of the IFN-β promoter (A549/pr(IFN-β).GFP) and the ISRE containing MxA promoter (A549/pr(ISRE).GFP) respectively. The assays were optimized, miniaturized and validated as suitable for HTS by achieving Z' Factor scores >0.6. A diversity screen of 15,667 compounds using the IFN induction reporter assay identified 2 hit compounds (StA-IFN-1 and StA-IFN-4) that were validated as specifically inhibiting IFNβ induction. Characterisation of these molecules demonstrated that StA-IFN-4 potently acts at, or upstream, of IRF3 phosphorylation. We successfully expanded this HTS platform to target viral interferon antagonists acting upon IFN-signalling. An additional assay was developed where the A549/pr(ISRE).GFP.RBV-P reporter cell line constitutively expresses the Rabies virus phosphoprotein. A compound inhibiting viral protein function will restore GFP expression. The assay was successfully optimized for HTS and used in an in-house screen. We further expanded this assay by placing the expression of RBV-P under the control of an inducible promoter. This demonstrates a convenient approach for assay development and potentiates the targeting of a variety of viral IFN antagonists for the identification of compounds with the potential to develop a novel class of antiviral drugs.

Declarations

I, **Zoe Olivia Gage**, hereby certify that this thesis (which is approximately 42,000 words) has been written by me, that it is the record of work carried out by me, and that it has not been submitted in any previous application for a higher degree. I was admitted as a research student in September 2012 as a candidate for the degree of **Doctor of Philosophy (PhD) in Molecular Virology**; the higher study for which this is a record and was carried out at the University of St. Andrews between 2012 and 2016.

Date ……..... Signature of candidate …….....

We hereby certify that the candidate has fulfilled the conditions of the Resolution and Regulations appropriate for the degree of Doctor of Philosophy at the University of St. Andrews, and that the candidate is qualified to submit this thesis in application for that degree.

Date ……..... Signature of supervisor …….....

Dr. C.S. Adamson

Date ……..... Signature of supervisor …….....

Prof. R.E. Randall

In submitting this thesis to the University of St Andrews I understand that I am giving permission for it to be made available for use in accordance with the regulations of the University Library for the time being in force, subject to any copyright vested in the work not being affected thereby. I also understand that the title and the abstract will be published, and that a copy of the work may be made and supplied to any *bona fide* library or research worker, that my thesis will be electronically accessible for personal or research use unless exempt by award of an embargo as requested below, and that the library has the right to migrate my thesis into new electronic forms as required to ensure continued access to the thesis.

The following is an agreed request by candidate and the supervisors regarding the electronic publication of this thesis: **Access to printed copy and electronic publication of thesis through the University of St Andrews.**

Date ……..... Signature of candidate …….....

Z.O. Gage

Date ……..... Signature of supervisor …….....

Dr. C.S. Adamson

Date ……..... Signature of supervisor …….....

Prof. R.E. Randall

Acknowledgments

There are so many people that have been instrumental in this. Firstly, I owe a lot to my supervisors, Cathy and Rick. Thank you for all the support, advice and discussion over the last 4 years. Rick, it's still all your fault, but I am so very grateful. Although it hasn't always been easy, I hope it's been worth it in the end. Secondly, I would like to thank everyone at the DDU who helped me with the assay development and screening. I'd especially like to thank David, Lorna, Manu, Scott and James… I'm sorry about the purple sinks!

Every member of the Adamson and Randall labs, past and present, you are extraordinary people. I'm lucky to have had the opportunity to work with you. Friends, colleagues, fellow PhD students, it's been fun. Our lunchtime giggles and your friendship has got me through.

To my husband, Oli, I wouldn't have made it without your unwavering support and understanding. Thank you for all of it. Aunty Jen, a pillar of strength and support, thank you. I did it!

Ma, this is for you. You made it happen. You are my inspiration. You believed in me. Always. "Thank you" just doesn't come close.

Table of Contents

List of Figures

List of Tables

Abbreviations

%	Percent(age)
2'5' OAS	Oligoadenylate synthase
293T	Human embryonic kidney cells
A549	Human adenocarcinomic alveolar epithelial cells
AAF	IFNα activation factor
AB	AlamarBlue
ADMET	Absorption, distribution, metabolism, elimination and toxicity
AMD	Actinomycin D
AP-1	Activating protein-1
BunV	Bunyamwera virus
BunVΔNSs	Recombinant Bunyamwera virus lacking NSs
CARD	Caspase activation and recruitment domain
CBP	Crebb binding protein
cDNA	Complimentary DNA
CDSs	Cytosolic DNA sensors
cGAS	cGAMP synthase
CHX	Cycloheximide
C_t	Cycle threshold
CV	Coefficient of variation
DAPI	4',6-diamidino-2-phenylindole
DC	Dendritic cell
DENV	Dengue virus
DMEM	Dulbecco’s modified eagle’s medium
DMSO	Dimethyl sulfoxide
DNA	Deoxyribonucleic acid

Dox	Doxycycline
ds	double-stranded
EBOV	Ebola virus
EC_{50}	Effective concentration 50
EDTA	Ethylenediaminetetraacetic acid
eIF	Eukaryotic initiation factor
EtOH	Ethanol
FACS	Fluorescent activated cell sorting
FBDD	Fragment-based drug discovery
FBS	Foetal bovine serum
FCS	Foetal calf serum
FITC	Fluorescein isothiocyanate
GAS	Gamma-activation sequence
GFP	Green fluorescent protein
HACAT	Human keratinocyte cell line
HAV	Hepatitis A virus
HBV	Hepatitis B virus
HCMV	Human cytomegalovirus
HCS	High-content screen(ing)
HCV	Hepatitis C virus
HEK	Human embryonic kidney
HIV	Human immunideficiency virus
HRP	Horseradish peroxidase
HSV	Herpes simplex virus
HTS	High-throughput screen(ing)
IAV	Influenza A virus
IC_{50}	Inhibitory concentration 50

IF	Immunofluorescence
IFI16	IFNγ-inducible protein 16
IFN	Interferon
IFNAR	Interferon α receptor
IKK	IκB kinase
IKKε/β	Inhibitor of NF-kB subunit ε/β
IP	Immunoprecipitation
IRAK	Interleukin 1 Receptor Associated Kinase
IRF	Interferon regulatory factor
ISG	Interferon stimulated gene
ISGF	Interferon stimulated gene factor
ISRE	Interferon stimulated response element
IκB	Inhibitor of κB
Jak	Janus kinase
KSHV	Kaposi's sarcoma-associated herpesvirus
LB	Lysogeny broth
LPS	Lipopolysaccharide
MAV	Marburg virus
MAVS	Mitochondrial antiviral signalling protein
MDA5	Melanoma differentiation-associated protein 5
MeV	Measles virus
ml	Mililitre
mM	Millimolar
MPNs	Myeloproliferative neoplasms
mRNA	Messenger RNA
MW	Molecular weight

MxA	Myxovirus resistence 1
NEMO	NF-kB essential modifier
NES	Nuclear export signal
NF-kB	Nuclear factor k-light-chain-enhancer of activated B cells
NiV	Nipah virus
NK	Natural killer
NLS	Nuclear localisation signal
nM	Nanomolar
NME	New molecular entity
NP	Nucleoprotein
PACT	PKR activator
PAMP	Pathogen associated molecular pattern
PBS	Phosphate buffered saline
PCD	Programmed cell death
PCR	Polymerase chain reaction
PRDs	Positive regulatory domains
PI3K	Phosphoinositide 3-kinase
pIC50	Log molar of IC50
PIV	Parainfluenza virus
PKC δ	protein kinase C δ
PKR	Protein kinase R
PML	Promyelocytic leukemia protein
PP1	Protein phosphatase 1
PRR	Pattern recognition receptor
QC	Quality control
qPCR	Quantitative PCR
RBV	Rabies virus

RBV-P	Rabies virus phosphoprotein
RFU	Raw fluorescent units
RIG-I	Retinoic acid-inducible gene I
RIP-1	Receptor-interacting protein 1
RLR	RIG-I-like receptor
RNA	Ribonucleic acid
RO5	Rule of 5
RSV	Respiratory syncytial virus
RT	Room temperature
Rux	Ruxolitinib
S/B	Signal-to-background ratio
SAR	Structure-activity relationship
SBDD	Structure-based drug design
SDS-PAGE	SDS-polyacrylamide gel electrophoresis
SeV	Sendai virus
SH2	Src homology 2
ss	single-stranded
STAT	Signal transducer and activator of transcription
STING	Stimulator of IFN Genes
TAB	TAK binding protein
TAK-1	Transforming growth factor β-activated kinase 1
TANK	TRAF family member-associated NF-kB activator
TaV	Thosea asigna virus
TBK1	TANK-binding kinase 1
TLR	Toll-like receptor
TR	Texas red
TRAF	Tumour necrosis factor receptor-associated factor

TRIF	Toll-like interleukin-1 resistance domain containing adaptor-inducing IFNβ
TRIM25	Tripartite motif-containing protein 25
uHTS	Ultra high-throughput screen(ing)
UPS	Ubiquitin proteosome system
v/v	volume to volume
VDC	V-degredation complex
Vero	African green monkey kidney epithelial cells
w/v	weight to volume
WB	Western blot
µg	Microgram
µL	Microlitre
µM	Micromolar

1. Introduction

1.1 The interferon system

The immune system is as ancient as the evolution of bacterial defence against bacteriophages and is implicated in inflammatory processes from tissue damage repair to protection from, and removal of potentially damaging foreign invaders (Kotwal et al., 2012). The interferon (IFN) response is an arm of the innate immune system that responds to infective challenge upon a cell, more frequently but not exclusively to viruses. Other functions of the IFN response include the regulation of cancer cell growth (Caraglia et al., 2013), suppression of inflammation (Gonzalez-Navajas et al., 2012) and involvement in macrophage differentiation (Hertzog, 2012). Infective challenge is detected by pattern recognition receptors (PRRs) present within a cell, which sense pathogen associated molecular patterns (PAMPs) (Kumar et al., 2011). These PAMPs can take many forms, from bacterial lipopolysaccharide (LPS) to nucleic acids and proteins (Yamamoto et al., 2002, Iwasaki, 2012). This crucial non-discriminatory mechanism of cellular defense is also necessary to abrogate any further damage to the cell and its neighbours. Additionally, its activation is a necessary step in the induction of the adaptive immune response, which instigates more tailored, longer lasting effects (Takeuchi and Akira, 2010).

IFN was first discovered in 1957 by Lindenmann and Isaacs, and is so named for its ability to ‘interfere’ with the course of a viral infection (Isaacs and Lindenmann, 1957). Interferons now encompass a group of cytokines that are germ line encoded, have far-reaching pleiotropic actions and have been

extensively reviewed (Randall and Goodbourn, 2008, Hoffmann et al., 2015, Ivashkiv and Donlin, 2014). Since the seminal discovery of IFNs, much work has focused on furthering our collective knowledge of the function of these chemical messengers and their mechanisms of action. There are numerous types of interferon, varying in their receptors and stimuli. The shared goal however is the cellular protection from invading pathogens. Type I IFNs encompass a group of 18 functional genes, including IFNα with 14 isoforms, β, of which there is a single isoform and others including ε, κ and ω (Gonzalez-Navajas et al., 2012, Ivashkiv and Donlin, 2014). They are ubiquitously expressed cytokines and are produced by all nucleated cells. Type II IFN (IFNγ) is produced by Natural killer (NK) and T cells and shares many similarities with type I IFNs in their mechanism of induction, although they are not produced as a direct result in viral infection (Schroder et al., 2004). Type III interferons known as IFNλ are more prominently expressed in epithelial cells (Koyama et al., 2008, Sommereyns et al., 2008). Although the induction of type III IFNs following viral challenge shares many similarities with the regulatory pathways of type I IFNs (Onoguchi et al., 2007), they are expressed in response to persistent, low-level or repeated infection (Wack et al., 2015, Lazear et al., 2015). Intriguingly, the more recently discovered IFNλ4 appears to be associated with poor clearance of Hepatitis C virus (Prokunina-Olsson et al., 2013, Hamming et al., 2013).

IFN production results in increased expression of hundreds of IFN stimulated genes (ISGs), including Trim 5α, Myxovirus resistence (Mx) GTPases, eukaryotic initiation factor 2α (eIF2α) and oligoadenylate synthase

(2’5’ OAS), many of which have direct antiviral actions and potentiate other cellular processes such as the induction of apoptosis, triggering dendritic cell (DC) maturation, and instigation of other aspects of the innate immune system such as the recruitment of NK cells (Baranek et al., 2012). IFNs are ultimately responsible for cellular resistance to infection, inducing an antiviral state of protection in neighbouring cells in response to, and for the prevention of, further spread. Furthermore, they are crucial for the activation and functionality of the adaptive immune system (Le Bon and Tough, 2002, Barra et al., 2010).

1.1.1 Type I IFN induction

The initial step in the complex IFN induction cascade is the detection of foreign material. Although as previously mentioned this stimulus can be LPS, for clarity here, the focus will be the detection of nucleic acids with regard to viral infection. In this case, the cell recognises self, from non-self using PRRs. Membrane bound Toll-like receptors (TLRs) embedded in cell and endosomal membranes detect extracellular foreign nucleic acids, whereas cytoplasmic PAMPs are recognized by Retinoic acid-inducible gene I (RIG-I) -like receptors (RLRs) (Broz and Monack, 2013). The induction of type I IFNs (IFNα/β) through TLR- and RLR-dependent signalling will be described below (Figure 1.1).

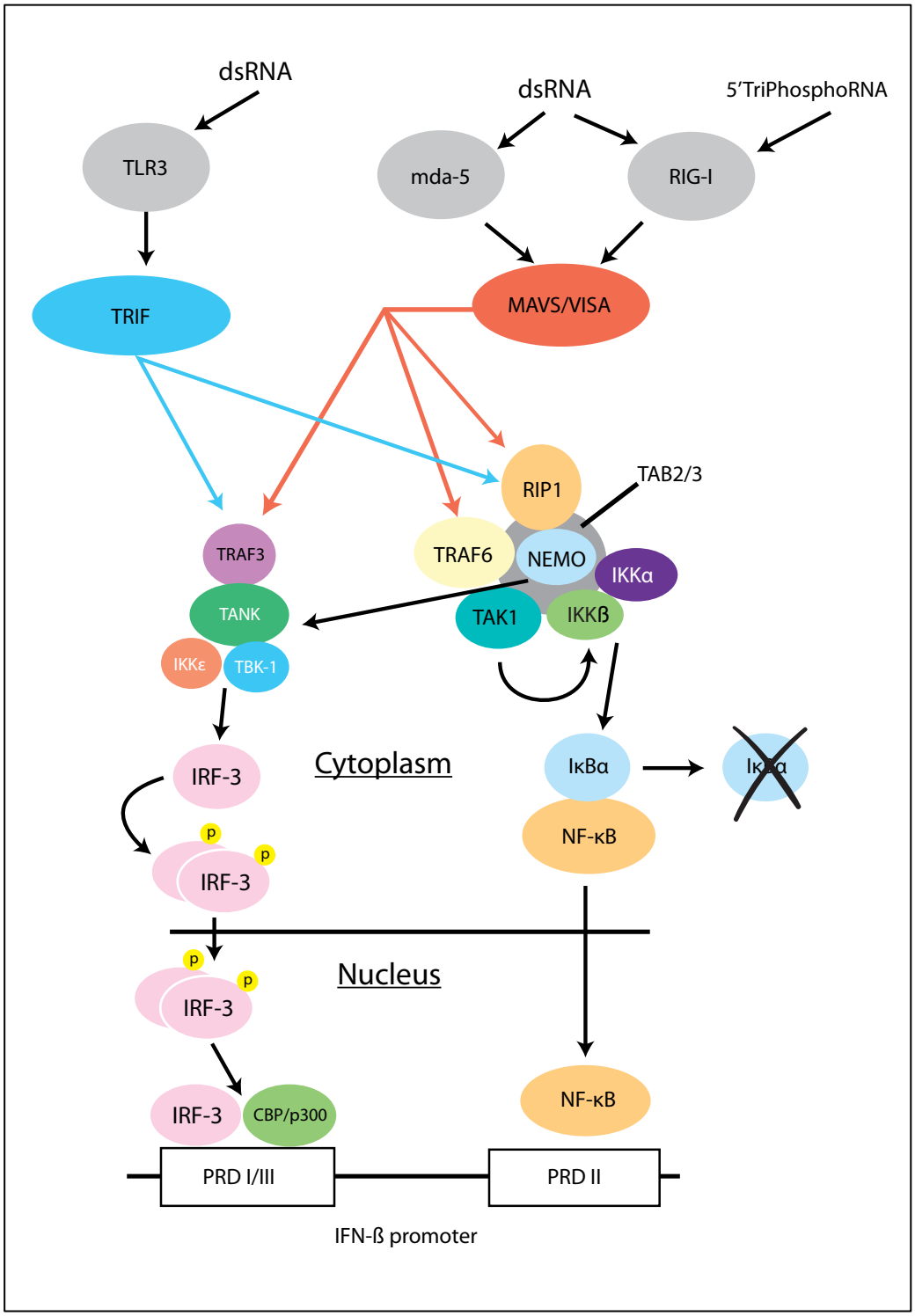

Figure 1.1: TLR3- and RLR-dependent induction of IFNβ gene expression.
In response to extracellular and endosomal dsRNA TLR3 recruits TRIF, whereas cytosolic dsRNA stimulates RLRs (MDA5, RIG-I), which activate VISA (MAVS/Cardif/IPS-1). Here the pathways converge culminating in IRF3 and NF-κB translocation to the nucleus. Binding to their respective PRDs in the IFNβ promoter instigates transcription. (Modified from Goodbourn and Randall, 2009)

1.1.1.1 TLR-dependent IFN induction

TLRs are membrane bound receptors present in two main cellular locations; the membranes of immune cells and endosomes (Takeda and Akira, 2004). TLRs 3, 7 and 9 are found in endosomal membranes and recognise double stranded (ds) RNA, single stranded (ss) RNA and unmethylated DNA respectively (Akira, 2011). TLR3-dependent IFN induction will be the primary focus here, as this study is concerned with IFN induction by dsRNA. The recognition of extracellular, endosomal and phagosomal dsRNA by TLR3 results in its dimerization and tyrosine phosphorylation (Sarkar et al., 2004). This leads to the recruitment of Toll-like Interleukin-1 resistance domain-containing adaptor inducing IFN-β (TRIF) and phosphoinositide 3-kinase (PI3K) (Yamamoto et al., 2003), which in turn causes the activation of the IFN regulatory factor 3 (IRF3) and nuclear factor κ-light-chain-enhancer of activated B cells (NF-κB) branches of the IFN induction pathway (Oshiumi et al., 2003).

The IRF3 branch of IFN induction is instigated by the recruitment of the E3 ubiquitin ligase Tumour necrosis factor receptor-associated factor (TRAF) 3 by TRIF upon TLR3 activation (Paz et al., 2011). TRAF3 associates with TRAF family member-associated NF-κB activator (TANK), which unites with TANK-binding kinase 1 (TBK-I) (Goubau et al., 2013). TBK-1 and inhibitor of NF-κB subunit ε (IKKε) cause the phosphorylation of IRF3, resulting in its dimerization and subsequent nuclear translocation in association with Crebb-binding protein (CBP)/p300 (Goubau et al., 2013, Perry et al., 2005). Nuclear IRF3 then associates with positive regulatory domains (PRDs) present in the IFNβ promoter (Panne et al., 2007)

The NF-κB branch is also initiated by TRIF, which engages TRAF6 and receptor-interacting protein-1 (RIP-I), which are both lysine-63 ubiquitinated (Hoesel and Schmid, 2013). The ubiquitination of RIP-I leads to NF-κB essential modifier (NEMO) association (Wu et al., 2006). The ubiquitination of both RIP-I and NEMO is sensed by the molecular chaperones TAK-binding protein (TAB) 2 and TAB3 (Kanayama et al., 2004), which instigate the association of transforming growth factor β-activated kinase-1 (TAK-I) (Deng et al., 2000). This forms the essential complex known as IκB kinase (IKK) (Wu et al., 2006). The TAK-I component of IKK causes the phosphorylation of IKKβ at serine 177 and 181 (Israel, 2010), leading to the ubiquitination and subsequent proteasomal degradation of inhibitor of κB (IκB), the suppressor of NF-κB (Li et al., 2000). This results in the release of NF-κB, exposing the nuclear localisation signal (NLS) present in its P65 (RelA) subunit (Zandi et al., 1997, Hoesel and Schmid, 2013). Nuclear NF-κB then associates with PRDs present in the IFNβ promoter (Panne et al., 2007).

The detection of endosomal ssRNA and DNA by TLR7 and TLR9 respectively results in the activation of a similar yet distinct signalling pathway to TLR3-dependent IFN induction (Figure 1.2) (Heil et al., 2004, Tabeta et al., 2004). TLR7 and TLR9 activation recruits the adaptor MyD88 as opposed to TRIF, and results in the enrolment of TRAF6, IRAK-1 and IRAK-4 (Reviewed by Takeuchi and Akira, 2010, Berke et al., 2013, Kawai and Akira, 2011). TRAF6 activation results in the release and nuclear localisation of NF-κB through RIP-I and TAK-1 signalling as discussed above (Hoesel and Schmid, 2013, Li et al., 2000). The transcription factor IRF7 is recruited in place of IRF3, and is brought

about by the phosphorylation of IRF7 by IRAK-1, a process that is independent of TBK-1 and IKKε (Huye et al., 2007). This results in the nuclear translocation of IRF7 and as with IRF3, association with the PRDs, subsequently inducing IFNα/β transcription.

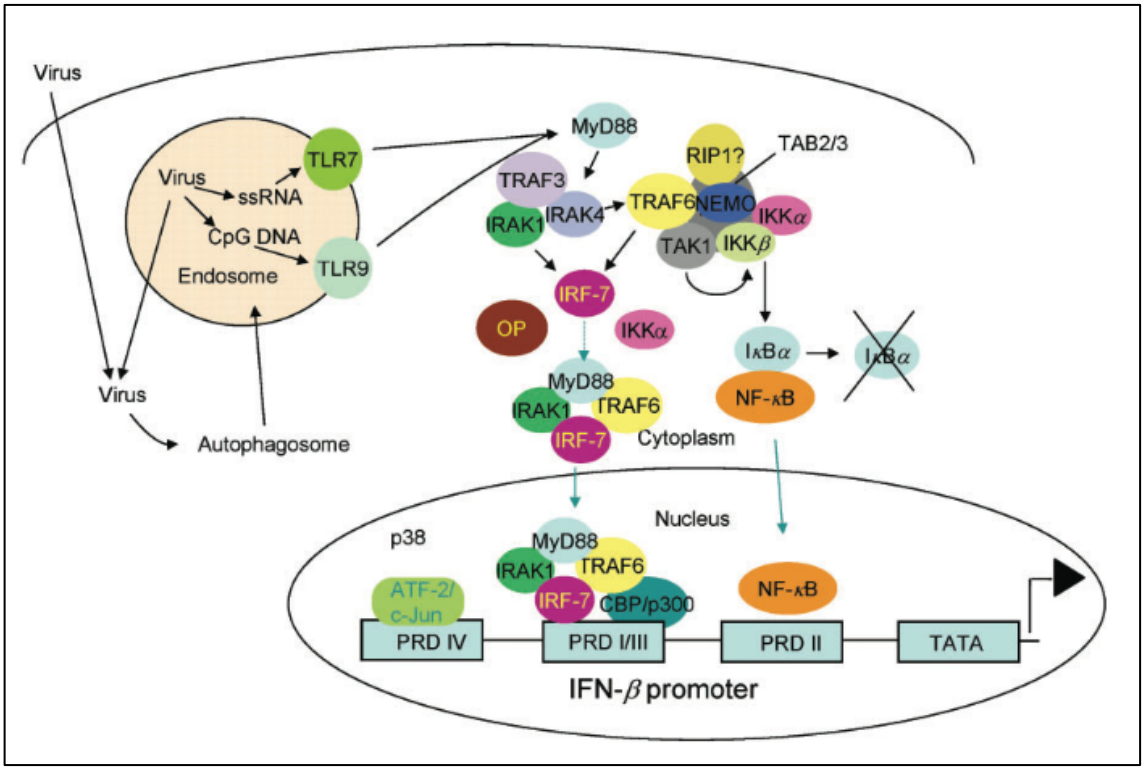

Figure 1.2: TLR7/9-dependent induction of IFNβ by ssRNA and DNA
TLR7 and 9 activation by endosomal ssRNA and DNA respectively initiates the TRAF3 and TRAF6-dependent signalling pathways through the adaptor molecule MyD88 (Randall and Goodbourn, 2008).

1.1.1.2 RLR-dependent IFN induction

Foreign nucleic acids that are cytosolic are sensed by helicases. Present in three main types, they are classed as the RLRs (Wu and Hur, 2015). RIG-I and MDA5 are RNA sensing molecules, which both associate with caspase activation and recruitment domains (CARDs) (Goubau et al., 2013). The final RLR, LGP2, appears to have a regulatory function, as it is lacking the CARD

domain required for IFN induction (Satoh et al., 2010). The subtle difference between the two IFN-inducing RLRs is the type of nucleic acids they sense. While RIG-I senses short, blunt RNA with a 5′ triphosphate, MDA5 is thought to sense long dsRNA (>2000 nt) although there remains some debate over this (da Conceicao et al., 2013, Kato et al., 2006, Baum et al., 2010). An additional structure, a 5′ triphosphate panhandle nucleic acid motif was also discovered to activate RIG-I (Schlee et al., 2009). Upon stimulation by nucleic acids, PP1α and PP1γ dephosphorylate RIG-I and MDA5 (Wies et al., 2013). Subsequently, their CARDs are exposed through conformational change and stimulate mitochondrial antiviral signalling protein (MAVS) (also known as VISA, Cardif and IPS-I) (Kawai et al., 2005). Upon the enrolment of MAVS, RLR-dependent induction follows the same signalling pathway as TLR3-dependent IFNα/β induction (Figure 1.1).

1.1.1.3 STING-dependent IFN induction

As cytosolic DNA is highly unusual in mammalian cells, detection independently of TLRs can also induce IFNα/β production (Ishii et al., 2006). Cyclic monophosphates are sensed by cGAMP synthase (cGAS) (Sun et al., 2013, Burdette et al., 2011), whereas DNA in DCs is sensed by the helicase DDX41 (Zhang et al., 2011), and in monocytes and some fibroblasts is detected by IFNγ-inducible protein 16 (IFI16) (Unterholzner et al., 2010). In all cases, these cytosolic DNA sensors (CDSs) initiate IFNα/β production through IRF3- and TBK1-dependent pathways (Figure 1.3) (Tanaka and Chen, 2012). The adaptor molecule Stimulator of IFN Genes (STING) is located on the surface of

the endoplasmic reticulum, and is essential for cytoplasmic DNA-mediated IFNα/β induction (Ishikawa and Barber, 2008, Ishikawa et al., 2009).

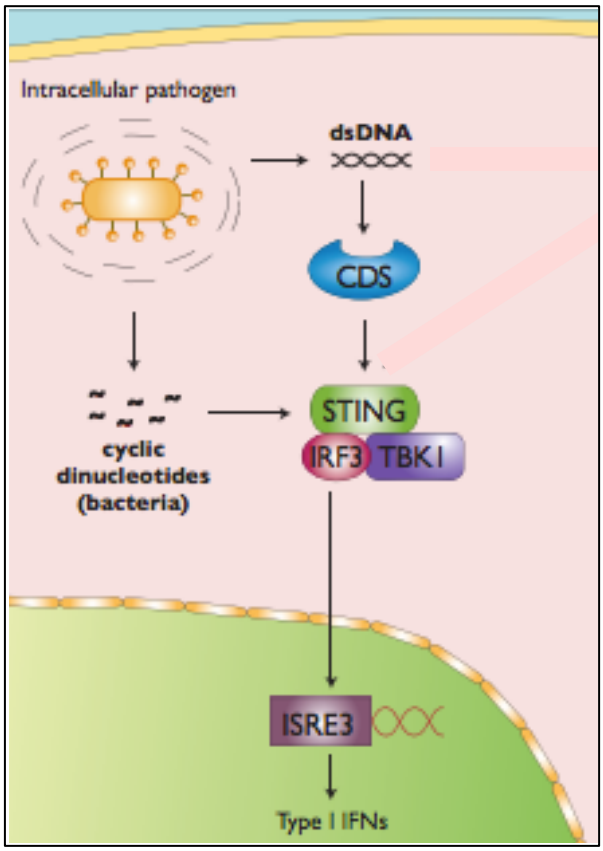

Figure 1.3: STING-dependent induction of IFNβ by Cytoplasmic DNA
Cytoplasmic DNA is detected by CDSs, which recruit the adaptor molecule STING, instigating the TBK-1 and IRF3-dependent type I IFN induction pathway (Adapted from the InvivoGen Insight newsletter, 2012 [http://www.invivogen.com])

Innate immune responses vary based on the characteristics of both the stimulus and the cell that detects the microbe. However, the pathways converge on a consensus set of signal transductions resulting in the activation of type I IFN responses and other proinflammatory cytokines facilitated by the induction of common signalling proteins including NF-κB and CBP (Schroder and Tschopp, 2010).

1.1.1.4 IFNβ promoter enhanceosome assembly

Regardless of the stimulus for type I IFN induction, it is heavily reliant on various transcription factors such as IRF3 and NF-κB associating with the relevant *cis* regulatory elements, the PRDs (Yang et al., 2004). TLR- and RLR-dependent signalling cascades result in the nuclear translocation of activated transcription factors such as IRF3 and NF-κB. Their association with PRDs present in the IFNα/β promoter is a synergistic process resulting in the formation of the IFNβ enhanceosome (Figure 1.4), potentiating transcriptional activation (Randall and Goodbourn, 2008, Maniatis et al., 1998). To initiate the transcription of IFNα/β, either IRF3 associates with PRD I or IRF7 with PRD III, whereas NF-κB interacts with PRD II (Panne et al., 2007). To complete enhanceosome assembly, activating protein-1 (AP-1) heterodimers composed of ATF-2C and c-Jun associate with PRD IV (Matsumoto and Seya, 2008).

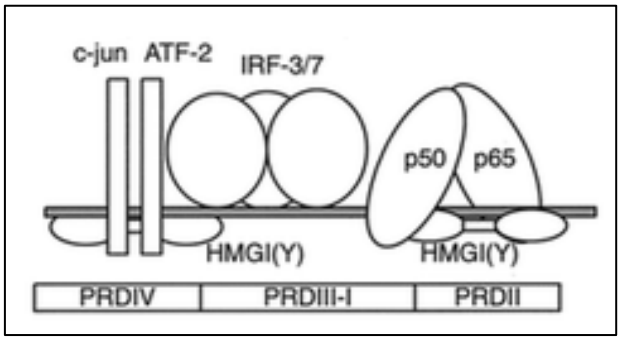

Figure 1.4: The IFNβ promoter enhanceosome.
The association of activated transcription factors with the PRDs present in the IFNβ promoter occurs in a cooperative manner. IRF subunits bind at PRDI and PRDIII, NF-κB (p50 & RelA) at PRDII and AP-1 (ATF-2 & c-Jun) at PRDIV, leading to transcriptional activation (Modified from Falvo et al., 2000).

1.1.2 Type I IFN signalling

Following the induction of type I IFN gene expression and its secretion from the cell, it attaches to specific membrane receptors on the cell surface

(Kim et al., 1997). All type I IFNs associate with the same IFN α/β receptor (IFNAR), minimally composed of two subunits, IFNAR-1 and IFNAR-2 (Figure 1.5) (Platanias, 2005). Prior to activation by IFN binding, the cytoplasmic tails of these membrane-spanning receptors associate with members of a tyrosine kinase family, Janus kinases (Jak) (Ivashkiv and Donlin, 2014). IFNAR-1 is bound to Tyk2 and IFNAR-2 to Jak1 (Kim et al., 1997). In addition to Jak1, IFNAR2 is bound by STAT1, which itself is weakly associated with STAT2 (Precious et al., 2005, Tang et al., 2007). The STAT1-IFNAR-2 association prior to IFN binding appears to occur only when STAT2 is present (Stancato et al., 1996, Li et al., 1996). Upon IFNα/β binding to the receptor subunits, ligand-induced dimerization of IFNAR-1 and -2 results in alterations in conformation and Janus kinase activation, where Jak1 phosphorylates Tyk2, which in turn phosphorylates Jak1 (Gauzzi et al., 1996). The now activate Tyk2 phosphorylates IFNAR1 at tyrosine 466, which creates a docking site for the SH2 domain of STAT2 (Stark et al., 1998, Yan et al., 1996). This facilitates a more robust association with STAT2 and subsequently, Tyk2 phosphorylates STAT2 at tyrosine 690, disabling its constitutive overriding nuclear export (Stark et al., 1998, Frahm et al., 2006). Concurrently, Jak1 phosphorylates STAT1 at tyrosine 701, resulting in its dissociation from IFNAR, and the formation of a stable heterodimer (Stark et al., 1998, Reich and Liu, 2006). NLS generation through SH2 domain interactions potentiates its transport to the nucleus, where it remains until it is dephosphorylated (Banninger and Reich, 2004). As a consequence of tyrosine phosphorylation, Interferon-stimulated gene factor 3 (ISGF-3) is formed with the purpose of transcriptional activation of ISGs. This

heterotrimeric complex is composed of the phosphorylated STAT1 and STAT2 proteins, and an additional transcription factor, Interferon Regulatory Factor 9 (IRF-9) (Yan et al., 1996, Stark et al., 1998).

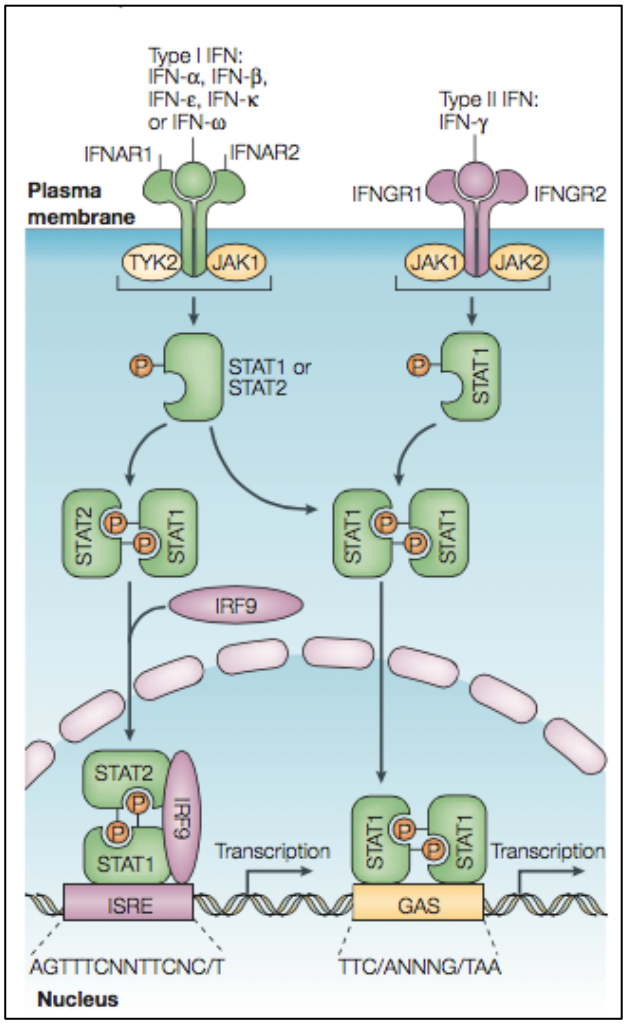

Figure 1.5: ISRE and GAS associated ISG induction by type I and type II IFN.
Although similar, the cascades triggered by type I and type II IFNS are distinct in the expression profiles they induce. Furthermore, it can be seen that cross-activation can occur due to STAT1 being a common component of all both signalling pathways. (Platanias, 2005)

An additional consequence of IFN binding is the IFNAR-2 induced activation of CBP/p300, which associates with both STAT2 and protein kinase C δ (PKC δ) (Uddin et al., 2002). CBP acetylates the ISGF-3 complex, creating a stable binding site for IRF9, which itself is then acetylated, a step crucial to ISGF-3-DNA binding (Tang et al., 2007). PKC δ phosphorylates STAT1 at

serine 727, promoting more efficient binding of ISGF-3 to the transcriptional apparatus upon nuclear translocation (Bonjardim et al., 2009). Recently phosphorylation of S287 in STAT2 was also found to have a regulatory role in IFNα/β signalling (Steen et al., 2013). Once in the nucleus, ISGF-3 binds with a high degree of specificity to the Interferon stimulated response element (ISRE) present in the promoter of ISGs through recognition of DNA sequences (Schoggins and Rice, 2011).

Type II interferons (IFNγ) have distinct receptors whose subunits are similarly termed IFNGR-1 and IFNGR-2, although in this case they are weakly associated with one another prior to IFN stimulation (Figure 1.5). Here, IFNGR-1 is associated with Jak1 and IFNGR-2 with Jak2 (Bach et al., 1997, Chen et al., 2004). Upon IFNγ binding, the two receptors are brought closer together, leading to the activation of Jak2, causing the *trans*-phosphorylation of Jak1 (Darnell, 1997). The activated kinases then phosphorylate a tyrosine rich region between amino acids 440 and 444 in IFNGR1, which creates binding sites for two STAT1 molecules, potentiating their interaction via SH2 domains (Varinou et al., 2003). Further phosphorylation of the STAT1 molecules at tyrosine 701 and serine 727 completes activation, resulting in their dissociation from the receptor complex. Dimerization of the STAT1 molecules occurs through detection of tyrosine phosphates in the SH2 domains leading to the subsequent nuclear translocation of the complex (Boehm et al., 1997). STAT1 homodimers bind to a distinct sequence in the promoter of ISGs known as Gamma-activation sequence (GAS), which results in their transcriptional induction (Decker et al., 1991b, Lew et al., 1991). This is separate from the ISRE of ISG promoters and

occurs in an IRF-9-independent manner (Takaoka and Yanai, 2006). The binding of the STAT1 homodimer and transcriptional activation of ISGs without the involvement of IRF-9 can also occur through IFNα/β signalling, which is known as the AAF complex (Decker et al., 1991a). Additionally, STAT1 and STAT2 can be phosphorylated as a result of both IFNα/β and IFNγ receptor binding, leading to "cross-activation", and represents a certain level of convergence of the pathways (Li et al., 1996). STAT1 however is a crucial component of both IFNα/β and IFNγ signalling cascades, rendering each type of IFN inactive without its presence (Patel et al., 2012).

1.1.3 The cellular impact of type I IFNs

The consequences of IFN induction are far reaching and have been reviewed extensively (Randall and Goodbourn, 2008, Darnell, 1997, Platanias, 2005, Takaoka and Yanai, 2006). Several hundred genes are categorised as ISGs, and to some extent the IFN response can be tailored, as a cell utilizes different sets of ISGs in order to control different viral infections (Bonjardim et al., 2009). Some ISGs are enzymes and are synthesised in their inactive form, requiring activation to instigate their anti-viral actions. GTPases known as Mx are induced by IFN signalling and have been shown to restrict the ability of viral components to move within a cell through nucleocapsid recognition (Haller and Kochs, 2011). Protein kinase R (PKR) is activated by association with its co-factors, dsRNA and PKR activator (PACT), leading to the phosphorylation of eIF2α (Nakayama et al., 2010, Li et al., 2006). The phosphorylation of eIF2α inhibits its action, thus leading to the cessation of translation (Deng et al., 2004). ISG56 has also been implicated in selectively inhibiting the translation of

parainfluenza virus 5 (PIV5) mRNA (Andrejeva et al., 2013). Another enzyme that has dsRNA as a co-factor, is 2′5′ OAS (Silverman, 2007). Here however, the activated enzyme catalyses the oligomerisation of ATP through an unusual 2′5′ phosphodiester bond. The oligoadenylates that result from this catalysis cause the activation of RNase L, which digests cellular and viral RNAs and has been postulated to lead to amplification of the IFN response through further activation of RLRs such as RIG-I and MDA5 (Malathi et al., 2007). Other implications of ISRE and GAS stimulation include the induction of a pro-apoptotic state through the activation of numerous factors including procaspases (Maher et al., 2007, Dai and Krantz, 1999, Chin et al., 1997). Cell cycle arrest has also been observed through cytostasis at the G_1/S interface. This has been comprehensively reviewed, and results in the inhibition of E2F specific expression, which includes genes crucial to S-phase (Ferrantini et al., 2007, Ferrantini et al., 2008, Dimova and Dyson, 2005, Asefa et al., 2004).

The plethora of cellular process affected by type I IFN signalling range from the actions of direct antiviral proteins to the limiting of translation and even cell cycle arrest. It is therefore not surprising that dysfunction is associated with the development of a wide range of diseases. Some of the pathologies associated with dysfunctional IFN responses will be discussed below.

1.1.4 Diseases associated with dysregulation of the IFN system

As with any biological process, there lies the potential for dysfunction within the IFN response. Although a multifactorial disease, it is believed that the Systemic Lupus Erythematosus (SLE) phenotype is exacerbated by chronic activation of the type I IFN response (Buers et al., 2016, Van Eyck et al., 2015,

Oliveira et al., 2015). Additionally, an increasing number of interferonopathies have been identified such as STING-associated vasculopathy with onset in infancy (SAVI) (Liu et al., 2014) and Aicardi-Goutières syndrome (AGS) (Ahn and Barber, 2014, Orcesi et al., 2009, Crow et al., 2006), where gain-of-function mutations in STING and MDA5 respectively result in aberrant activation and increased levels of type I IFN production (Liu et al., 2014, Oda et al., 2014). Although also caused by mutations in the gene encoding MDA5 (Rutsch et al., 2015), it was recently reported that mutations in the RIG-I encoding DDX58 gene are responsible for atypical Singleton-Merten syndrome (SMS) (Jang et al., 2015). The root of such dysfunction in AGS and SMS is the location of the genetic mutations that cause the disease. Both diseases arise from mutations located in the helicase domains of the associated RLRs, which are usually responsible for RNA binding during activation (Kato and Fujita, 2015, Wu and Hur, 2015). AGS is a genetically heterogeneous disorder however as loss-of-function mutations in enzymes responsible for DNA and RNA editing have also been shown to cause the same phenotype (Orcesi et al., 2009, Crow et al., 2006, Crow, 2015, Rice et al., 2013). As well as RLR-induced dysfunction, aberrant signalling in haematopoietic immune cells such as macrophages and T cells through TLR3 and TLR4, and subsequently TRIF and TRAM has recently been identified as having a causal role in the development of atherosclerosis (Lundberg et al., 2013).

In addition to autoimmune diseases, there is a strongly accepted causal link between dysfunctional type I IFN responses and cancer, including tumour development (Hosui et al., 2012). For example, phosphorylation events during

the activation of NF-κB resulting in atypical and aberrant activity have been implicated in solid tumour formation and inflammatory disease (Reviewed by Viatour et al., 2005). More specifically, IKKβ has been identified as a link between inflammatory responses and tumour formation in myeloid cells using a mouse model (Greten et al., 2004).

Although generally beneficial to the host during acute viral infection, type I IFN signalling during persistent infection, e.g. HIV and HCV, can have deleterious consequences (Wilson and Brooks, 2013). Due to the importance of type I IFN signalling in the recruitment of the adaptive immune response, it is increasingly thought of as the root cause of immunosuppression, where chronic activation can lead to atypical B and T cell activity and a reduced capacity to fight secondary infections (Snell and Brooks, 2015). In addition to immunosuppression and secondary infection, it has been shown that HIV patients undergoing treatment have heightened susceptibility to diseases linked to aberrant immune signalling including the aforementioned atherosclerosis (Subramanian et al., 2012, Cha et al., 2014).

Therefore, it is clear that although a crucial aspect of cellular protection against infection, tight regulation of type I IFN induction and signalling is necessary to prevent the development of potentially devastating diseases.

1.2 Modulating the IFN response

As a result of the far-reaching impact of the IFN response on cellular physiology, both in terms of viral infection and disease states, the ability to modulate the signalling pathways would be advantageous. Antagonism and activation of the response holds potential not only for clinical therapeutic intervention, but also as a tool to aid research into the IFN induction and signalling pathways. Additionally, the potency of the response has caused viruses to evolve mechanisms to circumvent both IFN induction and signalling. Chemical modification of the IFN response, and the mechanisms by which viruses circumvent its actions will be discussed below.

1.2.1 Chemical modulation of the IFN response

The interferon response is one of the most heavily studied signalling cascades in biology due to its broad ranging effects on cellular activity. As a result, it is viewed as an ideal target for the development of treatments for many diseases and infections (Theofilopoulos et al., 2005). Molecules that upregulate the IFN response for example, could be beneficial as antivirals. In the treatment of microbial infections a motive behind targeting a host pathway is the high level of drug resistance that can develop quickly when the target is the infecting organism. For example, in influenza virus treatment, some of the most commonly used drugs target the viral M2 ion channel. However, due to rapidly increasing levels of resistance, their use is no longer recommended (Lee and Yen, 2012, Jacob et al., 2016). Many current treatments place selective pressure directly onto the invading pathogen, increasing the likelyhood of resistance developing. Targeting a cellular pathway in the host circumvents this,

as it is less likely that the organism will evolve an escape mechanism, or in the least, it will occur more slowly (Lee and Yen, 2012). To this end, compounds that act as agonists to activate the IFN response could be used as broad-spectrum antivirals and as supportive therapy for immunocompromised patients.

Conversely, compounds that antagonize the IFN response are beneficial for the treatment of inflammatory and autoimmune disorders. A number of such molecules have been identified. Inhibitors of type I IFN induction such as TPCA-1, which inhibits IKKβ in the NF-κB pathway, have the potential for use in the treatment of autoimmune diseases such as arthritis (Podolin et al., 2005). It was found recently that sodium-potassium ATPase cardiac glycosides, commonly used in the treatment of congestive heart failure and arrhythmia, are potent inhibitors of IFNβ induction. Bufalin was identified in a cell-based assay to test 478 compounds for their ability to block the induction of type I IFN. The luciferase-based assay highlighted Bufalin as a potent inhibitor that decreased the expression of IFNβ by 90% with an IC_{50} of 43 nM (Ye et al., 2011). Molecules targeting type I IFN signalling are also available. The JAK1/2 inhibitor Ruxolitinib (Rux) for example, currently approved for the treatment of myeloproliferative neoplasms (MPNs), is also in phase II clinical trials to assess its use to treat psoriasis and a variety of cancers (Verstovsek et al., 2010, Quintas-Cardama et al., 2010, O'Shea et al., 2015).

Cancerous cells have vastly increased expression of NF-κB, a common and crucial component of the IFN response (Hasselbalch, 2012). The result of such aberrant over expression of this factor leads to increased and sustained

oxidative stress placed on cells. Recent research has found that histone deacetylase inhibitors, small molecule drugs widely used in the treatment of epilepsy and mood disorders, can have a highly beneficial application to cancer treatment (Bridle et al., 2013). This class of enzyme inhibitors has been shown to inhibit the transcriptional activation of genes that are typically activated upon infection and IFN treatment, resulting in the prevention of autoimmune responses.

Outwith the clinic, inhibitors of both type I IFN induction and signalling have been used to facilitate the growth of IFN sensitive viruses. Inhibition of IFN induction and signalling in this manner could be utilized in the production of live-attenuated viral vaccines and the growth of oncolytic viruses (Stewart et al., 2014, Jackson et al., 2016). Furthermore, their application to basic research could potentiate further study of these complex signalling cascades. For example, through the use of BX795, a TBK1 and IKKε inhibitor, it was demonstrated that serine 172 of TBK1 has a regulatory role in a feedback loop controlling its activation (Clark et al., 2009).

Due to the vast number of effector molecules involved in type I IFN induction and signalling, there is potential for novel target identification. Additionally, drug discovery could identify molecules that inhibit the IFN response, and may also unearth compounds that activate naturally occurring host proteins that have inhibitory functions, thus reducing the potential for drug associated side effects (Zhang et al., 2004). The complexity of these pathways suggests a vast number of yet undiscovered novel targets for the development of drugs. There are still many unknowns in the collective knowledge of the

molecular mechanisms behind the IFN response, and having the ability to transiently or reversibly inhibit the action of an effector molecule could be a powerful tool in the researcher's arsenal.

1.2.2 Viral antagonism of the IFN response

The IFN response places a large selective pressure on the ability of a virus to replicate and propagate an infection. As a result, nearly every virus has evolved at least one mechanism to circumvent the IFN response, highlighting the importance and potency of the system (Chen et al., 2010). A plethora of viral evasion strategies have evolved as a result of the inherently diverse nature of viruses. These will be discussed further, and as the ability of the Rabies virus to subvert IFN signalling is of particular importance to this study, it will be addressed independently.

1.2.2.1 The myriad of viral evasion stratagies

As IFN can elicit autocrine and paracrine actions, the ability of a virus to inhibit just one aspect of the IFN response, i.e. either IFN induction or IFN signalling, may not be sufficient to facilitate efficient viral replication and spread. Subsequently, most viruses have evolved mechanisms to antagonise both pathways of the IFN system. The often-multifunctional proteins that viruses encode to achieve this are termed IFN antagonists and collectively target every aspect of the IFN response (Figure 1.6). Viral antagonism of the IFN system can be broadly categorized as acting to (i) conceal PAMPs to prevent activation of IFN induction, (ii) inhibit host gene expression and (iii) alter or degrade signalling molecules (Reviewed by Ito et al., 2016). The concealment of PAMPs is a virus-targeted mechanism of evasion, whereas others that interfere with

gene expression and the signalling molecules of the cascades are directed against the host. Host-targeted evasion is achieved through 3 main mechanisms; (i) direct cleavage of effector molecules by viral proteases, (ii) sequestering and relocalisation of effector molecules, and (iii) recruitment of the cellular ubiquitin proteasome system (UPS) (Nag and Finley, 2012, Reviewed by Hoffmann et al., 2015).

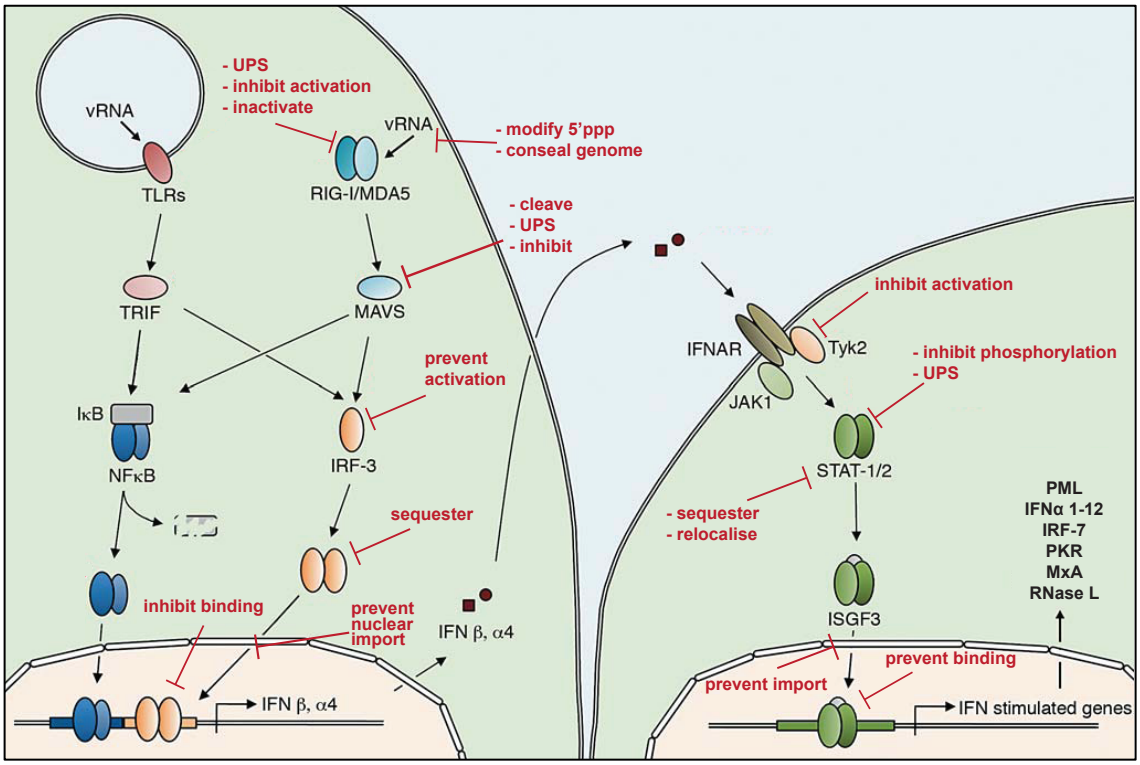

Figure 1.6: Viral strategies to evade the IFN response
Viruses have evolved a plethora of mechanisms to evade every step of the IFN induction and IFN signalling pathways, some of which are shown above. (Adapted from McInerney and Karlsson Hedestam, 2009)

Viruses have developed many strategies to avoid PAMP detection by cellular PRRs. For example, Herpes Simplex virus (HSV) and Influenza A viruses (IAV) replicate in the nucleus (Melroe et al., 2004, Weber et al., 2015), whereas Dengue virus (DENV) has adapted to replicate in the folds of the

endoplasmic reticulum in order to screen their genomes from cytoplasmic PRRS (Uchida et al., 2014). Some RNA viruses modify the 5'triphosphate of their genome to avoid RIG-I detection. Bunyaviruses (BunV) and Bornaviruses for example encode phosphatases that remove two phosphates, leaving an undetected 5'monophosphate (Wang et al., 2011b, Habjan et al., 2008), while others degrade excess cytoplasmic nucleic acids, such as Human Immunodeficiency virus (HIV), which utilises the cellular exonuclease TREX1 (Yan et al., 2010). Another mechanism to avoid detection by PRRs is to disguise the viral genome by ecapsidation in viral proteins such as IAV NS1, Ebola virus (EBOV) VP35 and Marburg virus (MAV) VP35 (Hatada and Fukuda, 1992, Ramanan et al., 2012, Cárdenas et al., 2006). Interestingly, Respiratory syncytial virus (RSV) hijacks the cellular protein La to conceal its RNA (Bitko et al., 2008).

Inhibiting the activation of RLR and adaptor molecules such as MAVS is also an effective approach to subvert IFN induction. Where some viruses directly degrade the PRR through UPS recruitment, such as the NS1 and NS2 proteins of RSV, others prevent its activation (Goswami et al., 2013). IAV NS1 for example binds TRIM25, preventing its oligomerization and subsequently inhibiting its ability to activate RIG-I through lysine-63 ubiquitination (Gack et al., 2009). Other viruses simply encode their own deubiquitinating enzymes, such as the Foot and mouth disease virus L^{Pro} and Kaposi's sarcoma-associated herpesvirus (KSHV) ORF64, which remove the lysine-63-linked ubiquitin from PRRs and subsequently inactivate them (Wang et al., 2011a, Inn et al., 2011). The ATPase activity of RIG-I is stimulated by PKR and PACT, however the NS1

protein of IAV and VP35 of EBOV target the latter to inhibit activation (Tawaratsumida et al., 2014, Luthra et al., 2013). The activation of RIG-I and MDA5 is also reliant on the dephosphorylation of their CARDs by PP1α and PP1γ, a step that is inhibited by Measles virus (MeV) V protein, which has a PP1 binding motif to bind and sequester these effector molecules (Davis et al., 2014). While the inhibition of an RLR such as RIG-I is an effective tactic in subverting IFN induction, inhibition of the downstream adaptor molecule MAVS, preventing induction from both MDA5 and RIG-I may be a more efficient tactic. For example, the $3C^{Pro}$ of Hepatitis A virus (HAV) and NS3-4A of HCV directly cleave MAVS, whereas HBV, which does not encode a protease, utilises protein X to instigate the UPS mediated degradation of MAVS (Yang et al., 2007, Li et al., 2005, Wei et al., 2010). Interestingly, MAVS function is also impeded by IAV, where the polymerase subunit PB1-F2 causes disruption of the mitochondrial membrane, thus inhibiting MAVS activity (Yoshizumi et al., 2014).

Invading viruses frequently target and inhibit downstream signalling in the IFN induction pathway. As one of the crucial effector molecules is IRF3 it is the focus of many evasion mechanisms. For example, KSHV encoded latency-associated nuclear antigen impedes IRF3 association with the IFNβ promoter by competing for binding (Cloutier and Flamand, 2010). Human cytomegalovirus (HCMV) has multiple mechanisms to subvert IRF3-dependent signalling using the virally encoded pp65, which has been reported to decrease the phosphorylation IRF3 and also prevent its nuclear translocation (Abate et al., 2004), a tactic also employed by the ICP0 protein of HCV (Melroe et al.,

2004). Simple binding and sequestration of cellular proteins is however just as effective at circumventing IFN induction. For example, Paramyxoviruses encode a multifunctional V protein, which, as well as directly binding to MDA5 to prevent its activation, also sequesters IRF3 (Irie et al., 2012). Additionally, some V proteins act as a decoy substrate for cellular TBK1 and IKKε and also cause the polyubiquitination of these signalling components (Lu et al., 2008).

Viruses also circumvent the IFN response by thwarting IFN signalling and the action of ISGs. Again, UPS and the subsequent proteasomal degradation of signalling effectors is a tactic employed by many viruses, including DENV, where NS5 causes the polyubiquitination and subsequent elimination of STAT2 (Morrison et al., 2013). The V protein of rubulaviruses in the paramyxoviridae family forms a V-degredation complex (VDC) with an E3 ubiquitin ligase, STAT1 and STAT2 (Ulane and Horvath, 2002). Interestingly, although both STATs are required for VDC assembly, only one will ultimately be degraded. For example, the VDC formed during PIV5 infection results in STAT1 degradation, whereas the VDC of PIV2 causes the elimination of STAT2 (Didcock et al., 1999, Parisien et al., 2001). The V protein of other paramyxoviruses such as Nipah virus (NiV) and the C protein of PIV1 sequester STAT molecules, although by slightly different mechanisms. Where NiV V relocalises unphosphorylated, nuclear STAT1 to the cytoplasm, PIV1 C results in the perinuclear aggregation of STAT1 to inhibit its phosphorylation (Schomacker et al., 2012, Rodriguez et al., 2002). Interestingly, Sendai virus (SeV), another respirovirus of paramyxoviridae appears to have a less specific mechanism for STAT inhibition. Although SeV C inhibits the tyrosine

phosphorylation of both STAT1 and STAT2 and the serine phosphorylation of STAT1, it has also been shown to impede the deactivation of STAT1 through disruption of dephosphorylation (Komatsu et al., 2002). The SeV C protein may therefore act through a general mechanism of dysregulating phosphorylation events. It has been shown that inhibition of the IFN signalling pathway also occurs through prevention of its activation. The phosphorylation of STATs is crucial to successful IFN signalling. The V protein of MeV blocks the nuclear translocation of STATs, but also binds to Jak1 impeding its ability to phosphorylate STATs and therefore blocks IFN signalling (Caignard et al., 2007, Caignard et al., 2009). Similarly, the E6 protein of human papilloma virus binds to Tyk2, resulting in a decrease in the phosphorylation of both STAT1 and STAT2 (Li et al., 1999).

1.2.2.2 Rabies and IFN antagonism

Rabies virus (RBV) of the lyssavirus genus in the Rhabdoviridae family is of particular interest to this study and is of significant global importance. Causing in excess of 55,000 human deaths annually, it is classified by the World Health Organisation as a neglected zoonotic disease (WHO, 2013, Wilde et al., 2016). To circumvent the induction of type I IFN, the N, L and P proteins encoded by the negative sense ssRNA genome encase the RNA to conceal it from detection by RIG-I (Tian et al., 2016). Additionally, residues 176 to 186 of RBV P have been shown to be crucial for the inhibition of IRF3 phosphorylation (Rieder et al., 2011). A recent report has demonstrated that the C-terminus of P from street strains of RBV inhibits the action of IKKε (Masatani et al., 2016). Interestingly, the inhibition of IKKε was not observed in any lab-adapted strains

tested. Clearly, the actions of RBV P are effective at inhibiting IFN induction. However, the pleiotropic nature of P is better demonstrated through its ability to subvert IFN signalling. RBV P only binds to STAT molecules that are tyrosine phosphorylated, presumably as it is more important to inhibit an active molecule as opposed to its inactive, repressed counterpart (Brzozka et al., 2006). Where the N-terminus of full length P (P1) is important for its role in genome replication, the C-terminus is crucial for STAT interactions (de Almeida Ribeiro et al., 2009, Ito et al., 2016). Additionally, the action of the C-terminus of P binding to STAT molecules appears to be conserved among lyssaviruses and is crucial for the lethality of RBV infection (Wiltzer et al., 2012, Wiltzer et al., 2014). N-terminal truncations give rise to 4 other isoforms of P (P2-P5) that appear to have distinct roles (Marschalek et al., 2012). For example, P1 and P2 have an NES which, when bound to phosphorylated STATs, results in their nuclear exclusion (Ito et al., 2010, Ito et al., 2016). Furthermore, monomeric P3 was reported to be nuclear and prevent the function of ISGF3 by preventing STATs binding to ISG promoters (Moseley et al., 2007a, Vidy et al., 2007). Interestingly, dimeric P3 was shown to prevent the nuclear import of STATs through association with microtubules (Moseley et al., 2007b). P1 and P3 have also been implicated in the subversion of ISG function by interacting with promyelocytic leukemia protein (PML), some isoforms of which have antiviral activity (Blondel et al., 2002).

It is clear that viruses have evolved a myriad of mechanisms that potently inhibit every aspect of the IFN response. Where DNA viruses generally have the genome capacity to encode numerous viral IFN antagonists, the limited

genomes of RNA viruses has resulted in the production of highly multifunctional proteins. This is exemplified through the pleiotropic NS1 protein of IAV, which has a plethora of mechanisms by which it subverts both IFN induction and IFN signalling. Due to the extent to which IFN antagonists facilitate virus replication, they provide an attractive target for clinical intervention. Recombinant viruses lacking a functional IFN antagonist could be used as an effective live-attenuated vaccine (Wressnigg et al., 2009). Conversely viral PAMPS, or synthetic versions, could make potent adjuvants in vaccine preparations (Hoffmann et al., 2015, Dalpke et al., 2002, Stahl-Hennig et al., 2009). On the other hand, compounds that modulate the function of viral IFN antagonists in the course of an infection could be developed into a novel class of antiviral drugs (Basu et al., 2009, Versteeg and García-Sastre, 2010). Furthermore, due to the high degree of similarity between the antagonists encoded by viruses of the same family and genus, active compounds could have a relatively broad spectrum of activity.

1.3 Drug discovery

The ever-increasing need for new drugs to treat the multitude of human diseases and infections in the clinic has placed enormous pressure on the pharmaceutical industry and academic research alike. To develop successful candidate drugs, a lengthy and iterative process of drug discovery followed by clinical trials is necessary to ensure the efficacy and safety of new therapeutics (Figure 1.7) (Hughes et al., 2011). Regardless of the approach used in different drug discovery programs, they all follow common themes and have shared goals. The overarching aim of all early stage drug discovery campaigns is to identify lead compounds that can be developed into candidate drugs to address unmet clinical need (Drewry and Macarron, 2010). The pre-clinical stages of the drug discovery process and the different approaches utilized will be discussed below. The use of high-throughput screening (HTS) and cell-based assays will be specifically addressed.

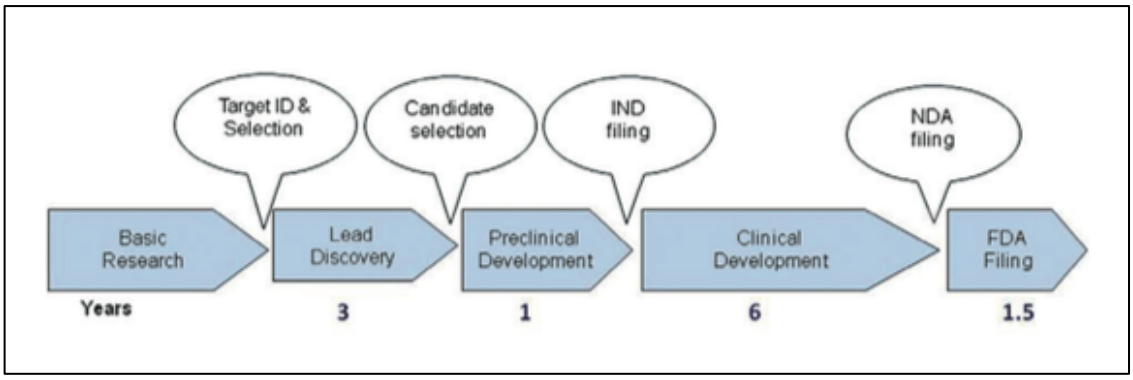

Figure 1.7: The development of a clinically approved drug.
From the inception of target identification, often from a basic research setting, to the approval of a new drug and its availability in the clinic is a lengthy, multistep process involving lead discovery, preclinical and clinical development (Hughes et al., 2011).

1.3.1 The process of drug discovery

The starting point of any drug discovery program is target identification. In many cases this is a specific protein, but a target can be any biological entity, including genes and RNA (Hughes et al., 2011). Additionally, a phenotypic screen can target a whole cellular pathway or process where many potential points of intervention may exist (An and Tolliday, 2010). Regardless of the type of target identified, they must meet certain criteria. Primarily, the target must be directly linked to a disease state, where it can be demonstrated that activation or inhibition of its activity will restore functionality and result in a reduction of disease-associated symptoms (Hughes et al., 2011). As a direct result of the advances in proteomics, genomics and sequencing, most especially with the completion of the human genome project in 2003, the number of potential targets has dramatically increased (Anderson, 2003). Additionally, the mining of biomedical data and direct sequencing of clinical samples has significantly increased the collective knowledge of disease-specific targets (Yap et al., 2016, Yang et al., 2009). It is estimated that biological space comprises approximately 30,000 disease-modifying genes, although only 10% of these may be disease causing (Overington et al., 2006). There is a great need for the identification of novel drug targets however, as all small molecule drugs currently available are directed against just 200 distinct protein targets (Bauer et al., 2010).

Following the identification of a target, a suitable assay must be developed in which the effect of test compounds can be assessed. This assay is then used to test different compounds to potentiate lead discovery. A lead is defined as a compound that displays the desired level of activity against a

specified target (Verlinde and Hol, 1994). Once identified, the lead molecule is validated for its potency, specificity and physiological relevance to the target (Clemons et al., 2014). As a result of the validation process, lead compounds are then chemically optimized, usually to produce a lead series, which provides pre-clinical drug candidates, termed new molecular entities (NMEs) (Hughes et al., 2011).

1.3.2 Approaches to drug discovery

Historically, lead identification in the 1970's relied heavily on observation. The activity of natural products for example, the side effects of currently available medicines, and even research presented at conferences (Kubinyi, 1995). As a result of advances in structural biology however, this dependence on "empirically-based" drug discovery began to decline and structure-based drug design (SBDD) emerged (Lipinski et al., 2001). The synthesis and testing of compounds on a larger scale was potentiated by developments in both combinatorial chemistry and automated robotics platforms (Baum, 1994, Patel and Gordon, 1996, Domanico, 1994), and the advent of high-throughput screening (HTS) made it possible to screen thousands of compounds in a reduced time (Hughes et al., 2011). As target knowledge has increased exponentially and NME output from the pharmaceutical industry has not followed suit, drug discovery programs are increasingly looking backward to historically successful in vivo phenotypic assays in search of innovative solutions to increase the productivity of lead discovery. Continued technological advances have lead to the development of many different types of HTS, from typical biochemical assays to more elaborate whole organism screens and ultra

high-throughput screens (uHTS) (Croston, 2002, Zlitni et al., 2009, Zon and Peterson, 2005).

1.3.3 High-throughput screening (HTS)

The first article to mention HTS was available on Pubmed in 1991, and it took a further 6 years for 10 HTS papers to be published in the same year (Macarron et al., 2011). Following target identification, it takes on average 11 to 13.5 years to develop a clinically approved drug at an estimated cost of $1.5 billion (Paul et al., 2010). Currently, there are few HTS derived NMEs in late stage drug development and clinical trials. This is seen by many as a result of the poorly constructed early compound libraries, which largely comprised non-drug-like molecules with little structural diversity, and were developed with little consideration for a compound's suitability for drug discovery (Bansal and Barnes, 2008, Dandapani and Marcaurelle, 2010). The primary purpose of HTS is to identify chemical starting points as quickly and efficiently as possible.

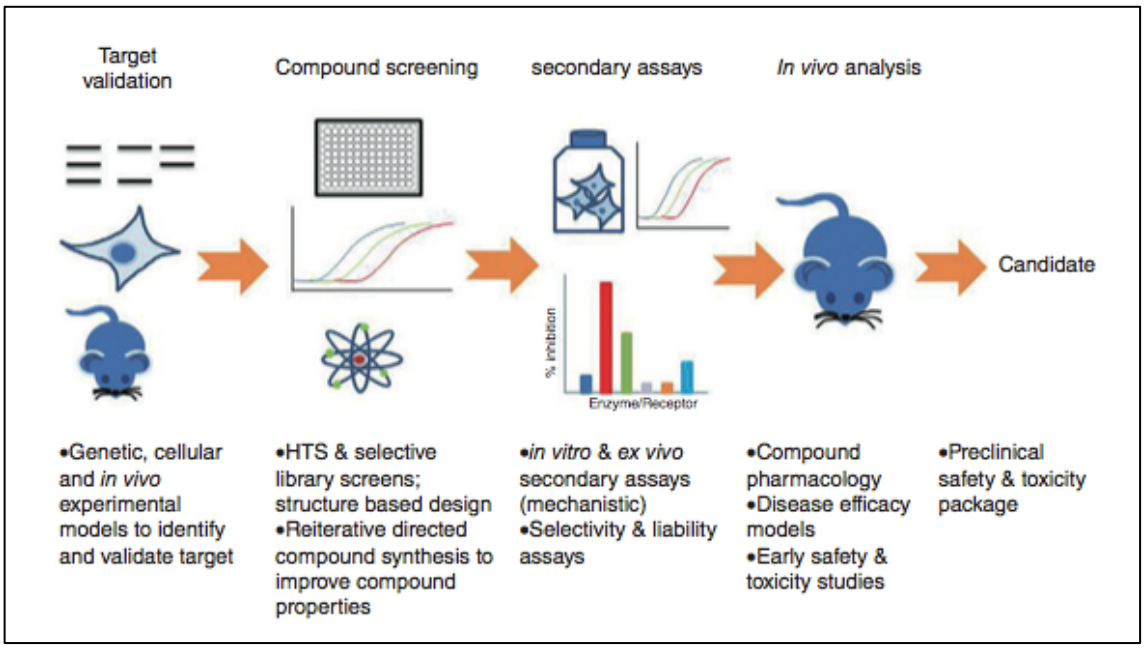

Figure 1.8: The workflow involved in early stage drug discovery.
Following validation of a target for drug discovery, compound screening programs including HTS aim to identify and optimize potent lead compounds, which are then analysed in secondary assays. Following successful characterisation, lead compounds are tested to assess safety and efficacy. If a compound successfully passes all these stages, it is deemed a preclinical candidate (Hughes et al., 2011).

Significant advances in the synthesis and testing of many thousands of compounds paved the way for HTS. Additionally, Lipinski observed that increased absorption and permeation of a compound was potentiated when a molecule has the following characteristics. (i) ≤ 5 hydrogen bond donors, (ii) ≤ 10 hydrogen bond acceptors, (iii) a molecular weight (MW) ≤ 500 and (iv), a CLogP ≤ 5, which is the logarithm of its partition coefficient, and is used as a measure of hydrophilicity (Lipinski et al., 2001). Following Lipinski's seminal publication and the founding of the "Rule of 5" (RO5), the make-up of screening libraries began to change, and compound collections were more thoughtfully developed (Lipinski, 2004). The continued evolution of screening libraries has placed increased emphasis on the use of small, simple molecules. This preference is due to the lead optimization process, which inevitably results in an

increase in MW and can result in issues with safety and tolerability in later stages of the drug development (Perola, 2010). As a result of the increased consideration of a compound's characteristics, two screening strategies have developed; (i) fragment-based screening and (ii) diversity screening.

Fragment-based drug discovery (FBDD) is based on the principle that small fragment molecules, although only binding weakly, can have "high quality interactions" with the target and so provide a solid basis from which to develop potent drugs (Scott et al., 2012). It is believed that hits with weak but appropriate binding kinetics are favourable to potent but flawed larger compounds. Additionally, classical HTS compound libraries require constant upkeep and funding to maintain their quality and diversity. As chemical space in the RO5 range (MW≤500) is estimated to be 10^{60} molecules (Barker et al., 2013), and there is predicted to be only 10^{7} fragment molecules that are RO3 compliant (comprising ≤11 atoms) (Fink and Reymond, 2007), FBDD immediately increases the range of chemical space that can be covered. FBDD relies heavily on molecules binding with high enough affinity to be detected, usually between 0.1 and 10 μM (Scott et al., 2012). As a result, screening is usually carried out at higher concentrations and requires very sensitive detection techniques (Law et al., 2009). As with SBDD, a strong collaboration between structural biology and synthetic chemistry is necessary, as is high quality 3D data. The fragment approach has proved to be a fruitful one, with the development of Zelboraf in 2011 (Murray et al., 2012). This enzyme inhibitor is used for the treatment of late-stage melanoma, and was the first FDA approved drug born from FBDD (Bollag et al., 2010). In contrast to FBDD, diversity

screening is based on classical HTS library composition that obeys Lipinski's RO5, although the focus here is maximization of the range of chemical space covered. Libraries are typically composed of a wide variety of chemical structures, with little similarity between compounds (Valler and Green, 2000).

As with SBDD, traditional biochemical HTS begins with a process of target identification and assay development. Typically, biochemical HTS assays simply test the affinity of a test compounds for the target. Following on from this and similarly to SBDD, the iterative process of lead optimization is pursued. In contrast to SBDD however, and as HTS can identify chemically distinct hits, there is potential for the development of multiple lead series. Furthermore, the starting point of biochemical HTS does not require any structural data pertaining to the target. Other approaches to HTS include focused, or knowledge-based screening, an extension of which has been the development of virtual screening. When there is substantial knowledge about a target, including its binding site and mode of action, there is the potential to use smaller compound collections, comprising molecules likely to have activity (Boppana et al., 2009). Knowledge-based screening has potentiated the development of virtual HTS (McInnes, 2007). Here, computerised compound sets are screened against a target using structure-based approaches that rely on the target structure, or ligand-based strategies where the chemistry of molecules known to bind the target is exploited (Lavecchia and Di Giovanni, 2013, Nagamani et al., 2011).

To potentiate HTS, the assay in question must meet certain criteria before screening can take place. This process of assay development considers the quality of the assay in terms of reproducibility and pharmacological

relevance (Zhang et al., 2012). The signal window, typically calculated as signal-to-background ratio (S/B), which considers the high and low signal, and the levels of variation observed, are used to assess assay quality (Zhang, 1999). The *Z*' factor is now a widely used statistic throughout the screening community as it assesses both the signal window of an assay (minimum and maximum means) and the variation seen within these populations, expressed as the standard deviation (StDev) (Zhang, 1999). The Z' factor has become the gold standard parameter used to gauge the suitability of an assay for HTS. An assay achieving a Z' factor of ≥ 0.5 is deemed an excellent assay, whereas if the Z' factor is between 0 and 0.5, it is viewed as marginal, and although could be used in HTS, further assay optimization and development is recommended (Clemons et al., 2014). Additionally, assay cost is a crucial aspect of assay development, which aims to minimize reagent usage, usually leading to assay miniaturization to reduce reagent volumes.

Regardless of assay format, lead identification (screening) follows successful assay development, where primary screening of thousands to millions of compounds aims to identify putative hit compounds. Assays targeted to antagonist identification are associated with higher initial hit rates as they usually detect a decrease in signal, which can also result from compounds that interfere with signal generation. A crucial process following primary screening is hit triage, which aims to eliminate putative hit compounds that are likely to be false positives. Remaining hits are then grouped based on structural similarities and secondary assays are carried out the further analyse activity and potency. The secondary assay stage of early drug discovery aims to test the potency of

lead compound(s) in cell-based assays to demonstrate their activity outwith engineered proteins and also identify any structure-activity relationships (SAR). Lead optimization, similar to the cyclic process of synthesis, testing and structural alteration utilized in SBDD and FBDD, ultimately aims to increase specificity and potency. This crucial process is time consuming and associated with high failure rates. From a primary HTS testing 200,000 to 1 million compounds, hundreds will be taken forward to the hit-to-lead and lead optimization phase, which may result in only 1 or 2 clinical candidates (Hughes et al., 2011).

Although the biochemical assays discussed above have been successful in generating new NMEs, output has been lower than expected. Lead-to-clinic has low numbers and is associated with high attrition rates. This may be for numerous reasons. Primarily, the activity of leads identified in traditional biochemical assays may not translate to the cellular environment used during pre-clinical testing (Clemons et al., 2014). Secondly, biochemical assays may not be the best option for targets that are outwith the norm of enzymes and receptors due to novel binding kinetics (Swinney, 2006). Historically, many successful drug discovery programs were less “target centric” and leads were often identified though phenotypic and in vivo assays (Kola and Landis, 2004). Furthermore, there was often no knowledge of the specific target or mechanism of action. As a result, screening centres and the pharmaceutical industry are increasingly looking to use cell-based assays with increased physiological relevance.

1.3.4 Cell-based assays in HTS

Biochemical assays used during primary screening simply assess the binding of a compound to a specific target. As a result of this, secondary assays used during hit validation are often associated with high attrition rates, by which time considerable time and money have been invested in the project. To overcome this, cell-based and phenotypic assays are increasingly used in early stage drug discovery as they not only illustrate the activity of a given compound, but also provide preliminary data regarding the ADMET (absorption, distribution, metabolism, elimination and toxicity) characteristics of the molecules (Zang et al., 2012). Additionally, cell-based assays have the capacity to identify both agonists and antagonists in a single screening campaign (Kunapuli et al., 2006, Guo et al., 2014).

Previously published research has provided proof of principle for using both a fluorescent cell-based assay and HTS for the identification of novel modulators of the IFN response (Enomoto et al., 2000, Guo et al., 2014). For example, a red fluorescent protein under the control of the ISRE promoter has been used in an HTS to identify immunostimulatory RNA (Nguyen et al., 2009). To date, most screens have been luciferase-based assays and utilise relatively small compound sets (Chen et al., 2008, Charlaftis et al., 2012, Ye et al., 2011, Patel et al., 2012, Zhu et al., 2010). Recently, cell-based HTS was used to discover agonists of the IFN response, with a view to developing broad-spectrum antivirals targeting infections to which there is high level of resistance to pre-existing therapies, or no current treatment options (Patel et al., 2012, Bedard et al., 2012, Martínez-Gil et al., 2012)

To design a cell-based assay for use in HTS, there are a number of criteria that need to be considered. Firstly, the target needs to be identified. In a cell-based phenotypic assay, this does not need to be a specific protein, but can be a signalling pathway as a whole. Secondly, the most appropriate cell system needs to be established. Although all cells are amenable to HTS, each have pros and cons associated with their use. Immortalized cell lines are simple to culture, reproducible and relatively cheap. However, the increased number of mutations necessary to render them immortal may alter their biological processes beyond physiological relevance (Ebert and Svendsen, 2010, Sharma et al., 2010). Primary cell lines and stem cells both produce physiologically relevant responses, although they have a limited culture life, and are difficult to handle (Ebert and Svendsen, 2010, Zang et al., 2012). Embryonic stem cells have an increased capacity for growth and differentiation, although their use is associated with moral issues. Chemically induced, pluripotent stem cells overcome these issues as they are artificially derived and can also be sourced directly from patients with a specific disease (Zang et al., 2012). Additionally, whole organism screens using parasites, zebra fish and even plants have been carried out (Zon and Peterson, 2005, Baragana et al., 2015, Agee and Carter, 2009).

Once an appropriate cell system has been chosen, the assay format needs to be addressed. The signal to be detected can range from a functional readout such as activation of secondary messengers and fluctuations in membrane potential, to phenotypic screens that assess cytokine production and cell migration (Zheng et al., 2013, Eggert et al., 2004, Yarrow et al., 2005, Kariv

et al., 1999, Chambers et al., 2003). Reporter genes including luciferase, β-galactosidase, and fluorophores such as green fluorescent protein (GFP) are also widely used (Zhang et al., 2012, Beck et al., 2005, Li et al., 2007). The final consideration for assay design is the detection method that will be used. Although somewhat linked to the format of the assay in terms of signal for functional assays, fluorescent-based phenotypic assays can be monitored by either uniform well measurements using plate readers or high content screening (HCS), where high quality, confocal-level microscopy is used to analyse individual cells (Gribbon and Sewing, 2003, Nichols, 2006).

As with other assays used in HTS, a stringent program of assay development and miniaturization is necessary. Although less simple to miniaturize compared to biochemical assays, cell-based, fluorescent end point assays are amenable to miniaturization as the signal window is not significantly affected (Kowski and Wu, 2000, Rudiger et al., 2001). The behaviour of the cell line and the assay are assessed at every step of assay development, where well-to-well, plate-to-plate, day-to-day and batch-to-batch reproducibility is closely monitored. This is achieved by the analysis of screening statistics such as the aforementioned S/B ratio, the percentage coefficient of variation (%CV) and the Z' factor (Sittampalam et al., 1997, Zhang, 1999). As cells respond rapidly to environmental changes, their sensitivity to the compound solvent, and fluctuations in temperature and humidity need to be considered (Zhang et al., 2012).

Following assay development, a pilot screen should be carried out, usually of 2,000 to 10,000 compounds to assess the behaviour of the finalized

assay (Voter et al., 2016, Clemons et al., 2014). Additionally, the inclusion of a reference molecule here is advantageous, although not always possible, especially for novel targets (Lu et al., 2015). Hit identification following primary HTS is based on the statistical analysis of the results. A predefined signal threshold, be it the top 1% of activity, or a fixed percentage minimum allows for hit triage, where increased stringency will decrease the number of putative hits, but potentially increases the number of false negatives (Malo et al., 2006). It is noteworthy that in cell-based HTS assays, off target effects can produce the same result as a hit. Additionally, in a phenotypic assay, the same phenotype can be achieved through compounds acting at different intervention points (Clemons et al., 2014). Putative leads resulting from hit identification are then subjected to secondary assays and counter screens designed to assess the specificity and potency of their activity. Following this, compounds are deemed confirmed hits, and enter the optimization pipeline. This usually involves compound set enrichment, where different compounds with chemotypes of high similarity to the hits are tested (Varin et al., 2011, Napolitano et al., 2016). Confirmed hits with novel structural properties and RO5 compliance are favourable as they are less likely to have off-target effects (Lipinski et al., 2001). Due to the inherent nature of cells to vary in their responses, hits can give rise to ambiguous results in different secondary assays (Burdine and Kodadek, 2004).

Due to the high attrition rates associated with lead optimization following biochemical HTS and SBDD, pharmaceutical companies have been searching for assays that have built-in hit triage, an unbiased lead identification process,

and that give an indication of the biological responses to compounds. Cell-based assays to provide an answer to this problem, and pharmaceutical companies appear to agree, as in 2006, cell-based assays constituted 53% of all HTS campaigns (Fox et al., 2006). It is important to note however, that in drug discovery there are no short cuts. Although cell-based assays allow for earlier focus on lead series that are likely to be successful, a lengthy process of lead optimization and preclinical testing will always be involved, regardless of the initial approach.

1.4 Research aims & objectives

The primary aim of this study was the development of a cell-based fluorescent assay to identify novel, small molecule modulators of the IFN response. Compounds that antagonize the IFN response have potential uses (i) as candidate drugs for the treatment of diseases associated with IFN dysfunction, (ii) in the production of live-attenuated viral vaccines and oncolytic viruses, and (iii) as tools to facilitate basic research. Conversely, compounds that agonize and therefore enhance IFN induction could be developed into therapeutics to boost the innate immune response in immunocompromised patients or for the indirect treatment of viral infections.

The main aims of this study were as follows:

- Develop a phenotypic assay to identify modulators of the IFN response
- Optimize and miniaturize the assay to an automated 384-well format
- Validate the suitability of the assay for use in an HTS campaign
- Carry out a diversity screen against 15,667 small molecules at the Drug Discovery Unit, University of Dundee
- Validate any hit compounds identified during screening and confirm their specificity
- Characterize the compounds with preliminary research into the cellular target and the mode of action of confirmed hits
- Expand the assay to enable the identification of molecules that modulate the function of the Rabies virus IFN antagonist (RBV-P) and subsequently carry out an in-house HTS.

2. Materials and Methods

2.1 Cell-lines, viruses, interferon and antibodies

2.1.1 Mammalian cell-lines

The mammalian cell-lines used in this study were Human embryonic kidney cells (293T) (Provided by Prof. Richard Iggo, University of Bordeaux), Human adenocarcinomic alveolar epithelial cells (A549) (ECACC 86012804) and African green monkey kidney epithelial cells (Vero) (ECACC 84113001). The human keratinocyte cell line, HACAT was utilized in the kinase activity assay carried out by Jordan Taylor at the University of Dundee.

In addition to the cell-lines detailed above, the following A549 derivatives were used.

- **A549/pr(IFNβ).GFP**: A549 cells with an enhanced green fluorescent protein (eGFP) gene under the control of the IFNβ promoter (Chen et al., 2010).
- **A549/pr(ISRE).GFP**: A549 cells with an eGFP gene under the control of the MxA promoter, which contains multiple Interferon stimulated response elements (ISRE) (Stewart et al., 2014).
- **A549/pr.(ISRE).GFP.RBV-P**: A549/pr(ISRE).GFP cells that stably express N-terminally V5-tagged P protein of Rabies virus (RBV) (generated by Dr. Andri Vasou).
- **A549/pr(ISRE).GFP.TetOne-Puro-RBV-P**: A549/pr(ISRE).GFP cells that express RBV P with an N-terminal V5-tag when induced with doxycycline (Dox) treatment.

2.1.2 Viruses and interferon

Cantell, a strain of Sendai virus (SeV) rich in defective interfering particles (DIs) (clarified allantoic fluid at 4000 HA units/ml, Charles River Laboratories) was used to stimulate the IFN induction pathway. Unless otherwise stated, SeV was used at a concentration of 40 HA units/ml. A recombinant Bunyamwera virus lacking the NSs gene (BunVΔNSs), rendering it IFN sensitive, was also used in this work (Stewart et al., 2014) (Provided by Prof. Richard Elliot, University of Glasgow). Purified IFNα (Roferon) (NHS, UK) was used to stimulate the IFN signalling pathway, and unless otherwise stated, used at a final concentration of 10^4 units/ml.

2.1.3 Antibodies

For the purposes of immunostaining western blot (WB) membranes and cell monolayers for immunofluorescent microscopy (IF), the primary and secondary-conjugated antibodies used are detailed below (Table 2.1).

Table 2.1: Antibodies used in western blotting and immunofluorescence

Target	Raised in	Source	WB Dilution	IF Dilution
Primary Antibodies				
β-Actin	Mouse	Sigma-Aldrich	1:10,000	-
SeV	Rabbit	Prof. Steve Goodbourn	-	1:500
IRF-3	Rabbit	Santa Cruz	-	1:200
pIRF-3 (Ser 396)	Rabbit	Cell Signalling	1:1000	-
pSTAT1 (Tyr 701)	Goat	Santa Cruz	1:150	-
MxA	Rabbit	Santa Cruz	1:750	-
GFP	Mouse	Roche	1:1000	-
V5	Mouse	Prof. Richard Randall	-	1:400
V5	Rabbit	AbD Serotec	1:1000	-
Secondary Antibodies				
α-Rabbit IRDye680	Goat	Li-Cor	1:10,000	-
α-Mouse IRDye800	Goat	Li-Cor	1:10,000	-
α-Goat HRP[1]	Donkey	Santa Cruz	1:2000	-
α-Rabbit FITC[2]	Goat	Sigma-Aldrich	-	1:200
α-Rabbit TR[3]	Donkey	Abcam	-	1:200
α-Mouse TR[3]	Goat	AbD Serotec	-	1:200

[1] Horseradish Peroxidase (HRP)

[2] Fluorescein isothiocyanate (FITC)

[3] Texas Red (TR)

The details of the antibodies used in the TLR3 experiment conducted by Jordan Taylor at the University of Dundee are detailed below.

Table 2.2: Antibodies used in TLR3 dependent kinase activity experiment; conducted at the University of Dundee

Target	Raised in	Source
pTBK1 (Ser 172)	Rabbit	Cell Signalling
TBK1		
pIKKε (Ser 172)		
pIRF3 (Ser 396)		
GAPDH		
α-Rabbit HRP	Goat	

2.2 Cloning

2.2.1 Polymerase chain reaction (PCR)

For purposes of gene amplification for sub-cloning into plasmids, all PCR reactions were performed using high-fidelity Pfu polymerase (Promega). A typical reaction contained the components detailed in Table 2.3 in a total volume of 50 μL. The 10× stock Pfu buffer with $MgSO_4$ (200 mM Tris-HCl (pH 8.8), 100 mM $(NH_4)_2SO_4$, 100 mM KCl, 1 mg/ml BSA, 1% (v/v) Triton X-100, 20 mM $MgSO_4$) was used. Details of the primers used throughout this work are given in Table 2.6. A thermocycler with heated lid (Biometra®, T-Personal) was used to carry out all PCR reactions, using the cycling conditions shown in Table 2.4.

Table 2.3: Regents used in a typical PCR reaction

Component	Stock Concentration	Final Concentration
Pfu Polymerase	2.5 u/μL	0.05 u/μL
Pfu buffer	10×	1×
dNTPs	10 mM	0.4 mM
Forward primer	100 μM	0.2 μM
Reverse primer	100 μM	0.2 μM
DMSO	100% (v/v)	4% (v/v)
Template DNA	100-500 ng/μL	50 ng
Water	-	-

Table 2.4: Cycling conditions of a typical PCR reaction

Step	Temperature (°C)	Time (Seconds)	Cycles
Polymerase activation	95	180	1
Denaturation	95	30	30
Annealing	55	30	
Extension	72	120 /kb	
	72	600	1

Table 2.5: Sources of DNA used in PCR reactions

Gene	Accession	Source
IFNβ	EF064725.1	Prof. R Randall
MxA	AK225885.1	Dr D Jackson
β-Actin	NC_000007.14	Amplified from A549 cDNA
RBV-P	ADJ29909.1	Dr A Vasou

Table 2.6: Primers used in PCR, qPCR and sequencing reactions

Name	Use	Sequence
IFNb qPCR Forward nt 41-62	qPCR PCR	GCTTCTCCACTACAGCTCTTTC
IFNb qPCR Reverse nt 134-155	qPCR PCR	CAGTATTCAAGCCTCCCATTCA
MxA qPCR Forward nt 570-590	qPCR PCR	GCCTGCTGACATTGGGTATAA
MxA qPCR Reverse nt 910-931	qPCR PCR	CCCTGAAATATGGGTGGTTCTC
Actin qPCR Forward nt 257-276	qPCR PCR	GGCACCACACCTTCTACAAT
Actin qPCR Reverse nt 679-640	qPCR PCR	CCTTAATGTCACGCACGATTTC
5' EcoRI-V5 (RBV-P)	PCR	GCGCGAATTCATGGGAAAGCCGATCCCAAACC
3' BamH1-RBV-P	PCR	GCGCGGATCCTCAGCAGCTGGTGTATCTGTTCAGG
pJet 1.2 Forward	Seq[1]	CGACTCACTATAGGGAGAGCGGC
pJet 1.2 Reverse	Seq[1]	AAGAACATCGATTTTCCATGGCAG
RBV-P nt510-527	Seq[1]	GGCCAGAATGGTGGCCCA
pLVX-TetOne Forward	Seq[1]	ATGTAAACCAGGGCGCCTAT
pLVX-TetOne Reverse	Seq[1]	CCTCCTGTCTTAGGTTAGTG
[1] Sequencing reactions (Seq)		

2.2.2 DNA gel electrophoresis and extraction

To analyse to results of PCR and restriction enzyme digest, DNA was separated by agarose gel electrophoresis. PCR reaction samples were mixed with the appropriate volume of 10× loading buffer (Bioline) and run on a 1 or 2% (w/v) agarose gel (Sigma-Aldrich) in TBE buffer (100 mM Tris base, 100 mM Boric acid, 2.5 mM EDTA) containing ethidium bromide (1 μg/ml) (Invitrogen).

Samples were loaded into the gel with a molecular weight marker (Bioline, 100 bp & 1kb) and run in TBE at 90 volts until bands were appropriately resolved. Bands of interest were excised from the gel and DNA purified using the QIAquick gel extraction kit (Qiagen) following manufacturer's instructions, with the exception of purified DNA elution, where nuclease-free water was used as opposed to EB buffer.

2.2.3 Sub-cloning into pJet shuttle vector

To facilitate sequencing and down-stream subcloning of amplified DNA fragments, PCR products were cloned into an intermediate vector. Purified PCR products were ligated into pJet1.2 (ThermoFischer). This CloneJet system allows for the direct ligation of blunt-ended PCR products into the pJet plasmid. One microliter of purified PCR product was incubated with 10 μL of 2× Buffer, 1 μL of pJet1.2 vector and 7 μL of nuclease-free water, and 1μL of T4 DNA ligase (5 units) at room temperature (RT) for 5 minutes. For bacterial transformation, the ligation reaction was then incubated, on ice, with 50 μL of chemically competent DH5α *E. coli* cells (provided by Dr D Jackson) for 15 minutes. The transformation mix was heat-shocked at 42°C for 45 seconds, followed by a period of recovery through incubation at 37°C for 30 minutes. The transformed DH5α cells were plated onto Lysogeny broth (LB) agar plates containing ampicillin (100 μg/ml), inverted and incubated at 37°C for 18 hours. Transformed colonies from the agar plates were inoculated into 4 ml of LB supplemented with 100 μg/ml ampicillin and incubated at 37°C in an orbital shaker (280 rpm) for 18 hours. Plasmid DNA was then extracted from the

cultures using QIAprep spin miniprep kit (Qiagen). Miniprep plasmid DNA was screened for the cloned insert using diagnostic restriction digest as per manufacturer's instructions (Promega). Briefly, plasmid DNA (3 μL), *BglII* restriction enzyme (5 units), 10× restriction digest buffer D (2 μL) and acetylated BSA (2 μg) were incubated at 37°C for 2 hours, followed by DNA gel electrophoresis. Gels were visualised under UV light, and plasmid DNA displaying the correct banding pattern was sequenced by DNA Sequencing & Services (MRCPPU, College of Life Sciences, University of Dundee, www.dnaseq.co.uk) using Applied Biosystems Big-Dye Ver 3.1 chemistry on an Applied Biosystems model 3730 automated capillary DNA sequencer.

2.2.4 Sub-cloning into lentiviral transfer vector

For construction of the lentiviral vector containing RBV-P, sequence verified pJet1.2 vectors and the pLVX-TetOne-Puro destination vector (Clontech) were digested with *BamHI* and *EcoRI* restriction enzymes (Promega). The digested vector was also dephosphorylated using calf intestinal alkaline phosphatase (New England Biolabs) to prevent re-ligation of the digested vector. Digestion reactions were separated by DNA gel electrophoresis followed by DNA extraction of the vector and insert as detailed above (2.2.2). Purified insert DNA (5μL) was incubated with 10 μL of 2× Buffer, 1 μL of pLVX-TetOne-Puro vector and 3 μL of nuclease-free water, and 1μL of T4 DNA ligase (5 units) at RT for 5 minutes. For bacterial transformation, the ligation reaction was then incubated, on ice, with 50 μL of chemically competent DH10b *E. coli* cells (Provided by Dr M Nevels) for 15 minutes. The transformation mix was heat-shocked at 42°C for 45 seconds, followed by a period of recovery through

incubation at 30°C for 1 hour. The transformed DH10b cells were plated onto LB agar plates containing ampicillin (100 μg/ml), inverted and incubated at 30°C for 24 hours. Transformed colonies from the agar plates were inoculated into 4 ml of LB supplemented with 100 μg/ml ampicillin and incubated at 30°C in an orbital shaker (280 rpm) for 24 hours. Plasmid DNA was then extracted from the cultures using QIAprep spin miniprep kit (Qiagen). Miniprep plasmid DNA was screened for the cloned insert using diagnostic restriction digest as detailed in section 2.2.3. where *BglII* restriction enzyme was substituted by *BamHI* and *EcoRI.* Following DNA gel electrophoresis, gels were visualised under UV light, and plasmid DNA displaying the correct banding pattern was sequenced by DNA Sequencing & Services. Upon verification that the recombinant pLVX-TetOne-Puro vector sequences were correct, miniprep DNA was transformed into DH10b *E.coli* cells, inoculated into 100 ml of LB supplemented with 100 μg/ml ampicillin and incubated at 30°C in an orbital shaker for 24 hours. To achieve higher DNA yield to facilitate transfection for lentivirus production, plasmid DNA was extracted from the 100 ml cultures using Qiagen Plasmid Maxi Kit as per manufacturer's instructions with the following alterations; (i) following isopropanol addition to precipitate eluted DNA; the reaction was incubated at -20°C for 1 hour, (ii) the wash step with ethanol addition to the pelleted DNA was carried out twice and (iii) following air-drying of the pellet, DNA was dissolved in nuclease-free water.

2.2.5 Genomic DNA Extraction

To verify the successful integration of the transfer vector cassette into the host cell chromosome following lentivirus transduction of cells, genomic DNA

was extracted. The DNA was then analysed by PCR using primers specific to RBV-P (Table 2.6) followed by DNA gel electrophoresis. Genomic DNA extraction was achieved using Blood and Cell Culture DNA Kit (Qiagen) and the Qiagen Genomic tip 20/G following manufacturer's instructions with the following alteration. Once air-drying of the pellet was complete, DNA was dissolved in nuclease-free water.

2.3 Cell culture

2.3.1 Cell maintenance

All the cell lines used in this study were maintained as monolayers in tissue culture flasks (25, 75, 175 or 225 cm^2) in high glucose Dulbecco's modified eagle's medium (DMEM) supplemented with 10% (v/v) Foetal bovine serum (FBS), 30 μg/ml penicillin and 50 μg/ml streptomycin (Pen-strep). Cells were incubated at 37°C with 5% CO_2. When confluency reached approximately 90%, cells were passaged with Trypsin-ethylenediaminetetraacetic acid (EDTA). For seeding of cells that would later be treated with IFNα, dissociation was achieved with 0.48 mM EDTA in phosphate-buffered saline (PBS) to avoid trypsin-mediated cleavage of the IFNα/β receptor.

2.3.2 Cryopreservation & resuscitation of cells

Stable cell lines produced by lentivirus transduction were stored as stocks in liquid nitrogen. Cell monolayers were maintained as detailed above. Once 90% confluency was achieved, cells were trypsinised and centrifuged at 1200 xg for 5 minutes. The cell pellet was resuspended in cryo-media (60%

(v/v) DMEM, 30% (v/v) FBS, 10% (v/v) DMSO) to achieve a concentration of 1×10^6 cells/ml. Cells were frozen in 1 ml aliquots at -80°C and transferred to liquid nitrogen for long-term storage. To resuscitate cells that had been in liquid nitrogen storage, the 1 ml vial was thawed at 37°C and centrifuged at 1200 xg for 5 minutes. The resultant cell pellet was resuspended in DMEM supplemented with 10% (v/v) FBS and Pen-strep, split 80/20 into two, 25 cm^2 tissue culture flasks and incubated at 37°C with 5% CO_2. Where selection was required, puromycin (2 μg/ml) was added to culture medium when monolayers reached 60% confluency or at first passage.

2.3.3 Growth of virus stocks

BunVΔNSs stocks were propagated in T75 cm^2 tissue culture flasks containing Vero cells at 95% confluency. Cells were infected with virus and incubated for 3 days in DMEM supplemented with 2% (v/v) FBS and L-glutamine (2 mM). Supernatant was collected and centrifuged at 1200 xg for 5 minutes. BunVΔNSs stocks were stored as 1 ml aliquots at -80°C.

2.3.4 Stable cell-line production

To modify the A549/pr(ISRE).GFP reporter cell line to express RBV-P by doxycycline induction, 2nd generation lentivirus technology was used. Lentiviruses are produced in 293T cells following transfection with 3 plasmids. These plasmids being (i) a transfer vector containing the integration cassette, which comprises a puromycin N-acetyl-transferase (PAC) gene, and so gives resistance to puromycin, and the gene of interest flanked by long terminal repeats, which facilitate integration into the host cell chromosome, (ii) a

packaging plasmid encoding Gag, Pol and Rev, and (iii) an envelope plasmid encoding the G glycoprotein of vesicular stomatis virus (VSV) (Zufferey et al., 1997, Naldini et al., 1996).

2.3.4.1 Lentivirus production

293T cells were seeded in T75 tissue culture flasks at 70 to 90% confluency for transfection. Using the 3 vector system for lentivirus production, 10μg of pLVX-TetOne-Puro-V5-RBV-P, 6 μg of pCMVR 8.91 packaging plasmid and 6 μg pVSV-G envelope plasmid were added to 1.5 ml of Optimem (Invitrogen) and incubated at room temperature for 5 minutes. Separately, 60 μl of Lipofectamine 2000 (Invitrogen) was added to 1.5 ml of Optimem. The plasmid and Lipofectamine mixes were then combined, and incubated at RT for a further 30 minutes to allow DNA containing liposomes to form. Culture medium was removed, and the plasmid-Lipofectamine-Optimem solution added drop-wise to the 293T cells, which are incubated at 37°C with 5% CO_2. Five hours post-transfection, 8 ml of antibiotic free DMEM supplemented with 10% (v/v) FBS was added. After a 48 hour incubation at 37°C with 5% CO_2, lentivirus containing media was collected and centrifuged at 3000 ×g for 10 minutes. The medium was then filtered through a 0.45 μm syringe filter and divided into 1 ml aliquots for storage at -70°C.

2.3.4.2 Transduction of A549/pr(ISRE).GFP cells

A549/pr(ISRE).GFP reporter cells were transduced with lentivirus at 50% confluency in T25 tissue culture flasks. Lentivirus preparations were thawed at 37°C and added to 1 ml of DMEM (serum and antibiotic free) supplemented

with polybrene (Sigma), to aid infection, at a final concentration of 8 μg/ml. The lentivirus-DMEM-polybrene mix was added to cell monolayers. Flasks were then centrifuged at 1000 ×g for 30 minutes and incubated at 37°C with 5% CO_2 for 2.5 hours. Two ml of DMEM supplemented with 10% (v/v) FBS was then added to the flasks, which were incubated as above for a further 48 hours.

Where repeated rounds of lentiviral transduction were required, following centrifugation for 30 minutes, cells were incubated for 1 hour. Following incubation, the lentivirus containing media was removed, and freshly prepared lentivirus-DMEM-polybrene mix applied to the cells as above. This was repeated as many times as required. Two ml of DMEM containing 10% (v/v) FBS was then added and the cells incubated for 48 hours as above.

2.3.4.3 Antibiotic selection of transduced cells

Following lentivirus transduction, antibiotic selection was used to isolate cells that had successfully integrated the transfer vector cassette into the host cell chromosome. Puromycin (Sigma) was added to cell culture medium at a final concentration of 2 μg/ml.

2.3.5 Fluorescent activated cells sorting (FACS)

Following multiple rounds of lentivirus transduction, the A549/pr(ISRE).GFP cell line required optimization. The expression of GFP was not consistent throughout the population and so was heterogeneous. Therefore, the cells were sorted on the basis of GFP expression to produce more homogenous expression. Fiona Rossi, of the Centre for Inflammation Research, The Queen's Medical Research Institute in Edinburgh carried this out.

The A549/pr(ISRE).GFP cell-lines adapted to include the Dox inducible expression of RBV-P required further optimization. To facilitate this optimization, FACS was employed to isolate cells expressing the lowest levels of GFP in the presence of antagonist. Cells were seeded into T25 tissue culture flasks at approximately 25% confluency in the presence or absence of Dox (1 μg/ml) (Sigma). Sixteen hours post-Dox treatment, cells were either treated with IFNα (10^4 units/ml) for 24 hours or left untreated. Cells were then trypsinized and centrifuged at 1200 xg for 5 minutes and the cell pellet resuspended in 2 ml of DMEM supplemented with 2% (v/v) FBS. For FACS analysis, cells were filtered into FACS tubes (Round bottom Falcon tubes with cell strainer cap) and analysed by flow cytometry in a FACSJazz cell sorter (BD Biosciences). All FACS sorting and initial analysis was completed by Dr. Elizabeth Randall. Briefly, the cell population to be sorted goes through a process of gating, where cell size (Forward Scatter (FSC)) and granularity (Side Scatter (SSC)) are assessed to eliminate cell debris, along with trigger pulse width, which removes cell doublets from the analysis. Single cells are then sorted on the basis of GFP fluorescence using laser excitation of 488 nm and identified by a 530/40 bandpass filter. Sorted cells are then isolated into 12-well tissue culture dishes and maintained for further analysis.

2.3.6 IFNβ induction assay

A549/pr(IFNβ).GFP reporter cells were maintained in tissue culture flasks and dissociated with Trypsin-EDTA. Cells were seeded at 9×10^4 cells/cm^2 in 96 or 384 well tissue culture plates (Corning) and incubated at 37°C with 5% CO_2. Unless specified, twenty-four hours post seeding, cells were infected with SeV

in DMEM supplemented with 10% (v/v) FBS and incubated at 37°C with 5% CO_2 for 18 hours, unless otherwise stated. Where necessary, prior to SeV infection, cells were treated with inhibitors at the indicated concentrations for 2 hours at 37°C. Cells were fixed with 5% (v/v) formaldehyde at room temperature, washed and phosphate buffered saline (PBS) added to each well. Cells were then analysed for GFP expression on an Infinite M200 Pro (Tecan) or EnVision (Perkin Elmer) plate reader at excitation/emission 484/518 nm or 485/535 nm respectively. Data was analysed by converting the signal in raw fluorescent units (RFU) to a signal-to-background (S/B) ratio of RFU of unactived cells and then calculating the mean (μ) and the standard deviation (σ) for a group of replicates. This was also used to calculate the Z′ Factor, comparing the signal of activated (SeV infected) and unactivated (untreated) cells. The formula for this calculation is below (Zhang, 1999). S/B ratio was calculated by dividing the mean signal (RFU) of activated cells by that of unactivated cells.

$$Z' \text{ Factor} = 1 - \frac{3 \times (\sigma_{Activated} + \sigma_{Unactivated})}{\mu_{Activated} - \mu_{Unactivated}}$$

2.3.7 IFN signalling assay

A549/pr(ISRE).GFP reporter cells were maintained in tissue culture flasks and dissociated with EDTA for seeding into 96 or 384 well tissue culture plates (Corning) at 9×10^4 cells/cm^2, followed by incubation at 37°C with 5% CO_2. To activate the IFN signalling pathway, cells were treated with 10^4 Uml^{-1} of IFN-α (Roferon, NHS) in DMEM supplemented with 10% (v/v) FBS 24 hours

post seeding. Where necessary, prior to INFα treatment, cells were treated with inhibitors at the indicated concentrations for 2 hours at 37°C. Following incubation at 37°C with 5% CO_2 for 42 hours, unless otherwise specified, cells were fixed with 5% (v/v) Formaldehyde at room temperature, washed and PBS added to each well. Cellular GFP expression was then analysed as above (2.3.6)

2.3.7.1 A549/pr(ISRE).GFP cells with constitutive antagonist expression

A derivative of the A549/pr(ISRE).GFP cell line, which constitutively expresses the P protein of Rabies virus (A549/pr(ISRE).GFP.RBV-P) was used for in-house HTS (2.4.2). A549/pr(ISRE).GFP.RBV-P cells were used in the IFN signalling assay as detailed above (2.3.7). Cells were analysed for GFP expression on an Infinite M200 Pro (Tecan) plate reader at excitation/emission 484/518 nm. As the expression of RBV-P inhibits the IFN signalling assay, GFP fluorescence is minimal. Therefore, the S/B ratio and Z' Factor cannot be used for quality control (QC) analysis. In this case, percentage coefficient of variation (CV %) was used to monitor fluctuations in the A549/pr(ISRE).GFP.RBV-P cell line.

$$CV\ \% = (\sigma/\mu)*100$$

2.3.7.2 A549/pr(ISRE).GFP cells with a doxycycline inducible expression system

Derivatives of the A549/pr(ISRE).GFP cell line were developed, where the expression of the P protein of Rabies virus (A549/pr(ISRE).GFP.TetOne-Puro.RBV-P) is induced with Dox treatment. These cell lines were used in the

IFN signalling assay above (2.3.7) with the following amendments. As the half-life of Dox is 48 hours, it was supplemented into the growth medium and topped up every 36 hours. Where appropriate, cells were seeded in the presence of Dox, which was also added at the same time as IFNα treatment. Unless otherwise stated, Dox was used at a final concentration of 1 μg/ml.

2.4 High-throughput screening

In this study, we embarked on 2 separate screening campaigns. The first utilized the IFNβ induction assay with the aim of identifying novel modulators the IFNβ induction pathway. In this screen we were primarily measuring a reduction in GFP expression, which would result from a test compound inhibiting the IFNβ induction pathway. The second screen, carried out in-house, utilized the IFN signalling assay and A549/pr(ISRE).GFP.RBV-P cells to identify novel modulators of RBV-P protein function. In this instance, if a test compound were to inhibit RBV-P function, GFP expression would be restored.

2.4.1 Screening compounds and inhibitors

IFN induction and signalling inhibitors BX-795, TPCA-1 and Ruxolitinib (Rux) (Selleck chemicals) were prepared in dimethyl sulfoxide (DMSO) as 10 mM stock. CYT387 (Selleck chemicals) was prepared in DMSO as a 20 mM stock. Unless otherwise stated, the inhibitors were used at 2 μM. Actinomycin D (AMD) and Cycloheximide (CHX) (Sigma), inhibitors of transcription and translation respectively, were prepared as 10 mg/ml stocks in DMSO and ethanol respectively, and, unless otherwise stated, used at 40 μg/ml.

Compounds constituting the Small Diversity Set of the Drug Discovery Unit (DDU) at the University of Dundee were stored as 10 mM stocks in DMSO and unless otherwise stated, used at 30 μM. Compounds constituting the Maybridge screening collection were stored as 10 mM stocks in DMSO and unless otherwise stated, used at 11.42 μM. Hit compounds identified during HTS, which were named StA-IFN-1 to StA-IFN-5 and compounds with high similarity to StA-IFN-1 and StA-IFN-4, and 2 molecules that constitute each half of these hit molecules are detailed below (Table 2.7). Compounds were purchased, prepared as 10 mM stocks in DMSO and used at 10 μM, unless otherwise stated. All compounds were stored at -80°C.

Table 2.7: Hit compounds and those with closely related structures

Name	Chemical Name	CAS	Source
StA-IFN-1	4-(1-Acetyl-1*H*-indol-3-yl)-5-methyl-2,4-dihydro-3*H*-pyrazol-3-one	300839-31-0	Chembridge
StA-IFN-2	4-{[4-(Thieno[3,2-*d*]pyrimidin-4-yl)-1,4-diazepan-1-yl]methyl}benzonitrile	930903-16-4	Enamine
StA-IFN-4	2-[(4,5-Dichloro-6-oxo-1(6*H*)-pyridazinyl)methyl]-8-methyl-4*H*-pyrido[1,2-*a*]pyrimidin-4-one	876916-52-8	Enamine
StA-IFN-5	6-Methyl-4-phenyl-*N*-(pyridin-4-yl)quinazolin-2-amine	610279-43-1	Mcule
StA-IFN-1-82S	3*H*-Pyrazol-3-one, 2,4-dihydro-4-(1*H*-indol-3-yl)-5-methyl-	3133225-48-8	Chembridge
StA-IFN-1-SF	3H-Pyrazol-3-one, 2,4-dihydro-5-methyl-	108-26-9	Enamine
StA-IFN-1-LF	Ethanone, 1-(1H-indol-1-yl)-	576-15-8	ChemDiv
StA-IFN-4-85S	3(2H) -Pyridazinone, 4,5-dichloro-2-[(6-methylimidazo[1,2-a]pyridin-2-yl)methyl]-	852902-22-8	Enamine
StA-IFN-4-SF	3(2H)-Pyridazinone, 4,5-dichloro-2-methyl-	933-76-6	Enamine
StA-IFN-4-LF	4H-Pyrido[1,2-a]pyrimidin-4-one, 2,8-dimethyl-	30247-64-4	ChemDiv

2.4.2 Diversity and dose response screening at the Drug Discovery Unit (DDU) University of Dundee

A single-point diversity screen of 15,667 compounds was carried out at the University of Dundee using the IFNβ induction assay detailed above (2.3.6).

The DDU small diversity set was provided in 384-well Echo plates. A549/pr(IFN).GFP cells were seeded into clear-bottomed black 384-well plates Test compound, at a final concentration of 30 μM (125 nl), was added to A549/pr(IFN).GFP cells using an Echo 550 liquid handler (Labcyte). Two hours post-compound addition, cells were infected with SeV (40 HA units/ml) for 18 hours. GFP expression was measured with an EnVision plate reader (Perkin Elmer) at excitation/emission 485/535 nm.

To test the potency of putative hits from the small diversity library, each compound was tested in the IFNβ induction reporter assay with and without SeV infection, and the IFN signalling assay to generate standard ten-point dose response curves. This was achieved through two-fold serial dilutions of test compounds added to seeded A549/pr(IFN).GFP or A549/pr(ISRE).GFP cells using an Echo 550 and overlord3 robotics software.

For all data analysis, the RFU of each well was measured, and normalised to a percentage effect (% effect) of the positive control, calculated as follows.

$$\% \text{ Effect} = ((RFU_{Unactivated} - RFU_{Test})/(RFU_{Unactivated} – RFU_{Activated})) * 100$$

ActivityBase XE (IDBS) was used for all data processing using % effect, with the utilisation of SARgen (IDBS) and Excel (Microsoft). For determination of potency, 4-parameter logistic fit (Minimum, maximum, hill slope and IC50) was used, being defined in reference to the negative log of the molar value at the point of inflection of a sigmoidal dose-response curve (pIC50). Additionally, all

assay plates were subject to QC analysis. The QC criteria for the acceptance of an assay plate is shown below:

- S/B Ratio ≥2
- CV % <8%
- Z' ≥0.5

2.4.3 In-house HTS using the Maybridge library

A single-point primary screen of 16,000 compounds was carried out in-house using the IFN signalling assay detailed above (2.3.7) with the A549/pr(ISRE).GFP.RBV-P reporter cell line. The Maybridge compound library, loaned by Prof Nicholas Westwood (University of St Andrews), was provided in 50 384-well plates. Compounds were at a concentration of 10 mM dissolved in DMSO and contained in columns 3 to 22. The screen was conducted in 4 batches; 2 batches of 12, and 2 batches of 13 plates. A549/pr(ISRE).GFP.RBV-P (columns 1-22) and A549/pr(ISRE).GFP (columns 23 to 24) cells were seeded in 384-well clear-bottomed, black tissue culture plates (Greiner Bio-one) at 9×10^4 cells/cm^2 and incubated at 37°C with 5% CO_2. The following day, cells were treated with 11.42 μM of test compound using a MiniTrak V Multi Position Dispenser (Perkin Elmer), which replicates the compound plate in the assay plate, for 2 hours. To activate the IFN signalling pathway, IFN-α in DMEM supplemented with 10% (v/v) FBS was added to cells in columns 2 to 23 followed by brief centrifugation at 1200 rpm for 1 minute. Following incubation at 37°C with 5% CO_2 for 42 hours, cells were fixed with 5% (v/v) Formaldehyde at room temperature, washed and PBS added to each well. With the exception of test compound transfer, all liquid handling was carried out using a Matrix

WellMate microplate dispenser (Thermo Scientific). Cellular GFP expression was analysed on an Infinite M200 Pro (Tecan) plate reader at excitation/emission 484/518 nm. Additionally, all assay plates were subject to QC analysis by monitoring CV % of A549/pr(ISRE).GFP.RBV-P cells and S/B ratio, CV % and Z' Factor of A549/pr(ISRE).GFP cells. All data analysis was conducted using Excel (Microsoft) and Prism6 (GraphPad) software.

2.5 Protein expression and modification analysis

To facilitate analysis of protein expression and phosphorylation levels under different treatment conditions, whole cell lysates were separated by SDS-polyacrylamide gel electrophoresis (SDS-PAGE) followed by transfer to membranes for western blotting. For different experiments, initial cell treatments post-seeding differ, however they converge on a standard set of techniques detailed below.

2.5.1 SDS-polyacrylamide gel electrophoresis (SDS-PAGE)

The procedures common to all experiments requiring SDS-PAGE are detailed here. A549 cells were seeded into 6-well plates at 4×10^4 cells/cm^2. Where appropriate the following day, cells were treated with compound for 2 hours. To activate the IFN induction pathway cells were infected with SeV. To induce the IFN signalling pathway, cells were treated with IFNα. Cells were lysed in disruption buffer (6M Urea, 4% (w/v) sodium dodceyl sulphate (SDS), 2 M β-mercaptoethanol), and to ensure denaturation of proteins were pulse sonicated at 10 amplitude microns (23kHz) for 10 seconds and heated to 95°C for 5 minutes. Cell lysates were separated by SDS-PAGE. Ten percent (v/v)

acrylamide gels were hand-cast using 30% (w/v) Protogel, Stacking buffer and Resolving buffer (National Diagnostics), the components of the gels are detailed below (Table 2.8). Gels were run at 100 volts for approximately 2 hours in 1× TGS buffer (25 mM Tris, 192 mM Glycine, 0.1% (w/v) SDS, pH8.3).

Table 2.8: Components of hand-cast SDS-PAGE gels

Reagent	10 % (v/v) Resolving Gel	4% (v/v) Stacking Gel
30% (w/v) Acrylamide (ProtoGel)	8.3 ml	1.3 ml
Resolving Gel Buffer (0.375 M Tris-HCl, 0.1% (w/v) SDS, pH 8.8)	6.3 ml	-
Stacking buffer (0.125 M Tris-HCl, 0.1% (w/v) SDS, pH 6.8)	-	2.5 ml
10% (w/v) Ammonium persulfate (APS)	250 µl	100 µl
TEMED (Tetramethylethylenediamine)	25 µl	10 µl
Water	8.5 ml	6.1 ml
Total Volume (for four gels)	25 ml	10 ml

Cell treatment conditions varied depending on the aim of individual experiments. The specifics of these different experiments following cell seeding and leading up to cell lysate collection are detailed below.

- **Detection of phosphorylated IRF3 (pIRF3)**: Cells were treated with compound for 2 hours, followed by SeV infection for 3.
- **Detection of phosphorylated STAT1 (pSTAT1)**: Cells were treated with compound for 2 hours, followed by IFNα treatments for 15 minutes.
- **Validation of the A549/pr(ISRE).GFP.RBV-P cell line**: A549/pr(ISRE).GFP and A549/pr(ISRE).GFP.RBV-P cells were treated with IFNα for 18 and 44 hours.

- **Validation of RBV-P protein expression from the pLVX-TetOne-Puro-RBV-P vector**: 293T cells were transfected with plasmid DNA using the Lipofectamine transfection protocol detailed in section 2.3.3.1, followed by incubation with Dox for 16 hours.
- **Validating the functionality of RBV-P in the A549/pr(ISRE).GFP. TetOne-Puro-RBV-P cell line**: A549/pr(ISRE).GFP and A549/pr(ISRE).GFP. TetOne-Puro-RBV-P cells were seeded in the presence or absence of Dox and treated with IFNα for 40 hours.

2.5.2 Western blotting and immunostaining of membranes

Following separation by SDS-PAGE, proteins were transferred to polyvinlidene difluoride (PVDF) membranes, activated in 100% (v/v) methanol (Thermo), using TransBlot Turbo semi-dry transfer system (Bio-Rad) in Towbin transfer buffer (25 mM Tris, 192 mM Glycine, 20% (v/v) methanol, pH8.3) at 1.3 Amps, 25 volts for 20 minutes. Membranes were blocked in blocking buffer (PBS, 0.1% (v/v) tween-20 and 5% (w/v) skimmed dried milk powder) and incubated with primary antibody (Table 2.1) at room temperature for 1 hour or overnight at 4°C. Membranes were then washed in 0.1% (v/v) tween-20 (PBS) and incubated with secondary antibody conjugated to a fluorophore or HRP (Table 2.1). Membranes were washed as above and protein detection performed using an Odyssey CLx near-infrared scanner (Licor) for fluorescently tagged secondary antibodies or enhanced chemiluminescence (ECL) for HRP-conjugated secondary antibodies.

2.6 Off-target effects of hit compounds

Following HTS and selection of hits to follow up, compounds were repurchased. We instigated a campaign of hit validation to confirm that the inhibition in GFP expression observed through screening was due to the action of a compound on the IFN induction pathway, and not through off-target, non-specific effects. This was achieved through assessing cell viability, cellular protein synthesis and virus infection and replication in the presence of hit compound.

2.6.1 Cell-viability assay

To assess the effect of compound on cell viability, the AlamarBlue (AB) reagent (Life Technologies) was used. A549 cells were seeded in 96-well plates and treated with a 10 point, 2-fold serial dilution of compound from 50 to 0.1 μM for 48 hours at 37°C with 5% CO_2. AB reagent (Life technologies) was added to cells to a final concentration of 10% (v/v) and incubated in the dark for 4 hours. Fluorescence was measured on an Infinite M200 Pro (Tecan) plate reader at excitation/emission 545/590 nm. The percentage reduction in AB used to assess cell viability is calculated by using 0% reduced (DMEM+AB) and 100% reduced (cells+DMEM+AB) controls.

2.6.2 Cellular and viral protein synthesis analysis

To assay cellular protein synthesis in the presence and absence of hit compounds, A549 cells were incubated with 10 μM of hit compound or the transcriptional inhibitor AMD for 24 and 48 hours. Cells were then metabolically labelled with L-[^{35}S]Met/Cys pro-mix (500 Ci mmol^{-1}, Perkin Elmer) for 1 hour.

After labelling, cells were lysed in disruption buffer containing 28 units/ml benzonase (Sigma) and proteins separated by SDS-PAGE (2.6.1). Gels were fixed, washed and imaged via coomassie brilliant blue stain. Bands were quantified using a FLA-5000 phosphoimager and Image Gauge software (FujiFilm). Down stream data analysis used Prism 6 (GraphPad) software.

To assess viral protein synthesis in the presence of hit compound, A549 cells were incubated with 10 μM of hit compound for 2 hours, followed by SeV infection for 18 hours. Metabolic labelling and processing of whole cell lysates was carried out as detailed above.

2.7 Analysis of IFNβ and MxA gene expression

To establish the activity of hit compounds out-with the GPF based reporter assays, their effect on IFNβ and MxA gene expression was assessed. This was achieved through total RNA extraction of compound treated, SeV infected cells, followed by reverse transcription of messenger RNA (mRNA) and quantitative PCR (qPCR) of the resultant complementary DNA (cDNA).

2.7.1 RNA extraction

A549 cells were seeding into 6-well plates at $3x10^5$ cells/ml (2 ml/well) and incubated at 37°C with 5% CO_2. The following day, confluent cell monolayers were treated with compound for 2 hours followed by either a 3-hour SeV infection or an 18-hour IFNα treatment. Total RNA was then extracted from the cells by standard Phenol-Chloroform extraction using TRIzol (ThermoFisher). Briefly, 1 ml of TRIzol reagent is added to each well to lyse the

cells. Cell lysates were collected and mixed with 200 μl of chloroform. To separate RNA, DNA and protein, the TRIZol-chloroform lysates were centrifuged at 12,000 ×g for 15 minutes at 4°C. The RNA-containing aqueous phase was then removed from the separated lysates. RNA was then mixed with 1μl of GlycoBlue coprecipitant (ThermoFisher) and 500 μl of isopropanol (IPA) and incubated at -20°C for up to 1 hour to aid RNA precipitation. The RNA-IPA was then centrifuged at 12,000 ×g for 10 minutes at 4°C and the resultant RNA pellet washed twice in 1 ml of 75% (v/v) ethanol (EtOH). The EtOH supernatant was removed from the RNA pellet, which was then air-dried and dissolved in nuclease-free water overnight at 4°C. The RNA was then used directly in cDNA synthesis or stored at -70°C.

2.7.2 Complementary DNA synthesis

Reverse transcription of purified RNA was completed using RevertAid First Strand cDNA Synthesis Kit (ThermoFisher), which utilizes a recombinant M-MuLV reverse transcriptase. Manufacturer's instructions were followed and are outlined below.

Total RNA (3 μg) was added to 1.5 μl of Oligo $d(T)_{18}$ primer (12.5μM) and nuclease-free water on ice and incubated at 65°C for 5 minutes. Once back on ice, 5× reaction buffer, RiboLock RNase inhibitor (20 units), and dNTPs (1 mM of each) and RevertAid M-MuLV Reverse Transcriptase (200 units) were added to the reaction. Following an hour's incubation at 42°C, the reaction was terminated by a 5-minute incubation at 70°C. Resultant cDNA was used directly in qPCR or stored at -70°C.

2.7.3 Quantitative PCR

Quantitative PCR is a highly sensitive technique that allows accurate determination of transcript levels within a given sample. In this study, qPCR was used to compare the levels of IFNβ mRNA in samples taken from cells treated with hit compounds and subsequently infected with SeV to activate the IFNβ induction pathway. MxA mRNA levels in samples from cells that had been treated with hit compound and subsequently incubated with IFNα to activate the IFN signalling pathway were also assessed. In this instance, absolute quantitation was used, as opposed to relative quantitation. To potentiate absolute quantitation, a DNA standard, of known concentration, matching the sequence to be amplified in the qPCR reaction is required. A 10-fold serial dilution of the standard allows the cycle threshold (C_t) values to be used to construct a standard curve, from which the quantity of DNA in the test samples can be calculated. The details of this process and the qPCR are given below.

2.7.3.1 Standard curve generation

Plasmids containing gene fragments of IFNβ, MxA and β-Actin to be amplified in the qPCR reactions were used to create a standard curve of known concentration against C_t value using a 6-point 10-fold serial dilution of DNA from 1 ng to 0.01 pg. These reactions are carried out in the same 96-well plate as the corresponding test sample reactions, detailed below. The qPCR results for the IFNβ standard are shown in figure 2.1. In addition to the internal controls in the qPCR reaction detailed below, the standard curve also potentiates assessment of the efficiency of the reaction through the R^2 value generated (Figure 2.1A). An example of the amplification plots generated for the DNA

standards is also shown (Figure 2.1B). The dissociation curve created during each reaction displays one clear peak (Figure 2.1C), suggesting high specificity of the primers and an absence of primer dimer formation. Standard and dissociation curves for the MxA and β-Actin primer sets are shown in Appendix 1.

2.7.3.2 qPCR of test samples

Primers specific to IFNβ (nt 40-155), MxA (nt 570-931) and Actin (nt 257-640) (Table 2.6) were used at 100 nM to assay cDNAs generated by reverse transcription (2.7.2) in qPCR reactions. In this study MESA Blue qPCR mastermIx (Eurogentec) containing SYBR Green I, an intercalating dye that fluoresces upon binding to DNA, and Rox, a reference dye that acts as an internal control to normalise any variations in mastermix concentration or reaction volume, were used. PCR reactions were set (Table 2.9) and were carried out in a Stratagene Mx3005P real-time PCR thermocycler using the specified cycling conditions (Table 2.10). Conversion of C_t value to DNA quantity (ng) was carried out by MxPro software (Stratagene). Further data analysis was carried out on Excel (Microsoft) and Prism6 (Graphpad).

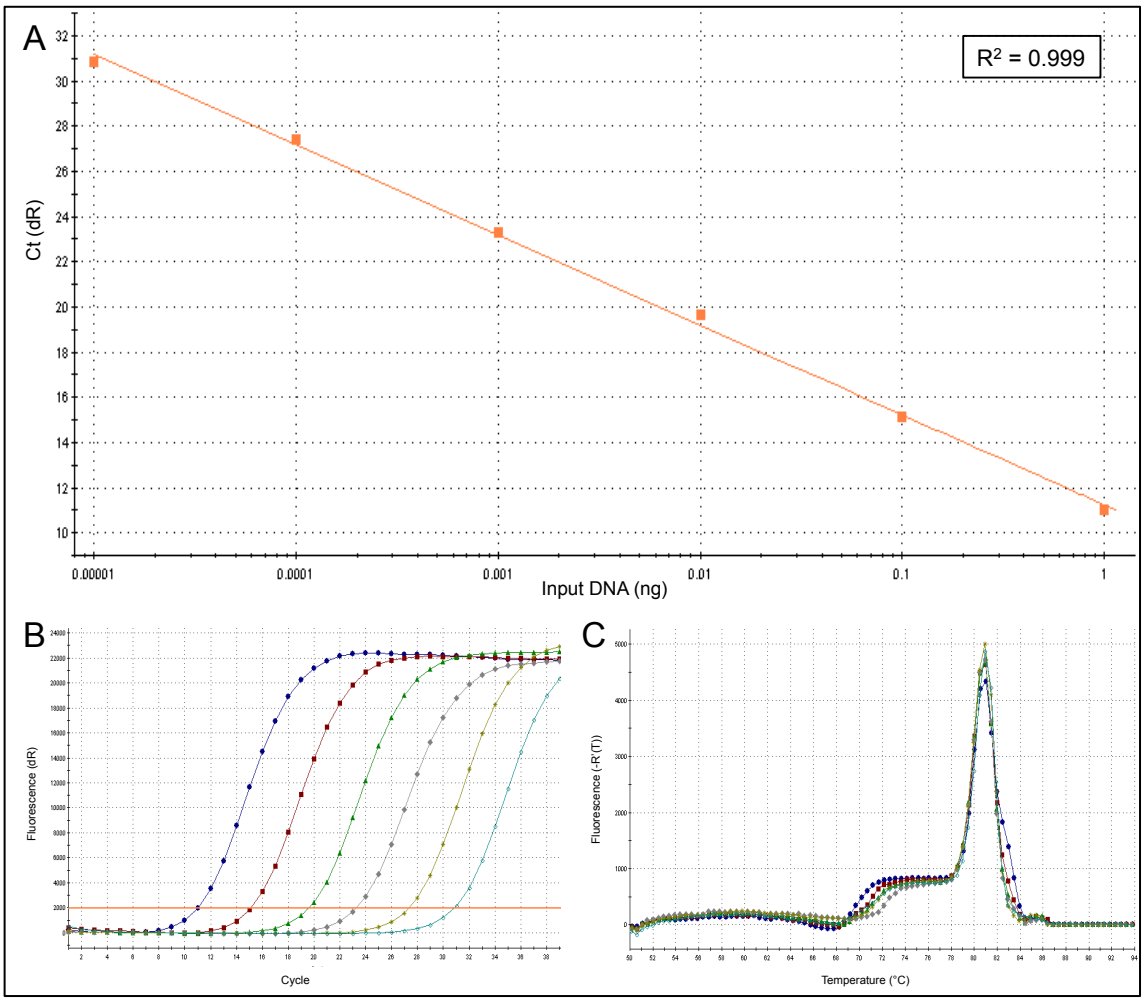

Figure 2.1: Data output of qPCR reactions using IFNβ standard template DNA.
pJet1.2 IFNβ nt 40-155 was used to create a 6-point standard curve using a 10-fold serial dilution from 1 ng to 0.01 pg, giving an R^2 value of 0.999 (**A**). The amplification plots for each of the 6 DNA concentrations show even spacing, with the highest DNA concentration corresponding to the lowest C_t value (**B**). The corresponding dissociation curve display a single clean peak with no indication of primer dimer formation (**C**).

Table 2.9: Components of a typical qPCR reaction

Component	Stock Concentration	Final Concentration
MESA Blue Mastermix	2×	1×
Forward primer	100 µM	100 nM
Reverse primer	100 µM	100 nM
cDNA	-	1 µl
Nuclease-free Water		

Table 2.10: Cycling conditions of a typical qPCR reaction

Step	Temperature (°C)	Time (Seconds)	Function
1 – Activation	60	120	Activates Mastermix
	95	600	Activates polymerase
2 – qPCR[1]	95	15	Denatures
	50	60	Anneals
	72	60	Extends[2]
3 – Dissociation curve	95	60	Denatures
	50	30	Anneals
	95	30	Denatures[3]
[1] Step 2 repeated through 40 cycles			
[2] Fluorescence read at the end of each extension step			
[3] Fluorescence read at each degree between 50 and 95°C during ramp			

2.8 Immunofluorescent microscopy

Immunofluorescent microscopy was used to analyse the nuclear localisation of IRF3 during SeV infection, in the presence or absence of hit compounds. It was also used to assess the impact of hit compounds on SeV infection itself. A549 cells were grown on 10 mm coverslips (Scientific Laboratory Supplies) and treated with inhibitors for 2 hours at 37°C. Cells were

then infected with SeV and processed as detailed below for the two different experiments. Details of the antibodies used can be found in table 2.1. Images were collected on a Nikon Microphot-FXA microscope at ×40 magnification with Imsol imaging software and processed using ImageJ64 software.

2.8.1 IRF-3 localisation analysis

At 4 hours post infection, cells were fixed (5% (v/v) formaldehyde in PBS) for 15 minutes, permeabilised (0.5% (v/v) NP-40, 10% (w/v) sucrose) for 10 minutes and washed (1% (v/v) FBS in PBS). Coverslips were incubated for 1 hour with anti-IRF3 antibody, followed by Texas red-conjugated secondary antibody and DAPI (Sigma). For quantification of nuclear translocation, images were anonymized and Dr Andri Vasou counted cells displaying nuclear or diffuse cytoplasmic staining of IRF3. The number of cells showing IRF3 nuclear localisation was converted to a percentage of total cells counted for each image.

2.8.2 Sendai virus infection analysis

Two hours post-compound treatment, cells were infected with SeV for 18 hours followed by fixation (5% (v/v) formaldehyde in PBS) for 15 minutes, permeabilisation (0.5% (v/v) NP-40, 10% (w/v) sucrose) for 10 minutes and washed (1% (v/v) FBS in PBS). Coverslips were incubated for 1 hour with anti-SeV antibody, followed by FITC-conjugated secondary antibody.

2.9 Plaque assays

In order to assess the growth of an IFN sensitive virus in the presence of hit compounds, plaque assays were performed, which allow quantification of viral replication. A549 cells were seeded into 12-well plates at 2.5×10^5 cells/ml. The following day, confluent monolayers were treated with compound for 2 hours where appropriate, and then infected with 100 μl of 10^{-6} BunVΔNSs in PBS supplemented with 2% (v/v) foetal calf serum (FCS). Following a 1 hour incubation at 37°C for adsorption, the inoculum was replaced with Avicel overlay (1× MEM, 1× GlutaMAX, 2% (v/v) newborn calf serum (NCS), 0.4% (v/v) $NaHCO_3$ and 0.6 % (w/v) Avicel), which, where appropriate also contained hit or control compound. Plaque assays were incubated for 3 days at 37°C with 5% CO_2 followed by fixation with 5% (v/v) formaldehyde in PBS for 1 hour at 4°C. Cells monolayers were washed with water and plaques visualised by Coomassie Brilliant Blue stain (0.1% (w/v) Coomassie R250, 10% (v/v) Glacial acetic acid and 40% (v/v) Methanol). To facilitate quantification of plaque size, plates were scanned at 600 d.p.i. and images amplified to 400%. PixelStick (Plum Amazing) was used to measure plaque size. The plaque size in pixels was normalized to the DMSO + SeV control to illustrate fold-increase.

3. Development of a cell-based assay to identify modulators of the type I IFN response

3.1 Introduction

Two GFP reporter cell lines, A549/pr(IFNβ).GFP and A549/pr(ISRE).GFP, previously generated in the lab provide a simple method to detect activation of the IFN response through fluorescence. These cells lines have previously been used to monitor the activity of known inhibitors of the IFN induction and signalling pathways (Stewart et al., 2014). We sought to demonstrate that these cell lines could be utilized in an automated HTS to identify novel compounds that modulate the IFN response. In order to execute a robust screen and have confidence in the results obtained, the assay in question requires optimization to (i) maximize the signal-to-background (S/B) ratio, (ii) minimize variation between replicates and (iii) minimize the timescale of the assay. In collaboration with the Drug Discovery Unit (DDU) at the University of Dundee, we instigated a campaign of assay development in which we sought to optimize every step in both the IFN induction assay, utilizing the A549/pr(IFNβ).GFP reporter cell line and the IFN signalling assay, utilizing the A549/pr(ISRE).GFP cell line. Following this period of optimization, both assays were validated for their ability to identify novel modulators of the IFN response by using compounds known to inhibit various components of the pathways. Following successful assay validation, the assays were miniaturized and automated to a 384-well HTS format to generate final assay parameters, which

illustrated that both GFP reporter assays had been successfully optimized for use in HTS.

3.2 Results

3.2.1 IFN induction assay development

The IFN induction assay utilizes the A549/pr(IFNβ).GFP cell line, which has an eGFP gene under the control of the IFNβ promoter. When A549/pr(IFNβ).GFP cells are infected with a Sendai virus (SeV) stock rich in defective interfering (DI) particles to activate the IFN induction pathway, GFP is expressed (Figure 3.1A). Using a fluorescent plate reader, the signal expressed in raw fluorescent units (RFU), potentiates quantification of GFP fluorescence. By normalizing the RFU of activated cells to that of unactivated cells (background fluorescence), S/B ratio can be established (Figure 3.1B). A compound that enhances or inhibits the IFN induction pathway would result in increased or decreased GFP expression respectively. With the aim of developing a high-throughput automated assay to identify molecules that modulate IFNβ induction, we sought to optimize a cell-based assay using the A549/pr(IFNβ).GFP reporter cell line. To achieve this, we assessed the following parameters; (i) SeV inoculum concentration, (ii) SeV infection length, (iii) length of cell seeding prior to infection, (iv) length of formaldehyde fixation of cells following infection and (iv) seeding density of cells. As each parameter was optimized, it was taken forward for use in the next step of the optimization campaign.

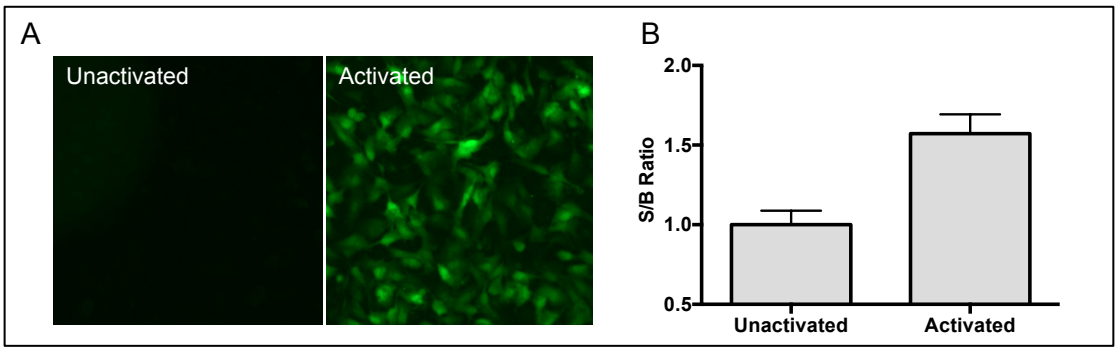

Figure 3.1: A cell-based assay to monitor the IFN induction pathway
The A549/pr(IFNβ).GFP cell line, with a GFP gene under the control of the IFNβ promoter proveds a straightforward method to monitor the IFN induction pathway. Upon infection of the A549/pr(IFNβ).GFP cell line with a DI rich stock of SeV, the IFN induction pathway is activated resulting in expression of GFP (**A**). This fluorescence provides a parameter by which the activation of the IFNβ promoter can be monitored and quantified using a fluorescent plate reader at excitation and emission wavelengths of 484 and 518 nm respectively (**B**). Data represents 3 independent repeats each conducted in quadruplicate (n=4) and error bars display standard deviation (StDeV).

The initial step in the optimization process was to determine the optimal concentration of SeV for maximal activation of the IFNβ promoter and thus GFP expression, whilst minimizing reagent usage. To achieve this, A549/pr(IFNβ).GFP cells were infected with a 2-fold dilution series of virus for 20 hours. Fluorescence was measured following formaldehyde fixation on a Tecan Infinate Pro plate reader at excitation/emission of 484/518nm. Maximal GFP expression was observed between 200 and 12.5 HA units/ml, after which S/B ratio begins to reduce in a dose-dependent manner (Figure 3.2A). As maximal GFP expression is required without wasting reagents, an SeV inoculum concentration of 40 HA units/ml was deemed to be the most appropriate for this assay; it is a convenient dilution to perform (1:100) and does not approach the stage at which S/B ratio begins to reduce.

SeV is cytopathic in cell culture as it induces programmed cell death (PCD) (Garcin et al., 1998), resulting in high levels of apoptosis and monolayer

disruption during infection (Iseni et al., 2002). We therefore sought to ascertain the point at which GFP expression was optimal during infection. We assume that when S/B ratio is at its highest, the cell monolayer has undergone minimal disruption from the SeV infection and as such the maximum number of cells expressing GFP are present. A549/pr(IFNβ).GFP cells were infected with SeV, and following 8, 12, 16 and 19 hours of infection, cells were fixed and GFP expression measured. S/B ratio is significantly increased at 16 and 19 hours post-infection ($p<0.0001$) (Figure 3.2B). As an aim of this optimization was to minimize the timescale of the assay where possible, a 16-hour infection was deemed most appropriate as incubation with SeV for 3 hours longer did not significantly impact GFP expression.

The length of time that cells are given to recover following trypsinisation prior to infection may also be a factor that impacts the level of SeV induced cell death. To investigate this, A549/pr(IFNβ).GFP cells were seeded and incubated for 18 and 24 hours. Cells were then infected with SeV for 16 hours, fixed and GFP fluorescence measured. From the levels of GFP expression observed, a 24-hour incubation following cell seeding prior to infection was optimal (Figure 3.2C). Although slight, a significant increase in S/B ratio is observed when compared with cells that were incubated for 16 hours before SeV addition ($p<0.0002$). By assessing the impact of SeV inoculum concentration, cell seeding length prior to infection and infection length itself, variability observed within the assay resulting from SeV induced cell death was reduced, whilst also optimizing S/B ratio.

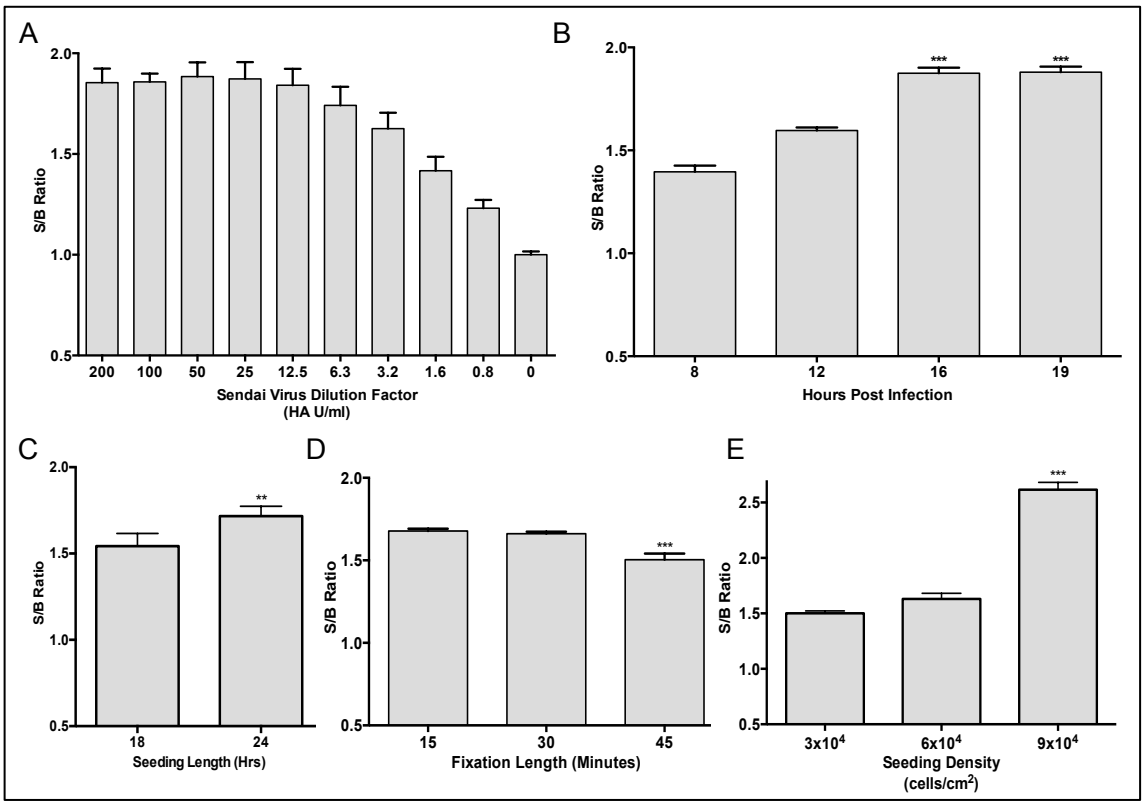

Figure 3.2: Optimization of the IFN induction reporter assay.
A549 reporter cells with a GFP gene under the control of the IFNβ promoter were used to optimize an assay for HTS. The level of eGFP reporter gene expression is presented as signal-to-background ratio (S/B ratio). Optimization steps aimed to maximize S/B ratio and minimize the time-scale of the assay. SeV input was assessed in A549/pr(IFNβ).GFP reporter cells using a 2-fold dilution series of SeV and fluorescence was monitored (**A**). Length of SeV infection was assessed (**B**), as was the incubation period between cell seeding and infection (**C**). By fixing cells for various lengths of time 16 hours post-infection, the effect of formaldehyde fixation on GFP signal was assessed (**D**). Reporter cells were seeded at various cell densities and infected with SeV. Fluorescence was measured 18 hours post-infection (**E**). Data is representative of three independent experiments that were each conducted in quadruplicate (n=4) and error bars indicate StDev. Statistical significance was assessed using one-way ANOVA to compare the S/B ratios achieved under differing assay conditions (*** $p<0.0001$, ** $p<0.0002$).

Additional factors unrelated to SeV infection may also impact the variability and S/B ratio observed in the IFN induction assay. Owing to the scale of HTS, batches of multiple 384-well plates will be processed at the same time. To ensure that the cells and virus infection are consistent, and that GFP expression is comparable between plates, fixation is necessary. Therefore, we aimed to assess the impact of formaldehyde fixation on GFP fluorescence. To

study this, A549/pr(IFNβ).GFP cells were seeded and infected with SeV. Cells were then fixed with a final concentration of 5% formaldehyde in PBS for 15, 30 and 45 minutes. We observed that S/B ratio was significantly reduced following 45 minutes of formaldehyde fixation ($p<0.0001$) (Figure 3.2D). Furthermore, an increase in variability was observed when cells were fixed for longer than 30 minutes. As the assay development process aims to minimize the timescale and variability of the assay where possible, and no significant difference in S/B ratio is observed between formaldehyde incubations of 15 and 30 minutes, a fixation length of 15 minutes was considered optimal.

In order for cells to respond to treatment with a physiologically representative response, they must be at a density at which they are functioning as normal. Furthermore, in a cell-based assay S/B ratio is inherently linked to the cell-number in each well. To assess how cell density may impact GFP expression in our assay, A549/pr(IFNβ).GFP cells were seeded at 3, 6 and 9×10^4 cells/cm^2 of cell growth area for 24 hours. Following SeV infection and formaldehyde fixation, GFP was measured to assess S/B ratio and associated variability between replicates. S/B ratio is not significantly increased when cell density doubles from 3×10^4 to 6×10^4 cells/cm^2 (Figure 3.2E). However, when cells are seeded at a density of 9×10^4 cells/cm^2 of growth area, a statistically significant increase in S/B ratio is observed ($p<0.0001$). Interestingly, variability also appears to increase slightly with each increase in cell density, although the increase in S/B ratio more than compensated for this.

Owing to this campaign of assay development, the optimized assay resulted in a S/B ratio of 2.6±0.06 from cell seeding at 9×10^4 cells/cm^2 of growth

area, 24 hours prior to infection with 40 HA units/ml of SeV for 16 hours followed by 15 minutes of formaldehyde fixation. As such, S/B ratio was successfully optimized whilst minimizing assay variability and timescale.

In order to validate the IFN induction assay for use in HTS, we needed to verify its ability to identify novel inhibitors of the IFNβ induction pathway. To achieve this, chemical compounds reported to inhibit components of the IFN induction pathway were used in the IFN induction reporter assay. BX795, which inhibits TBK1 in the course of IRF3 activation (Clark et al., 2009), and TPCA-1, an IKKβ inhibitor acting during NF-κB activation (Podolin et al., 2005) were used. A549/pr(IFNβ).GFP cells were seeded into 96-well plates. Twenty-four hours post-seeding, cells were treated with a 2-fold serial dilution of either BX795, TPCA-1, or the equivalent volumes of DMSO for 2 hours followed by a SeV infection. Cells were fixed and GFP expression measured. Percentage inhibition in GFP expression was calculated by converting the RFU signal of DMSO treated cells that were unactivated (uninfected), with that of DMSO treated, activated (infected) cells to normalize to 100% and 0% inhibition respectively. The equation used to calculate percentage inhibition in GFP expression can be found in chapter 2 (2.4.1). A clear dose-dependent inhibition of GFP expression was observed in the presence of both inhibitors (Figure 3.3). BX-795 completely inhibited GFP expression at 25 μM with an IC_{50} of 5.2 μM, displaying a classic sigmoidal dose-response curve. TPCA-1 on the other hand achieved a lower maximum GFP inhibition of 72% at 25 μM, however it also has a lower IC_{50} of 3.1 μM.

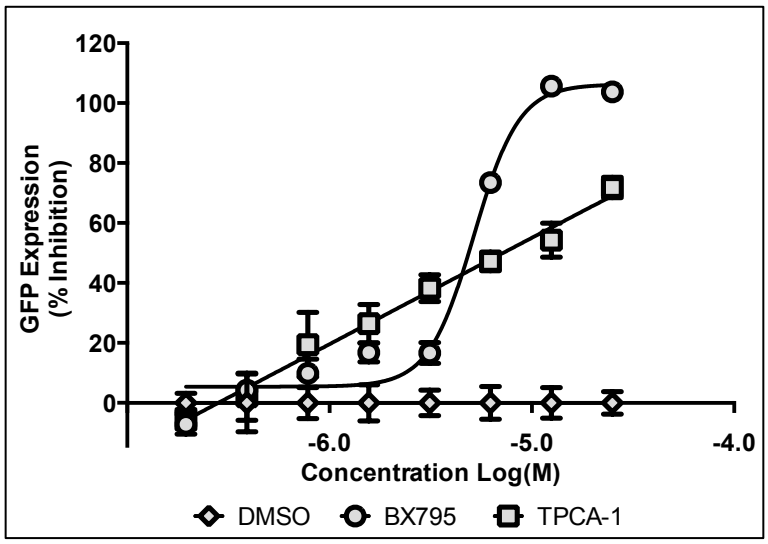

Figure 3.3: Inhibition of IFNβ promoter driven GFP expression by chemical antagonists. Small molecules BX795 and TPCA-1, reported to inhibit the TBK1 and IKKβ in the course of IFN induction were used to verify the A549/pr(IFNβ).GFP reporter assay**.** The IFN-induction pathway and hence GFP expression was activated by SeV infection. GFP expression in the presence of a 2-fold serial dilution of BX795 and TPCA-1 was measured 16 hours post-infection. Data represents 3 independent repeats each conducted in quadruplicate (n=4); error bars display StDev.

The inhibition of GFP expression observed in activated A549/pr(IFNβ).GFP cells treated with BX795 and TPCA-1 validates this assay and provides proof-of-principle that it can used in HTS. Due to proof-of-principle confirmation and the encouraging results obtained through the assay development campaign, it was believed that an HTS to identify novel modulators of IFN induction would be successful.

3.2.2 IFN signalling assay development

The IFN signalling assay utilizes the A549/pr(ISRE).GFP cell line, which has an eGFP gene under the control of an MxA promoter, which contains ISREs. When A549/pr(ISRE).GFP cells are treated with purified IFNα, the IFN signalling pathway is activated, and results in GFP expression (Figure 3.4). However, the levels of GFP expressed in activated A549/pr(ISRE).GFP cells

appears more heterogeneous (Figure 3.4A) with a lower S/B ratio (Figure 3.4B) than that observed in the A549/pr(IFNβ).GFP cell line (Figure 3.1). To facilitate successful assay development and subsequent HTS of a cell-based assay, we required a S/B ratio of at least 2. Therefore, maximizing the S/B ratio in the A549/pr(ISRE).GFP cell line was necessary to render it more amenable to assay development and potentiate the use of the IFN signalling assay in HTS.

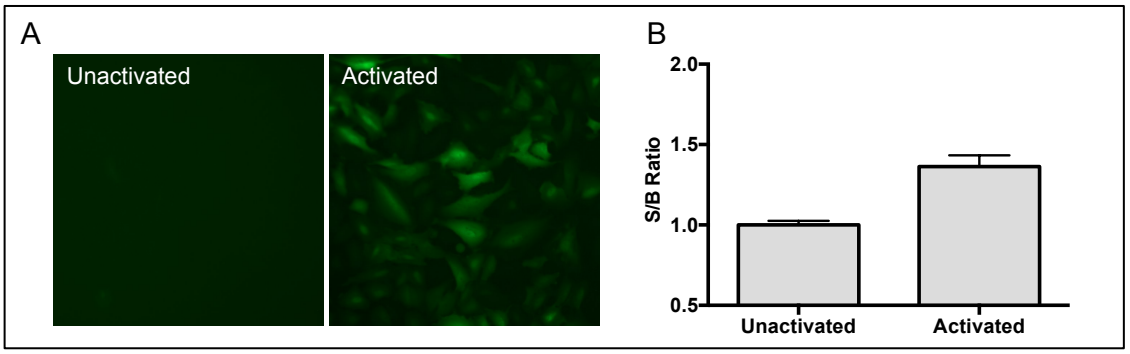

Figure 3.4: A cell-based assay to monitor the IFN signaling pathway
To monitor activation of IFN signalling, an A549 reporter cell line with an eGFP gene under the control of the ISRE containing MxA promoter had been previously generated. Upon treatment of the A549/pr(ISRE).GFP cell line with purified IFNα, the IFN signaling pathway is activated resulting in expression of GFP (**A**). This fluorescence provides a parameter by which the activation of the MxA promoter and thus ISG expression through IFN signaling can be monitored, and quantified using a fluorescent plate reader at excitation and emission wavelengths of 484 and 518 nm respectively (**B**). Data represents 3 independent repeats each conducted in quadruplicate (n=4) and error bars display StDeV.

We sought to optimize GFP expression in the A549/pr(ISRE).GFP reporter cell line through multiple rounds of transduction with lentivirus containing the pr(ISRE).GFP integration cassette. Parental A549/pr(ISRE).GFP cells, generated previously to this study, had undergone a single round of lentivirus transduction followed by fluorescent activated cell sorting (FACS) to isolate cells expressing the highest levels of GFP following IFNα treatment. We theorized that multiple lentiviral transductions, increasing the number of

integration events with the pr(ISRE).GFP expression cassette would significantly increase GFP expression in A549/pr(ISRE).GFP cells without having a detrimental affect on the cells. This was achieved by transducing the parental A549/pr(ISRE).GFP cell line 3 times with lentivirus, followed by incubation for 72 hours to allow the cells to recover. The cells were then transduced a further 4 times to produce the A549/pr(ISRE).GFP.L8 cell line. GFP expression and intensity of fluorescence was increased dramatically between cells that have a single integration compared to those that have 8 (Figure 3.5A). In an effort to produce a cell line that exhibits more homogenous expression of GFP with more consistent levels of fluorescence throughout the population, these cells were analysed by FACS. Fiona Rossi at The Queen's Medical Research Institute, Edinburgh, carried out this work. The A549/pr(ISRE).GFP cells that had undergone a total of 8 lentiviral transductions were left untreated (unactivated) or treated with IFNα for 20 hours to activate the IFN signalling pathway (activated). From the population of cells activated with IFNα, those expressing the highest levels of GFP were isolated. The flow cytometry profiles of untreated and IFN-treated A549/pr(ISRE).GFP.L8 cells and the sorted cell population (A549/pr(ISRE).GFP.L8F) are shown (Figure 3.5B).

To assess the impact that repeated rounds of lentivirus transduction with the pr(ISRE).GFP integration cassette and FACS had in the context of the IFN signalling assay, A549/pr(ISRE).GFP, A549/pr(ISRE).GFP.L8 and A549/pr(ISRE).GFP.L8F cells were seeded into 96-well plates and left untreated or treated with IFNα. Following IFNα treatment to activate the IFN

signalling pathway, cells were fixed with 5% formaldehyde and GFP expression measured. Surprisingly, the level of GFP expression observed in A549/pr(ISRE).GFP.L8 cells was only slightly higher than that of the parental A549/pr(ISRE).GFP cell line. Following FACS however, a dramatic increase in S/B ratio was seen (Figure 3.5C). From the data presented here, we successfully increased GFP expression in the IFN signalling assay by repeated rounds of lentivirus transduction in the A549/pr(ISRE).GFP cell line. The S/B ratio was dramatically improved upon FACS to select against cells that, in the presence of IFNα, had low levels of GFP expression. Overall, this optimization process increased the S/B ratio from 1.5 to 2.3. For the remainder of this chapter, and all other chapters, the A549/pr(ISRE).GFP.L8F cell line was used. For simplicity, it will be referred to as A549/pr(ISRE).GFP.

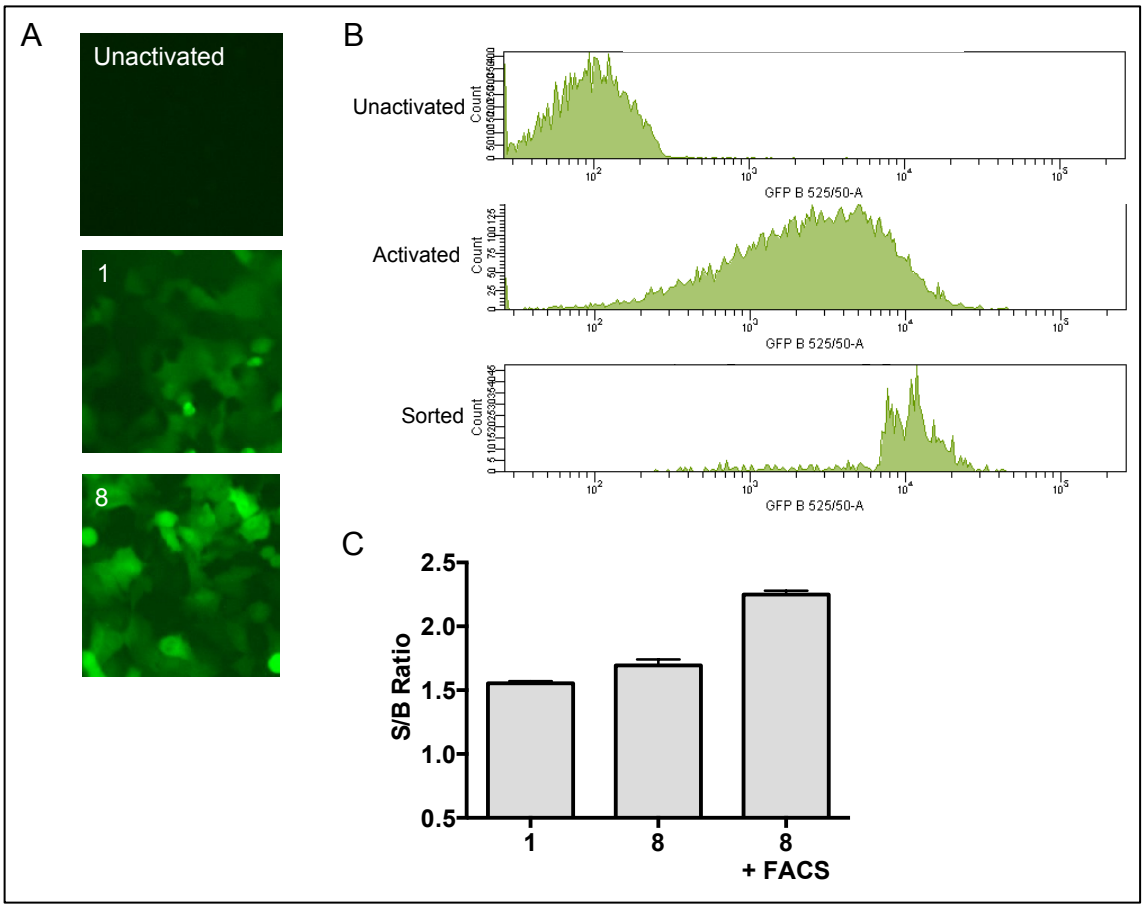

Figure 3.5: Optimization of the A549/pr(ISRE).GFP reporter cell line through multiple lentivirus transductions and FACS

To maximize the S/B ratio of GFP expression in A549/pr(ISRE).GFP reporter cells, repeated lentivirus transductions were performed, followed by cell sorting on the basis of GFP fluorescence. A549/pr(ISRE).GFP cells were transduced a further 7 times with lentivirus with an integration cassette containing the MxA promoter and GFP gene. (**A**) Parental A549/pr(ISRE).GFP (**1**) and multiply transduced (**8**) cells were treated with IFNα to activate the IFN signaling pathway, and visualized to assess GFP expression compared to untreated A549/pr(ISRE).GFP cells. (**B**) To establish the signal window of the IFN signaling assay when cells are activated and unactivated, A549/pr(ISRE).GFP cells that had undergone multiple transductions were analyzed for GFP expression following incubation with and without IFNα by flow cytometry. Cells were then subjected to FACS on the basis of GFP fluorescence. Activated cells expressing the highest levels of GFP were sorted and isolated (A549/pr(ISRE).GFP.L8F). (**C**) The GFP expression levels of sorted cells (A549/pr(ISRE).GFP.L8F) was compared to unsorted cells that had also undergone multiple lentivirus transductions (A549/pr(ISRE).GFP.L8) and the parental A549/pr(ISRE).GFP cell line following IFNα treatment was assessed. Data represents 3 independent repeats, each conducted in quadruplicate (n=4). Error bars display StDev.

To identify molecules that modulate IFN signalling, we sought to optimize a cell-based assay using the A549/pr(ISRE).GFP reporter cell line. To achieve this, we aimed to investigate the impact the following parameters; (i) concentration of IFNα treatment, (ii) use of dissociation reagent, and (iii) length of IFNα treatment. As each parameter was optimized, it was taken forward for use in the next step of the optimization process. The previously optimized parameters for cell density, seeding length and formaldehyde fixation gained from development of the IFN induction assay were also used here.

The initial step in the optimization process was to determine the concentration of IFNα required for optimal activation of the IFN signalling pathway and thus GFP expression, whilst minimizing reagent usage. To achieve this, A549/pr(ISRE).GFP cells were treated with a 2-fold dilution series of IFNα. Fluorescence was measured following formaldehyde fixation on a Tecan Infinite Pro plate reader at excitation/emission of 484/518nm. Maximal GFP expression was observed between 40,000 and 20,000 units/ml, after which S/B ratio begins to decline in a dose-dependent manner (Figure 3.6A). As maximal GFP expression is required without wasting reagents, an IFNα concentration of 10,000 units/ml was deemed to be the most appropriate for the assay. Although maximal S/B ratio is no achieved at this concentration, variability is lower; it is a convenient dilution to perform (1:100) and does not approach the point at which S/B ratio dramatically decreases.

To activate the IFN signalling pathway, IFNα binds to the IFNα/β receptor found on the surface of cells. Trypsin is routinely used in cell culture for passage and seeding of cells into multi-well plates. If trypsin cleaves the IFNα/β

receptor, the potential exists for a reduction in receptor numbers, which would have a negative impact on IFNα binding and thus activation of the IFN signalling pathway. The ExPASy website PeptideCutter (http://web.expasy.org/peptide_cutter/) predicts 54 trypsin cleavage sites in the IFNα/β receptor protein sequence (Accession: CAA42992.1). As such, this could impact the S/B ratio of the IFN signalling assay. To investigate this further, we made single cell suspensions of A549/pr(ISRE).GFP cells by treating cell monolayers with either trypsin-EDTA or EDTA alone and then compared their ability to respond to IFNα. Cells were left untreated or treated with IFNα for 24 hours. GFP expression was measured following formaldehyde fixation. The use of trypsin did not impact the background signal or variability of unactivated A549/pr(ISRE).GFP cells (Figure 3.6B). However, following treatment with IFNα, there was a significant increase in GFP expression in cells that had been seeded following EDTA treatment alone, compared to cells treated with trypsin-EDTA ($p<0.0001$). This suggests that trypsin does cleave the IFNα/β receptor, leading to a lower level of IFN signalling pathway activation in the presence of IFNα.

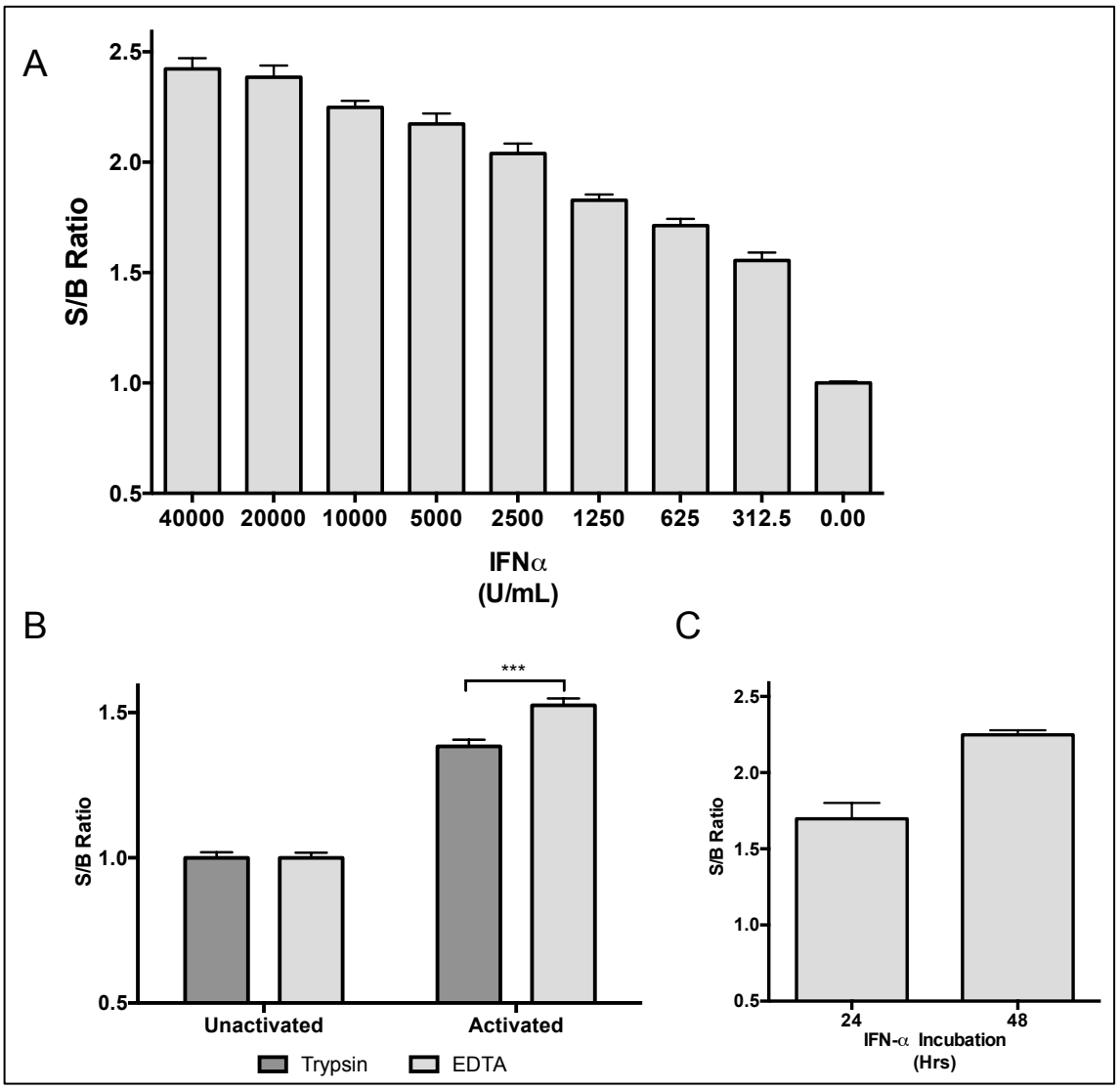

Figure 3.6: Optimization of the IFN signaling assay.
A549 reporter cells with a GFP gene under the control of the ISG containing MxA promoter were used to optimize an assay for HTS in successive steps. The level of GFP reporter gene expression is presented as signal-to-background ratio (S/B ratio). Optimization steps aimed to maximize S/B ratio and minimize the time-scale of the assay. IFNα input was assessed in A549/pr(ISRE).GFP reporter cells using a 2-fold serial dilution of IFNα and fluorescence was monitored (**A**). The method of monolayer dissociation prior to cell seeding was assessed for its impact on GFP expression. A549/pr(ISRE).GFP reporter cells were dissociated with either trypsin or EDTA (0.48 mM) before seeding and IFNα treatment (**B**). The length of IFNα incubation was assessed (**C**). Data represents three independent experiments that were each conducted in triplicate (n=3) and error bars indicate StDev. Statistical significance was assessed using one-way ANOVA to compare the S/B ratios achieved under differing assay conditions (*** $p<0.0001$).

Following the discovery that trypsin treatment prior to cell seeding negatively impacts S/B ratio, we next assessed the length of IFNα treatment

that results in optimal GFP expression. To achieve this, A549/pr(ISRE).GFP cells were treated with IFNα, and 24 and 48 hours post-IFNα treatment, GFP expression was measured. There was a dramatic increase in S/B ratio at 48 hours post-treatment (Figure 3.6C). As the aim of this assay development was to maximize S/B ratio, a 48-hour IFNα incubation was deemed most appropriate as it increased GFP expression by 0.5-fold above that of a 24-hour treatment length. Owing to this process of development, the optimized assay included cell seeding at a density of 9×10^4 cells/cm^2 following treatment with EDTA only, and treating cells with 10,000 units/ml of IFNα for 48 hours, and achieved a S/B ratio of 2.2.

In order to validate the IFN signalling assay for use in HTS, we needed to verify that it could be used to identify novel inhibitors of the IFN signalling pathway. To achieve this, Ruxolitinib (Rux), and CYT387, which both inhibit JAK1/2 in the course of STAT activation (Quintas-Cardama et al., 2010, Pardanani et al., 2009) were tested in the IFN signalling assay. Twenty-four hours post-seeding, A549/pr(ISRE).GFP cells were treated with a 2-fold serial dilution of either Rux, CYT387, or the equivalent volumes of DMSO for 2 hours followed by IFNα treatment. The percentage inhibition in GFP expression was calculated as before (3.2.1). A clear dose-dependent inhibition of GFP expression was observed in the presence of both inhibitors (Figure 3.7). Both compounds completely inhibited GFP expression at 25 μM. Rux had an IC_{50} of 0.53 μM and CYT387 had an IC_{50} of 2.03 μM.

The inhibition in GFP expression seen in activated A549/pr(ISRE).GFP cells treated with Rux or CYT387 validated this assay and provides proof-of-

principle that it can be used successfully in HTS to identify novel modulators of IFN signalling would be successful.

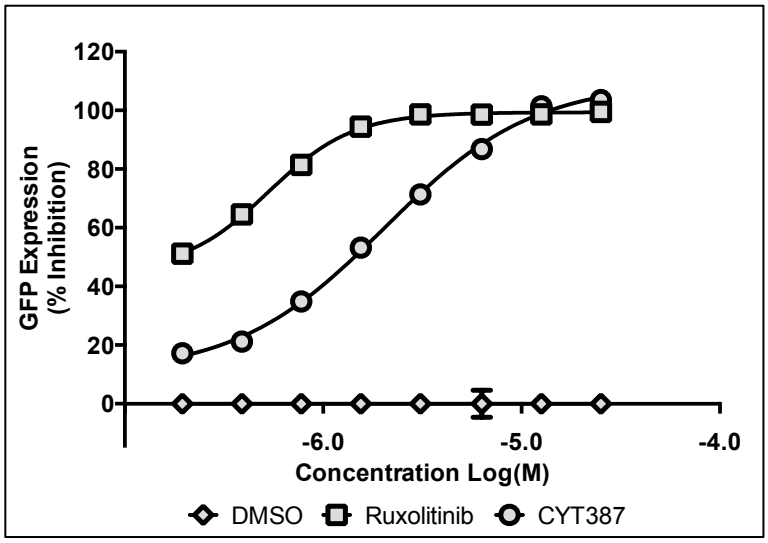

Figure 3.7: Inhibition of ISRE driven GFP expression by chemical antagonists.
Small molecules Ruxolitinib and CYT387 have been reported to inhibit the Jak1 component of the IFN-signaling pathway. The compounds were used to verify the A549/pr(ISRE).GFP reporter assay**.** The IFN-signaling pathway and hence eGFP expression was activated by IFNα treatment. GFP expression in the presence of Ruxolitinib and CYT387 at various concentrations was measured post-IFNα treatment. Data represents 3 independent repeats each conducted in quadruplicate (n=4); error bars display StDev.

3.2.3 Final assay parameters

The assay development campaigns detailed above for both the IFN induction and the IFN signalling assays were carried out in St Andrews with the aim of subsequently using automated liquid handling at the DDU at the University of Dundee. For this, we needed to miniaturize the assays from a 96- to a 384-well plate format, which is more amenable to HTS as it reduces the necessary plate number by 75%. It also facilitates reduction of the assay volume from 120 μl to 60 μl, allowing for conservation of valuable reagents. To achieve this, both assays were assessed at the DDU after automating as much of the assay as possible. This included the use of an Echo 555 liquid handler,

which can accurately transfer as little as 2.5 nl of test compound. Cell seeding, addition of SeV and IFNα were carried out with a Matrix WellMate microplate dispenser. Initially, washing of fixed plates wasto be carried out using a BioTek ELx405 Select CW microplate washer. However, troubleshooting of inconsistent washing, revealed high levels of variability. Therefore, the wash step was the only high throughput aspect of the assays that was done manually. Following miniaturization and automation of the IFNβ induction and IFN signalling reporter assays at the DDU, their performance was compared to pre-set QC parameters set by the DDU (Table 3.1). Both assays performed well, with each assay parameter well within its associated QC limits. This provided confidence that we had successfully developed robust and reproducible assays as the S/B ratio was above 2.8 in both cases. A powerful statistic used to assess the overall performance of an assay, which gives an indication of its suitability to HTS is the Z' factor (Zhang, 1999). This statistic takes into consideration both the signal window (S/B ratio) and the variability of the assay. As such, it provides a convenient statistic that describes the critical aspects of an assay's behaviour. The closer the Z' factor is to 1 (and above 0.5), the more robust and reliable an assay. In this case, a Z' factor above 0.6 was achieved, indicating a high level of reproducibility and that both assays were robust.

Table 3.1: Performance of the IFN induction and signaling assays compared to pre-set QC standards. Following assay development, the reporter cell lines were optimized for HTS. The performance of the A549/pr(IFNβ).GFP IFN induction and A549/pr(ISRE).GFP IFN signalling assays following optimization to an automated 384-well format were compared to pre-set quality control standards.

	QC Approval	IFNβ Induction Assay	IFN Signalling Assay
Z' Factor	> 0.5	0.67 ± 0.03	0.7 ± 0.05
S/B ratio	> 2	3.1 ± 0.53	2.8 ± 0.06
Activated CV (%)	< 8	6.7 ± 0.59	4.9 ± 0.93
Unactivated CV (%)	< 8	3.1 ± 0.53	2.5 ± 0.66

3.3 Summary

Through extensive assay development, we successfully optimized two fluorescent cell-based assays for use in HTS. Furthermore, through the use of known chemical antagonists of IFN induction and signalling, these assays were validated for their suitability to identify novel modulators of the two pathways. Activation of the IFN induction pathway in the A549/pr(IFNβ).GFP assay is dependent upon SeV infection. Although the DI rich Cantell strain of SeV used in this study is a very potent inducer of IFN, its inherent properties such as PCD induction meant that close optimization was necessary. This was achieved through assessing general assay conditions such as seeding density, and closely monitoring the impact of SeV induced cell death by studying the effect of infection length and inoculum concentration. The IFN signalling assay, utilizing the A549/pr(ISRE).GFP reporter cell line required additional optimization prior to general assay development, to maximize the GFP signal window. This was

achieved by multiple lentivirus transductions of the parental cell line followed by FACS selection of the most responsive cells. This signal optimization, followed by subsequent assay development successfully maximized S/B ratio while minimizing variation. As a result of the optimization campaigns on both the IFN induction and IFN signalling assay, their behaviour was highly reproducible. Furthermore, the assays were validated for their ability to identify chemical modulators of the pathways, and successfully miniaturized to an automated 384-well plate format amenable to HTS.

4. High-throughput screening to identify novel modulators of the IFN response

4.1 Introduction

As a result of the successful assay development and validation carried out in St Andrews, and the subsequent miniaturization of the IFN induction and IFN signalling assays at the DDU, an HTS campaign was pursued. At this point either assay could be taken forward for HTS, and the IFN induction pathway was chosen. There are already many commercially available inhibitors of the IFN signalling pathway, and although commercial inhibitors of the IFN induction pathway are also available, they are mainly focused on inhibition of the kinases involved in IFN activation. Therefore, the potential exists to identify compounds that modulate novel targets. As such, we proposed that there was greater scope for discovery of novel modulators of IFN induction and so pursued a single-point diversity screen utilizing the IFN induction assay and A549/pr(IFNβ).GFP cell line.

The small diversity set of the DDU compound library, consisting of 15,667 small molecules, was used at an initial screening concentration of 30 μM. Following successful primary screening, putative hit compounds were taken forward to dose-response screens. This screening aimed to determine the potency of a given hit compound. Dose-response screening utilized a 10-point 2-fold serial dilution of compound, in this case from 50 μM to 0.1 μM, to construct a 4-parameter logistic fit using % inhibition in GFP expression. This facilitates determination of potency through the construction of a dose-response

curve by using minimum and maximum % inhibition in GFP expression, hill slope and XC_{50}. Where the term XC_{50} is used, 'X' denotes a compound where activity is either antagonistic (inhibition, IC_{50}) or agonistic (enhancement, EC_{50}). During dose-response screening, XC_{50} values are routinely reported as pXC_{50}, where the negative log of the molar concentration is used. As such, the higher pXC_{50} value, the lower the molar XC_{50} concentration. For reference, a conversion table is provided (Table 4.1).

Table 4.1: Conversion table of the μM and corresponding negative log molar concentration

μM	Log(-M)
50.0	4.3
25.0	4.6
12.5	4.9
10.0	5.0
6.3	5.2
5.0	5.3
3.1	5.5
1.6	5.8
0.8	6.1
0.4	6.4
0.2	6.7
0.1	7.0
0.05	7.3

Three dose-response screens were carried out to investigate the activity of hit compounds in (i) inhibition of IFN induction, (ii) enhancement of IFN induction and (iii) assess their specificity. This screening aimed to determine the potency of putative hit compounds in the IFN induction assay, but also eradicate false positives by eliminating hits that fail to produce a curve from the parameters detailed above. This process is beneficial as it allows for timely

reduction in compound numbers, allowing further studies to focus on a smaller number of confirmed hits.

Following dose-response screening, a confirmed hit warranting further investigation was first analysed by liquid chromatography-mass spectrometry (LC-MS) to assess the purity and confirm the identity of the compound used in screening. Confirmed hit compounds that passed LC-MS were repurchased and investigated further through a campaign of hit validation, aiming to re-test the compound from a fresh stock to confirm its direct action on the IFN induction pathway and also eliminate false-positives acting through off-target effects.

4.2 Results

4.2.1 Diversity HTS to identify compounds that modulate the IFN induction pathway

The successful optimization and validation of the IFN induction assay detailed in chapter three provided confidence that a diversity screen to identify novel modulators of the IFN induction pathway could be successfully completed. As such, we embarked on a screening campaign using the Small Diversity Set (15,667 compounds) of the compound library at the DDU. This compound collection is composed of small molecules selected as appropriate starting points for drug discovery that all comply with Lipinski's rule of 5 (Lipinski et al., 2001). For HTS, A549/pr(IFNβ).GFP cells were seeded into clear-bottomed black 384-well plates laid out as shown (Figure 4.1A). Cells in columns 1 to 22 were treated with test compound. SeV infection of columns 1 to 22 and column 24 followed. Column 24 was untreated but infected with SeV

(activated) provide a 0% inhibition control. Column 23 was left untreated and uninfected (unactivated) to provide a 100% inhibition control. GFP expression was measured using an Envision plate reader. Screening was carried out in 4 batches of 12 384-well plates over the course of 2 weeks.

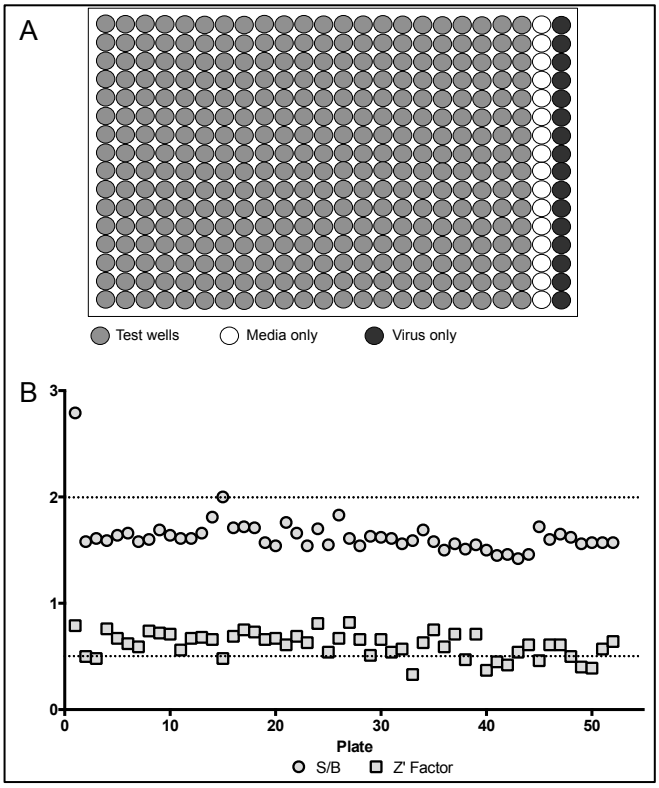

Figure 4.1: Single point diversity HTS to identify compounds that modulate the IFN induction pathway

A single point diversity screen using the A549/pr(IFNβ).GFP reporter assay and the DDU small diversity set (n = 15,667 compounds) was performed at a compound concentration of 30 μM. (**A**) A schematic of 384-well plate layout; wells in columns 1-22 contain a single test compound and SeV infected cells, wells in column 23 contain uninfected cells that represent maximum eGFP inhibition (100%, Unactivated) and wells in column 24 contain untreated SeV infected cells that represent baseline eGFP inhibition (0%, Activated). (**B**) Plot of Z' factor and S/B ratio for each assay plate in the primary screen. Dotted lines indicate QC approval limits for Z' factor (0.5) and S/B ratio (2).

Table 4.2: Screen statistics of the IFN induction assay, measured as Z' factor, S/B ratio, and % co-efficient of variation (CV) and compared to DDU preset QC standards.

	QC Approval	Diversity Screen
Z' Factor	> 0.5	0.6 ± 0.1
S/B	> 2	1.6 ± 0.2
Activated CV (%)	< 8	4.4 ± 1.8
Unactivated CV (%)	< 8	2.4 ± 1.4

The behaviour of the screen in terms of QC statistics was monitored between plates and between batches. The screen performed as expected with the exception of a dramatic drop in S/B ratio (Table 4.2). Assay development saw a consistent S/B ratio of 3.1±0.53, while this fell during primary screening to 1.6±0.2. Although not inconsequential, the Z' factor remained at 0.6 and % CV for both activated and unactivated cells was consistently below 4.5%. Although the unexpected drop in S/B ratio may call into question the validity of the screen, the consistency of the arguably more important Z' factor suggests that the screen remained robust (Figure 4.1B). Percentage effect of GFP inhibition for each compound was calculated using fluorescence, in RFU, of uninfected cells to set the 100% maximum (Unactivated) and untreated, SeV infected cells to set the 0% baseline (Activated). Of the 15,667 compounds tested, percentage effect of inhibition in GFP expression produced a normal distribution of results, centred at 10 to 20% inhibition (Figure 4.2A). A compound resulting in less that -50% inhibition in GFP expression and being 2 standard deviations outside of the test well average for the plate was considered a putative enhancer of IFN induction (Figure 4.2B). Likewise, a compound achieving 50% or more inhibition in GFP expression and being 2 standard deviations away

from the test well average for the plate was considered a putative inhibitor of IFN induction (Figure 4.2C).

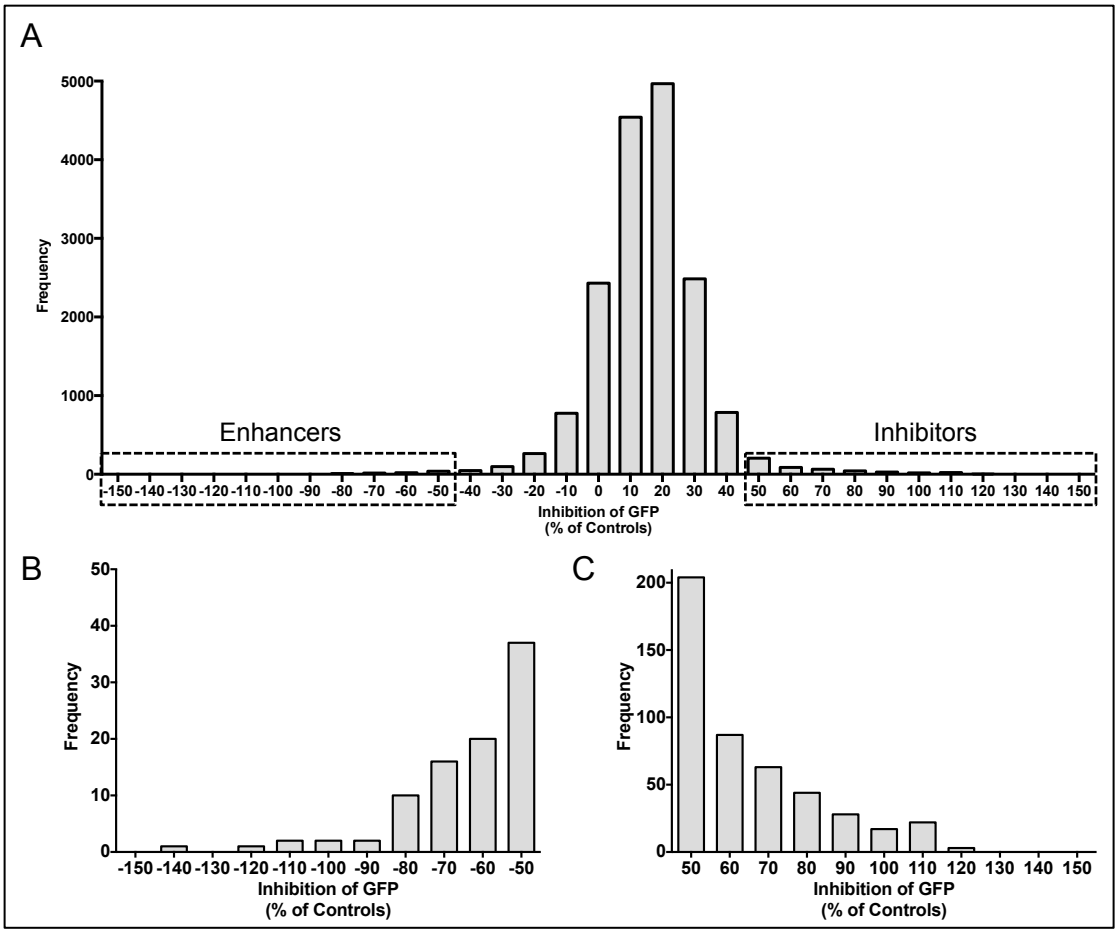

Figure 4.2: Percentage inhibition in GFP expression of compounds tested in a single point diversity HTS to identify modulators the IFN induction pathway
(**A**) Screen output is represented as % inhibition of eGFP expression and plotted as a frequency distribution of all compounds tested. (**B**) Compounds that inhibit GFP expression from -50 to -150% were designated as potential enhancers of IFN induction and plotted as a frequency distribution. (**C**) Compounds that inhibit GFP expression by 50% or more were designated potential inhibitors of IFN induction and plotted as a frequency distribution.

From these initial selection criteria, 264 of the 15,667 compounds screened were considered putative hits. A compound that was duplicated was withdrawn, along with any that had shown possible toxicity in past DDU screens. The information regarding compound toxicity was established by using

legacy data at the DDU. This data is compiled from all screens carried out in the department. One such example of how this data was used can be seen in an historical screen carried out at the DDU investigating compound action on intracellular parasites. In the course of this screen, mammalian host cell number was monitored. As such, information regarding a compounds impact on cell number was available. If a putative hit compound from our screen had caused a reduction in cell number in the previous screen, it was likely to be toxic to the mammalian host cell and as such was eliminated from further analysis. This process of hit triage reduced our putative hit compound number to 245, composed of 200 inhibitors and 45 enhancers of GFP expression. Therefore, the primary screening campaign yielded an initial hit rate of 1.56%.

With the aim of identifying novel compounds that modulate the IFN induction pathway we utilized the A549/pr(IFNβ).GFP reporter cell line and successfully carried out an automated HTS campaign with 15,667 test compounds, which identified 245 putative hits. Although a drop in S/B ratio was observed, the Z' factor remained comparable to that achieved during assay development, reinforcing the integrity of the primary screen, which had a respectable hit rate of 1.56%.

4.2.2 Dose response screening of putative hit compounds that modulate the IFN induction pathway

In order to confirm the activity of putative hit compounds identified during primary diversity screening, we embarked on a campaign of dose-response screening. The purpose of dose-response screening is 2-fold in that it not only allows the establishment of potency of putative hit compounds, but can also

facilitate the identification of false-positive hits. In this case, there were 245 putative hit compounds to test. Primary diversity screening sought to identify compounds that modulate the IFN induction pathway, which could therefore result in either inhibition or enhancement of GFP expression. In order to maximize the information gained from dose-response screening, we carried out 3 separate screens. The classical IFN induction assay with SeV infection facilitated the study of inhibitors of IFN activation (i), while the IFN induction assay without SeV infection allowed for greater scrutiny of putative hits that may enhance pathway activation (ii), and to aid in the elimination of false positives, putative hit compounds were also subjected to a specificity screen (iii) in the IFN signalling assay utilizing the A549/pr(ISRE).GFP cell line. A compound that is active in both the IFN induction and signalling assays is either acting through non-specific, off-target means or could have dual activity. The plate layout used in all 3 of the screens is shown (Figure 4.3A), where columns 1 to 10 and 13 to 22 contain a 10-point 2-fold serial dilution of test compound from 50 μM to 0.1 μM. As with the primary screen, a 100% inhibition control of untreated, unactivated cells (in columns 11 and 23) and a 0% inhibition baseline control of untreated, activated cells (in columns 12 and 24) was included.

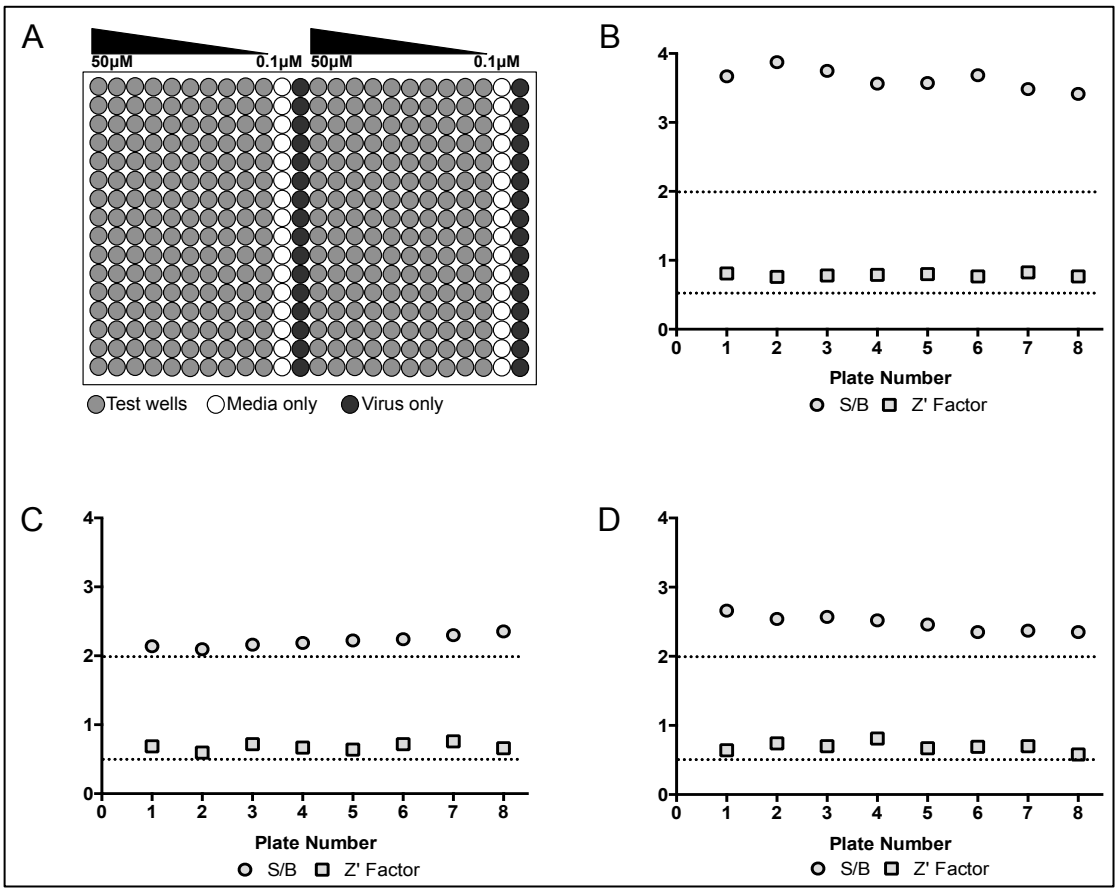

Figure 4.3: Secondary dose-response screening using the IFN induction and signalling reporter assays.
Putative hit compounds were subjected to secondary screening in the A549/pr(IFNβ).GFP and A549/pr(ISRE).GFP reporter assays to generate 10-point dose-response curves for potency determination. (**A**) A schematic of 384-well plate layout; wells in columns 1-10 and 13-22 contain a single test compound in a 2-fold dilution series from 50 to 0.1 μM and SeV infected or IFNα treated cells, wells in column 11 and 23 contain uninfected cells that represent maximum eGFP inhibition (100%, Unactivated) and wells in column 12 and 24 contain untreated SeV infected or IFNα treated cells that represent baseline eGFP inhibition (0%, Activated). (**B-D**) Plots of Z' factor and S/B ratio for each assay plate in the 3 secondary dose-response screens. Dotted lines indicate QC approval limits for Z' factor and S/B. All 245 putative hit compounds were analyzed in the A549/pr(IFNβ).GFP reporter assay with (**B**) and without (**C**) SeV infection to confirm the activity of compounds that inhibited or enhanced GFP expression during primary screening respectively. To eliminate false positive hits, compounds were also tested in the A549/pr(ISRE).GFP reporter assay (**D**) where SeV infection is replaced by IFNα treatment.

The IFN inhibitor dose-response screen followed the IFN induction assay protocol using the A549/pr.(IFNβ).GFP reporter cell line with SeV infection of wells containing test compound. The purpose of this was to further investigate compounds that resulted in a reduction in GFP expression in the primary

screen. The IFN inhibitor screen behaved exceptionally with clear restoration of the S/B ratio to above 3, and each plate passing both the S/B ratio and Z' factor QC approval limits (Figure 4.3B).

The IFN enhancer dose-response screen was used to further investigate putative hits that enhanced GFP expression. This assay utilized the A549/pr.(IFNβ).GFP reporter cell line following the same protocol as the IFN induction assay with one exception; wells containing test compound (columns 1 to 10 and 13 to 22) were not infected with SeV. Here the 0% enhancement baseline control was untreated, uninfected (unactivated) cells in columns 11 and 23 and the 100% enhancement control was untreated, infected (activated) cells in columns 12 and 24. As was observed in the IFN inhibitor dose-response screen, each plate passed both the S/B ratio and Z' factor QC approval limits (Figure 4.3C). Although a slight drop in S/B ratio was seen in comparison, it remained above the QC approval limit of 2.

To aid in the identification of any non-specific hits, a specificity screen utilizing the IFN signalling assay and A549/pr.(ISRE).GFP reporter cell line was carried out. Here, wells containing test compound were treated with IFNα. A putative hit compound that resulted in reduced GFP expression in this assay is likely to be activating through off-target actions. It is possible however that a compound with activity in both the IFN induction and IFN signalling assays is real, and as such, these dual inhibitors should not be disregarded completely. This screen followed the same plate layout as the IFN inhibitor dose-response screen, where SeV infection was substituted with IFNα treatment. The screen behaved as expected, where the S/B ratio averaged 2.2 and Z' factor was 0.68.

Thus, it was a robust screen as each plate passed the S/B ratio and Z' factor QC approval limits (Figure 4.3D). The dose-response screening performed to further investigate the 245 putative hit compounds behaved well, with each QC approval limit, including % CV being cleared (Table 4.3).

Table 4.3: Screen statistics for the 3 dose-response screens performed, measured as robust Z' factor, S/B ratio, and co-efficient of variation (CV) and compared to DDU preset QC limits.

	QC Approval	IFN Inhibitor	IFN Enhancer	Specificity (ISRE)
Z' Factor	> 0.5	0.8 ± 0.02	0.7 ± 0.05	0.7 ± 0.07
S/B	> 2	3.6 ± 0.1	2.2 ± 0.1	2.5 ± 0.1
Activated CV (%)	< 8	5.4 ± 0.9	4.0 ± 0.5	5.2 ± 1.8
Unactivated CV (%)	< 8	3.9 ± 0.8	4.0 ± 1.6	5.1 ± 0.8

At this stage of the screening process, to be considered a confirmed hit, a compound's activity must result in the production of a dose-response curve that allows pXC_{50} determination. As such, it must achieve clear maximum and minimum effects in the assay. The hill slope of a dose-response curve is an important indication of the potency of a molecule. A steeper hill slope (≥1) indicates that a compound has higher potency. Therefore, to designate a hit as confirmed, it must also produce an acceptable hill slope around 1. The determination of a compound's pXC_{50} value potentiates efficient hit characterization, allowing the elimination of compounds that fail to produce a dose-response curve. A compound with a pXC_{50} value of 4.3, equivalent to 50 μM, and the highest concentration tested, was designated as inactive and as

such, a false-positive. Any compound achieving a pXC_{50} of 5 or above (≤10 μM) was categorized as a confirmed hit warranting further study. Although a compound with a pXC_{50} value between 4.4 and 5 is not disregarded as inactive, it is deemed as less potent, and so further investigation may not be worthwhile. This procedure potentiates efficient triage of hit compounds, using rational parameters to reduce the number of compounds warranting further investigation. Analysis of the pIC_{50} values generated for each compound in the IFN inhibitor dose-response screen identified a 109 putative hits that failed to produce a dose-response curve, with a pIC_{50} of 4.3 (Figure 4.4A). From the 200 potential inhibitors of IFN induction, 41 had a pIC_{50} of 5 or more. Therefore, the IFN inhibitor dose-response screen identified 20% as confirmed hits indicating good levels of potency. The IFN enhancer dose-response screen identified all but 3 compounds (242) as inactive, having pEC_{50} values of 4.3 (Figure 4.4B). The 3 compounds that successfully produced dose-response curves had a pEC_{50} value between 4.5 and 4.7, suggesting a lack of potency. The specificity screen, carried out to facilitate elimination of false-positive hits and identify any potential dual inhibitors of both pathways identified 83 putative hits with no activity (pIC_{50} values of 4.3) and 63 compounds with a pIC_{50} of 5 or more (Figure 4.4C).

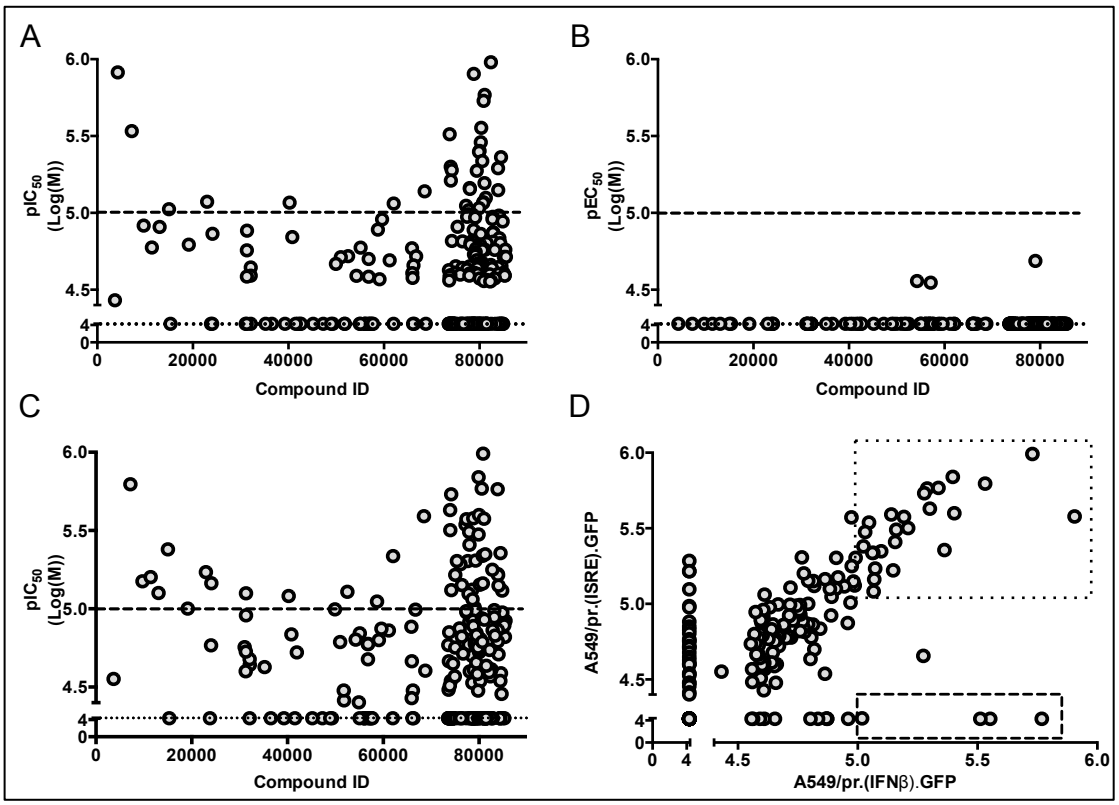

Figure 4.4: pIC50 and pEC50 values generated through secondary dose-response screening using the IFN induction and signalling reporter assays.
Potency determination of putative hit compounds derived from the dose-response curves generated in the A549/pr(IFNβ).GFP reporter assay with (A) and without (B) SeV infection to generate pIC50 and pEC50 values respectively, and the A549/pr(ISRE).GFP reporter assay (C) to give pIC50. Hits with a pXC_{50} of 4.3 (IC_{50} 50 μM) were deemed inactive (dotted line) and hits with a $pXC_{50} \geq 5$ ($IC_{50} \leq 10$ μM) were deemed favorable (dashed line). pIC_{50} values derived from dose-response curves generated for each hit tested in the A549/pr(IFNβ).GFP with Sev infection and A549/pr(ISRE).GFP reporter assays were plotted against one another. Boxed hits represent confirmed hit compounds that specifically inhibit the IFN-induction pathway (dashed line) or those that show comparable activity in both the A549/pr(IFNβ).GFP and A549/pr(ISRE).GFP reporter assays (dotted line) and have a $pIC_{50} \geq 5$ ($IC_{50} \leq 10$ μM). Dose response curves, pIC_{50} values and statistics were generated using ActivityBase XE software.

Taken alone, the information provided by the specificity screen is limited. The aim of this screen was to see whether putative hits inhibiting IFN induction were specific. Therefore, the pIC_{50} value generated for each compound in the IFN inhibitor dose-response screen was plotted against the corresponding value generated in the specificity screen (Figure 4.4D). This provides a straightforward method for identifying hits specific to the IFN induction pathway,

with pIC_{50} values above 5, but showed no activity in the IFN signalling pathway, achieving pIC_{50} values in the specificity screen of 4.3. Hits achieving very similar levels of inhibition in both assays could be false positives, or compounds that have dual activity in the both pathways, and so could warrant further investigation.

As a result of the dose-response screening, 41 compounds were designated as confirmed hits, inhibiting IFN induction with pIC_{50} values of 5 or above. Of these 41 hits, 6 achieved pIC_{50} values in the specificity screen of less than 5. Therefore, dose-response screening focused further investigation of 41 confirmed inhibitors of IFN induction down to 6, which are more likely to be real hits, specific to the pathway we are aiming to target. These confirmed hit compounds were designated StA-IFN-1, -2, -3, -4, -5, and -6, and their associated pIC_{50} values are shown (Table 4.4). In this case, dose-response screening was also an effective tool for eliminating hits that are unlikely to yield results further down the validation pipeline. The IFN enhancer dose-response screen identified 3 compounds with dose-dependent activity, although the levels of potency achieved were not convincing enough to warrant further investigation. Overall, the dose-response screening campaign was effective at focusing further investigative efforts on hit compounds with levels of potency and specificity amenable to future characterization and chemical optimization.

Table 4.4: pIC_{50} values of 6 confirmed hit compounds that specifically inhibit IFNβ promoter driven GFP expression, showing minimal to no activity in the A549/pr(ISRE).GFP reporter assay.

	StA-IFN-1	StA-IFN-2	StA-IFN-3	StA-IFN-4	StA-IFN-5	StA-IFN-6
A549/pr(IFNβ).GFP	5.5	5.6	5.8	5.0	5.0	5.3
A549/pr(ISRE).GFP	4.3	-	4.3	4.4	4.3	4.7

4.2.3 Validation of novel hit compounds that inhibit the IFN induction pathway

As a result of the dose-response campaign that followed the primary diversity screen, 6 compounds were identified as specifically inhibiting GFP expression in the IFN induction assay. To ensure that the molecules used during screening were correct, the purity and identity of the compounds required verification. Therefore, all 245 putative hit compounds were subjected to LC-MS at the DDU. Compounds StA-IFN-3 and StA-IFN-6 did not pass this stage of testing, as LC-MS of these molecules failed to produce a mass ion. Therefore, investigation of these compounds was not carried forward.

To further scrutinize the 4 confirmed hit compounds that passed LC-MS, they were repurchased from commercial sources and their activity verified. This was achieved by re-testing the compounds in the IFN induction and IFN signalling reporter assays. Cells were treated with a 9-point, 2-fold serial dilution of compounds StA-IFN-1, StA-IFN-2, StA-IFN-4 or StA-IFN-5 or the equivalent volume of DMSO. Following pathway activation for the appropriate length of time, GFP expression was measured. The activity of StA-IFN-1 (Figure 4.5A) and StA-IFN-4 (Figure 4.5B) remained specific for the IFN induction pathway,

as they failed to produce an adequate dose-response curve in the IFN signalling assay. Conversely, StA-IFN-2 (Figure 4.5C) and StA-IFN-5 (Figure 4.5D) did not exhibit specificity, where the dose-response curves observed in the IFN induction and IFN signalling assays are comparable. As a result, StA-IFN-2 and StA-IFN-5 were not carried forward to further hit validation studies. StA-IFN-1 and StA-IFN-4 maintained their specific activity upon repurchase and re-testing, reinforcing the validity of these compounds as specifically inhibiting the IFN induction pathway. The activity of these compounds is broadly comparable to that of TPCA-1, a known inhibitor of IKKβ, bearing in mind that StA-IFN-1 and StA-IFN-4 are small druggable molecules, designed to be starting points for medicinal chemistry and optimization (Table 4.5).

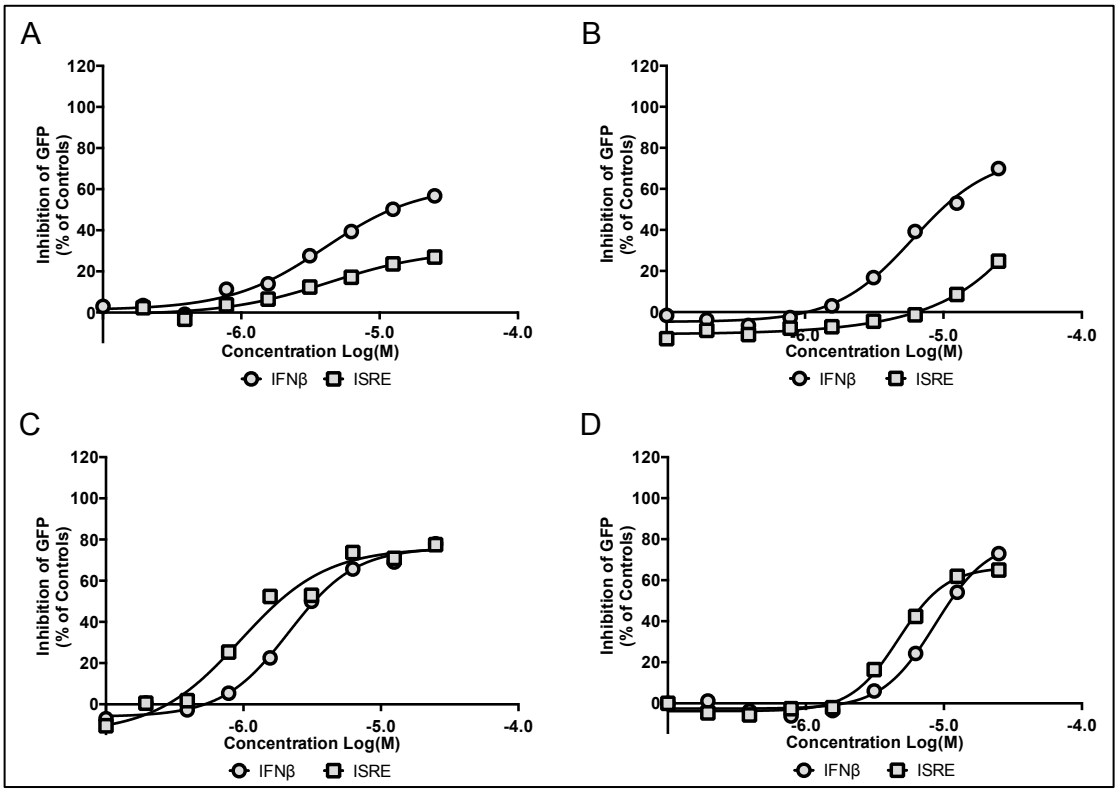

Figure 4.5: **Potency and specificity of confirmed hit compounds in the IFN induction and signalling reporter assays.**
Confirmed hit compounds were repurchased and tested in the A549/pr(IFNβ).GFP and A549/pr(ISRE).GFP reporter assays. Cells were treated with a 9-point, 2-fold serial dilution of StA-IFN-1 (**A**), StA-IFN-4 (**B**), StA-IFN-2 (**C**) and StA-IFN-5 (**D**) for 2 hours prior to stimulation of A549/pr(IFNβ).GFP and A549/pr(ISRE).GFP cells with SeV or IFNα respectively. Data represents 3 independent experiments, each conducted in triplicate (n=3); error bars show StDev.

Table 4.5: Dose response curve parameters of repurchased hit compounds, StA-IFN-1 and StA-IFN-4, retested in the A549/pr(IFNβ).GFP reporter assay and compared to those of the IKKβ inhibitor, TPCA-1.

	Max (%)	Min (%)	IC_{50} (μM)	Hill Slope
StA-IFN-1	61	-5	4.1	1.4
StA-IFN-4	77	-5	6.7	1.5
TPCA-1	88	-6	1.1	0.9

Up to this point, compound activity had been assessed using GFP expression as a marker of pathway activation. Furthermore, hit compounds had

been designated as specific through their lack of potency in the IFN signalling reporter assay. It was therefore necessary to verify that the activity of StA-IFN-1 and StA-IFN-4 was not due to other potential off-target effects. Additionally, it was necessary to validate the hit compounds by assessing their effect on cellular markers for IFN induction.

To eradicate the possibility that StA-IFN-1 and StA-IFN-4 had off-target effects that would mimic IFN induction pathway inhibition, we aimed to analyse cellular processes in the presence and absence of hit compounds. To achieve this, we studied levels of protein synthesis in A549 cells treated with DMSO, the transcriptional inhibitor actinomycin D (AMD), StA-IFN-1 or StA-IFN-4. Cells were metabolically labelled with ^{35}S cysteine/methionine mix to assess the levels of ^{35}S incorporation (Figure 4.6A). As expected, quantification of band intensity clearly showed AMD inhibiting cellular protein synthesis (Figure 4.6B). However, no such reduction in the levels of ^{35}S incorporation were observed following treatment with StA-IFN-1 or StA-IFN-4, suggesting they were not acting through inhibition of cellular protein synthesis. We also aimed to assess cell viability in the presence of these compounds. To achieve this, A549 cells were treated with DMSO, the translational inhibitor cycloheximide (CHX), StA-IFN-1 or StA-IFN-4 and an AlamarBlue cell viability assay carried out. As expected, cells exhibit a dose-dependent reduction in viability following CHX treatment. In contrast to this, cells treated with StA-IFN-1 (Figure 4.6C) and StA-IFN-4 (Figure 4.6D) only exhibited a reduction in viability at the highest concentration tested (50μM). This further supported the theory that hit

compounds StA-IFN-1 and StA-IFN-4 do not elicit inhibitory effects on the IFN induction pathway through non-specific off-target effects.

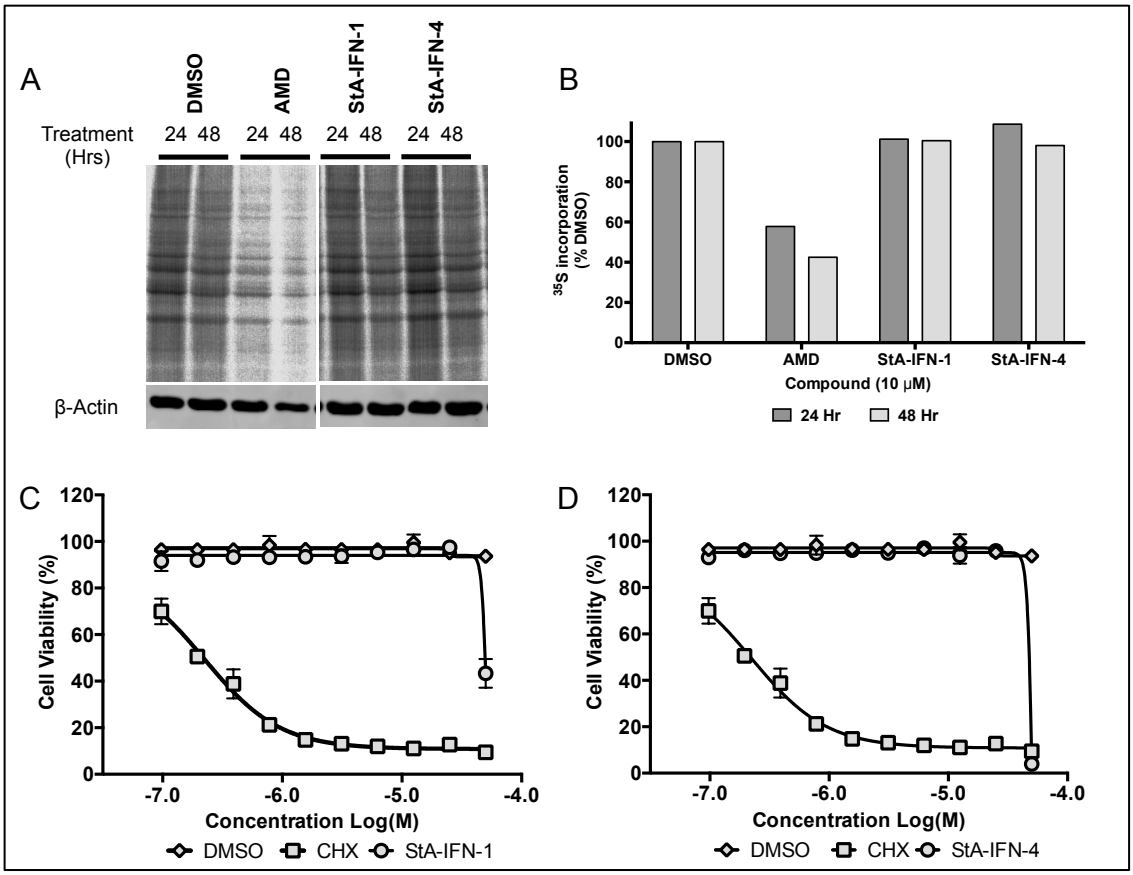

Figure 4.6: Elimination of off-target effects associated with hit compounds StA-IFN-1 and StA-IFN-4 impacting cell viability

Cellular protein synthesis in the presence of StA-IFN-1 and StA-IFN-4 was assessed with the use of the transcriptional inhibitor AMD as a control. A549 cells were treated with compound for 24 or 48 hours and labeled metabolically with [^{35}S]Met/Cys promix. Whole cell lysates were visualized (**A**) by SDS-PAGE followed by coomassie brilliant blue stain and phosphoimage analysis to quantitate levels of global protein synthesis compared to the DMSO control (**B**). The effect of StA-IFN-1 (**C**) and StA-IFN-4 (**D**) on cell viability was assessed with an AlamarBlue Assay and the translational inhibitor CHX as a control. A549 cells were treated with compound for 48 hours prior to AlalmarBlue reagent addition and viability assessed by fluorescence. Data is representative of three independent experiments that were each conducted in quadruplicate (n = 4). Error bars indicate StDev.

There is a possibility that StA-IFN-1 and StA-IFN-4 may be appearing as IFN induction inhibitors by acting on the SeV used to activate the pathway. If

this were the case, inhibition of SeV entry into the cells and subsequent reduction in cellular PAMPs would result in dose-dependent inhibition of the IFN induction pathway. To investigate this, immunofluorescence was carried out on compound treated, infected cells to detect viral proteins. No viral proteins were detected in mock-infected cells (Figure 4.7A). However, in cells treated with DMSO or either of the hit compounds, viral proteins were clearly seen. The staining of SeV proteins appeared comparable between the DMSO control and compound treated cells, suggesting that there was no impact on SeV entry into cells. This implied that StA-IFN-1 and StA-IFN-4 were not effecting SeV infection in the IFN induction assay.

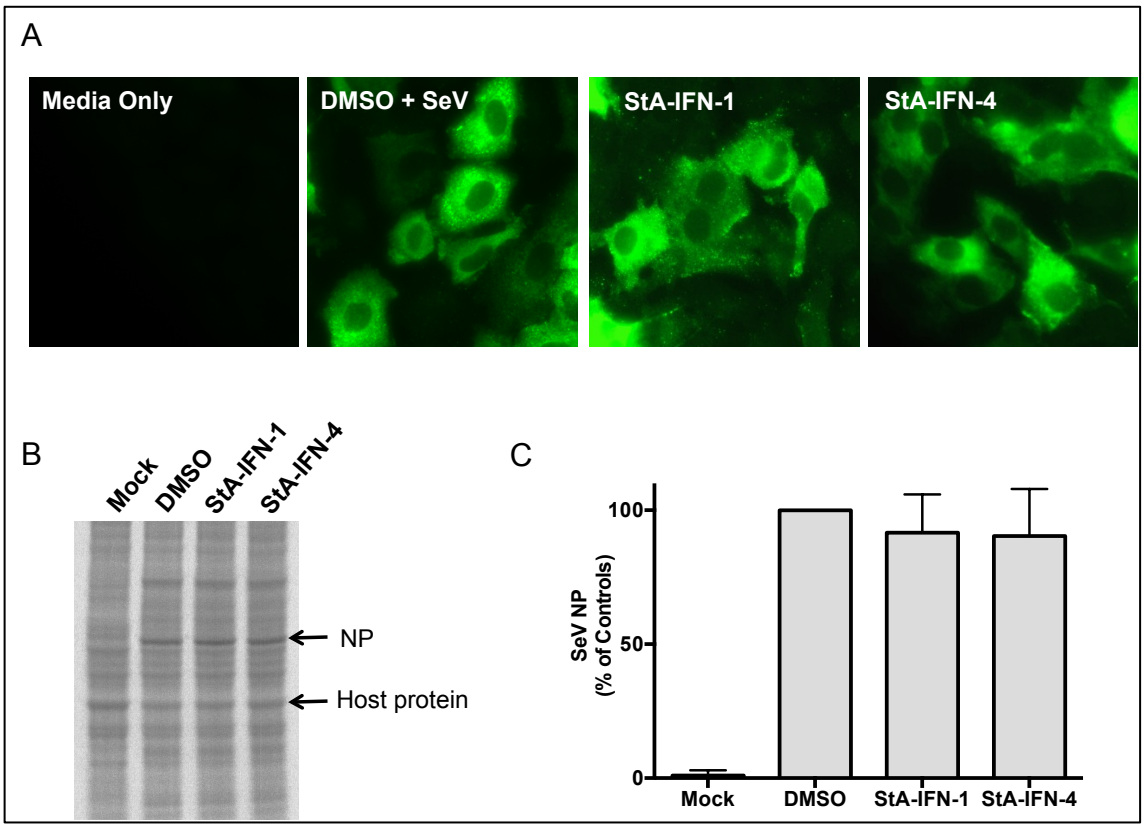

Figure 4.7: Elimination of off-target effects associated with hit compounds StA-IFN-1 and StA-IFN-4 impacting SeV

The effect of StA-IFN-1 and StA-IFN-4 on SeV infection and replication was assessed. A549 cells were treated with compound and infected with SeV for eighteen hours. Cells were then fixed, permeabilized and probed with anti-SeV antibody followed by FITC-conjugated secondary antibody. Cells were visualized with a Nikon Microphot-FXA microscope at 40x magnification (**A**). A549 cells were treated with compound and infected with SeV. Eighteen hours post-infection cells were labeled metabolically with [^{35}S]Met/Cys promix. Whole cell lysates were visualized by SDS-PAGE and coomassie brilliant blue followed by phosphoimage analysis (**B**) to quantitate SeV nucleoprotein (NP) levels (**C**). NP band intensity was normalized to a host cell protein and quantified relative to the DMSO control, set at 100%. Data represents the mean of three independent experiments (n=3); error bars indicate StDev.

To further investigate compound effect on viral replication, A549 cells were treated as above and metabolically labelled with ^{35}S cysteine/methionine mix to assess the levels of ^{35}S incorporation. SeV nucleoprotein (NP) was clearly visible (Figure 4.7B), and from the associated quantification (Figure 7.7C), NP was undetectable in mock treated cells. However, it was easily quantified in DMSO treated, SeV infected cells. The same levels of SeV NP were detected in StA-IFN-1 and StA-IFN-4 treated cells, where no significant

difference was seen. Therefore, taking both the immunofluorescence images and the NP expression levels into consideration, it was clear that neither StA-IFN-1 nor StA-IFN-4 target SeV. This gives further confidence that they act to inhibit the IFN induction pathway specifically.

To investigate cellular markers of IFN induction, the expression of IFNβ mRNA resulting from pathway activation was assessed by qRT-PCR. Quantitative RT-PCR using RNA extracted from cells treated with DMSO, TPCA-1, StA-IFN-1 or StA-IFN-4 and subsequently infected was used to monitor expression levels. As was expected, TPCA-1, the IKKβ inhibitor, significantly reduced the levels of IFNβ mRNA by 78% ($p<0.005$) (Figure 4.8A). StA-IFN-1 reduced IFNβ mRNA expression to a lesser extent, showing levels of 45% compared to the DMSO, SeV control ($p<0.005$). Interestingly, in the presence of StA-IFN-4, greater inhibition of the induction pathway was observed, with only 13% of IFNβ mRNA expressed compared to SeV infection alone. The clear inhibition of IFNβ mRNA expression in the presence of StA-IFN-1 and StA-IFN-4 further validated them as inhibitors of IFN induction, outwith the GFP reporter cells used thus far.

In order to ensure pathway specificity, StA-IFN-1 and StA-IFN-4 were assessed for activity in the IFN signalling pathway. We utilized qRT-PCR to analyse MxA mRNA expression in cells treated with DMSO, the Jak inhibitor Rux, StA-IFN-1 or StA-IFN-4 and subsequently treated with IFNα to activate IFN signalling. Rux reduced MxA mRNA expression by almost 99% compared to IFNα treatment in the absence of inhibitors ($p<0.0001$) (Figure 4.8B). Conversely, StA-IFN-1 and StA-IFN-4 had no significant impact upon MxA

mRNA expression following IFN signalling pathway activation. Taken together, the data obtained from qRT-PCR provided further evidence that compounds StA-IFN-1 and StA-IFN-4 inhibit the induction of IFNβ, exhibiting pathway specificity, as they have no activity on the IFN signalling pathway.

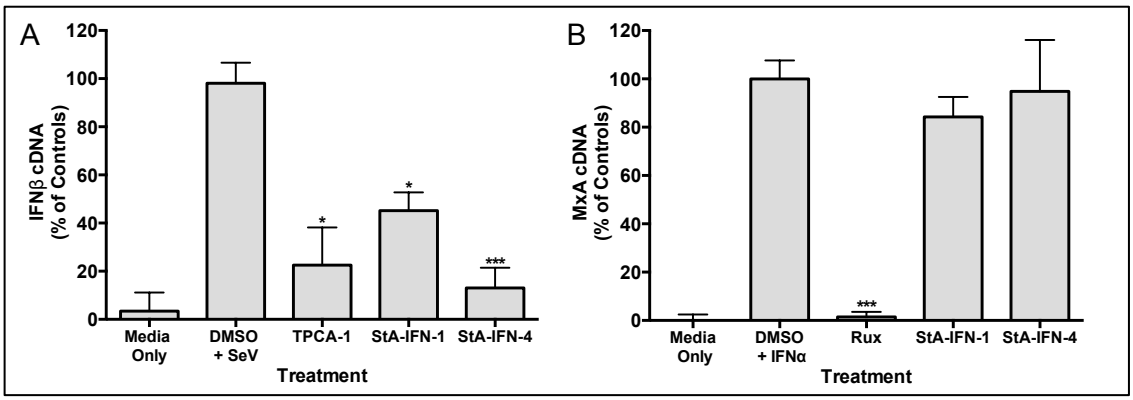

Figure 4.8: Hit compounds StA-IFN-1 and StA-IFN-4 effect on IFNβ and MxA transcript levels

The effect of StA-IFN-1, StA-IFN-4 and known inhibitory compounds on IFNβ and MxA mRNA levels was assessed. A549 cells were treated with compound 2 hours prior to activation. Three hours post-SeV infection and 18 hours post-IFNα treatment, total cellular RNA was extracted and reverse transcribed. The resultant cDNA was used to qPCR amplify either IFNβ (**A**) or MxA (**B**) sequences using appropriate primers. C_t values were subjected to absolute quantitation using a 6-point standard curve with DNA of known concentration and converted into % cDNA of controls. Data represents the mean of three independent experiments, each conducted in triplicate (n=3); error bars indicate StDev. Statistical significance was assessed using One-way ANOVA to compare compound treatment with the DMSO + SeV control (*** = $p<0.0001$, *=$p<0.005$).

4.3 Summary

Successful assay development to optimize and validate the IFN induction and IFN signalling assays facilitated an HTS campaign to identify novel modulators of IFN induction. A screening campaign was instigated, using the small diversity set at the DDU, comprising 15,667 small molecules. The diversity screen was carried out in an automated 384-well format utilizing the IFN induction reporter assay. Primary screening saw a dramatic drop in S/B

ratio to 1.6 compared to 3.1 following assay development. The Z' factor was consistent however at 0.67, indicating that the screen remained robust. Of 15,667 compounds screened, 245 were identified as putative hit molecules, 200 showing inhibitory activity and 45 enhancing GFP expression, yielding a primary hit rate of 1.56%. To validate these hit compounds and determine their potency, we embarked on a campaign of dose-response screening. Using 2-fold serial dilutions of hit compounds, construction of 10-point dose-response curves facilitated XC_{50} determination.

Three screens were performed.

I. IFN inhibitor screen to further investigate putative hit compounds with inhibitory activity
II. IFN enhancer screen using the IFN induction assay without SeV infection to study possible enhancers of IFN induction
III. Specificity screen using the IFN signalling assay to identify compounds with dual activity or non-specific, off-target effects

Of the 200 putative inhibitors of IFN induction, 6 showed activity specific to the IFN induction pathway, as they were shown to lack potency in the specificity screen. All but 3 of the potential enhancers of IFN induction were deemed inactive. Following LC-MS to confirm the identity and purity of the screening compounds, the remaining 4 most promising hits were repurchased for further testing. Two of these hit compounds, StA-IFN-2 and StA-IFN-5 failed to display specificity to the IFN induction pathway following retesting. StA-IFN-1 and StA-IFN-4 however continued to exhibit activity specific to IFN induction. Additionally, we excluded the possibility that this inhibition was due to off-target

effects such as SeV inhibition or by compromising cell viability. Furthermore, we confirmed that StA-IFN-1 and StA-IFN-4 have direct activity on the inhibition of IFN induction as RT-qPCR saw a significant decrease in IFNβ mRNA expression in their presence.

5. Characterization of novel compounds that inhibit the IFN induction pathway

5.1 Introduction

As a result of successful diversity screening, dose-response studies and hit validation, two compounds, StA-IFN-1 and StA-IFN-4, were identified as having specific activity to the inhibition of IFN induction. To further investigate the action of these compounds in the IFN induction pathway, we instigated studies to identify the cellular target of these compounds, assess any structure-activity relationships regarding their activity and determine whether StA-IFN-1 and StA-IFN-4 can increase the growth of IFN sensitive viruses.

The activity of StA-IFN-1 and StA-IFN-4 in the IRF3 branch of the IFN induction pathway was investigated in a number of different ways: (i) Immunofluorescent microscopy was utilized to determine the levels of IRF3 nuclear translocation in the presence and absence of the compounds. (ii) IRF3 phosphorylation is critical for its activation and we therefore assessed the levels of phosphorylated IRF3 in the presence of hit compounds following SeV induced pathway activation. (iii) To further scrutinize the activity of the compounds in this pathway, which is heavily dependent on the activity of cellular kinases, StA-IFN-1 and StA-IFN-4 were tested for activity on kinases that act upstream of IRF3 phosphorylation.

To characterize specific aspects of the structures of StA-IFN-1 and StA-IFN-4 that may be important for their activity, we carried out an investigation into

any previous publications that may include these compounds, or substructures within the molecules. Web-based database searches suggested that the compound activity observed in our study was novel. Subsequently, we instigated studies using compounds with a high level of similarity to StA-IFN-1 and StA-IFN-4 and components of the molecules that have structural identity to distinct portions of the original hit compounds. As we have previously shown that inhibitors of the IFN response can increase the growth of BunVΔNSs, an IFN sensitive virus (Stewart et al., 2014), we sought to assess the activity of StA-IFN-1 and StA-IFN-4 in the broader context of the IFN response. Effective replication of BunVΔNSs in the presence of StA-IFN-1 and StA-IFN-4 would suggest that these compounds are blocking the IFN response.

5.2 Results

5.2.1 Mode of action studies

As StA-IFN-1 and StA-IFN-4 were identified through phenotypic screening, the mechanism of action of these compounds remains unknown. We therefore sought to determine their cellular target(s). Firstly, we measured the impact of StA-IFN-1 and StA-IFN-4 on the nuclear translocation of activated IRF3, a crucial step in the induction of IFN. To achieve this, we used immunofluorescent microscopy to assess IRF3 localisation in SeV infected A549 cells incubated in the presence, or absence, of the compounds (Figure 5.1A). In the absence of infection, IRF3 is primarily cytoplasmic. Following DMSO treatment and SeV infection however, 60% of the cells exhibited clear nuclear staining (Figure 5.1B). Strikingly, StA-IFN-4 caused a highly significant

inhibition of IRF3 translocation, approaching 100% ($p<0.0001$). As was expected, BX795, which inhibits TBK1 in the course of IRF3 activation, significantly reduced nuclear IRF3 to 20% ($p<0.0001$), although very high levels of variation were observed. StA-IFN-1 resulted in a significant ($p<0.005$) 20% reduction in nuclear translocation of IRF3 compared to the DMSO control. Although StA-IFN-1 caused a significant reduction in IRF3 translocation, the level of inhibition seen by StA-IFN-4 is far superior, even compared to that of BX795.

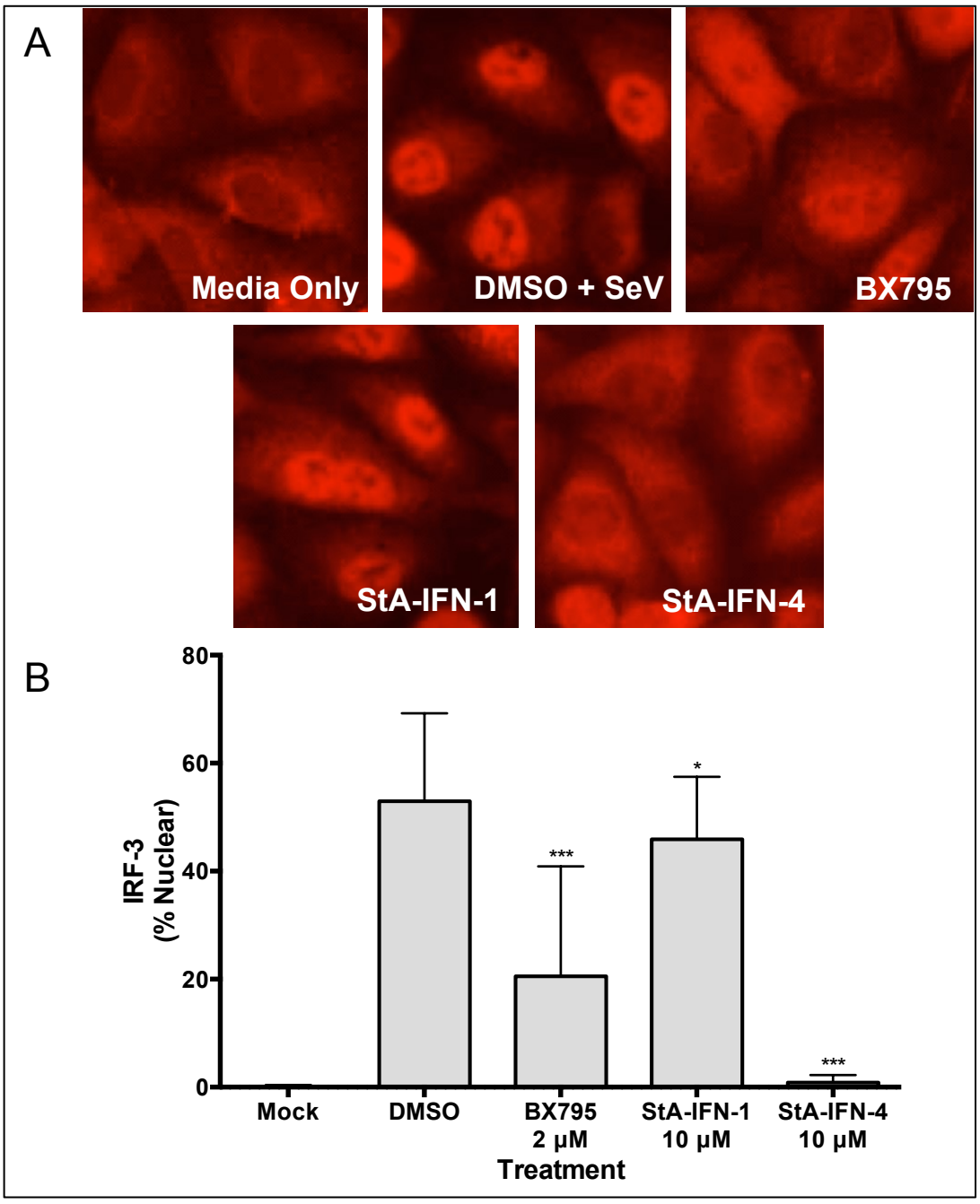

Figure 5.1: Effect of StA-IFN-1 and StA-IFN-4 on nuclear translocation of IRF3.
The effect of StA-IFN-1, StA-IFN-4 and BX795 on the translocation of IRF3 following SeV infection. A549 cells were treated with compound for 2 hours, followed by infection with SeV for 3 hours. Cells were fixed, permeabilized and incubated with anti-IRF3 antibody, followed by Texas red-conjugated secondary antibody. Cells were visualized with a Nikon Microphot-FXA microscope at 40x magnification (**A**). Images were annonymized and the number of cells displaying diffuse cytoplasmic and nuclear staining quantified by Dr Andri Vasou (**B**). Data is presented as percentage of cells displaying nuclear staining of IRF3 and is representative of 3 individual repeats (n=3). Error bars display StDev and the statistical significance of cells exhibiting nuclear IRF3 following compound treatment compared to the DMSO + SeV control using one-way ANOVA (***=p<0.0001, *=p<0.005).

The translocation of IRF3 is a consequence of its phosphorylation and subsequent homodimerization, which exposes a nuclear localization signal. A reduction in IRF3 phosphorylation would suggest the compounds are acting upstream in the pathway, where no decrease in levels of phosphorylated IRF3 (pIRF3) would suggest compound activity is targeted to inhibit dimerization or nuclear translocation. Therefore we assessed the impact of StA-IFN-1 and StA-IFN-4 on levels of pIRF3 following activation of the IFN induction pathway (Figure 5.2A). The most dramatic reduction was observed following treatment with StA-IFN-4, where the level of pIRF3 decreased by 92% ($p<0.0001$). BX795 resulted in a 56% reduction in pIRF3 compared to the control, although again, high levels of variation were observed (Figure 5.2B). StA-IFN-1 results in a small yet significant decrease in IRF3 phosphorylation of 32% ($p<0.005$). It was necessary to ensure that the action of StA-IFN-1 and StA-IFN-4 upon pIRF3 was not due to a global inhibition of phosphorylation. The phosphorylation of STAT1 is a crucial step in the IFN signalling pathway, distinct from phosphorylation events in the IFN induction pathway. Therefore, we investigated the impact of StA-IFN-1 and StA-IFN-4 on the levels of phosphorylated STAT1 (pSTAT1) (Figure 5.2C). As was expected, Rux, a Jak1/2 inhibitor, resulted in a dramatic 85% decrease in pSTAT1 ($p<0.0001$) (Figure 5.2D). Conversely, no such impact on the levels of pSTAT1 following StA-IFN-1 or StA-IFN-4 treatment was observed, suggesting that the hit compounds are not acting as general inhibitors of phosphorylation.

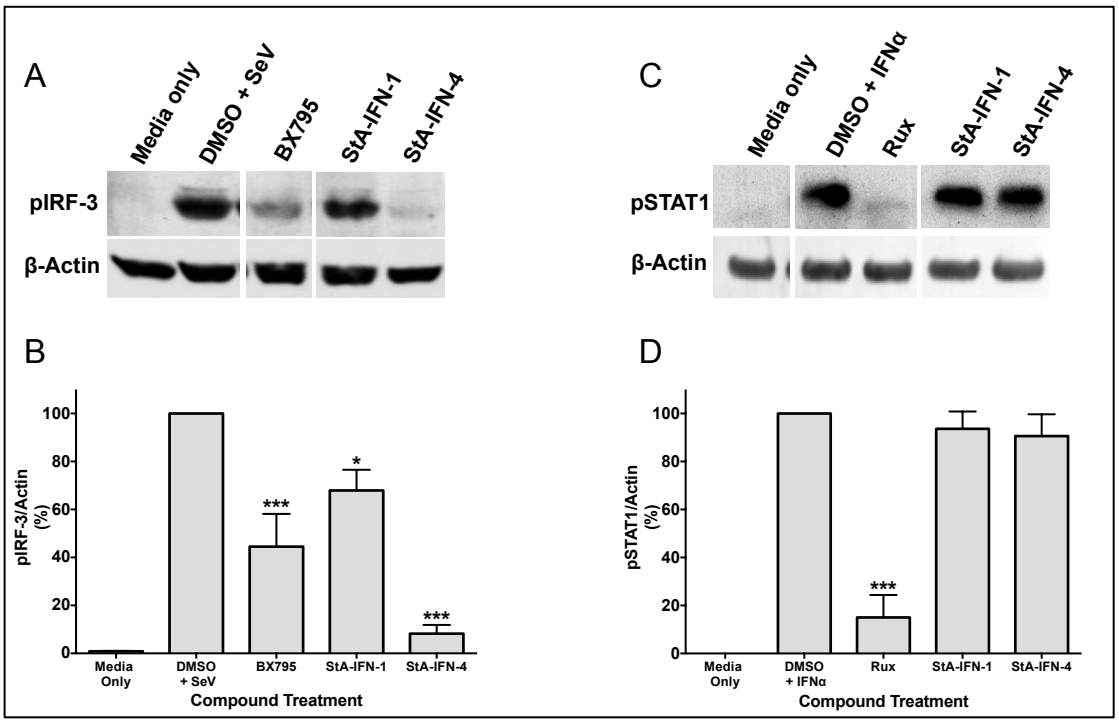

Figure 5.2: Effect of StA-IFN-1 and StA-IFN-4 on phosphorylation of IRF3.
The effect of StA-IFN-1, StA-IFN-4 and BX795 on the phosphorylation of IRF3 following SeV infection. A549 cells were treated with compound for 2 hours, followed by infection with SeV to activate the IFNβ induction pathway for 3 hours. Whole cell lysates were subjected to SDS-PAGE and western blot. Membranes were probed with anti-pIRF3 and anti-βActin antibodies followed by IRDye680 or IRDye800-conjugated secondary antibody respectively (**A**). Bands were visualized and quantified as % pIRF3 relative to actin (**B**)**.** The effect of StA-IFN-1, StA-IFN-4 and Rux on the phosphorylation of STAT1 following IFNα treatment was also assessed. A549 cells were treated with compound for 2 hours, followed by incubation with IFNα to activate the IFN signalling pathway for 15 minutes. Whole cell lysates were subjected to SDS-PAGE and western blot. Membranes were probed with anti-pSTAT1 or anti-βActin antibodies followed by HRP or IRDye800-conjugated secondary antibody respectively (**C**). Bands were visualized and quantified as % pSTAT1 relative to actin (**D**)**.** Data representative of 3 individual repeats (n=3). Error bars display StDev and statistical significance of pIRF3 and pSTAT1 levels compared to the DMSO + SeV or IFNα control was determined by one-way ANOVA (***=$p<0.0001$, *=$p<0.005$).

Taken together, we have shown that StA-IFN-4 significantly reduces the phosphorylation and subsequent nuclear translocation of IRF3. This suggests that StA-IFN-4 is not acting upon the dimerization or translocation of IRF3, but either directly upon its phosphorylation, or further upstream in the IFN induction pathway. As StA-IFN-1 resulted in only small levels of inhibition in these

experiments, it may have more potent activity elsewhere in the IFN induction pathway.

IRF3 is activated by phosphorylated kinases, TBK1 and IKKε. In an effort to further scrutinize the activity of StA-IFN-1 and StA-IFN-4 in IRF3-dependent IFN induction, we instigated studies to assess their action on TBK1 and IKKε. Philip Cohen has a well-established assay to investigate compounds with inhibitory activity against kinases (Clark et al., 2009). Therefore, in collaboration with Philip Cohen, hit compounds StA-IFN-1 and StA-IFN-4, were studied for their ability to inhibit the phosphorylation of TBK1 (pTBK1) and IKKε (pIKKε) following TLR3 activation by Poly(I:C). In contrast to the results we obtained, where IFN was induced through SeV activated RIG-1 (Figure 5.2), no reduction in pIRF3 levels were observed in the presence of either StA-IFN-1 or StA-IFN-4 (Figure 5.3). Indeed, here the data suggests that neither compound causes a reduction in the phosphorylation of IRF3, TBK1 or IKKε following TLR-induced activation.

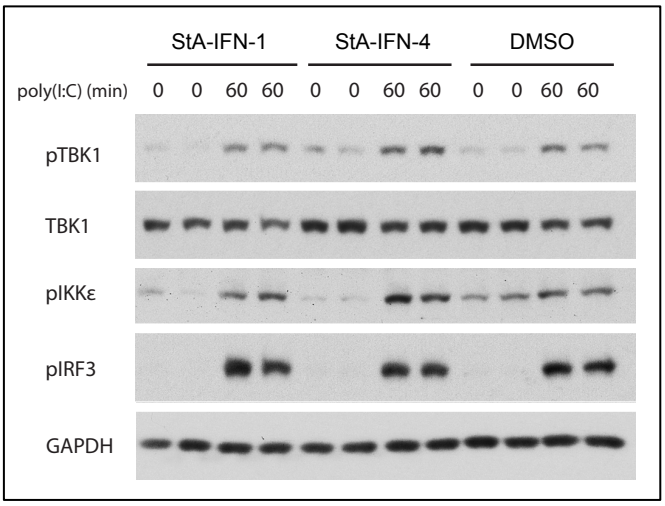

Figure 5.3: Effect of hit compounds on TLR3 induced kinase activity
The activity of StA-IFN-1 and StA-IFN-4 on TLR3 activation of the IFN induction pathway. HACAT cells were incubated with 10 μM of compound. Two hours post-compound treatment, cells were treated with 10 μg/ml of Poly(I:C) for 1 hour to activate TLR3. Whole cell lysates were subjected to SDS-PAGE and western blot. Membranes were probed with anti-pTBK1, anti-TBK1, anti-pIKKε, anti-pIRF3 and anti-GAPDH antibodies followed by goat anti-rabbit HRP-conjugated secondary antibody. Jordan Taylor carried out this work in the lab of Philip Cohen at the university of Dundee.

From this study, we have identified that StA-IFN-4 causes a significant reduction in the phosphorylation of IRF3 and its subsequent translocation to the nucleus following RIG-I mediated IFN induction by SeV infection. StA-IFN-1 on the other hand exhibited lower levels of activity that were less significant. However, no such reduction in pIRF3 was observed through TLR3 dependent IFN induction with Poly(I:C). The disparity in the levels of pIRF3 observed in experiments using different activators of IFN induction suggests that StA-IFN-1 and StA-IFN-4 may be acting upstream of the TBK1/IKKε activation step, where induction of the pathway is distinct between different PAMPs.

5.2.2 Structure-activity relationships (SAR)

To further characterize hit compounds StA-IFN-1 and StA-IFN-4, we hoped to gain an understanding of the structural components of the molecules

that are important for inhibition of IFN induction. We first endeavoured to identify if these molecules had previously been characterized. If they have shown activity in previous studies, we could gain an understanding of any structure-activity relationships relating to these compounds. To investigate this, the SciFinder database (American Chemical Society, scifinder.cas.org) was utilized. Searches based on the chemical structures of StA-IFN-1 and StA-IFN-4 were carried out to identify any substructures within the compounds that have shown activity similar to that observed in our study. This investigation suggested that the compounds were novel as no previous compound characterization was identified.

StA-IFN-1 obeys Lipinski's rule of 5 with a molecular weight of 255.3, 1 hydrogen bond acceptor and 5 hydrogen bond donors. SciFinder database searches identified a compound with 82% similarity (StA-IFN-1-82S). StA-IFN-1 (Figure 5.4A) has an acetyl group, whereas this is missing in StA-IFN-1-82S (Figure 5.4B). The chemical structure of StA-IFN-1 can be broadly divided into two smaller compounds, an acetyl indole group (StA-IFN-1-LF) (Figure 5.4C) and a pyrazolone (StA-IFN-1-SF) (Figure 5.4D). We sought to investigate the activity of StA-IFN-1-82S, StA-IFN-1-LF and StA-IFN-1-SF in relation to StA-IFN-1. To achieve this, the compounds were used in the IFN induction reporter assay to assess inhibition of GFP expression. StA-IFN-1 had far superior activity, showing the highest levels of inhibition (38%) (Figure 5.4E). StA-IFN-1-LF was the only other compound tested that exhibited activity, reducing GFP expression by 13%. Both StA-IFN-1-82S and StA-IFN-1-SF resulted in no inhibition of GFP expression, exhibiting the same trend as DMSO. Interestingly,

both StA-IFN-1 and StA-IFN-1-LF have the acetyl indole structure, suggesting that it may be important for inhibition of IFN induction.

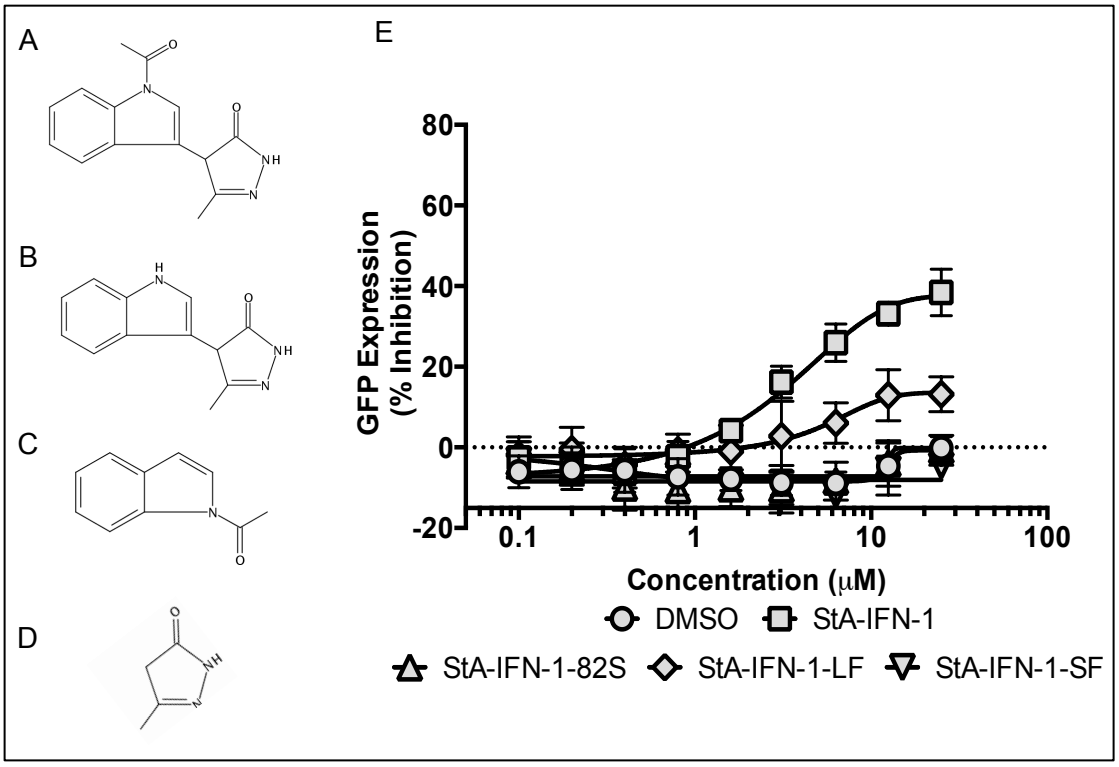

Figure 5.4: Investigating StA-IFN-1 structure-activity relationships
The activity of compounds with structural similarity to StA-IFN-1 were analysed in the IFN induction reporter assay. The chemical structure of StA-IFN-1 (**A**), an 82% similar molecule (StA-IFN-1-82S) (**B**), and molecules representing large (StA-IFN-1-LF) (**C**) and small (StA-IFN-1-SF) (**D**) fragments of the original compound are shown. A549/pr(IFNβ).GFP cells were treated with compounds 2 hours prior to infection with SeV. Eighteen hours post infection, cells were fixed and GFP expression analyzed (**E**). Data represents 2 independent replicates, each conducted in triplicate (n=6) where errors bars show StDev.

StA-IFN-4 obeys Lipinski's rule of 5 with a molecular weight of 337.2, 6 hydrogen bond acceptors and no hydrogen bond donors. SciFinder database searches identified a compound with 85% similarity (StA-IFN-4-85S). StA-IFN-4 is composed of a pyridoprymindine and a dichloro pyridazinone (Figure 5.5A), whereas the pyridoprymidine is substituted for an imidazolprymindine in StA-IFN-4-85S (Figure 5.5B). The chemical structure of StA-IFN-4 can be broadly

divided into two smaller compounds, the pyridoprymidine (StA-IFN-4-LF) (Figure 5.5C) and the dichloro pyridazinone (StA-IFN-4-SF) (Figure 5.5D). We sought to investigate the activity of StA-IFN-4-85S, StA-IFN-4-LF and StA-IFN-4-SF in relation to StA-IFN-4. Initially, the compounds were used in the IFN induction reporter assay to monitor inhibition of GFP expression. StA-IFN-4 had the highest level of activity, resulting in over 60% inhibition (Figure 5.5E). StA-IFN-4-85S exhibited a slight decrease in activity compared to the parental compound, although still achieved 40% inhibition in GFP expression. Surprisingly, the smallest molecule, StA-IFN-4-SF, also appeared to be active in inhibiting IFN induction, causing a 28% decrease in GFP expression. StA-IFN-4-LF did not significantly inhibit GFP expression, exhibiting the same trend as DMSO. Interestingly, StA-IFN-4, StA-IFN-4-85S and StA-IFN-4-SF all have the same dichloro pyridazinone structure and although to varying degrees, all inhibit IFN induction.

In order to further investigate the activity of the StA-IFN-4-like molecules independently of the GFP reporter assay, qRT-PCR was used to assess the level of IFNβ mRNA expression following compound treatment and activation of the IFN induction pathway. As expected, BX795, a TBK1 inhibitor, significantly reduced the levels of IFNβ mRNA present by 99% ($p<0.0001$) (Figure 5.5F). Treatment with StA-IFN-4 at 10 μM exhibited similar levels of IFNβ mRNA as shown previously (Figure 4.8A). Furthermore, when treated with 20 μM, inhibition is increased to 97% ($p<0.0001$). The 3 compounds with high levels of similarity to StA-IFN-4 showed significantly less inhibition at 10 μM compared to 20 μM (Figure 5.5F). IFN-4-85S significantly decreased IFN induction, achieving

73% at 10 μM (p<0.001) and 52% at 20 μM (p<0.0001). In contrast to the results of the IFN induction reporter assay, both of the fragment compounds, StA-IFN-4-LF and StA-IFN-4-SF, achieved similar levels of IFNβ mRNA expression. However here, StA-IFN-4-LF yielded more significant decreases in IFNβ mRNA expression.

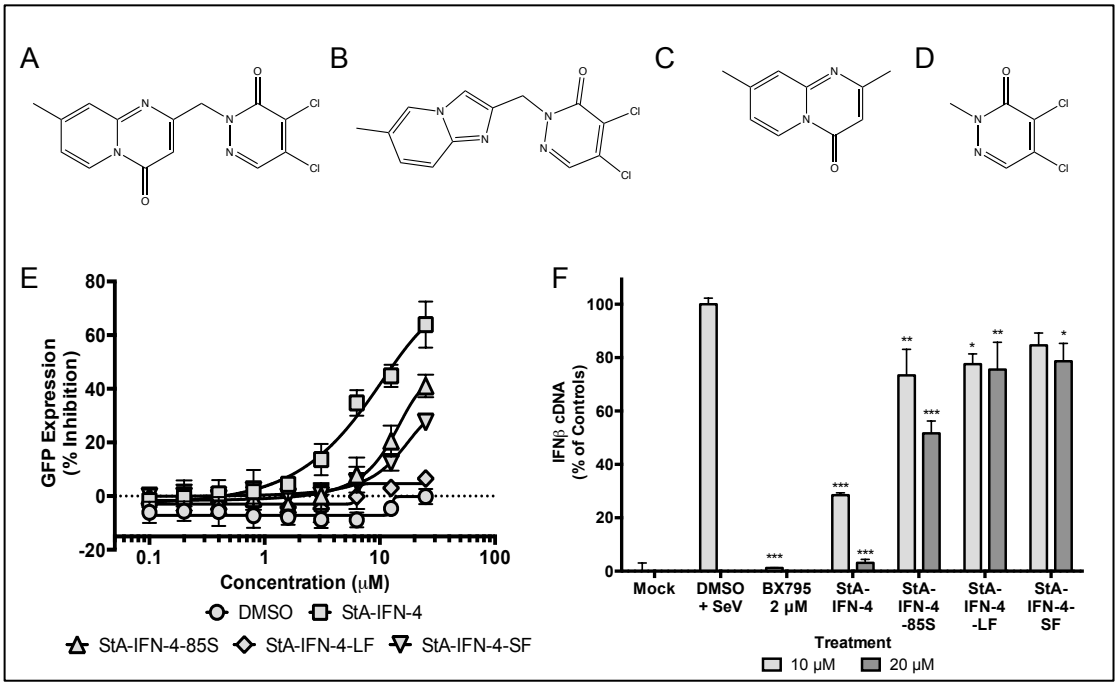

Figure 5.5: Investigating StA-IFN-4 structure-activity relationships
The activity of compounds with structural similarity to StA-IFN-4 was analysed. The chemical structures of StA-IFN-4 (**A**), a molecule with 85% similarity (StA-IFN-4-85S) (**B**), and molecules representing large (StA-IFN-4-LF) (**C**) and small (StA-IFN-4-SF) (**D**) fragments of the original compound are shown. A549/pr(IFNβ).GFP cells were treated with compound 2 hours prior to SeV infection. Eighteen hours post-infection GFP expression was analyzed (**E**). Compound effect on IFNβ mRNA levels was assessed. A549 cells were treated with compound for 2 hours. Three hours post infection, total cellular RNA was extracted and reverse transcribed. The resultant cDNA was used to qPCR amplify IFNβ sequences using appropriate primers. C_t values were subjected to absolute quantitation using a 6-point standard and converted into % cDNA of controls (**F**). Data represents 2 independent repeats, each conducted in triplicate (n=6). Errors bars show StDev. Statistical significance was assessed using One-way ANOVA to compare compound treatment with the DMSO + SeV control (*** = p<0.0001, **=p<0.001, *=p<0.005).

We endeavoured to investigate how the structure of hit compounds StA-IFN-1 and StA-IFN-4 affected their ability to inhibit IFN induction. By using

molecules with high levels of similarity to the parental compound, and compounds constituting distinct structures within StA-IFN-1 and StA-IFN-4, we have learnt that the acetyl indole of StA-IFN-1 (StA-IFN-1-LF) appears to be crucial for its activity. Conversely, the dichloro pyridazinone of StA-IFN-4 (StA-IFN-4-SF) showed more activity in the inhibition of IFN induction in the GFP reporter assay. However, both StA-IFN-4-LF and StA-IFN-4-SF showed similarly low levels of inhibition in the RT-qPCR assay.

5.2.3 Inhibition of IFN induction and the growth of an IFN sensitive virus

We have previously demonstrated that inhibitors of the IFN response can restore the replication of an IFN sensitive virus in A549 cells (Stewart et al., 2014). BunVΔNSs is IFN sensitive and so replicates poorly in cell culture as a result of the deletion of NSs, the gene encoding its viral IFN antagonist. Therefore, we wanted to assess the growth of BunVΔNSs in the presence of StA-IFN-1 and StA-IFN-4. To achieve this, plaque assays were carried out on A549 cells treated with compound. As is clear, BunVΔNSs produces pinpoint plaques when inhibitory compounds are not present (Figure 5.6A). In agreement with previously published work (Stewart et al., 2014), the size of BunVΔNSs plaques is significantly increased by 6-fold in the presence of the Ikkβ inhibitor TPCA-1 ($p<0.0001$) (Figure 5.6B). Interestingly, StA-IFN-1 caused a 2-fold increase in plaque size ($p<0.0005$). However, StA-IFN-4 did not have a potent impact on plaque size, although a slight increase was observed ($p<0.04$).

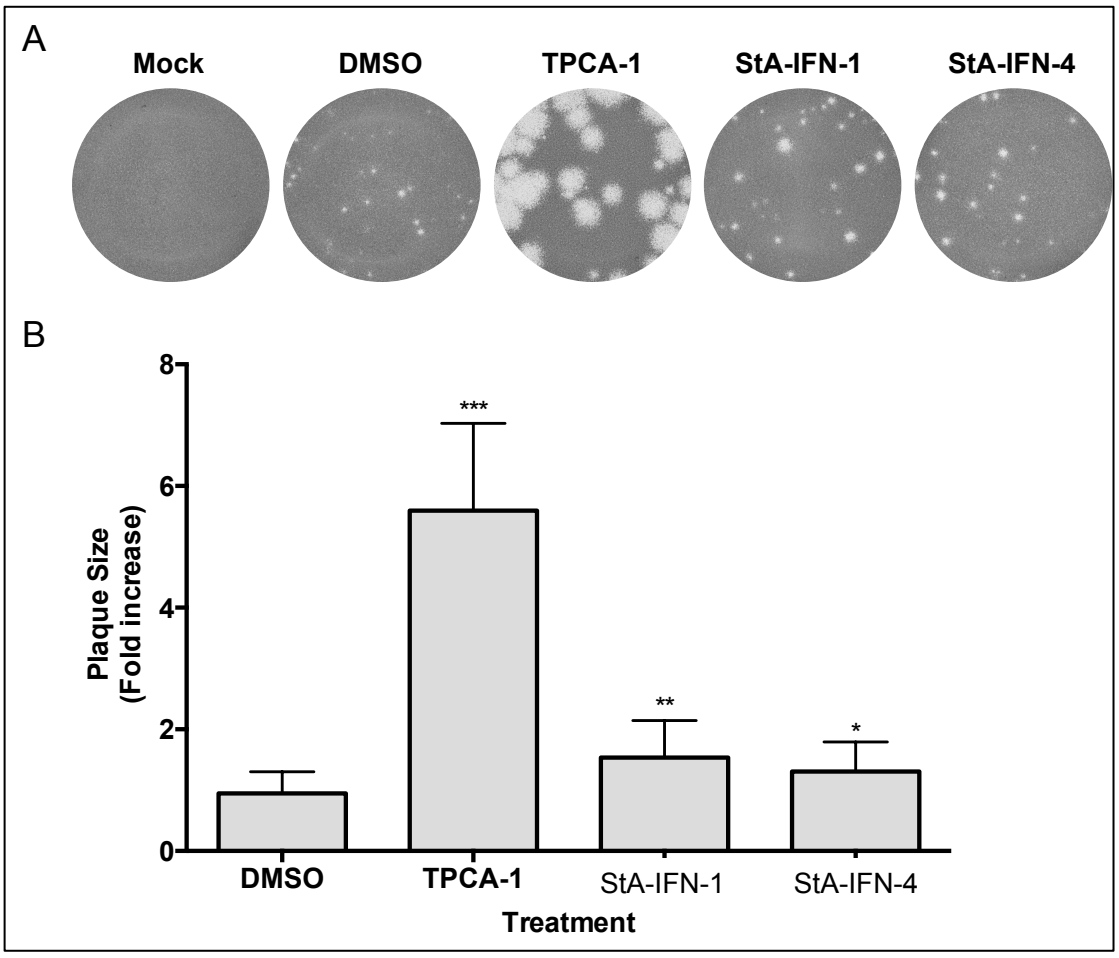

Figure 5.6: Effect of hit compounds on the replication of an IFN sensitive virus
The effect of StA-IFN-1 and StA-IFN-4 on the growth of an IFN sensitive virus, BunVΔNSs, was assessed. A549 cells were treated with compound and infected with BunVΔNSs for 1 hour. Plaque size was visualized by crystal violet staining 3 days post-infection (**A**). Plaque sizes were measured and are presented as fold increase above that of the DMSO-only control (**B**). Data represents 2 independent experiments (n≥53). Statistical significance was determined by one-way ANOVA where each condition was compared to the DMSO-only control (***=p<0.0001, **=p<0.0005, *=p<0.04).

As StA-IFN-4 exhibited such low levels of activity in the plaque assays, we postulated that this could be a result of compound degradation. Therefore, we assessed the stability of StA-IFN-1 and StA-IFN-4. To achieve this, culture media containing the compounds was incubated alone or with A549 cells, and media samples containing StA-IFN-1 and StA-IFN-4 were used in the IFN induction reporter assay. The level of GFP inhibition observed for StA-IFN-1

does not differ between samples incubated in media alone or in the presence of cells, however the extent of GFP inhibition begins to decline 3-days post-treatment (Figure 5.7A). In contrast to this, when StA-IFN-4 was incubated in the presence of cells, activity dropped dramatically after 24-hours, whereas in media alone, activity was retained (Figure 5.7B). To further investigate the reduction in StA-IFN-4 activity, media samples were also used to assess pIRF3 levels (Figure 5.7C). Through quantification of band intensity, we observed that StA-IFN-4-mediated inhibition of pIRF3 dramatically decreased when incubated with A549 cells (Figure 5.7D). Conversely, it remained potent at inhibiting IRF3 phosphorylation when incubated in media alone. This suggests that the compound is stable for up to 8 days in cell culture media. However, StA-IFN-4 loses activity when A549 cells are present, suggesting that it is metabolised rapidly in cell culture. This indicates that the small plaque size observed in the presence of StA-IFN-4 is not necessarily due to lack of activity, but instead a result of compound instability in cell culture. StA-IFN-1 on the other retains activity for up to 4 days regardless of the presence of cells.

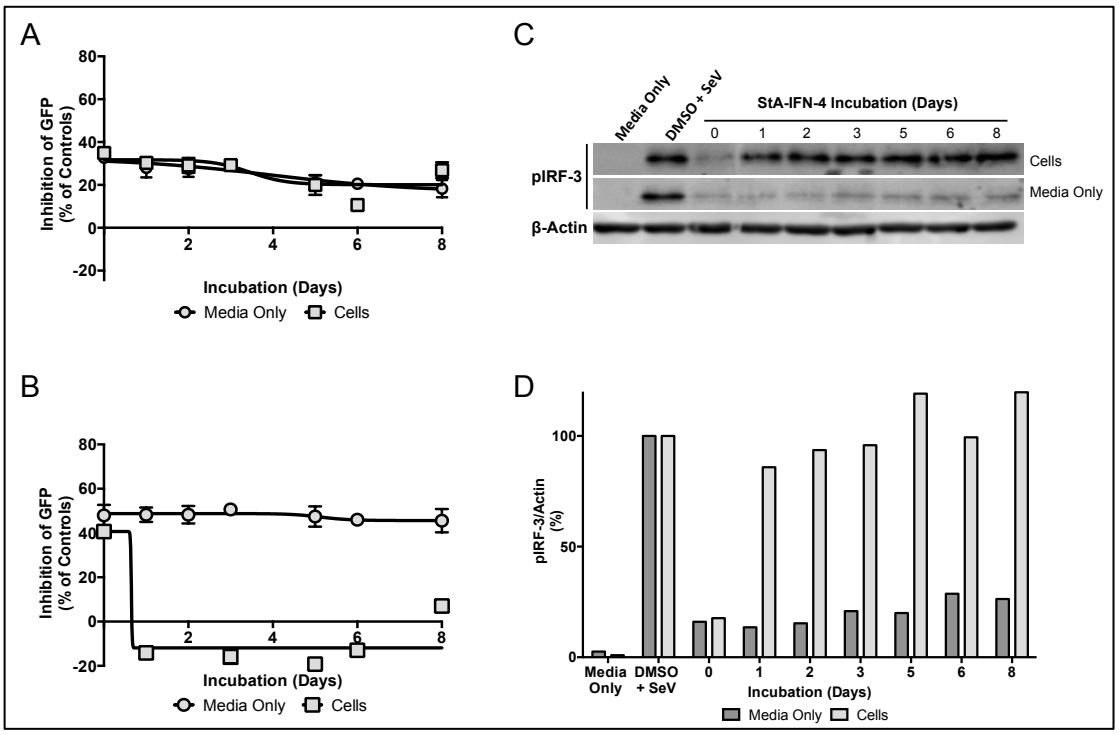

Figure 5.7: Stability of hit compound activity
By incubating compounds in media alone or in the presence of A549 cells the stability of StA-IFN-1 and StA-IFN-4 was assessed. Media samples were taken for up to 8 days. A549/pr(IFNβ).GFP cells were treated with the samples of StA-IFN-1 (**A**) or StA-IFN-4 (**B**) for 2 hours, prior to infection with SeV. Eighteen hours post infection, cells were fixed and GFP expression analyzed. Data is representative of 2 independent experiments each conducted in triplicate (n=3). Error bars indicate StDev. Monitoring phosphorylation of IRF3 also assessed the activity of IFN-4. A549 cells were treated with compound samples for 2 hours, followed by infection with SeV to activate the IFNβ induction pathway for 3 hours. Whole cell lysates were subjected to SDS-PAGE and western blot (**C**). Membranes were probed with anti-pIRF3 and anti-βActin antibodies followed by IRDye680 or IRDye800-conjugated secondary antibody respectively. Bands were visualized and quantified as % pIRF3 relative to actin (**D**). Data is representative of 2 independent experiments.

5.3 Summary

As a result of HTS and associated hit validation, two compounds, StA-IFN-1 and StA-IFN-4 were identified as inhibitors of the IFN induction pathway. In order to further characterize the inhibitory activity of these compounds, we sought to determine their mechanism of action in the IFN induction pathway. Through assessment of nuclear translocation and phosphorylation of IRF3, we observed that StA-IFN-4 significantly reduced both of these events. Although

still significant, StA-IFN-1 exhibited much lower levels of activity. This suggested that StA-IFN-4 acts at, or upstream of IRF3 phosphorylation. The activity of these compounds appears to be specific to SeV-induced RIG-1 activation of IFN induction however, as no inhibition in the phosphorylation of IRF3, TBK1 or IKKε was observed following TLR3-dependent, Poly(I:C) stimulation of the IFN induction pathway.

To gain an insight into how the structures of StA-IFN-1 and StA-IFN-4 impact their activity, we conducted preliminary structure-activity relationship studies. Compounds with a high degree of structural similarity to, or substructures from within, the parental compounds were tested in the IFN induction reporter assay. Here, we learnt that the acetyl indole of StA-IFN-1 was important for activity. This work also suggested that the dichloro pyridazinone of StA-IFN-4 was important for inhibition of the IFN induction pathway, although these results were not definitive. In order to assess the activity of the compounds in the context of the IFN response as a whole, we sought to determine if StA-IFN-1 and StA-IFN-4 increased the growth of an IFN sensitive virus. Plaque assays using the IFN sensitive BunVΔNSs were carried out. StA-IFN-1 and StA-IFN-4 resulted in a small increase in BunVΔNSs plaque size. As the increase in plaque size resulting from StA-IFN-4 treatment was small, we postulated that compound degradation might be the cause. Indeed, by assessing compound stability in cell culture and media alone, we observed that StA-IFN-4 is rapidly metabolised by cells in culture, although it remains stable when incubated in media alone. From this work, we have successfully gained an insight into the cellular target of StA-IFN-4 in the IFN induction pathway, and

ascertained which aspects of both molecules may be more important for their inhibitory activity. Furthermore, we have successfully shown that these compounds can inhibit the cellular IFN response, resulting in slightly increased growth of an IFN sensitive virus.

6. An assay to screen for novel antiviral compounds

6.1 Introduction

Due to the potency of the cellular IFN response, viruses have evolved strategies to circumvent its actions. One way in which viruses achieve this is through the expression of viral IFN antagonists, which are often multi-functional proteins. Owing to the importance of functional IFN antagonists to the establishment of a viral infection, they present an attractive target for antiviral drug discovery. A virus that does not have a functional IFN antagonist is severely restricted in its ability to replicate (Stewart et al., 2014). Therefore, a compound that renders the viral IFN antagonist non-functional will aid the cellular IFN response in controlling an infection and prevent virus spread. With the aim of identifying candidate molecules with antiviral activity, we postulated that the IFN signalling reporter assay presents a simple platform to facilitate this work. To this end, a derivative of the A549/pr(ISRE).GFP cell line was generated to constitutively express the phosphoprotein of Rabies virus (RBV-P). Following validation of the A549/pr(ISRE).GFP.RBV-P cell line it was used in an in-house diversity HTS with the aim of identifying compounds that modulate RBV-P function, resulting in restoration of GFP expression.

As the A549/pr(ISRE).GFP.RBV-P cell line used in screening constitutively expresses RBV-P, the assay was complex, as it was necessary to include the parental A549/pr(ISRE).GFP cell line in assay plates. In an effort to streamline this assay and optimize it for use in future screening campaigns, we instigated a campaign of assay development in which RBV-P was under the

control of an inducible promoter. Following validation of the functionality of RBV-P under Dox inducible expression, we aimed to optimize the cell line using multiple rounds of lentivirus transduction and FACS.

6.2 Results

6.2.1 Assay validation

The IFN antagonist of Rabies virus, RBV-P, blocks the IFN signalling pathway by sequestering STATs in the cytoplasm, thus preventing their nuclear accumulation. To target RBV-P, Dr Andri Vasou generated a derivative of the parental A549/pr(ISRE).GFP cell line that constitutively expresses RBV-P. To validate this cell line, we first compared GFP expression in the parental A549/pr(ISRE).GFP and A549/pr(ISRE).GFP-RBV-P cell lines in the IFN signalling reporter assay. A549/pr(ISRE).GFP.RBV-P cells do not respond to pathway activation. Regardless of IFNα concentration, GFP expression remains the same as untreated cells (Figure 6.1A). This suggests that the RBV-P expressed is functional and successfully blocks the IFN signalling pathway. To confirm this, the expression levels of the ISG, MxA, were assessed. A549/pr(ISRE).GFP cells stimulated with IFNα expressed high levels of GFP and MxA, indicating successful activation of the IFN signalling pathway (Figure 6.1B). Where RBV-P is expressed, the expression of GFP and MxA remains undetectable, irrespective of IFNα treatment. This confirms that the expression of RBV-P results in functional protein that is effective at blocking the IFN signalling pathway.

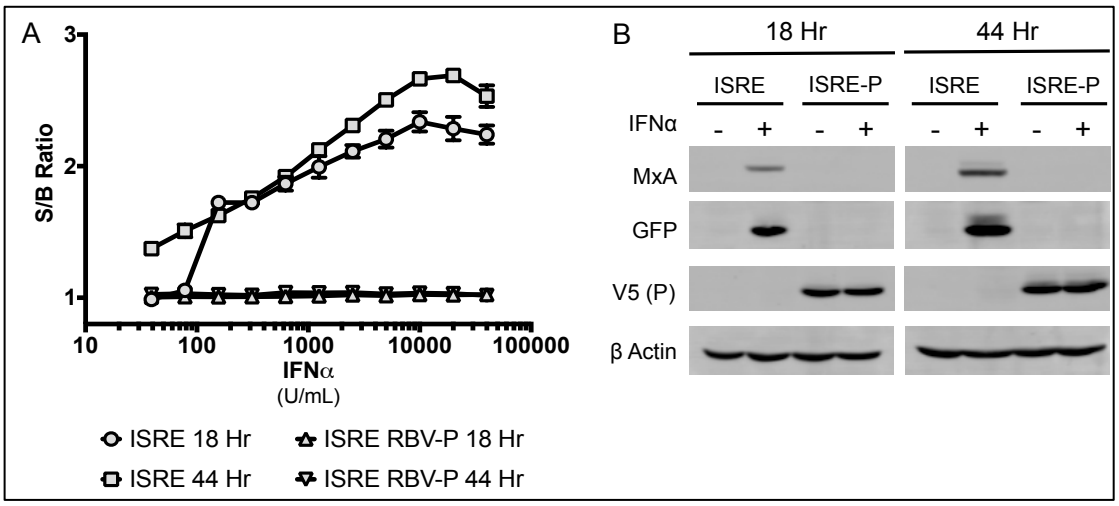

Figure 6.1: IFN signaling pathway inhibition by Rabies virus P protein
To assess the functionality of RBV-P, A549/pr.(ISRE).GFP and A549/pr.(ISRE).GFP.RBV-P cell lines were used in the IFN signalling reporter assay. (**A**) Cells were seeded and treated with a 2-fold serial dilution of IFN-α (40,000 to 39 U/mL) for 18 and 44 hours. Cells were then fixed and fluorescence measured using the Tecan Infinate Pro plate reader. Data is representative of 2 independent repeats, each conducted in quadruplicate (n=4). Error bars display StDev. (**B**) Cells were treated with or without IFNα for 18 and 44 hours. Total cell lysates were collected and subject to SDS-PAGE followed by western blot. Membranes were probed with primary antibodies raised against MxA, GFP, V5 tag and β-Actin, followed by IRDye800 and IRDye680 conjugated secondary antibodies. Data shown is representive of 2 independent repeats.

6.2.2 In-house HTS

Successful validation of the A549/pr(ISRE).GFP.RBV-P cell line demonstrated that is was suitable for use in an in-house HTS to identify small molecules that modulate the function of RBV-P. We embarked on a screening campaign using the Maybridge Screening Collection (16,000 compounds), comprising small molecules selected as appropriate starting points for drug discovery as they all comply with Lipinski's rule of 5 (Lipinski et al., 2001). As A549/pr(ISRE).GFP.RBV-P cells display the same level of fluorescence irrespective of IFNα stimulation, the parental A549/pr(ISRE).GFP cell line was included in each assay plate as an internal control, allowing us to monitor GFP expression (Figure 6.2A). As such, A549/pr(ISRE).GFP cells in column 23, untreated and activated with IFNα provide a 100% restoration control. Column

24 was left untreated and unactivated to provide a 0% restoration control. This also allows for QC parameters to be determined for each assay plate, as if the A549/pr(ISRE).GFP cell line produces results that do not pass the QC criteria, the A549/pr(ISRE).GFP.RBV-P cells are also likely to fail. A549/pr(ISRE).GFP.RBV-P cells were seeded into columns 1 to 22 and A549/pr(ISRE).GFP cells into columns 23 and 24 in clear-bottomed black 384-well plates. In column 1, A549/pr(ISRE).GFP.RBV-P cells were left untreated and unactivated, whereas in column 2, cells were untreated and activated with IFNα. This allowed us to monitor the behaviour of the A549/pr(ISRE).GFP.RBV-P cell line in the absence of test compound.

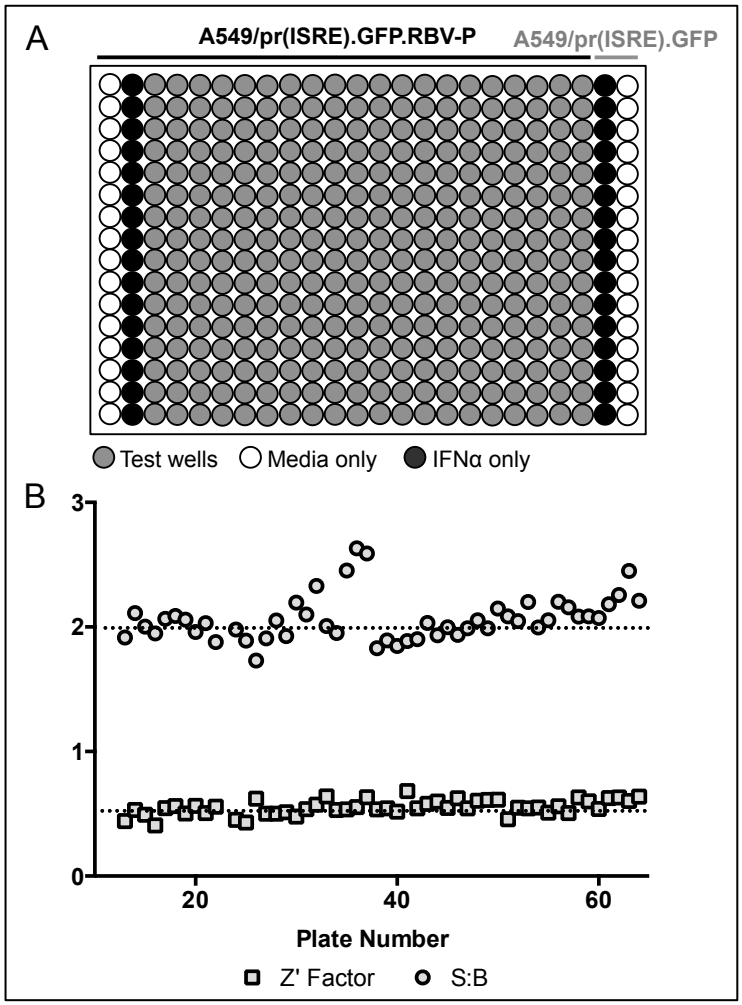

Figure 6.2: Performance of a single point HTS to identify compounds that modulate RBV-P protein function

A single point HTS using the A549/pr(ISRE).GFP and A549/pr(ISRE).GFP.RBV-P cell lines against the Mayrbidge compound library (n=16,000 compounds) at a concentration of 11.42 μM was performed. (**A**) A schematic of the 384-well plate layout used for screening; wells in columns 1-22 contain the A549/pr(ISRE).GFP.RBV-P cell line and 23-24 contain A549/pr(ISRE).GFP cells. Columns 3-22 were treated with a single test compound and IFNα, wells in columns 1 and 24 were untreated (Unactivated) and wells in columns 2 and 23 contain IFNα treated cells (Activated). (**B**) Plate metrics representing Z' Factor and S/B ratio for A549/pr(ISRE).GFP cells, plotted for each plate of the HTS compared to preset quality control standards (dotted lines).

The behaviour of the screen in terms of QC statistics was monitored both between plates and between batches. The screen was performed successfully, behaving as expected (Table 6.1). The consistency of the S/B ratio and Z' factor of A549/pr(ISRE).GFP cells (Figure 6.2B), and the percentage CV of both cell lines demonstrate that the screen was robust. Therefore, fold increase in GFP

for each compound was calculated using fluorescence, in RFU of each test well normalized to that of activated A549/pr(ISRE).GFP.RBV-P cells. Fold change in GFP expression produced a very narrow normal distribution of results for the 16,000 compounds tested, centred at 1 to 1.25-fold increase (Figure 6.3A). To verify the shape of the frequency distribution, a narrower range of fold change was also used (Figure 6.3B). A compound resulting in a fold increase in GFP expression that was 2 standard deviations away from the test well average for the plate resulted in it being considered a putative hit. From these initial selection criteria, 56 of the 16,000 compounds screened were considered putative hits yielding an initial hit rate of 0.35%. Unlike the IFN inhibitor screening campaign, the toxicity of a compound was less relevant, as a compound causing a restoration in GFP expression is unlikely to have toxic effects on the cells.

Table 6.1: Primary screen statistics of the RBV-P IFN signalling assay represented as Z' factor, S/B ratio and coefficient of variation (CV) compared to preset quality control standards. Screen statistics were generated using Microsoft Excel and the associated formulae.

		QC Approval	Primary Screen
A549/pr(ISRE).GFP	**Z' Factor**	> 0.5	0.54 ± 0.06
	S/B	> 2	2.04 ± 0.18
	Activated CV (%)	< 8	6.85 ± 1.32
	Unactivated CV (%)	< 8	1.74 ± 0.49
A549/pr(ISRE).GFP. RBV-P	**Activated CV (%)**	< 8	2.28 ±0.97
	Unactivated CV (%)	< 8	2.00 ± 0.73

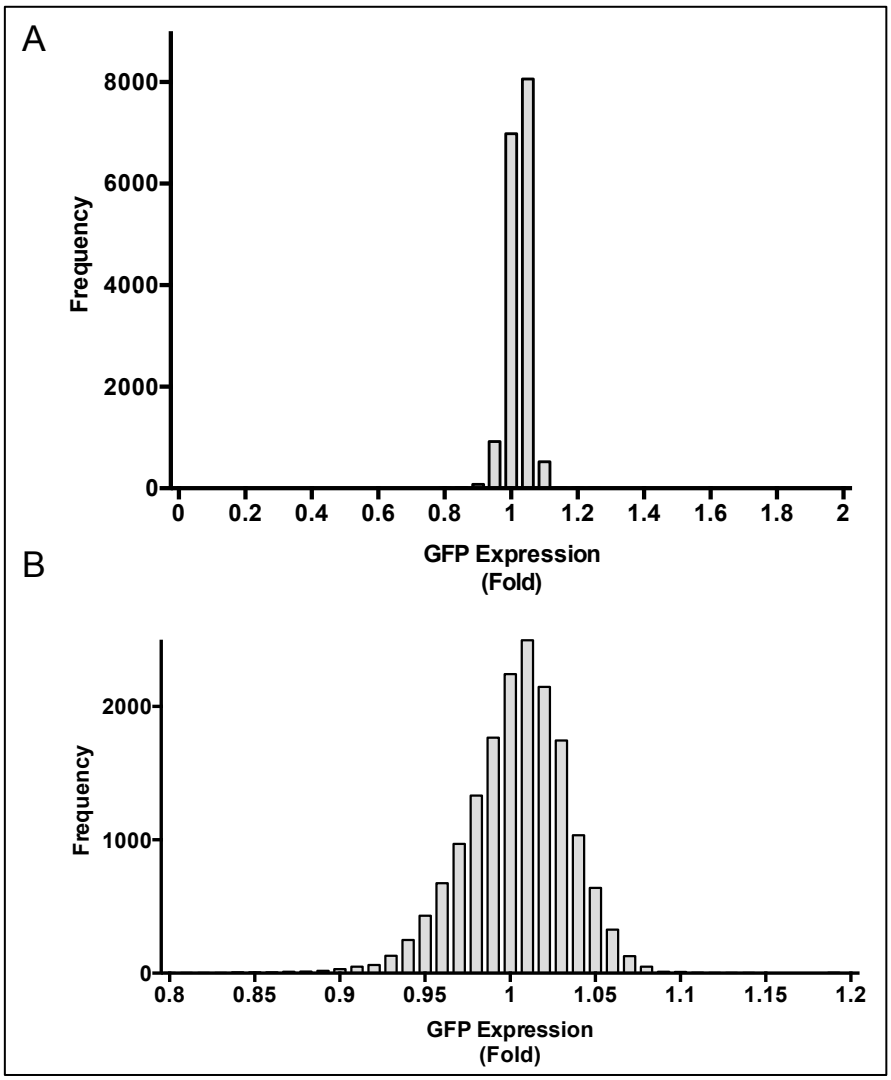

Figure 6.3: Data output from a single point HTS to identify compounds that modulate RBV-P protein function

Data obtained during the single point HTS was analyzed by comparing the fluorescence of A549/pr(ISRE).GFP.RBV-P cells to the parental A549/pr(ISRE).GFP cell line. Raw data (RFU) was converted to fold increase in GFP expression where IFNα treated (activated) A549/pr(ISRE).GFP.RBV-P cells set the background level (1). Screen output is plotted as a frequency distribution of the fold increase in GFP expression of all compounds tested (n=16,000) (**A**) and a smaller range of expression levels demonstrate the normal distribution of results (**B**).

With the aim of identifying novel compounds that modulate the function of RBV-P in the IFN signalling pathway we utilized the A549/pr(ISRE).GFP.RBV-P reporter cell line and successfully carried out an automated HTS against 16,000 test compounds, which identified 56 putative

hits. By utilizing the A549/pr(ISRE).GFP reporter cell line during screening, we were able to monitor GFP expression. The Z' factor remained above 0.5 and a S/B ratio >2 was consistently observed, reinforcing the integrity of the primary screen.

6.2.3 Dose response screening of putative hit compounds

In order to confirm the activity of putative hit compounds, determine their potency and identify any false-positive hits, we embarked on a campaign of dose-response screening. In this case, 56 putative hit compounds were tested using a 9-point 2-fold serial dilution of test compound from 25 μM to 0.1 μM. As compounds modulating RBV-P function would result in restoration of GFP expression, we needed to be aware that compounds with autofluorescent properties could be identified as hits. To identify false positives that exhibit autofluorescence, three dose-response screens were carried out. We tested each compound in the A549/pr(ISRE).GFP.RBV-P cell line (i) with and (ii) without IFNα treatment to activate the IFN signalling pathway and (iii) in A549 cells lacking a GFP reporter gene. If a compound exhibits the same levels of fluorescence in the absence of IFNα to activate IFN signalling and in a cell line without a GFP gene, they are autofluorescent and therefore false positive hits.

The 3 dose-response screens performed to further investigate the 56 putative hit compounds behaved well, with each assay achieving a percentage CV well below that of the 8% approval limit (Figure 6.4A). Unfortunately, all 56 putative hit compounds tested were either inactive or exhibited some degree of autofluorescence. As such, the compounds were categorized into 3 groups;

compounds displayed (i) high-level autofluorescence (Figure 6.4B), (ii) low-level autofluorescence (Figure 6.4C) or (iii) inactivity (Figure 6.4D).

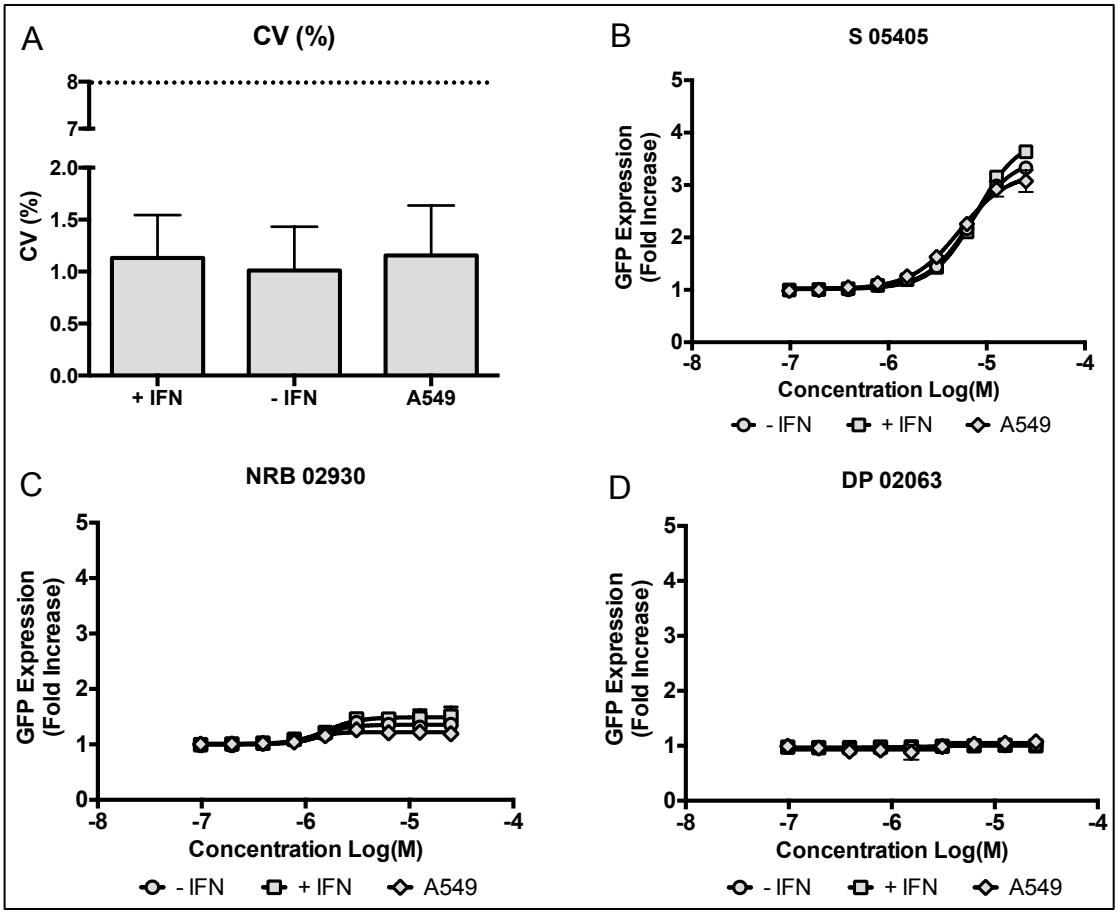

Figure 6.4: Dose-response screening of putative hit compounds using A549 cells and the A549 pr.(ISRE).GFP.RBV-P reporter assay

Compounds showing activity during primary HTS screening were subjected to secondary screening to generate a 9-point dose response curve using a 2-fold serial dilution from 25 to 0.1 μM in the A549/pr.(ISRE).GFP.RBV-P reporter cell-line with (+IFN) or without (-IFN) IFNα treatment and A549 cells lacking a GFP gene (A549). Between-plate screen statistics showing coefficient of variation (CV) of the 3 conditions used, compared to preset quality control standards (Dotted line) (**A**). Compounds were categorized as displaying high-level auto-fluorescence (**B**), low-level auto-fluorescence (**C**) or as being inactive (**D**), where a representative example of each is shown.

With the aim of identifying compounds that modulate the antagonistic activity of RBV-P in the IFN signalling pathway, diversity HTS against 16,000 compounds at 11.42 μM resulted in the identification of 56 putative hits. These compounds were taken forward to secondary dose-response screening to

determine potency. All 56 putative hit compounds displayed either no activity or autofluorescence, and as such were broadly characterized as being inactive, highly autofluorescent or exhibiting low-level autofluorescence.

6.2.4 An inducible expression assay

A limitation of the HTS performed was the constitutive expression of RBV-P. As such, to ascertain the possible S/B ratio in this assay and the level of potential restoration in GFP expression a compound could achieve, it was necessary to include the parental A549/pr(ISRE).GFP cell line in screening. Therefore, we hypothesized that using an inducible expression system to express the IFN antagonist target would produce an assay requiring a single cell line that, under different treatment conditions, would provide all the necessary controls. Primarily, working with a single cell line would greatly simplify the assay, thus decreasing the potential for variation. Additionally, comparisons of signal and variation would have increased validity if all results were derived from the same cell line. Secondly, we theorized that the high levels of RBV-P expression in the constitutive cell line were saturating the IFN signalling pathway, decreasing the potential for hit identification. To this end, we aimed to develop an assay in which RBV-P was expressed under the control of an inducible promoter. This would enable maximum and minimum levels of GFP expression to be determined and allow greater control over the expression levels of RBV-P. Successful development of such an assay would provide proof-of-principle for its application to HTS. Further to this, we aimed to optimize the assay to maximize the signal window achieved when the IFN antagonist is or is not expressed.

6.2.4.1 Assay development

To generate a derivative of the parental A549/pr(ISRE).GFP cell line, which contained the RBV-P gene under the control of a Dox inducible promoter, we utilized the LVX-Tet-One transfer vector. The expression of V5-tagged RBV-P from the newly constructed transfer vector was tested in transiently transfected 293T cells. RBV-P is clearly expressed in cells transfected with the transfer vector containing the gene and subsequently treated with Dox (Figure 6.5). The pLVX-Tet-One vector tightly regulates expression from the inducible cassette, as no RBV-P is detected in transfected cells where Dox treatment was withheld. This provided confidence that the pLVX-Tet-One-RBV-P vector was functional.

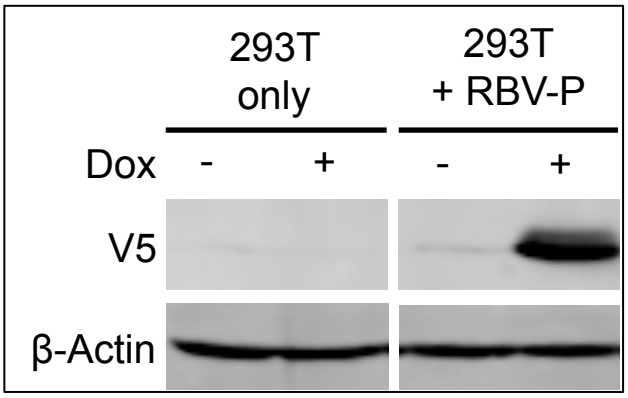

Figure 6.5: An IFN signaling reporter assay to incorporate the inducible expression of the Rabies virus phosphoprotein
A transient transfection of the pLVX-Tet-One-RBV-P plasmid was performed in 293T cells followed by treatment of the cells with Dox. Total cell lysates were subjected to separation on SDS-PAGE gel followed by western blot. Membranes were probed for N-terminally V5 tagged P protien to ensure successful expression from the plasmid.

Following verification that the pLVX-Tet-One-RBV-P plasmid was functional and resulted in the expression of V5-tagged RBV-P, lentivirus stock produced with this transfer vector was used to transduce parental A549/pr(ISRE).GFP cells, producing the A549/pr(ISRE).GFP.Tet-One-RBV-P

cell line. To verify that the Tet-One-RBV-P cassette was integrated into the A549/pr(ISRE).GFP chromosome, we amplified the RBV-P sequence from genomic DNA (gDNA) extracted from A549/pr(ISRE).GFP.Tet-One-RBV-P cells and used the pLVX-Tet-One-RBV-P plasmid as a control (Figure 6.6). The RBV-P sequence is not present in gDNA extracted from parental A549/pr(ISRE).GFP cells. This suggested that the V5-tagged RBV-P gene had been successfully integrated into the host cell chromosome.

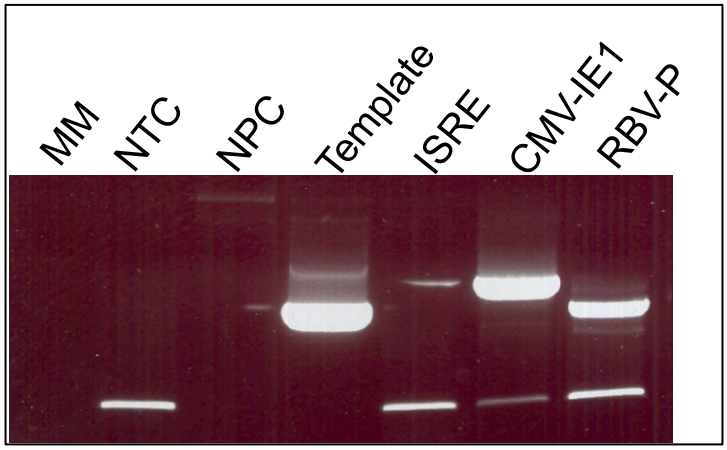

Figure 6.6: Confirmation of RBV-P gene integration into chromosomal DNA
Following transduction of the target cells with lentivirus, genomic DNA was extracted and PCR amplified to confirm chromosomal integration of the Rabies P gene. Lanes contain the following; MM – Mastermix only, NTC – No template control (primers only), NPC – No primer control (template only), Template – parental lentiviral plasmid, ISRE – parental A549/pr(ISRE).GFP cells (untransduced), CMV-IE1 – control cell line transformed using the same lentivirus technology and RBV-P – resultant A549/pr(ISRE).GFP.Tet-One-RBV-P cell line following lentiviral transduction.

Although we had confirmed that the A549/pr(ISRE).GFP.Tet-One-RBV-P cell line contained the RBV-P gene, we needed to verify that the protein was expressed and that it was functional. To achieve this, A549/pr(ISRE).GFP and A549/pr(ISRE).GFP.Tet-One-RBV-P cells were used in the IFN signalling reporter assay. Untreated A549/pr(ISRE).GFP and A549/pr(ISRE).GFP.Tet-One-RBV-P cells show no fluorescence, achieving a S/B ratio of 1 (Figure

6.7A). When treated with a 2-fold serial dilution of IFNα however, A549/pr(ISRE).GFP and A549/pr(ISRE).GFP.Tet-One-RBV-P cells exhibit comparable dose-dependent expression of GFP as a result of successful IFN signalling pathway activation. In the presence of Dox and IFNα, A549/pr(ISRE).GFP.Tet-One-RBV-P cells exhibit greatly reduced S/B ratio in comparison to cells treated only with IFNα. Although suggesting that induction of RBV-P expression by Dox treatment is successful and results in the production of functional protein, GFP expression is not completely inhibited. To investigate the effect of Dox concentration on RBV-P expression, A549/pr(ISRE).GFP and A549/pr(ISRE).GFP.Tet-One-RBV-P cells were again used in the IFN signalling assay, and treated with a 2-fold serial dilution of Dox. In the presence of IFNα, low Dox concentrations (0.03 to 0.06 μg/ml) result in comparable levels of GFP expression in A549/pr(ISRE).GFP.Tet-One-RBV-P and A549/pr(ISRE).GFP cells (Figure 6.7B). At higher Dox concentrations, GFP expression in A549/pr(ISRE).GFP.Tet-One-RBV-P cells is reduced by up to 50% compared to the parental A549/pr(ISRE).GFP cell line. However, a reduction in S/B ratio is also observed in the A549/pr(ISRE).GFP cell line as Dox concentrations increase.

Thus far, assessment of RBV-P functionality has been carried out in the IFN signalling reporter assay. We therefore endeavoured to evaluate the effect of RBV-P in the context of the IFN signalling pathway itself by comparing the levels of MxA and GFP expression in both A549/pr(ISRE).GFP and A549/pr(ISRE).GFP.Tet-One-RBV-P cell lines. Dox treatment does not impact the IFN signalling pathway as A549/pr(ISRE).GFP cells exhibit the same levels

of MxA and GFP expression irrespective of Dox (Figure 6.7C). Strong expression of MxA and GFP was also observed in IFNα treated A549/pr(ISRE).GFP.Tet-One-RBV-P cells. Upon Dox induction, RBV-P is strongly expressed, and there is a marginal decrease in GFP expression, but not MxA, which remains unaltered. This suggests that RBV-P does not successfully inhibit the IFN signalling pathway.

Variation in RBV-P expression within the cell population was investigated using immunofluorescent microscopy of A549/pr(ISRE).GFP and A549/pr(ISRE).GFP.Tet-One-RBV-P cells. Dox treatment does not impede the expression of GFP following IFNα treatment in A549/pr(ISRE).GFP cells (Figure 6.7D). In the absence of Dox, both cell lines express comparable levels of GFP, indicating successful activation of the IFN signalling pathway. A549/pr(ISRE).GFP.Tet-One-RBV-P cells treated with both Dox and IFNα show clear expression of both GFP and RBV-P. Interestingly, cells that express GFP do not appear to express RBV-P, and in cells where RBV-P is detected, GFP is not expressed. This suggests that although RBV-P is successfully expressed and functional, the cell population is heterogeneous and therefore there are cells present that do not contain the inducible RBV-P gene.

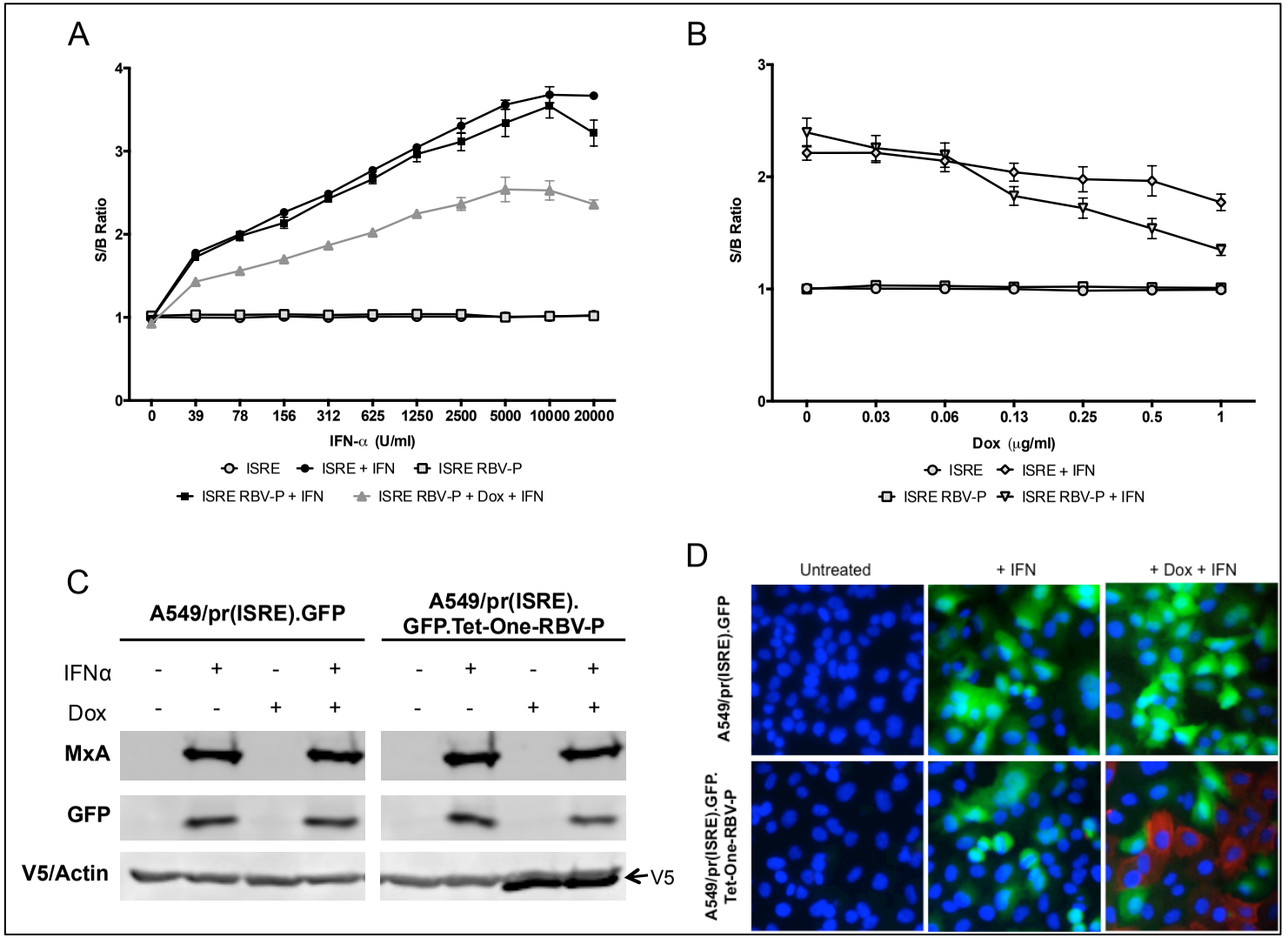

Figure 6.7: Assessing the functionality and expression of Rabies virus phosphoprotein in an inducible reporter assay.
Legend overleaf

Figure 6.7: Assessing the functionality and expression of Rabies virus phosphoprotein in an inducible reporter assay

Following generation of the A549/pr(ISRE).GFP.Tet-One-RBV-P cell line, the functionality of the expressed protein was assessed. The IFN signaling assay using A549/pr(ISRE).GFP and A549/pr(ISRE).GFP.Tet-One-RBV-P cell lines was performed using a 2-fold dilution series of IFN-α (**A**) or Dox (**B**) to assess GFP expression in the presence and absence of Rabies phosphoprotein. Cellular expression levels of GFP, Rabies phosphoprotein and the ISG MxA were assessed in the presence and absence of IFN-α and Dox by SDS-PAGE separation and western blotting of whole cell lysates (**C**). To further investigate the expression of GFP and phosphoprotein in the cell population, immunofluorescent microscopy was utilized. A549/pr(ISRE).GFP and A549/pr(ISRE).GFP.Tet-One-RBV-P cells were seeded onto coverslips and either left untreated, incubated with IFN-α only or with Dox followed by IFN-α treatment. Cells were fixed and probed with α-V5 primary and Texas red-conjugated secondary antibodies and DAPI (**D**). Data is representative of 3 independent repeats, each conducted in triplicate (n=3). Error bars display StDev.

To reduce the heterogeneity of the population and maximize RBV-P mediated inhibition of GFP expression, further optimization of the cell line was required. We aimed to increase the homogeneity of the cell line by selecting against cells that poorly express RBV-P using FACS, which can isolate thousands of cells with the same expression profiles from a given population. The levels of GFP expression in the RBV-P expressing cell line was assessed in comparison to the parental A549/pr(ISRE).GFP cell line. In the presence of RBV-P and IFNα, a fluorescent profile similar to that of unactivated A549/pr(ISRE).GFP cells should be observed, as the IFN signalling pathway would be inhibited. The GFP expression profile of the A549/pr(ISRE).GFP population exhibited a clear shift in fluorescence following IFNα treatment, where one clear peak is observed (Figure 6.8A). As expected, A549/pr(ISRE).GFP.Tet-One-RBV-P cells treated only with IFNα exhibited the same profile as the parental cell line (Figure 6.8B). When Dox treatment is included to induce RBV-P expression, there is a clear decrease in fluorescence, although a second lesser peak of high fluorescence was observed (Figure

6.8C), where a sub-population of cells exhibiting high GFP expression was present. FACS was used to select for the population of cells that, in the presence of Dox and IFNα, expressed low levels of GFP. The expression profile of these sorted cells exhibited a more defined peak of low fluorescence (Figure 6.8D). However, although reduced, the second peak of cells expressing high levels of GFP was not eradicated.

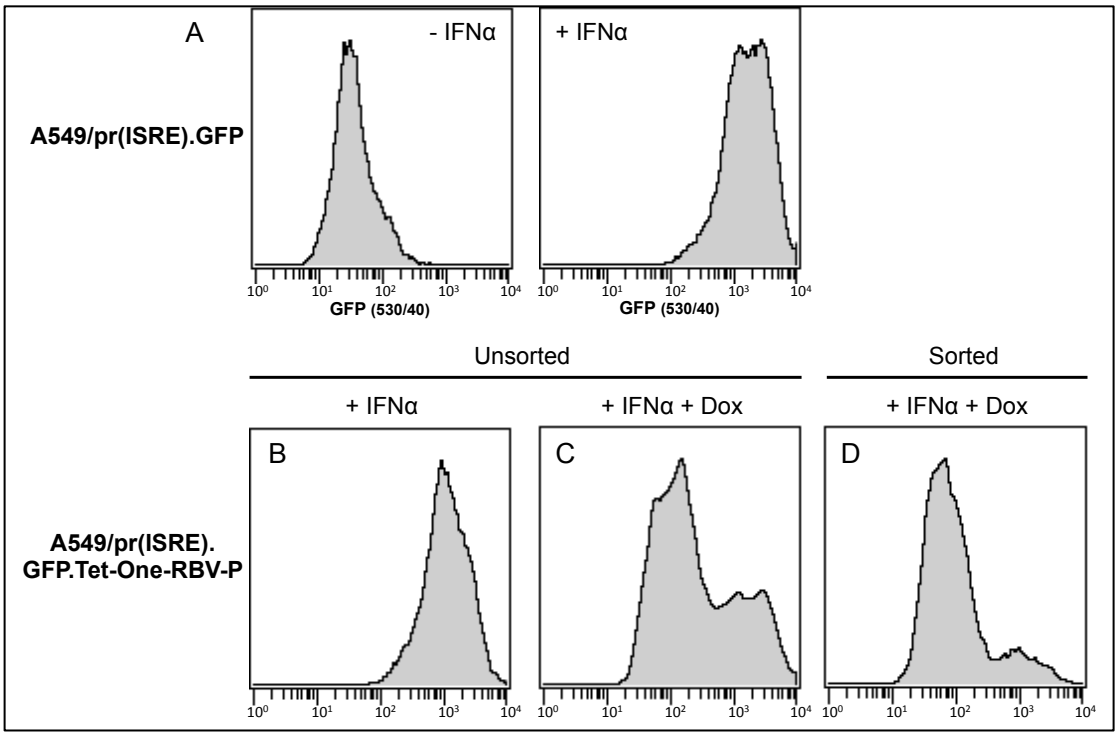

Figure 6.8: Optimization of viral IFN antagonist expression through FACS
To maximize the inhibitory effect of viral IFN antagonists on the IFN signalling pathway, we sought to optimize the fluorescent signal window through FACS. The parental A549/pr(ISRE).GFP cells were analyzed for GFP expression following incubation with and without IFNα to establish the original signal window of the IFN signaling assay (**A**). Cell lines expressing the IFN antagonist of Rabies virus (**B-D**) were then either left untreated or treated with Dox, followed by incubation with IFNα and subjected to FACS analysis on the basis of GFP fluorescence. Cells treated with both Dox and IFNα (**C**) were sorted, and those expressing the lowest levels of GFP isolated. The GFP fluorescent profile of sorted cells in the presence of Dox and IFNα is shown (**D**).

We previousliy utilized multiple rounds of lentivirus transduction to optimize the A549/pr(ISRE).GFP cell line. Therefore, we used the same approach to reduce the heterogeneity of the A549/pr(ISRE).GFP.Tet-One-RBV-P cell line, which were subjected to six rounds of lentivirus transduction. We used FACS to compare GFP expression in cells that had undergone 1 and 6 rounds of transduction. Following IFNα treatment, the GFP expression profiles observed in A549/pr(ISRE).GFP cells (Figure 6.9A), and A549/pr(ISRE).GFP.Tet-One-RBV-P cells, which had undergone 1 (Figure 6.9B) or 6 (Figure 6.9C) lentiviral transductions all exhibited high levels of GFP fluorescence, producing a single defined peak. Following Dox induction of RBV-P expression, A549/pr(ISRE).GFP.Tet-One-RBV-P cells that had been transduced once with lentivirus again displayed 2 peaks (Figure 6.9D). Interestingly, A549/pr(ISRE).GFP.Tet-One-RBV-P cells that had been transduced 6 times displayed a single peak comparable to that observed in untreated A549/pr(ISRE).GFP cells (Figure 6.9E). Only a slight shoulder was observed however, where a small number of cells continued to express high levels of GFP.

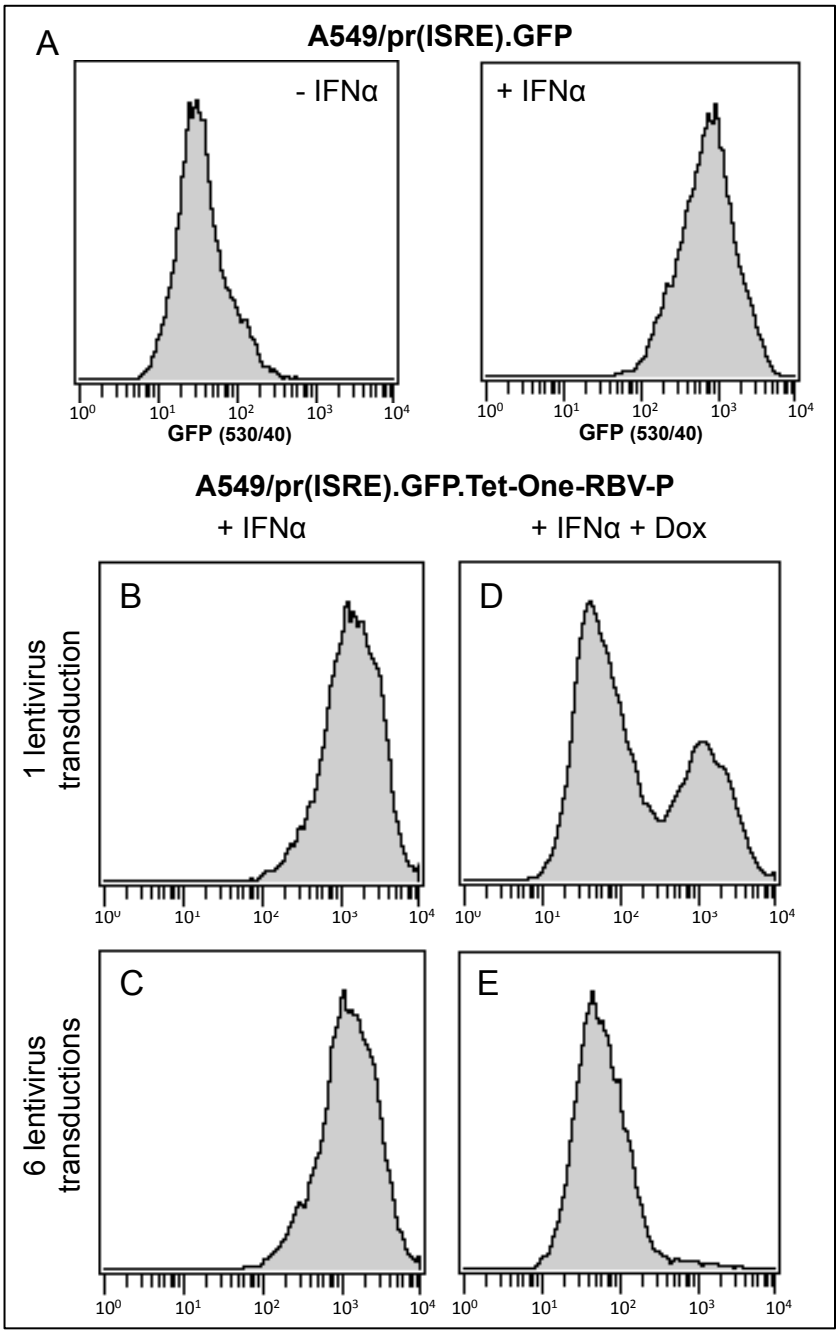

Figure 6.9: Optimization of viral IFN antagonist expression through repeated lentivirus transduction

To optimize the inhibitory effect of RBV-P expression on the IFN signalling assay, we sought to maximize the fluorescent signal window through repeated lentivirus transduction of cells. The parental reporter cell line (A549/pr(ISRE).GFP) (**A**) was transduced once or 6 times with lentivirus containing the gene encoding RBV-P. Cells were then either left untreated (**B&C**) or treated with Dox (**D&E**), followed by incubation with IFNα. All cells were subjected to FACS analysis on the basis of GFP fluorescence.

6.3 Summary

Validation of the A549/pr(ISRE).GFP.RBV-P cell line in the IFN signalling reporter assay potentiated a successful primary screening campaign against 16,000 compounds, which identified 56 putative hits. Following potency assessment of these hits through dose-response screening, all 56 compounds exhibited inactivity or some degree of autofluorescence and as such were categorized as false positive hits. With the aim of developing a less complex assay that required a single cell line for HTS, we developed a derivative of the A549/pr(ISRE).GFP cell line where the expression of RBV-P was under the control of a Dox inducible promoter. Although functional protein resulted from Dox treatment of this cell line, heterogeneous expression resulted in inconsistent levels of IFN signalling pathway inhibition within the population. Therefore, using FACS, we sought to select for cells expressing functional antagonist that was successfully blocking IFN signalling. As this did not sufficiently optimize the cell lines, they were transduced a further 5 times with lentivirus containing the inducible integration cassette. Through repeated rounds of lentivirus transduction, we have successfully optimized the A549/pr(ISRE).GFP.Tet-One-RBV-P cell line, resulting in the production of a population with more homogeneous expression of RBV-P. These results further support repeated rounds of lentivirus transduction as a method to achieve an optimal signal window, potentiating successful optimization of an assay for use in HTS.

7. Discussion

Through the use of GFP reporter cell lines, we successfully developed and validated two cell-based assays to identify modulators of the IFN induction and signalling pathways. We performed a robust phenotypic HTS with the IFN induction reporter assay, which has the potential to target all components involved in RIG-I-induced, IRF3-dependent IFN induction. The screen identified 2 compounds, StA-IFN-1 and StA-IFN-4 that specifically inhibit IFN induction. The potency of these compounds is in the micromolar range, and along with other dose-response parameters for hill slope, and maximum and minimum percentage effects, are broadly comparable to the IKKβ inhibitor, TPCA-1. We did not know the cellular targets of StA-IFN-1 and StA-IFN-4, as the assay used to identify them was phenotypic. Therefore, we instigated target deconvolution studies to characterize their target(s), which is discussed below.

7.1 Target deconvolution

Data mining and target set enrichment can be a powerful tool to direct target deconvolution. Although not crucial for clinical approval of a candidate drug (Perola, 2010), target elucidation of a hit compound can be valuable to medicinal chemistry to further optimize the compound in terms of potency and specificity. We identified that StA-IFN-1 and StA-IFN-4 were novel in their ability to inhibit IFN induction through the use of SciFinder database searches and so

extended the investigation into the cellular targets of StA-IFN-1 and StA-IFN-4 through preliminary target deconvolution studies.

7.1.1 StA-IFN-4

StA-IFN-4 is a novel inhibitor of IFN induction, as SciFinder database searches against its structure gave no indication as to the compound's mechanism of action or cellular target within the pathway. Although a patent detailing a compound with 74% similarity to StA-IFN-4 has been published, it details the use of Imidazo pyridines as GABA receptor agonists (Fang et al., 2011, Goodacre et al., 2006). To characterize the antagonistic action of StA-IFN-4 in IFN induction, we first assessed its effect on IRF3. We discovered that StA-IFN-4 is a potent inhibitor of IRF3 phosphorylation and subsequent nuclear translocation, suggesting that the cellular target of StA-IFN-4 must be at, or upstream, of IRF3 phosphorylation. To investigate this further, we assessed the affect of StA-IFN-4 on the kinases TBK1, and IKKε, which are responsible for IRF3 phosphorylation. In contrast to the IRF3 experiments conducted in A549 cells, where SeV activated IFN induction, StA-IFN-4 had no impact on the levels of IRF3, TBK1 or IKKε phosphorylation where IFN induction in HACAT cells was activated by Poly(I:C). Although the difference in cell line may have a causal role in the differences observed in pIRF3 levels, the most likely reason for this discrepancy is the nature of the inducer used to activate the IFN induction pathway. As poly(I:C) is introduced to cells in liposomes via transfection, it is a potent activator of TLR3-dependent IFN induction (Naumann et al., 2013, Matsumoto and Seya, 2008). SeV Cantell on the other hand is a well-characterized ligand of RIG-I (Martinez-Gil et al., 2013). This difference would

suggest that the cellular target of StA-IFN-4 is upstream of TRAF3 recruitment, as this is where the signalling cascades instigated by TLR3 and RIG-I converge (Figure 7.1). Therefore, StA-IFN-4 could target MAVS or RIG-I. Additionally, it could target the cellular regulators of these signalling molecules such as TRIM25, PP1α, PP1γ and TRAF 2, 5 and 6 (Gack et al., 2009, Wies et al., 2013, Liu et al., 2013). In order to strengthen the kinase data, the experiment should be repeated to test RIG-I and TRL3-dependent kinase activity in parallel, and also to include an appropriate control compound, such as the TBK1 inhibitor BX795.

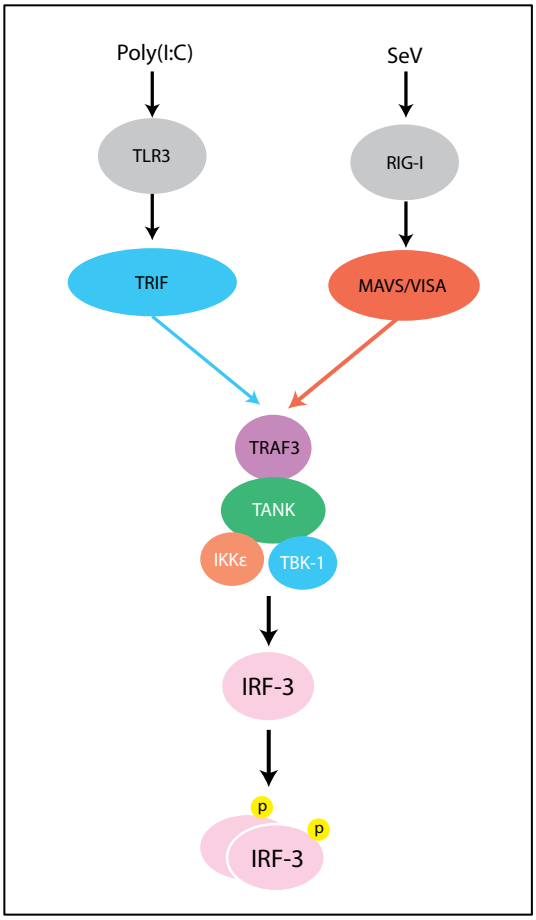

Figure 7.1: TL3- and RIG-I-dependent activation of IRF3.
Poly(I:C) induced activation of IRF3 signals through TLR3 and TRIF, whereas SeV is sensed by RIG-I, and induces IRF3 phosphorylation through MAVS. TRIF- and MAVS-dependent signalling converges at TRAF3 recruitment. (Modified from Goodbourn and Randall, 2009)

To further investigate the activity of StA-IFN-4 upstream of TRAF3, co-immunoprecipitation (IP) experiments could be utilised. As RIG-I-dependent IFN induction relies on the dephosphorylation of RIG-I by PP1 proteins, this interaction could be studied through IP of RIG-I followed by western blotting for PP1α and PP1γ (Wies et al., 2013). The levels of phosphorylated RIG-I could be examined in the presence and absence of StA-IFN-4. Furthermore, the interaction between RIG-I and its regulator TRIM25 can be detected through IP experiments (Gack et al., 2007). If, in the presence of StA-IFN-4, this interaction were undetectable, it would suggest that the target is either of these two proteins or upstream effector molecules such as PP1 proteins. Likewise, the association of MAVS with TRIM25, and MAVS CARD with RIG-I CARD could be studied using IP to assess these interactions in the presence of StA-IFN-4 (Castanier et al., 2012, Nistal-Villan et al., 2010).

As a result of this preliminary investigation into the target of StA-IFN-4, we have identified that it is acting at, or upstream, of IRF3 phosphorylation. Furthermore, it is suggested that StA-IFN-4 is acting upon RIG-I, MAVS or their modulators, as no inhibition of TLR3-dependent IFN induction was observed. Further deconvolution studies are required to verify the exact cellular target of StA-IFN-4. Other approaches that could be used for this are discussed below (7.1.3).

7.1.2 StA-IFN-1

As with StA-IFN-4, we carried out SciFinder searches of published patent and research literature relating to the structure of StA-IFN-1, which revealed that it is also a novel antagonist of IFN induction. These searches did not

highlight its specific mode of action in the IFN induction pathway. In fact, literature relating to this compound was limited to an 87% similar molecule identified as binding to BRPF1, a transcriptional scaffolding protein (Zhu and Caflisch, 2016), and a molecule with ~70% similarity patented as an inhibitor of tyrosine kinases involved in angiogenesis (Arnold et al., 2002). In contrast to StA-IFN-4, StA-IFN-1 did not potently inhibit IRF3 phosphorylation of nuclear translocation. Although we cannot rule out the possibility that StA-IFN-1 is acting downstream of IRF3 nuclear translocation, by inhibiting IFNβ enhanceosome assembly for example, we postulated that its target might be elsewhere in the IFN induction pathway. The compound with 70% similarity identified through SciFinder suggests that StA-IFN-1 may be a kinase inhibitor. It may therefore inhibit a kinase involved in the NF-κB branch of the IFN induction cascade, such as TAK-1, IKKβ or IKKα (Israel, 2010). To investigate this further, the impact of StA-IFN-1 on the nuclear translocation of NF-κB subunits could be assessed via immunofluorescent microscopy (Unterholzner et al., 2011). Additionally, as NF-κB activation is dependent on the proteasomal degradation of IκBα (Li et al., 2000), the levels of this cellular effector in the presence of StA-IFN-1 could also be monitored. More specifically, as TAK-1 is responsible for IKKβ phosphorylation in the course of NF-κB activation (Israel, 2010), monitoring the levels of pIKKβ in the presence of StA-IFN-1 could indicate that TAK-1 is the cellular target. However, it is worth noting that TAK-1 is a serine kinase, and the 70% similar compound identified is responsible for inhibiting tyrosine kinases.

As a result of this preliminary study into the cellular target of StA-IFN-1, we have identified that, unlike StA-IFN-4, it is not a potent inhibitor of IRF3 phosphorylation or nuclear translocation. Although StA-IFN-1 may inhibit downstream events in the IRF3 branch of the IFN induction cascade, it is likely that it may also target elsewhere such as the NF-κB branch of IFN induction. Structural similarity searches suggest that StA-IFN-1 may be a kinase inhibitor and as such may target TAK-1, IKKβ or IKKα. Further target deconvolution studies will be necessary to verify the exact cellular target of StA-IFN-1. The approaches that could be used for this are discussed below (7.1.3).

7.1.3 Further approaches to target deconvolution.

Although a case-independent systematic approach to target deconvolution is yet to be established, there are numerous methods that can be employed to identify the target of a hit molecule. Through the characterisation of StA-IFN-1 and StA-IFN-4 we had identified that the latter acts at or upstream of IRF3 phosphorylation. Here, we will discuss 3 methods that could be employed to elucidate the exact targets of StA-IFN-1 and StA-IFN-4.

7.1.3.1 Functional screening of IFN induction pathway effector molecules

A targeted approach that could be used to identify the cellular targets of StA-IFN-1 and StA-IFN-4 is the use of expression vectors encoding signalling factors involved in the IFN induction pathway. This approach has been successfully applied to identify the cellular targets of the viral IFN antagonists expressed by Vaccinia virus and Poxvirus. The overexpression of MAVS activates the IFN induction pathway (Unterholzner et al., 2011). In the presence

of an IFN antagonist acting at or downstream of MAVS, induction is inhibited. However, if the target of the antagonist is upstream of MAVS, induction is unimpeded. As such, this provides a convenient method for target identification and could be applied to test StA-IFN-4. If the target of StA-IFN-4 is MAVS, IFN induction would be blocked. If, on the other hand, StA-IFN-4 inhibits RIG-I or a regulator of MAVS or RIG-I, then IFN will be induced as normal. Similarly, this approach has been used to identify the cellar target of IFN antagonists acting upon the NF-κB branch of IFN induction. Ectopic overexpression of IKKα, IKKβ, and TRAF6 induce the expression of a luciferase gene under the control of an NF-κB dependent promoter (DiPerna et al., 2004). If a molecule targets downstream of these signalling molecules, luciferase expression will be impeded. This approach could also be applied to StA-IFN-1 to establish whether it targets the NF-κB branch of the IFN induction pathway and indicate its point of action. However, to date, this method has only been used to identify the target of overexpressed viral proteins following the overexpression of cellular signalling molecules. It remains to be seen therefore whether it is a suitable method for small molecule target deconvolution, as the compound may not be potent enough to interfere with the pathway to a detectable level.

7.1.3.2 Global approaches to target deconvolution

Historically, target deconvolution has involved affinity-based approaches based on immunoprecipitation and chromatography (Reviewed by Lomenick et al., 2010, Titov and Liu, 2012, McFedries et al., 2013). Although a powerful approach, it relies on the conjugation of a small molecule to an affinity tag such as biotin, or a solid matrix such as agarose, which can reduce the activity of the

compound. More recently, a technique has been developed, which negates the need for small molecule conjugation. Drug affinity responsive target stability (DARTS) suggests that when bound to a ligand (small molecule), the stability of a protein is increased, and thus is less susceptible to protease cleavage (Lomenick et al., 2010, Lomenick et al., 2009). For target deconvolution of StA-IFN-1 and StA-IFN-4, cell lysates would be incubated with or without the compounds. As the compounds were identified through a phenotypic screen where the IFN induction pathway was activated, the cell lysates should be taken from both activated and unactivated cells. Following protease digestion, protein samples are separated on 1-dimensional SDS-PAGE gels, which are then stained with Silver staining or Coomassie blue for example (Figure 7.2A). Visual analysis of the differences in the banding patterns between the two samples can identify changes in the abundance of specific proteins, which can then be identified by LC-MS. If protein levels are too low to assess visually, direct LC-MS followed by subtractive analysis of results from the two samples and other label-free approaches could be utilized (Wiener et al., 2004).

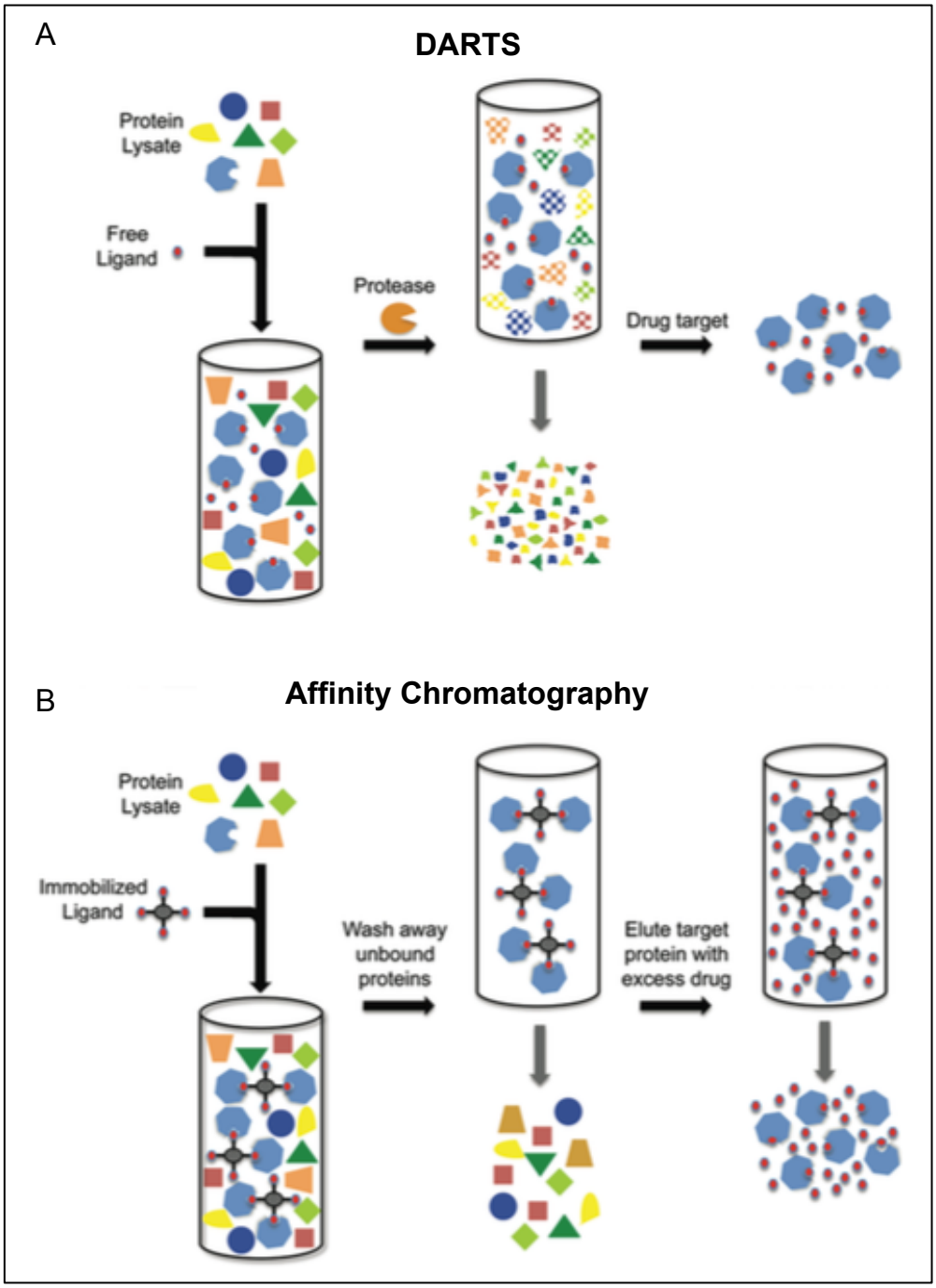

Figure 7.2: Schematic representation of two global approaches to target deconvolution. DARTS relies on the decreased protease susceptibility of the binding partner upon small molecule binding (**A**) whereas affinity chromatography-based target elucidation requires the small molecule to be immobilized in order to capture its interaction partner (**B**). (Adapted from Lomenick et al., 2010)

One of the most commonly used approaches to target elucidation is affinity-chromatography (Titov and Liu, 2012, McFedries et al., 2013). Cell lysates are incubated with affinity-tagged compound followed by standard immunoprecipitation protocols and LC-MS or western blotting to identify the bound proteins (Figure 7.2B). As these approaches rely on the conjugation of a small molecule to an affinity tag such as biotin, or a solid matrix such as agarose, these methods require considerable knowledge of SAR relating to the compound as to not ablate activity once immobilised. To determine the regions of StA-IFN-1 and StA-IFN-4 that may be amenable to conjugation, we tested molecules with high levels of similarity to the parental compounds and fragments of the structures. These experiments suggest that the acetyl indole of StA-IFN-1 and the dichloro pyridazinone of StA-IFN-4 are crucial for their inhibitory activity. Therefore, in order to use affinity chromatography to elucidate the target of StA-IFN-1, a biotin affinity-tag could be attached to the pyrazolone structure. Loss of this group did not ablate the activity of StA-IFN-1, although it was reduced. Similarly, the pyridopyrimidine group of StA-IFN-4 appeared dispensable, and as such a biotin tag could be attached here. In order to maximize the knowledge pertaining to mode of action, SAR and potentiate target elucidation, medicinal chemistry to optimize the potency of StA-IFN-1 and StA-IFN-4 may be necessary before affinity-based approaches to target deconvolution are utilized.

As a result of preliminary investigations into the targets of StA-IFN-1 and StA-IFN-4, we have identified StA-IFN-4 as a potent inhibitor of IRF3-dependent IFN induction. As such, StA-IFN-4 could be targeting RIG-I, MAVS or one of

their effector molecules. The reduced activity of StA-IFN-1 in comparison to StA-IFN-4 against IRF3 activation suggests that its cellular target may be involved in the NF-κB branch of IFN induction. To further elucidate the cellular targets of these compounds, various approaches can be employed ranging from targeted IP analysis and signalling molecule activity studies to more global methods such as DARTS and affinity chromatography.

7.2 Applications of IFN induction inhibitors

The IFN response is a potent first line of cellular defence against invading pathogens. However, aberrant activation of IFN induction and signalling either as a result of persistent viral infection or autoimmunity has potentially devastating effects. Compounds that inhibit IFN induction have potential uses in the clinic as therapeutics to treat diseases associated with dysfunction in the IFN system. Furthermore, IFN induction inhibitors could have applications in the biotechnology industry for the production of live-attenuated viral vaccines and oncolytic viruses, and could also be powerful tools for use in the research environment.

Inhibitors of the IFN response can be used to increase the growth of IFN sensitive viruses, including oncolytic viruses and live-attenuated viral vaccines (Jackson et al., 2016, Cataldi et al., 2015, Stewart et al., 2014). We assessed the replication of BunVΔNSs, a recombinant virus lacking its viral IFN antagonist (Weber et al., 2002), in the presence of StA-IFN-1 and StA-IFN-4. BunVΔNSs has a reduced plaque size in cell culture, whereas in the presence of TPCA-1, plaque size is increased by 6-fold. The plaque size in the presence of both StA-IFN-1 and StA-IFN-4 significantly increased to almost 2-fold, and although marginal, these results are promising for further compound optimization. Due to its potent inhibition of IRF3, it was interesting that only a marginal increase in plaque size was observed in the presence of StA-IFN-4. We demonstrated that the lack of potency of StA-IFN-4 on BunVΔNSs plaque size was a result of instability in tissue culture, causing a rapid loss of compound activity. Therefore, to increase the stability of StA-IFN-4 medicinal chemistry is required. BunV is

sensed by RIG-I and has also been shown to activate PKR, which induces NF-κB and IRF1-dependent pathways and also has direct antiviral activity (Streitenfeld et al., 2003). Therefore, to further assess StA-IFN-1 and StA-IFN-4 for their ability to increase the growth of IFN sensitive viruses, plaque assays using viruses known to activate specific PRRs, such as IAV PR8 (Hale et al., 2008), could be used.

To the best of our knowledge, there are no known chemical antagonists of MAVS, and only one chemical modulator of RIG-I activity. Bufalin, an FDA approved cardiac glycoside, appears to inhibit the ATPase activity of RIG-I by increasing the intracellular sodium concentration (Ye et al., 2011). If StA-IFN-4 specifically inhibits RIG-I or MAVS, it has various potential uses. For example, it could provide a straightforward method to transiently inhibit RIG-I or MAVS in a research environment. To achieve knockdown such as this currently, the use of expensive reagents such as short-interfering RNA, or the lengthy development of stable cell lines is required (Jiang et al., 2012, Schmolke et al., 2012, Spengler et al., 2015). Furthermore, knowledge regarding the mode of binding of a molecule specific to RIG-I could be used to highlight the mechanistic differences between RLRs. Targeting of RIG-I, MAVS or any their regulatory molecules such as TRIM25, PP1α or PP1γ, suggests that StA-IFN-4 could be a clinical candidate for use in the treatment of diseases associated with RLR dysfunction such as AGS, SMS and SLE (Buers et al., 2016, Rice et al., 2014, del Toro Duany et al., 2015, Miner and Diamond, 2014).

As the precise target of StA-IFN-1 remains unknown, we can only speculate as to its specific application. If it does act in the NF-κB branch of IFN

induction, StA-IFN-1 has potential applications in the treatment of cancers and the aforementioned production of IFN sensitive viruses. Due to the involvement of NF-κB in the regulation of many cellular pathways, it has been the target of many drug discovery programs, and as such hundreds of modulators have already been identified (Ahmad et al., 2013, Herrington et al., 2015, Gilmore and Herscovitch, 2006).

The potential uses of IFN induction inhibitors are numerous, ranging from clinical treatments to basic research tools. StA-IFN-1 and StA-IFN-4 although specifically inhibiting IFN induction require further characterization and medicinal chemistry to improve their potency before they can be considered NMEs.

7.3 Design and optimization of cell-based assays for HTS

The use of cell-based assays in HTS has increased dramatically in recent years due to their potential to indicate more biologically relevant characteristics of test compounds (Clemons et al., 2014). Due to the sensitivity of cells and the potential for variation within a population, optimization is crucial for an assay to be successful. Below, we will discuss some of the aspects involved in the successful development of phenotypic and targeted cell-based assays.

7.3.1 Phenotypic assays

We successfully used a phenotypic fluorescent assay in HTS following the development of a reporter cell-line to monitor IFN induction. The IFN induction assay performed exceptionally following optimization achieving Z' factors of >0.6 and S/B ratios >3, which are above pre-set industry standards (Iversen et al., 2006, Zhang, 1999). Although a S/B ratio of 3 may be regarded as relatively low in comparison to other reporter systems such as luciferase, where the S/B ratio can range from 79 to >11,000 (Guo et al., 2014, Martínez-Gil et al., 2012, Patel et al., 2012), the Z' factors achieved by these assays ranged between 0.3 and 0.7. Therefore, the excellent Z' factors achieved by our assays are comparable to those of reporter assays associated with a large signal window.

Typically, a high S/B ratio giving a larger signal window is advantageous to HTS and although an accurate and sensitive method (Zhang et al., 2012), the

use of enzyme reporters such as firefly and Renilla luciferase have been associated with compound interference from screening libraries (Auld et al., 2008). Therefore, we believed that the use of GFP as a reporter would give rise to a more robust assay, less amenable to off-target compound interference. Although there remains the possibility that compounds in screening libraries could interfere with the generation of a fluorescent reporter signal, no detection method is capable of differentiating between real activity and interference (Gribbon and Sewing, 2003). That being said, the inclusion of a secondary reference signal could increase the robustness of an assay (Cali et al., 2008). For example, we could have included a constitutively expressed fluorophore in the IFN induction assay. The expression of mCherry for example, with excitation and emission wavelengths distinct from the GFP signal being assayed (Kremers et al., 2011), would potentiate the differentiation between test and control signals. This could reduce the false positive hit rate of the primary diversity screen by identifying compounds that interfere with signal generation, such as translational inhibitors, as both signals would be affected. Nevertheless, the IFN induction assay was optimized and validated as suitable for use in an HTS, where we successfully identified two specific inhibitors.

We also validated the IFN signalling assay for use in HTS following cell line optimization and assay development. Prior to optimization, both the IFN induction and signalling assays had comparable levels of variability, although the initial S/B ratio of the A549/pr(ISRE).GFP cell line was below 2. Therefore, we sought to increase the signal window of the IFN signalling assay, theorizing that repeated rounds of lentivirus transduction could achieve this. Different

methods for the titration of lentivirus stock show inconsistency (Geraerts et al., 2006), and as such they cannot be quantified in the same way as infectious viruses. The same principle of multiplicity of infection (MOI) can be applied, where plaque-forming units is substituted for transducing units. Working on the principle that one lentivirus results in one integration event per cell, applying the Poisson distribution suggests that only 62% of cells will be successfully transduced from an MOI of 1 (Fields et al., 2013). By increasing the rounds of lentivirus transduction, we effectively increase the MOI. Thus, following multiple rounds of transduction, each cell in the population should have at least one integration event. For the A549/pr(ISRE).GFP cell line, multiple rounds of lentiviral transduction followed by FACS significantly increased S/B ratio, potentiating the successful optimization and validation of the IFN signalling assay for HTS. Due to the excellent performance of the IFN induction and signalling assays in HTS, they have the potential to be used in HCS, where multiplexing of assays is potentiated (Nichols, 2006). As such, the IFN induction and signalling assays could be combined into one cell line. To achieve this, one of the promoters would need to drive the expression of a distinct fluorophore, such as the aforementioned mCherry. HCS is a powerful approach and multiplexing the IFN induction and signalling assays potentiates the screening of a compound library against both assays simultaneously, immediately allowing the identification of compounds acting specifically upon either pathway.

Phenotypic assays are powerful tools for use in HTS as they not only indicate the biological activity of a test compound, but also, as we have demonstrated, have the potential to identify compounds with distinct targets.

The IFN induction assay was successfully optimized and validated for use in an HTS where it identified two specific inhibitors. The IFN signalling assay was also optimized and validated as suitable for HTS, and as such could be used to identify modulators of the IFN signalling pathway. Both GFP reporter assays produce excellent Z' factors comparable to other reporter assays such as luciferase-based systems.

7.3.2 Targeted cell-based assays

As the IFN induction and signalling assays were successfully optimized and validated for use in HTS, we postulated that we could expand the assays and develop a platform to target viral IFN antagonists. We developed and validated an assay using the IFN signalling reporter cell line, in which RBV-P was constitutively expressed. The function of RBV-P antagonising IFN signalling results in the inhibition of GFP expression, and therefore, a compound that modulates RBV-P function will result in a restoration of GFP signal. We successfully performed an in-house HTS of 16,000 small molecules that performed well and remained robust throughout, identifying 56 putative hit compounds that resulted in an increase in GFP signal. During dose-response screening, all putative hits were eliminated as they either displayed inactivity or autofluorescence. As the A549/pr(ISRE).GFP.RBV-P cell line expresses high levels of RBV-P, we hypothesised that it may be saturating the IFN signalling pathway. Thus, a small molecule at a relatively low concentration of 11.42 μM may simply not be potent enough to modulate the protein-protein interaction of RBV-P with STATs (Kuenemann et al., 2016, Bakail and Ochsenbein, 2016). Therefore, the case may be that RBV-P is simply not a druggable target. If the

binding of RBV-P to STAT molecules is very rapid and highly stable, a small molecule may not be able to disrupt the interaction. A possible solution to this would be to alter the order in which the assay is performed. RBV-P binds only to phosphorylated STAT molecules (Wiltzer et al., 2014, Brzozka et al., 2006), which occurs only upon IFN signalling pathway activation. Therefore, compound treatment of the cells prior to IFNα treatment would allow for their binding to RBV-P and blockage of the interaction with phosphorylated STAT upon activation of IFN signalling. As small molecule compound libraries require constant upkeep and maintenance, an additional consideration as to why no modulators of RBV-P function were identified may be the size and age of the library used. The Maybridge library at just 16,000 compounds has undergone countless freeze-thaw cycles, which could expedite compound loss. A study by Kozikowski *et al* demonstrated that although not due to considerable levels of compound degradation, loss was observed following just 5 freeze-thaw cycles, most probably due to compound precipitation (Kozikowski et al., 2003).

To simplify the assay to require only one cell line, and have greater control over the levels of RBV-P expressed, we further developed this assay format with a derivative of the IFN signalling reporter cell line where RBV-P gene expression is under the control of a Dox inducible promoter. Initially, the expressed viral protein did not fully block the IFN signalling pathway. We hypothesized that this was due to inconsistent levels of RBV-P expression within the cell population, and confirmed this through immunofluorescent microscopy illustrating that RBV-P and GFP expression were indeed heterogeneous and appeared mutually exclusive. Additionally, the

corresponding FACS profile of this cell line showed 2 distinct sub-populations. As with the parental A549/pr(ISRE).GFP cell line, we successfully optimized the inducible expression cell line through multiple rounds of lentivirus transduction followed by FACS. Although requiring further characterization, we have optimized the inducible RBV-P assay, and demonstrated a straightforward method by which an HTS appropriate assay, targeting a specific viral protein, can be developed. Furthermore, the inducible assay format can be applied to a variety of viral IFN antagonists, including those of high containment category viruses, as whole, live virus is not required. This may be a more favourable approach for pharmaceutical companies to adopt, as it does not require expensive high containment facilities. An interesting option for further expansion of the assay would be through the use of a dual reporter cell line as previously discussed, where the IFNβ promoter drives the expression of GFP and another fluorophore is under the control of the MxA promoter. Thus, when used in HTS, it could potentiate the simultaneous detection of hit compounds that modulate the IFN induction or signalling functions of a viral IFN antagonist.

We have successfully expanded the IFN signalling assay to develop an screening platform to target viral IFN antagonists, which could identify compounds with potential uses as antiviral drugs. Through the use of an inducible expression system and multiple rounds of lentivirus transduction, we have demonstrated the flexibility of this assay format, and highlighted approaches that potentiate successful assay optimization.

7.4 Concluding remarks

With the primary aim of developing a fluorescent-based phenotypic assay for use in HTS to identify novel modulators of the IFN response, we instigated a campaign of optimization of two reporter assays to monitor the activity of the IFN induction and IFN signalling pathways. Through successful optimization and validation, the IFN induction assay was used in an HTS against 15,667 small molecules that culminated in the identification of 2 specific IFN induction inhibitors. Although not inconsequential, StA-IFN-1 is arguably less interesting in comparison to StA-IFN-4, which appears to target the IFN induction pathway upstream of TRAF3, potentially directed against RIG-I or MAVS. Both compounds warrant further investigation and chemical optimization to improve potency and pinpoint their mode of action. Nevertheless, they provide an exciting starting point for the development of novel therapeutics against RLR-associated diseases and as chemical tools to expedite the growth of live-attenuated viral vaccines and oncolytic viruses.

We also demonstrate the optimization of the signal window of a fluorescent assay through the use of multiple lentiviral transduction and FACS. Additionally, we extended the IFN signalling assay to incorporate the expression of the RBV IFN antagonist and demonstrate the development of a target-specific fluorescent assay through the use if an inducible expression system. This assay can be easily manipulated to target the IFN antagonists of different clinically relevant viruses, including those typically requiring high containment facilities.

References

ABATE, D. A., WATANABE, S. & MOCARSKI, E. S. 2004. Major human cytomegalovirus structural protein pp65 (ppUL83) prevents interferon response factor 3 activation in the interferon response. *J Virol,* 78**,** 10995-1006.

AGEE, A. & CARTER, D. 2009. Whole-organism screening: plants. *Cell-Based Assays for High-Throughput Screening: Methods and Protocols***,** 77-95.

AHMAD, A., BIERSACK, B., LI, Y., KONG, D., BAO, B., SCHOBERT, R., B. PADHYE, S. & H. SARKAR, F. 2013. Targeted Regulation of PI3K/Akt/mTOR/NF-κB Signaling by Indole Compounds and their Derivatives: Mechanistic Details and Biological Implications for Cancer Therapy. *Anti-Cancer Agents in Medicinal Chemistry- Anti-Cancer Agents),* 13**,** 1002-1013.

AHN, J. & BARBER, G. N. 2014. Self-DNA, STING-dependent signaling and the origins of autoinflammatory disease. *Curr Opin Immunol,* 31**,** 121-6.

AKIRA, S. 2011. Innate immunity and adjuvants. *Philosophical transactions of the Royal Society of London. Series B, Biological sciences,* 366**,** 2748-55.

AN, W. F. & TOLLIDAY, N. 2010. Cell-based assays for high-throughput screening. *Molecular biotechnology,* 45**,** 180-186.

ANDERSON, A. C. 2003. The Process of Structure-Based Drug Design. *Chemistry & Biology,* 10**,** 787-797.

ANDREJEVA, J., NORSTED, H., HABJAN, M., THIEL, V., GOODBOURN, S. & RANDALL, R. E. 2013. ISG56/IFIT1 is primarily responsible for interferon-induced changes to patterns of parainfluenza virus type 5 transcription and protein synthesis. *J Gen Virol,* 94**,** 59-68.

ARNOLD, L., BERLANGA, J. M. C., CALDERWOOD, D. J., FERNANDEZ, I. F., MOSET, M. M. & RAFFERTY, P. 2002. *2-pyrazolin-5-ones as tyrosine kinase inhibitors*.

ASEFA, B., KLARMANN, K. D., COPELAND, N. G., GILBERT, D. J., JENKINS, N. A. & KELLER, J. R. 2004. The interferon-inducible p200 family of proteins: a perspective on their roles in cell cycle regulation and differentiation. *Blood Cells, Molecules, and Diseases,* 32**,** 155-167.

AULD, D. S., SOUTHALL, N. T., JADHAV, A., JOHNSON, R. L., DILLER, D. J., SIMEONOV, A., AUSTIN, C. P. & INGLESE, J. 2008. Characterization of chemical libraries for luciferase inhibitory activity. *J Med Chem,* 51**,** 2372-86.

BACH, E. A., AGUET, M. & SCHREIBER, R. D. 1997. The IFNγ receptor: a paradigm for cytokine receptor signaling. *Annual review of immunology,* 15**,** 563-591.

BAKAIL, M. & OCHSENBEIN, F. 2016. Targeting protein–protein interactions, a wide open field for drug design. *Comptes Rendus Chimie,* 19**,** 19-27.

BANNINGER, G. & REICH, N. C. 2004. STAT2 nuclear trafficking. *J Biol Chem,* 279**,** 39199-206.

BANSAL, A. T. & BARNES, M. R. 2008. Genomics in drug discovery: the best things come to those who wait. *Current opinion in drug discovery & development,* 11**,** 303-311.

BARAGANA, B., HALLYBURTON, I., LEE, M. C., NORCROSS, N. R., GRIMALDI, R., OTTO, T. D., PROTO, W. R., BLAGBOROUGH, A. M., MEISTER, S., WIRJANATA, G., RUECKER, A., UPTON, L. M., ABRAHAM, T. S., ALMEIDA, M. J., PRADHAN, A., PORZELLE, A., MARTINEZ, M. S., BOLSCHER, J. M., WOODLAND, A., NORVAL, S., ZUCCOTTO, F., THOMAS, J., SIMEONS, F., STOJANOVSKI, L., OSUNA-CABELLO, M., BROCK, P. M., CHURCHER, T. S., SALA, K. A., ZAKUTANSKY, S. E., JIMENEZ-DIAZ, M. B., SANZ, L. M., RILEY, J., BASAK, R., CAMPBELL, M., AVERY, V. M., SAUERWEIN, R. W., DECHERING, K. J., NOVIYANTI, R., CAMPO, B., FREARSON, J. A., ANGULO-BARTUREN, I., FERRER-BAZAGA, S., GAMO, F. J., WYATT, P. G., LEROY, D., SIEGL, P., DELVES, M. J., KYLE, D. E., WITTLIN, S., MARFURT, J., PRICE, R. N., SINDEN, R. E., WINZELER, E. A., CHARMAN, S. A., BEBREVSKA, L., GRAY, D. W., CAMPBELL, S., FAIRLAMB, A. H., WILLIS, P. A., RAYNER, J. C., FIDOCK, D. A., READ, K. D. & GILBERT, I. H. 2015. A novel multiple-stage antimalarial agent that inhibits protein synthesis. *Nature,* 522**,** 315-20.

BARANEK, T., MANH, T. P., ALEXANDRE, Y., MAQBOOL, M. A., CABEZA, J. Z., TOMASELLO, E., CROZAT, K., BESSOU, G., ZUCCHINI, N., ROBBINS, S. H., VIVIER, E., KALINKE, U., FERRIER, P. & DALOD, M. 2012. Differential responses of

immune cells to type I interferon contribute to host resistance to viral infection. *Cell host & microbe,* 12**,** 571-84.
BARKER, A., KETTLE, J. G., NOWAK, T. & PEASE, J. E. 2013. Expanding medicinal chemistry space. *Drug Discov Today,* 18**,** 298-304.
BARRA, N. G., GILLGRASS, A. & ASHKAR, A. A. 2010. Effective control of viral infections by the adaptive immune system requires assistance from innate immunity. *Expert review of vaccines,* 9**,** 1143-1147.
BASU, D., WALKIEWICZ, M. P., FRIEMAN, M., BARIC, R. S., AUBLE, D. T. & ENGEL, D. A. 2009. Novel influenza virus NS1 antagonists block replication and restore innate immune function. *Journal of virology,* 83**,** 1881-1891.
BAUER, R. A., WURST, J. M. & TAN, D. S. 2010. Expanding the range of 'druggable' targets with natural product-based libraries: an academic perspective. *Curr Opin Chem Biol,* 14**,** 308-14.
BAUM, A., SACHIDANANDAM, R. & GARCÍA-SASTRE, A. 2010. Preference of RIG-I for short viral RNA molecules in infected cells revealed by next-generation sequencing. *Proceedings of the National Academy of Sciences,* 107**,** 16303-16308.
BAUM, R. M. 1994. Combinatorial Approaches Provide Fresh Leads for Medicinal Chemistry. *Chemical & Engineering News Archive,* 72**,** 20-26.
BECK, V., PFITSCHER, A. & JUNGBAUER, A. 2005. GFP-reporter for a high throughput assay to monitor estrogenic compounds. *Journal of biochemical and biophysical methods,* 64**,** 19-37.
BEDARD, K. M., WANG, M. L., PROLL, S. C., LOO, Y. M., KATZE, M. G., GALE, M., JR. & IADONATO, S. P. 2012. Isoflavone agonists of IRF-3 dependent signaling have antiviral activity against RNA viruses. *J Virol,* 86**,** 7334-44.
BERKE, I. C., LI, Y. & MODIS, Y. 2013. Structural basis of innate immune recognition of viral RNA. *Cellular microbiology,* 15**,** 386-94.
BITKO, V., MUSIYENKO, A., BAYFIELD, M. A., MARAIA, R. J. & BARIK, S. 2008. Cellular La protein shields nonsegmented negative-strand RNA viral leader RNA from RIG-I and enhances virus growth by diverse mechanisms. *Journal of virology,* 82**,** 7977-7987.
BLONDEL, D., REGAD, T., POISSON, N., PAVIE, B., HARPER, F., PANDOLFI, P. P., DE THE, H. & CHELBI-ALIX, M. K. 2002. Rabies virus P and small P products interact directly with PML and reorganize PML nuclear bodies. *Oncogene,* 21**,** 7957-7970.
BOEHM, U., KLAMP, T., GROOT, M. & HOWARD, J. 1997. Cellular responses to interferon-γ. *Annual review of immunology,* 15**,** 749-795.
BOLLAG, G., HIRTH, P., TSAI, J., ZHANG, J., IBRAHIM, P. N., CHO, H., SPEVAK, W., ZHANG, C., ZHANG, Y. & HABETS, G. 2010. Clinical efficacy of a RAF inhibitor needs broad target blockade in BRAF-mutant melanoma. *Nature,* 467**,** 596-599.
BONJARDIM, C. A., FERREIRA, P. C. & KROON, E. G. 2009. Interferons: signaling, antiviral and viral evasion. *Immunology letters,* 122**,** 1-11.
BOPPANA, K., DUBEY, P., JAGARLAPUDI, S. A., VADIVELAN, S. & RAMBABU, G. 2009. Knowledge based identification of MAO-B selective inhibitors using pharmacophore and structure based virtual screening models. *European journal of medicinal chemistry,* 44**,** 3584-3590.
BRIDLE, B. W., CHEN, L., LEMAY, C. G., DIALLO, J. S., POL, J., NGUYEN, A., CAPRETTA, A., HE, R., BRAMSON, J. L., BELL, J. C., LICHTY, B. D. & WAN, Y. 2013. HDAC Inhibition Suppresses Primary Immune Responses, Enhances Secondary Immune Responses, and Abrogates Autoimmunity During Tumor Immunotherapy. *Mol Ther*.
BROZ, P. & MONACK, D. M. 2013. Newly described pattern recognition receptors team up against intracellular pathogens. *Nat Rev Immunol,* 13**,** 551-65.
BRZOZKA, K., FINKE, S. & CONZELMANN, K. K. 2006. Inhibition of interferon signaling by rabies virus phosphoprotein P: activation-dependent binding of STAT1 and STAT2. *J Virol,* 80**,** 2675-83.
BUERS, I., NITSCHKE, Y. & RUTSCH, F. 2016. Novel interferonopathies associated with mutations in RIG-I like receptors. *Cytokine & growth factor reviews,* 29**,** 101-107.
BURDETTE, D. L., MONROE, K. M., SOTELO-TROHA, K., IWIG, J. S., ECKERT, B., HYODO, M., HAYAKAWA, Y. & VANCE, R. E. 2011. STING is a direct innate immune sensor of cyclic di-GMP. *Nature,* 478**,** 515-8.

BURDINE, L. & KODADEK, T. 2004. Target identification in chemical genetics: the (often) missing link. *Chemistry & biology,* 11**,** 593-597.

CAIGNARD, G., BOURAÏ, M., JACOB, Y., TANGY, F. & VIDALAIN, P.-O. 2009. Inhibition of IFN-α/β signaling by two discrete peptides within measles virus V protein that specifically bind STAT1 and STAT2. *Virology,* 383**,** 112-120.

CAIGNARD, G., GUERBOIS, M., LABERNARDIÈRE, J.-L., JACOB, Y., JONES, L. M., I-MAP, T. I. M. P., WILD, F., TANGY, F. & VIDALAIN, P.-O. 2007. Measles virus V protein blocks Jak1-mediated phosphorylation of STAT1 to escape IFN-α/β signaling. *Virology,* 368**,** 351-362.

CALI, J. J., NILES, A., VALLEY, M. P., O'BRIEN, M. A., RISS, T. L. & SHULTZ, J. 2008. Bioluminescent assays for ADMET. *Expert opinion on drug metabolism & toxicology,* 4**,** 103-120.

CARAGLIA, M., DICITORE, A., MARRA, M., CASTIGLIONI, S., PERSANI, L., SPERLONGANO, P., TAGLIAFERRI, P., ABBRUZZESE, A. & VITALE, G. 2013. Type I interferons: ancient peptides with still under-discovered anti-cancer properties. *Protein and peptide letters,* 20**,** 412-423.

CÁRDENAS, W. B., LOO, Y.-M., GALE, M., HARTMAN, A. L., KIMBERLIN, C. R., MARTÍNEZ-SOBRIDO, L., SAPHIRE, E. O. & BASLER, C. F. 2006. Ebola virus VP35 protein binds double-stranded RNA and inhibits alpha/beta interferon production induced by RIG-I signaling. *Journal of virology,* 80**,** 5168-5178.

CASTANIER, C., ZEMIRLI, N., PORTIER, A., GARCIN, D., BIDÈRE, N., VAZQUEZ, A. & ARNOULT, D. 2012. MAVS ubiquitination by the E3 ligase TRIM25 and degradation by the proteasome is involved in type I interferon production after activation of the antiviral RIG-I-like receptors. *BMC biology,* 10**,** 1.

CATALDI, M., SHAH, N. R., FELT, S. A. & GRDZELISHVILI, V. Z. 2015. Breaking resistance of pancreatic cancer cells to an attenuated vesicular stomatitis virus through a novel activity of IKK inhibitor TPCA-1. *Virology,* 485**,** 340-354.

CHA, L., BERRY, C. M., NOLAN, D., CASTLEY, A., FERNANDEZ, S. & FRENCH, M. A. 2014. Interferon-alpha, immune activation and immune dysfunction in treated HIV infection. *Clin Transl Immunology,* 3**,** e10.

CHAMBERS, C., SMITH, F., WILLIAMS, C., MARCOS, S., LIU, Z., HAYTER, P., CIARAMELLA, G., KEIGHLEY, W., GRIBBON, P. & SEWING, A. 2003. Measuring intracellular calcium fluxes in high throughput mode. *Combinatorial chemistry & high throughput screening,* 6**,** 355-362.

CHARLAFTIS, N., FEARON, D. T., SCHOENEMEYER, A. & MORLEY, P. J. 2012. siRNA high-throughput kinase library screen identifies protein kinase, DNA-activated catalytic polypeptide to play a role in MyD88-induced IFNA2 activation and IL-8 secretion. *Biotechnol Appl Biochem,* 59**,** 6-14.

CHEN, B., ZONG, Q., CIBOTTI, R., MORRIS, C., CASTANEDA, J., NAIMAN, B., LIU, D., GLODEK, A., SIMS, G. P., HERBST, R., HORRIGAN, S. K., KIENER, P. A., SOPPET, D., COYLE, A. J. & AUDOLY, L. 2008. Genomic-based high throughput screening identifies small molecules that differentially inhibit the antiviral and immunomodulatory effects of IFN-alpha. *Mol Med,* 14**,** 374-82.

CHEN, J., BAIG, E. & FISH, E. N. 2004. Diversity and relatedness among the type I interferons. *Journal of interferon & cytokine research,* 24**,** 687-698.

CHEN, S., SHORT, J. A., YOUNG, D. F., KILLIP, M. J., SCHNEIDER, M., GOODBOURN, S. & RANDALL, R. E. 2010. Heterocellular induction of interferon by negative-sense RNA viruses. *Virology,* 407**,** 247-55.

CHIN, Y. E., KITAGAWA, M., KUIDA, K., FLAVELL, R. A. & FU, X.-Y. 1997. Activation of the STAT signaling pathway can cause expression of caspase 1 and apoptosis. *Molecular and cellular biology,* 17**,** 5328-5337.

CLARK, K., PLATER, L., PEGGIE, M. & COHEN, P. 2009. Use of the pharmacological inhibitor BX795 to study the regulation and physiological roles of TBK1 and IKKε: A distinct upstream kinase mediates ser172 phosphorylation and activation. *Journal of Biological Chemistry*.

CLEMONS, P. A., TOLLIDAY, N. J. & WAGNER, B. K. 2014. *Cell-Based Assays for High-Throughput Screening*, Springer.

CLOUTIER, N. & FLAMAND, L. 2010. Kaposi sarcoma-associated herpesvirus latency-associated nuclear antigen inhibits interferon (IFN) beta expression by competing with IFN regulatory factor-3 for binding to IFNB promoter. *J Biol Chem,* 285**,** 7208-21.

CROSTON, G. E. 2002. Functional cell-based uHTS in chemical genomic drug discovery. *Trends in biotechnology,* 20**,** 110-115.

CROW, Y. J. 2015. Type I interferonopathies: Mendelian type I interferon up-regulation. *Current opinion in immunology,* 32**,** 7-12.

CROW, Y. J., HAYWARD, B. E., PARMAR, R., ROBINS, P., LEITCH, A., ALI, M., BLACK, D. N., VAN BOKHOVEN, H., BRUNNER, H. G., HAMEL, B. C., CORRY, P. C., COWAN, F. M., FRINTS, S. G., KLEPPER, J., LIVINGSTON, J. H., LYNCH, S. A., MASSEY, R. F., MERITET, J. F., MICHAUD, J. L., PONSOT, G., VOIT, T., LEBON, P., BONTHRON, D. T., JACKSON, A. P., BARNES, D. E. & LINDAHL, T. 2006. Mutations in the gene encoding the 3'-5' DNA exonuclease TREX1 cause Aicardi-Goutieres syndrome at the AGS1 locus. *Nat Genet,* 38**,** 917-20.

DA CONCEICAO, T. M., RUST, N. M., BERBEL, A. C., MARTINS, N. B., DO NASCIMENTO SANTOS, C. A., DA POIAN, A. T. & DE ARRUDA, L. B. 2013. Essential role of RIG-I in the activation of endothelial cells by dengue virus. *Virology,* 435**,** 281-92.

DAI, C. & KRANTZ, S. B. 1999. Interferon γ induces upregulation and activation of caspases 1, 3, and 8 to produce apoptosis in human erythroid progenitor cells. *Blood,* 93**,** 3309-3316.

DALPKE, A. H., ZIMMERMANN, S., ALBRECHT, I. & HEEG, K. 2002. Phosphodiester CpG oligonucleotides as adjuvants: polyguanosine runs enhance cellular uptake and improve immunostimulative activity of phosphodiester CpG oligonucleotides in vitro and in vivo. *Immunology,* 106**,** 102-112.

DANDAPANI, S. & MARCAURELLE, L. A. 2010. Grand Challenge Commentary: Accessing new chemical space for 'undruggable' targets. *Nat Chem Biol,* 6**,** 861-863.

DARNELL, J. E. 1997. STATs and gene regulation. *Science,* 277**,** 1630-1635.

DAVIS, M. E., WANG, M. K., RENNICK, L. J., FULL, F., GABLESKE, S., MESMAN, A. W., GRINGHUIS, S. I., GEIJTENBEEK, T. B., DUPREX, W. P. & GACK, M. U. 2014. Antagonism of the phosphatase PP1 by the measles virus V protein is required for innate immune escape of MDA5. *Cell host & microbe,* 16**,** 19-30.

DE ALMEIDA RIBEIRO, E., LEYRAT, C., GÉRARD, F. C., ALBERTINI, A. A., FALK, C., RUIGROK, R. W. & JAMIN, M. 2009. Binding of rabies virus polymerase cofactor to recombinant circular nucleoprotein–RNA complexes. *Journal of molecular biology,* 394**,** 558-575.

DECKER, T., LEW, D. & DARNELL, J. 1991a. Two distinct alpha-interferon-dependent signal transduction pathways may contribute to activation of transcription of the guanylate-binding protein gene. *Molecular and cellular biology,* 11**,** 5147-5153.

DECKER, T., LEW, D. J., MIRKOVITCH, J. & DARNELL JR, J. E. 1991b. Cytoplasmic activation of GAF, an IFN-gamma-regulated DNA-binding factor. *The EMBO Journal,* 10**,** 927.

DEL TORO DUANY, Y., WU, B. & HUR, S. 2015. MDA5—filament, dynamics and disease. *Current opinion in virology,* 12**,** 20-25.

DENG, J., LU, P. D., ZHANG, Y., SCHEUNER, D., KAUFMAN, R. J., SONENBERG, N., HARDING, H. P. & RON, D. 2004. Translational repression mediates activation of nuclear factor kappa B by phosphorylated translation initiation factor 2. *Mol Cell Biol,* 24**,** 10161-8.

DENG, L., WANG, C., SPENCER, E., YANG, L., BRAUN, A., YOU, J., SLAUGHTER, C., PICKART, C. & CHEN, Z. J. 2000. Activation of the IκB kinase complex by TRAF6 requires a dimeric ubiquitin-conjugating enzyme complex and a unique polyubiquitin chain. *Cell,* 103**,** 351-361.

DIDCOCK, L., YOUNG, D., GOODBOURN, S. & RANDALL, R. 1999. The V protein of simian virus 5 inhibits interferon signalling by targeting STAT1 for proteasome-mediated degradation. *Journal of virology,* 73**,** 9928-9933.

DIMOVA, D. K. & DYSON, N. J. 2005. The E2F transcriptional network: old acquaintances with new faces. *Oncogene,* 24**,** 2810-26.

DIPERNA, G., STACK, J., BOWIE, A. G., BOYD, A., KOTWAL, G., ZHANG, Z., ARVIKAR, S., LATZ, E., FITZGERALD, K. A. & MARSHALL, W. L. 2004. Poxvirus protein N1L targets

the I-kappaB kinase complex, inhibits signaling to NF-kappaB by the tumor necrosis factor superfamily of receptors, and inhibits NF-kappaB and IRF3 signaling by toll-like receptors. *J Biol Chem,* 279**,** 36570-8.

DOMANICO, P. L. 1994. Discovery research: innovation and automation. *Chemometrics and intelligent laboratory systems,* 26**,** 115-121.

DREWRY, D. H. & MACARRON, R. 2010. Enhancements of screening collections to address areas of unmet medical need: an industry perspective. *Current opinion in chemical biology,* 14**,** 289-298.

EBERT, A. D. & SVENDSEN, C. N. 2010. Human stem cells and drug screening: opportunities and challenges. *Nature Reviews Drug Discovery,* 9**,** 367-372.

EGGERT, U. S., KIGER, A. A., RICHTER, C., PERLMAN, Z. E., PERRIMON, N., MITCHISON, T. J. & FIELD, C. M. 2004. Parallel chemical genetic and genome-wide RNAi screens identify cytokinesis inhibitors and targets. *PLoS Biol,* 2**,** e379.

ENOMOTO, K., AONO, Y., MITSUGI, T., TAKAHASHI, K., SUZUKI, R., PREAUDAT, M., MATHIS, G., KOMINAMI, G. & TAKEMOTO, H. 2000. High Throughput Screening for Human Interferon-y Production Inhibitor Using Homogenous Time-Resolved Fluorescence. *Journal of Biomolecular Screening,* 5**,** 263-268.

FALVO, J. V., PAREKH, B. S., LIN, C. H., FRAENKEL, E. & MANIATIS, T. 2000. Assembly of a functional beta interferon enhanceosome is dependent on ATF-2–c-Jun heterodimer orientation. *Molecular and cellular biology,* 20**,** 4814-4825.

FANG, Q. K., WU, F. X., GROVER, P. T., HOPKINS, S. C., CAMPBELL, U., CHYTIL, M. & SPEAR, K. L. 2011. *Imidazo[1,2-a]pyridine compounds as gaba-a receptor modulators*.

FERRANTINI, M., CAPONE, I. & BELARDELLI, F. 2007. Interferon-α and cancer: mechanisms of action and new perspectives of clinical use. *Biochimie,* 89**,** 884-893.

FERRANTINI, M., CAPONE, I. & BELARDELLI, F. 2008. Dendritic cells and cytokines in immune rejection of cancer. *Cytokine & growth factor reviews,* 19**,** 93-107.

FIELDS, B. N., KNIPE, D. M. & HOWLEY, P. M. 2013. *Fields virology,* Philadelphia, Wolters Kluwer Health/Lippincott Williams & Wilkins.

FINK, T. & REYMOND, J.-L. 2007. Virtual exploration of the chemical universe up to 11 atoms of C, N, O, F: assembly of 26.4 million structures (110.9 million stereoisomers) and analysis for new ring systems, stereochemistry, physicochemical properties, compound classes, and drug discovery. *Journal of chemical information and modeling,* 47**,** 342-353.

FOX, S., FARR-JONES, S., SOPCHAK, L., BOGGS, A., NICELY, H. W., KHOURY, R. & BIROS, M. 2006. High-throughput screening: update on practices and success. *Journal of biomolecular screening,* 11**,** 864-869.

FRAHM, T., HAUSER, H. & KOSTER, M. 2006. IFN-type-I-mediated signaling is regulated by modulation of STAT2 nuclear export. *J Cell Sci,* 119**,** 1092-104.

GACK, M. U., ALBRECHT, R. A., URANO, T., INN, K. S., HUANG, I. C., CARNERO, E., FARZAN, M., INOUE, S., JUNG, J. U. & GARCIA-SASTRE, A. 2009. Influenza A virus NS1 targets the ubiquitin ligase TRIM25 to evade recognition by the host viral RNA sensor RIG-I. *Cell Host Microbe,* 5**,** 439-49.

GACK, M. U., SHIN, Y. C., JOO, C. H., URANO, T., LIANG, C., SUN, L., TAKEUCHI, O., AKIRA, S., CHEN, Z., INOUE, S. & JUNG, J. U. 2007. TRIM25 RING-finger E3 ubiquitin ligase is essential for RIG-I-mediated antiviral activity. *Nature,* 446**,** 916-920.

GARCIN, D., TAYLOR, G., TANEBAYASHI, K., COMPANS, R. & KOLAKOFSKY, D. 1998. The Short Sendai Virus Leader Region Controls Induction of Programmed Cell Death. *Virology,* 243**,** 340-353.

GAUZZI, M. C., VELAZQUEZ, L., MCKENDRY, R., MOGENSEN, K. E., FELLOUS, M. & PELLEGRINI, S. 1996. Interferon-α-dependent activation of Tyk2 requires phosphorylation of positive regulatory tyrosines by another kinase. *Journal of Biological Chemistry,* 271**,** 20494-20500.

GERAERTS, M., WILLEMS, S., BAEKELANDT, V., DEBYSER, Z. & GIJSBERS, R. 2006. Comparison of lentiviral vector titration methods. *BMC biotechnology,* 6**,** 1.

GILMORE, T. D. & HERSCOVITCH, M. 2006. Inhibitors of NF-kappaB signaling: 785 and counting. *Oncogene,* 25**,** 6887-99.

GONZALEZ-NAVAJAS, J. M., LEE, J., DAVID, M. & RAZ, E. 2012. Immunomodulatory functions of type I interferons. *Nature reviews. Immunology,* 12**,** 125-35.

GOODACRE, S. C., STREET, L. J., HALLETT, D. J., CRAWFORTH, J. M., KELLY, S., OWENS, A. P., BLACKABY, W. P., LEWIS, R. T., STANLEY, J. & SMITH, A. J. 2006. Imidazo [1, 2-a] pyrimidines as functionally selective and orally bioavailable GABAAα2/α3 binding site agonists for the treatment of anxiety disorders. *Journal of medicinal chemistry,* 49**,** 35-38.

GOODBOURN, S. & RANDALL, R. E. 2009. The regulation of type I interferon production by paramyxoviruses. *Journal of interferon & cytokine research : the official journal of the International Society for Interferon and Cytokine Research,* 29**,** 539-47.

GOSWAMI, R., MAJUMDAR, T., DHAR, J., CHATTOPADHYAY, S., BANDYOPADHYAY, S. K., VERBOVETSKAYA, V., SEN, G. C. & BARIK, S. 2013. Viral degradasome hijacks mitochondria to suppress innate immunity. *Cell research,* 23**,** 1025-1042.

GOUBAU, D., DEDDOUCHE, S. & E SOUSA, C. R. 2013. Cytosolic sensing of viruses. *Immunity,* 38**,** 855-869.

GRETEN, F. R., ECKMANN, L., GRETEN, T. F., PARK, J. M., LI, Z.-W., EGAN, L. J., KAGNOFF, M. F. & KARIN, M. 2004. IKKβ links inflammation and tumorigenesis in a mouse model of colitis-associated cancer. *Cell,* 118**,** 285-296.

GRIBBON, P. & SEWING, A. 2003. Fluorescence readouts in HTS: no gain without pain? *Drug Discovery Today,* 8**,** 1035-1043.

GUO, F., ZHAO, X., GILL, T., ZHOU, Y., CAMPAGNA, M., WANG, L., LIU, F., ZHANG, P., DIPAOLO, L., DU, Y., XU, X., JIANG, D., WEI, L., CUCONATI, A., BLOCK, T. M., GUO, J. T. & CHANG, J. 2014. An interferon-beta promoter reporter assay for high throughput identification of compounds against multiple RNA viruses. *Antiviral Res,* 107**,** 56-65.

HABJAN, M., ANDERSSON, I., KLINGSTRÖM, J., SCHÜMANN, M., MARTIN, A., ZIMMERMANN, P., WAGNER, V., PICHLMAIR, A., SCHNEIDER, U. & MÜHLBERGER, E. 2008. Processing of genome 5′ termini as a strategy of negative-strand RNA viruses to avoid RIG-I-dependent interferon induction. *PloS one,* 3**,** e2032.

HALE, B. G., RANDALL, R. E., ORTIN, J. & JACKSON, D. 2008. The multifunctional NS1 protein of influenza A viruses. *J Gen Virol,* 89**,** 2359-76.

HALLER, O. & KOCHS, G. 2011. Human MxA protein: an interferon-induced dynamin-like GTPase with broad antiviral activity. *Journal of Interferon & Cytokine Research,* 31**,** 79-87.

HAMMING, O. J., TERCZYNSKA-DYLA, E., VIEYRES, G., DIJKMAN, R., JORGENSEN, S. E., AKHTAR, H., SIUPKA, P., PIETSCHMANN, T., THIEL, V. & HARTMANN, R. 2013. Interferon lambda 4 signals via the IFNlambda receptor to regulate antiviral activity against HCV and coronaviruses. *EMBO J,* 32**,** 3055-65.

HASSELBALCH, H. C. 2012. Chronic inflammation as a promotor of mutagenesis in essential thrombocythemia, polycythemia vera and myelofibrosis. A human inflammation model for cancer development? *Leuk Res*.

HATADA, E. & FUKUDA, R. 1992. Binding of influenza A virus NS1 protein to dsRNA in vitro. *Journal of General Virology,* 73**,** 3325-3329.

HEIL, F., HEMMI, H., HOCHREIN, H., AMPENBERGER, F., KIRSCHNING, C., AKIRA, S., LIPFORD, G., WAGNER, H. & BAUER, S. 2004. Species-specific recognition of single-stranded RNA via toll-like receptor 7 and 8. *Science,* 303**,** 1526-1529.

HERRINGTON, F. D., CARMODY, R. J. & GOODYEAR, C. S. 2015. Modulation of NF-κB Signaling as a Therapeutic Target in Autoimmunity. *Journal of biomolecular screening***,** 1087057115617456.

HERTZOG, P. J. 2012. Overview. Type I interferons as primers, activators and inhibitors of innate and adaptive immune responses. *Immunology and cell biology,* 90**,** 471.

HOESEL, B. & SCHMID, J. A. 2013. The complexity of NF-κB signaling in inflammation and cancer. *Molecular cancer,* 12**,** 1.

HOFFMANN, H.-H., SCHNEIDER, W. M. & RICE, C. M. 2015. Interferons and viruses: an evolutionary arms race of molecular interactions. *Trends in immunology,* 36**,** 124-138.

HOSUI, A., KLOVER, P., TATSUMI, T., UEMURA, A., NAGANO, H., DOKI, Y., MORI, M., HIRAMATSU, N., KANTO, T., HENNIGHAUSEN, L., HAYASHI, N. & TAKEHARA, T. 2012. Suppression of signal transducers and activators of transcription 1 in hepatocellular carcinoma is associated with tumor progression. *Int J Cancer,* 131**,** 2774-84.

HUGHES, J. P., REES, S., KALINDJIAN, S. B. & PHILPOTT, K. L. 2011. Principles of early drug discovery. *Br J Pharmacol,* 162**,** 1239-49.
HUYE, L. E., NING, S., KELLIHER, M. & PAGANO, J. S. 2007. Interferon regulatory factor 7 is activated by a viral oncoprotein through RIP-dependent ubiquitination. *Molecular and cellular biology,* 27**,** 2910-2918.
INN, K.-S., LEE, S.-H., RATHBUN, J. Y., WONG, L.-Y., TOTH, Z., MACHIDA, K., OU, J.-H. J. & JUNG, J. U. 2011. Inhibition of RIG-I-mediated signaling by Kaposi's sarcoma-associated herpesvirus-encoded deubiquitinase ORF64. *Journal of virology,* 85**,** 10899-10904.
IRIE, T., KIYOTANI, K., IGARASHI, T., YOSHIDA, A. & SAKAGUCHI, T. 2012. Inhibition of interferon regulatory factor 3 activation by paramyxovirus V protein. *J Virol,* 86**,** 7136-45.
ISAACS, A. & LINDENMANN, J. 1957. Virus interference. I. The interferon. *Proceedings of the Royal Society of London. Series B-Biological Sciences,* 147**,** 258-267.
ISENI, F., GARCIN, D., NISHIO, M., KEDERSHA, N., ANDERSON, P. & KOLAKOFSKY, D. 2002. Sendai virus trailer RNA binds TIAR, a cellular protein involved in virus‐induced apoptosis. *The EMBO Journal,* 21**,** 5141-5150.
ISHII, K. J., COBAN, C., KATO, H., TAKAHASHI, K., TORII, Y., TAKESHITA, F., LUDWIG, H., SUTTER, G., SUZUKI, K., HEMMI, H., SATO, S., YAMAMOTO, M., UEMATSU, S., KAWAI, T., TAKEUCHI, O. & AKIRA, S. 2006. A Toll-like receptor-independent antiviral response induced by double-stranded B-form DNA. *Nat Immunol,* 7**,** 40-8.
ISHIKAWA, H. & BARBER, G. N. 2008. STING is an endoplasmic reticulum adaptor that facilitates innate immune signalling. *Nature,* 455**,** 674-8.
ISHIKAWA, H., MA, Z. & BARBER, G. N. 2009. STING regulates intracellular DNA-mediated, type I interferon-dependent innate immunity. *Nature,* 461**,** 788-92.
ISRAEL, A. 2010. The IKK complex, a central regulator of NF-kappaB activation. *Cold Spring Harb Perspect Biol,* 2**,** a000158.
ITO, N., MOSELEY, G. W., BLONDEL, D., SHIMIZU, K., ROWE, C. L., ITO, Y., MASATANI, T., NAKAGAWA, K., JANS, D. A. & SUGIYAMA, M. 2010. Role of interferon antagonist activity of rabies virus phosphoprotein in viral pathogenicity. *J Virol,* 84**,** 6699-710.
ITO, N., MOSELEY, G. W. & SUGIYAMA, M. 2016. The importance of immune evasion in the pathogenesis of rabies virus. *Journal of Veterinary Medical Science*.
IVASHKIV, L. B. & DONLIN, L. T. 2014. Regulation of type I interferon responses. *Nat Rev Immunol,* 14**,** 36-49.
IVERSEN, P. W., EASTWOOD, B. J., SITTAMPALAM, G. S. & COX, K. L. 2006. A Comparison of Assay Performance Measures in Screening Assays: Signal Window, Z' Factor, and Assay Variability Ratio. *Journal of Biomolecular Screening,* 11**,** 247-252.
IWASAKI, A. 2012. A virological view of innate immune recognition. *Annu Rev Microbiol,* 66**,** 177-96.
JACKSON, J. D., MARKERT, J. M., LI, L., CARROLL, S. L. & CASSADY, K. A. 2016. STAT1 and NF-κB Inhibitors Diminish Basal Interferon-Stimulated Gene Expression and Improve the Productive Infection of Oncolytic HSV in MPNST Cells. *Molecular Cancer Research,* 14**,** 482-492.
JACOB, A., SOOD, R., CHANU, K. V., BHATIA, S., KHANDIA, R., PATERIYA, A., NAGARAJAN, S., DIMRI, U. & KULKARNI, D. 2016. Amantadine resistance among highly pathogenic avian influenza viruses (H5N1) isolated from India. *Microbial pathogenesis,* 91**,** 35-40.
JANG, M. A., KIM, E. K., NOW, H., NGUYEN, N. T., KIM, W. J., YOO, J. Y., LEE, J., JEONG, Y. M., KIM, C. H., KIM, O. H., SOHN, S., NAM, S. H., HONG, Y., LEE, Y. S., CHANG, S. A., JANG, S. Y., KIM, J. W., LEE, M. S., LIM, S. Y., SUNG, K. S., PARK, K. T., KIM, B. J., LEE, J. H., KIM, D. K., KEE, C. & KI, C. S. 2015. Mutations in DDX58, which encodes RIG-I, cause atypical Singleton-Merten syndrome. *Am J Hum Genet,* 96**,** 266-74.
JIANG, X., KINCH, L. N., BRAUTIGAM, C. A., CHEN, X., DU, F., GRISHIN, N. V. & CHEN, Z. J. 2012. Ubiquitin-induced oligomerization of the RNA sensors RIG-I and MDA5 activates antiviral innate immune response. *Immunity,* 36**,** 959-73.

KANAYAMA, A., SETH, R. B., SUN, L., EA, C.-K., HONG, M., SHAITO, A., CHIU, Y.-H., DENG, L. & CHEN, Z. J. 2004. TAB2 and TAB3 activate the NF-κB pathway through binding to polyubiquitin chains. *Molecular cell,* 15**,** 535-548.

KARIV, I., STEVENS, M. E., BEHRENS, D. L. & OLDENBURG, K. R. 1999. High throughput quantitation of cAMP production mediated by activation of seven transmembrane domain receptors. *Journal of biomolecular screening,* 4**,** 27-32.

KATO, H. & FUJITA, T. 2015. RIG-I-like receptors and autoimmune diseases. *Curr Opin Immunol,* 37**,** 40-5.

KATO, H., TAKEUCHI, O., SATO, S., YONEYAMA, M., YAMAMOTO, M., MATSUI, K., UEMATSU, S., JUNG, A., KAWAI, T., ISHII, K. J., YAMAGUCHI, O., OTSU, K., TSUJIMURA, T., KOH, C. S., REIS E SOUSA, C., MATSUURA, Y., FUJITA, T. & AKIRA, S. 2006. Differential roles of MDA5 and RIG-I helicases in the recognition of RNA viruses. *Nature,* 441**,** 101-5.

KAWAI, T. & AKIRA, S. 2011. Toll-like receptors and their crosstalk with other innate receptors in infection and immunity. *Immunity,* 34**,** 637-50.

KAWAI, T., TAKAHASHI, K., SATO, S., COBAN, C., KUMAR, H., KATO, H., ISHII, K. J., TAKEUCHI, O. & AKIRA, S. 2005. IPS-1, an adaptor triggering RIG-I- and Mda5-mediated type I interferon induction. *Nature immunology,* 6**,** 981-8.

KIM, S. H., COHEN, B., NOVICK, D. & RUBINSTEIN, M. 1997. Mammalian type I interferon receptors consists of two subunits: IFNaR1 and IFNaR2. *Gene,* 196**,** 279-286.

KOLA, I. & LANDIS, J. 2004. Can the pharmaceutical industry reduce attrition rates? *Nature reviews Drug discovery,* 3**,** 711-716.

KOMATSU, T., TAKEUCHI, K., YOKOO, J. & GOTOH, B. 2002. Sendai virus C protein impairs both phosphorylation and dephosphorylation processes of Stat1. *FEBS letters,* 511**,** 139-144.

KOTWAL, G. J., HATCH, S. & MARSHALL, W. L. 2012. Viral infection: an evolving insight into the signal transduction pathways responsible for the innate immune response. *Advances in virology,* 2012**,** 131457.

KOWSKI, T. J. & WU, J. J. 2000. Fluorescence polarization is a useful technology for reagent reduction in assay miniaturization. *Combinatorial chemistry & high throughput screening,* 3**,** 437-444.

KOYAMA, S., ISHII, K. J., COBAN, C. & AKIRA, S. 2008. Innate immune response to viral infection. *Cytokine,* 43**,** 336-41.

KOZIKOWSKI, B. A., BURT, T. M., TIREY, D. A., WILLIAMS, L. E., KUZMAK, B. R., STANTON, D. T., MORAND, K. L. & NELSON, S. L. 2003. The effect of freeze/thaw cycles on the stability of compounds in DMSO. *J Biomol Screen,* 8**,** 210-5.

KREMERS, G.-J., GILBERT, S. G., CRANFILL, P. J., DAVIDSON, M. W. & PISTON, D. W. 2011. Fluorescent proteins at a glance. *Journal of Cell Science,* 124**,** 157-160.

KUBINYI, H. 1995. Strategies and recent technologies in drug discovery. *Die Pharmazie,* 50**,** 647-662.

KUENEMANN, M. A., LABBE, C. M., CERDAN, A. H. & SPERANDIO, O. 2016. Imbalance in chemical space: How to facilitate the identification of protein-protein interaction inhibitors. *Sci Rep,* 6**,** 23815.

KUMAR, H., KAWAI, T. & AKIRA, S. 2011. Pathogen recognition by the innate immune system. *International reviews of immunology,* 30**,** 16-34.

KUNAPULI, P., LEE, S., ZHENG, W., ALBERTS, M., KORNIENKO, O., MULL, R., KREAMER, A., HWANG, J.-I., SIMON, M. I. & STRULOVICI, B. 2006. Identification of small molecule antagonists of the human mas-related gene-X1 receptor. *Analytical biochemistry,* 351**,** 50-61.

LAVECCHIA, A. & DI GIOVANNI, C. 2013. Virtual screening strategies in drug discovery: a critical review. *Current medicinal chemistry,* 20**,** 2839-2860.

LAW, R., BARKER, O., BARKER, J. J., HESTERKAMP, T., GODEMANN, R., ANDERSEN, O., FRYATT, T., COURTNEY, S., HALLETT, D. & WHITTAKER, M. 2009. The multiple roles of computational chemistry in fragment-based drug design. *Journal of computer-aided molecular design,* 23**,** 459-473.

LAZEAR, H. M., NICE, T. J. & DIAMOND, M. S. 2015. Interferon-lambda: Immune Functions at Barrier Surfaces and Beyond. *Immunity,* 43**,** 15-28.

LE BON, A. & TOUGH, D. F. 2002. Links between innate and adaptive immunity via type I interferon. *Current opinion in immunology,* 14**,** 432-436.
LEE, S. M. & YEN, H. L. 2012. Targeting the host or the virus: Current and novel concepts for antiviral approaches against influenza virus infection. *Antiviral Res,* 96**,** 391-404.
LEW, D. J., DECKER, T., STREHLOW, I. & DARNELL, J. 1991. Overlapping elements in the guanylate-binding protein gene promoter mediate transcriptional induction by alpha and gamma interferons. *Molecular and Cellular Biology,* 11**,** 182-191.
LI, Q., ESTEPA, G., MEMET, S., ISRAEL, A. & VERMA, I. M. 2000. Complete lack of NF-kappaB activity in IKK1 and IKK2 double-deficient mice: additional defect in neurulation. *Genes & Development,* 14**,** 1729-1733.
LI, S., LABRECQUE, S., GAUZZI, M. C., CUDDIHY, A. R., WONG, A. H., PELLEGRINI, S., MATLASHEWSKI, G. J. & KOROMILAS, A. E. 1999. The human papilloma virus (HPV)-18 E6 oncoprotein physically associates with Tyk2 and impairs Jak-Stat activation by interferon-α. *Oncogene,* 18.
LI, S., PETERS, G. A., DING, K., ZHANG, X., QIN, J. & SEN, G. C. 2006. Molecular basis for PKR activation by PACT or dsRNA. *Proc Natl Acad Sci U S A,* 103**,** 10005-10.
LI, X., LEUNG, S., QURESHI, S., DARNELL, J. E. & STARK, G. R. 1996. Formation of STAT1-STAT2 heterodimers and their role in the activation of IRF-1 gene transcription by interferon. *Journal of Biological Chemistry,* 271**,** 5790-5794.
LI, X., SHEN, F., ZHANG, Y., ZHU, J., HUANG, L. & SHI, Q. 2007. Functional characterization of cell lines for high-throughput screening of human neuromedin U receptor subtype 2 specific agonists using a luciferase reporter gene assay. *European journal of pharmaceutics and biopharmaceutics,* 67**,** 284-292.
LI, X. D., SUN, L., SETH, R. B., PINEDA, G. & CHEN, Z. J. 2005. Hepatitis C virus protease NS3/4A cleaves mitochondrial antiviral signaling protein off the mitochondria to evade innate immunity. *Proc Natl Acad Sci U S A,* 102**,** 17717-22.
LIPINSKI, C. A. 2004. Lead- and drug-like compounds: the rule-of-five revolution. *Drug Discov Today Technol,* 1**,** 337-41.
LIPINSKI, C. A., LOMBARDO, F., DOMINY, B. W. & FEENEY, P. J. 2001. Experimental and computational approaches to estimate solubility and permeability in drug discovery and development settings. *Advanced Drug Delivery Reviews,* 46**,** 3-26.
LIU, S., CHEN, J., CAI, X., WU, J., CHEN, X., WU, Y.-T., SUN, L. & CHEN, Z. J. 2013. MAVS recruits multiple ubiquitin E3 ligases to activate antiviral signaling cascades. *Elife,* 2**,** e00785.
LIU, Y., JESUS, A. A., MARRERO, B., YANG, D., RAMSEY, S. E., MONTEALEGRE SANCHEZ, G. A., TENBROCK, K., WITTKOWSKI, H., JONES, O. Y., KUEHN, H. S., LEE, C. C., DIMATTIA, M. A., COWEN, E. W., GONZALEZ, B., PALMER, I., DIGIOVANNA, J. J., BIANCOTTO, A., KIM, H., TSAI, W. L., TRIER, A. M., HUANG, Y., STONE, D. L., HILL, S., KIM, H. J., ST HILAIRE, C., GURPRASAD, S., PLASS, N., CHAPELLE, D., HORKAYNE-SZAKALY, I., FOELL, D., BARYSENKA, A., CANDOTTI, F., HOLLAND, S. M., HUGHES, J. D., MEHMET, H., ISSEKUTZ, A. C., RAFFELD, M., MCELWEE, J., FONTANA, J. R., MINNITI, C. P., MOIR, S., KASTNER, D. L., GADINA, M., STEVEN, A. C., WINGFIELD, P. T., BROOKS, S. R., ROSENZWEIG, S. D., FLEISHER, T. A., DENG, Z., BOEHM, M., PALLER, A. S. & GOLDBACH-MANSKY, R. 2014. Activated STING in a vascular and pulmonary syndrome. *N Engl J Med,* 371**,** 507-18.
LOMENICK, B., HAO, R., JONAI, N., CHIN, R. M., AGHAJAN, M., WARBURTON, S., WANG, J., WU, R. P., GOMEZ, F., LOO, J. A., WOHLSCHLEGEL, J. A., VONDRISKA, T. M., PELLETIER, J., HERSCHMAN, H. R., CLARDY, J., CLARKE, C. F. & HUANG, J. 2009. Target identification using drug affinity responsive target stability (DARTS). *Proc Natl Acad Sci U S A,* 106**,** 21984-9.
LOMENICK, B., OLSEN, R. W. & HUANG, J. 2010. Identification of direct protein targets of small molecules. *ACS chemical biology,* 6**,** 34-46.
LU, H. R., WHITTAKER, R., PRICE, J. H., VEGA, R., PFEIFFER, E. R., CERIGNOLI, F., TOWART, R. & GALLACHER, D. J. 2015. High Throughput Measurement of Ca++ Dynamics in Human Stem Cell-Derived Cardiomyocytes by Kinetic Image Cytometery: A Cardiac Risk Assessment Characterization Using a Large Panel of Cardioactive and Inactive Compounds. *Toxicol Sci,* 148**,** 503-16.

LU, L. L., PURI, M., HORVATH, C. M. & SEN, G. C. 2008. Select paramyxoviral V proteins inhibit IRF3 activation by acting as alternative substrates for inhibitor of kappaB kinase epsilon (IKKe)/TBK1. *J Biol Chem,* 283**,** 14269-76.

LUNDBERG, A. M., KETELHUTH, D. F., JOHANSSON, M. E., GERDES, N., LIU, S., YAMAMOTO, M., AKIRA, S. & HANSSON, G. K. 2013. Toll-like receptor 3 and 4 signalling through the TRIF and TRAM adaptors in haematopoietic cells promotes atherosclerosis. *Cardiovasc Res,* 99**,** 364-73.

LUTHRA, P., RAMANAN, P., MIRE, C. E., WEISEND, C., TSUDA, Y., YEN, B., LIU, G., LEUNG, D. W., GEISBERT, T. W. & EBIHARA, H. 2013. Mutual antagonism between the Ebola virus VP35 protein and the RIG-I activator PACT determines infection outcome. *Cell host & microbe,* 14**,** 74-84.

MACARRON, R., BANKS, M. N., BOJANIC, D., BURNS, D. J., CIROVIC, D. A., GARYANTES, T., GREEN, D. V., HERTZBERG, R. P., JANZEN, W. P., PASLAY, J. W., SCHOPFER, U. & SITTAMPALAM, G. S. 2011. Impact of high-throughput screening in biomedical research. *Nat Rev Drug Discov,* 10**,** 188-95.

MAHER, S., ROMERO-WEAVER, A., SCARZELLO, A. & GAMERO, A. 2007. Interferon: cellular executioner or white knight? *Current medicinal chemistry,* 14**,** 1279-1289.

MALATHI, K., DONG, B., GALE, M. & SILVERMAN, R. H. 2007. Small self-RNA generated by RNase L amplifies antiviral innate immunity. *Nature,* 448**,** 816-819.

MALO, N., HANLEY, J. A., CERQUOZZI, S., PELLETIER, J. & NADON, R. 2006. Statistical practice in high-throughput screening data analysis. *Nature biotechnology,* 24**,** 167-175.

MANIATIS, T., FALVO, J., KIM, T., KIM, T., LIN, C., PAREKH, B. & WATHELET, M. Structure and function of the interferon-β enhanceosome. Cold Spring Harbor Symposia on Quantitative Biology, 1998. Cold Spring Harbor Laboratory Press, 609-620.

MARSCHALEK, A., DRECHSEL, L. & CONZELMANN, K.-K. 2012. The importance of being short: the role of rabies virus phosphoprotein isoforms assessed by differential IRES translation initiation. *European journal of cell biology,* 91**,** 17-23.

MARTÍNEZ-GIL, L., AYLLON, J., ORTIGOZA, M. B., GARCÍA-SASTRE, A., SHAW, M. L. & PALESE, P. 2012. Identification of Small Molecules with Type I Interferon Inducing Properties by High-Throughput Screening. *PloS one,* 7**,** e49049.

MARTINEZ-GIL, L., GOFF, P. H., HAI, R., GARCIA-SASTRE, A., SHAW, M. L. & PALESE, P. 2013. A Sendai virus-derived RNA agonist of RIG-I as a virus vaccine adjuvant. *J Virol,* 87**,** 1290-300.

MASATANI, T., OZAWA, M., YAMADA, K., ITO, N., HORIE, M., MATSUU, A., OKUYA, K., TSUKIYAMA-KOHARA, K., SUGIYAMA, M. & NISHIZONO, A. 2016. Contribution of the interaction between the rabies virus P protein and I-kappa B kinase ϵ to the inhibition of type I IFN induction signalling. *Journal of General Virology,* 97**,** 316-326.

MATSUMOTO, M. & SEYA, T. 2008. TLR3: interferon induction by double-stranded RNA including poly (I: C). *Advanced drug delivery reviews,* 60**,** 805-812.

MCFEDRIES, A., SCHWAID, A. & SAGHATELIAN, A. 2013. Methods for the elucidation of protein-small molecule interactions. *Chemistry & biology,* 20**,** 667-673.

MCINERNEY, G. M. & KARLSSON HEDESTAM, G. B. 2009. Direct cleavage, proteasomal degradation and sequestration: three mechanisms of viral subversion of type I interferon responses. *J Innate Immun,* 1**,** 599-606.

MCINNES, C. 2007. Virtual screening strategies in drug discovery. *Current opinion in chemical biology,* 11**,** 494-502.

MELROE, G. T., DELUCA, N. A. & KNIPE, D. M. 2004. Herpes simplex virus 1 has multiple mechanisms for blocking virus-induced interferon production. *J Virol,* 78**,** 8411-20.

MINER, J. J. & DIAMOND, M. S. 2014. MDA5 and autoimmune disease. *Nat Genet,* 46**,** 418-9.

MORRISON, J., LAURENT-ROLLE, M., MAESTRE, A. M., RAJSBAUM, R., PISANELLI, G., SIMON, V., MULDER, L. C., FERNANDEZ-SESMA, A. & GARCIA-SASTRE, A. 2013. Dengue virus co-opts UBR4 to degrade STAT2 and antagonize type I interferon signaling. *PLoS Pathog,* 9**,** e1003265.

MOSELEY, G. W., FILMER, R. P., DEJESUS, M. A. & JANS, D. A. 2007a. Nucleocytoplasmic distribution of rabies virus P-protein is regulated by phosphorylation adjacent to C-terminal nuclear import and export signals. *Biochemistry,* 46**,** 12053-12061.

MOSELEY, G. W., ROTH, D. M., DEJESUS, M. A., LEYTON, D. L., FILMER, R. P., POUTON, C. W. & JANS, D. A. 2007b. Dynein light chain association sequences can facilitate nuclear protein import. *Mol Biol Cell,* 18**,** 3204-13.

MURRAY, C. W., VERDONK, M. L. & REES, D. C. 2012. Experiences in fragment-based drug discovery. *Trends in Pharmacological Sciences,* 33**,** 224-232.

NAG, D. K. & FINLEY, D. 2012. A small-molecule inhibitor of deubiquitinating enzyme USP14 inhibits Dengue virus replication. *Virus research,* 165**,** 103-106.

NAGAMANI, S., SOURAV, D. & NAGAMAN, S. 2011. Current Trends in Virtual High Throughput Screening Using Ligand-Based and Structure-Based Methods. *Combinatorial Chemistry & High Throughput Screening,* 14**,** 872-888.

NAKAYAMA, Y., PLISCH, E. H., SULLIVAN, J., THOMAS, C., CZUPRYNSKI, C. J., WILLIAMS, B. R. & SURESH, M. 2010. Role of PKR and Type I IFNs in viral control during primary and secondary infection. *PLoS Pathog,* 6**,** e1000966.

NALDINI, L., BLÖMER, U., GALLAY, P., ORY, D., MULLIGAN, R., GAGE, F. H., VERMA, I. M. & TRONO, D. 1996. In vivo gene delivery and stable transduction of nondividing cells by a lentiviral vector. *Science,* 272**,** 263-267.

NAPOLITANO, F., SIRCI, F., CARRELLA, D. & DI BERNARDO, D. 2016. Drug-set enrichment analysis: a novel tool to investigate drug mode of action. *Bioinformatics,* 32**,** 235-241.

NAUMANN, K., WEHNER, R., SCHWARZE, A., PETZOLD, C., SCHMITZ, M. & ROHAYEM, J. 2013. Activation of dendritic cells by the novel Toll-like receptor 3 agonist RGC100. *Clin Dev Immunol,* 2013**,** 283649.

NGUYEN, D. N., KIM, P., MARTINEZ-SOBRIDO, L., BEITZEL, B., GARCIA-SASTRE, A., LANGER, R. & ANDERSON, D. G. 2009. A novel high-throughput cell-based method for integrated quantification of type I interferons and in vitro screening of immunostimulatory RNA drug delivery. *Biotechnol Bioeng,* 103**,** 664-75.

NICHOLS, A. 2006. High content screening as a screening tool in drug discovery. *High Content Screening: A Powerful Approach to Systems Cell Biology and Drug Discovery***,** 379-387.

NISTAL-VILLAN, E., GACK, M. U., MARTINEZ-DELGADO, G., MAHARAJ, N. P., INN, K. S., YANG, H., WANG, R., AGGARWAL, A. K., JUNG, J. U. & GARCIA-SASTRE, A. 2010. Negative role of RIG-I serine 8 phosphorylation in the regulation of interferon-beta production. *J Biol Chem,* 285**,** 20252-61.

O'SHEA, J. J., SCHWARTZ, D. M., VILLARINO, A. V., GADINA, M., MCINNES, I. B. & LAURENCE, A. 2015. The JAK-STAT pathway: impact on human disease and therapeutic intervention*. *Annual review of medicine,* 66**,** 311-328.

ODA, H., NAKAGAWA, K., ABE, J., AWAYA, T., FUNABIKI, M., HIJIKATA, A., NISHIKOMORI, R., FUNATSUKA, M., OHSHIMA, Y., SUGAWARA, Y., YASUMI, T., KATO, H., SHIRAI, T., OHARA, O., FUJITA, T. & HEIKE, T. 2014. Aicardi-Goutieres syndrome is caused by IFIH1 mutations. *Am J Hum Genet,* 95**,** 121-5.

OLIVEIRA, L., SINICATO, N. A., POSTAL, M., APPENZELLER, S. & NIEWOLD, T. B. 2015. Dysregulation of antiviral helicase pathways in systemic lupus erythematosus. *DNA helicases: expression, functions and clinical implications***,** 48.

ONOGUCHI, K., YONEYAMA, M., TAKEMURA, A., AKIRA, S., TANIGUCHI, T., NAMIKI, H. & FUJITA, T. 2007. Viral infections activate types I and III interferon genes through a common mechanism. *The Journal of biological chemistry,* 282**,** 7576-81.

ORCESI, S., LA PIANA, R. & FAZZI, E. 2009. Aicardi-Goutieres syndrome. *Br Med Bull,* 89**,** 183-201.

OSHIUMI, H., MATSUMOTO, M., FUNAMI, K., AKAZAWA, T. & SEYA, T. 2003. TICAM-1, an adaptor molecule that participates in Toll-like receptor 3-mediated interferon-beta induction. *Nat Immunol,* 4**,** 161-7.

OVERINGTON, J. P., AL-LAZIKANI, B. & HOPKINS, A. L. 2006. How many drug targets are there? *Nat Rev Drug Discov,* 5**,** 993-996.

PANNE, D., MANIATIS, T. & HARRISON, S. C. 2007. An atomic model of the interferon-β enhanceosome. *Cell,* 129**,** 1111-1123.

PARDANANI, A., LASHO, T., SMITH, G., BURNS, C. J., FANTINO, E. & TEFFERI, A. 2009. CYT387, a selective JAK1/JAK2 inhibitor: in vitro assessment of kinase selectivity and preclinical studies using cell lines and primary cells from polycythemia vera patients. *Leukemia,* 23**,** 1441-5.

PARISIEN, J.-P., LAU, J. F., RODRIGUEZ, J. J., SULLIVAN, B. M., MOSCONA, A., PARKS, G. D., LAMB, R. A. & HORVATH, C. M. 2001. The V protein of human parainfluenza virus 2 antagonizes type I interferon responses by destabilizing signal transducer and activator of transcription 2. *Virology,* 283**,** 230-239.

PATEL, D. A., PATEL, A. C., NOLAN, W. C., ZHANG, Y. & HOLTZMAN, M. J. 2012. High Throughput Screening for Small Molecule Enhancers of the Interferon Signaling Pathway to Drive Next-Generation Antiviral Drug Discovery. *PloS one,* 7**,** e36594.

PATEL, D. V. & GORDON, E. M. 1996. Applications of small-molecule combinatorial chemistry to drug discovery. *Drug Discovery Today,* 1**,** 134-144.

PAUL, S. M., MYTELKA, D. S., DUNWIDDIE, C. T., PERSINGER, C. C., MUNOS, B. H., LINDBORG, S. R. & SCHACHT, A. L. 2010. How to improve R&D productivity: the pharmaceutical industry's grand challenge. *Nat Rev Drug Discov,* 9**,** 203-14.

PAZ, S., VILASCO, M., WERDEN, S. J., ARGUELLO, M., JOSEPH-PILLAI, D., ZHAO, T., NGUYEN, T. L., SUN, Q., MEURS, E. F., LIN, R. & HISCOTT, J. 2011. A functional C-terminal TRAF3-binding site in MAVS participates in positive and negative regulation of the IFN antiviral response. *Cell Res,* 21**,** 895-910.

PEROLA, E. 2010. An analysis of the binding efficiencies of drugs and their leads in successful drug discovery programs. *Journal of medicinal chemistry,* 53**,** 2986-2997.

PERRY, A. K., GANG, C., ZHENG, D., HONG, T. & CHENG, G. 2005. The host type I interferon response to viral and bacterial infections. *Cell research,* 15**,** 407-422.

PLATANIAS, L. C. 2005. Mechanisms of type-I- and type-II-interferon-mediated signalling. *Nature reviews. Immunology,* 5**,** 375-86.

PODOLIN, P. L., CALLAHAN, J. F., BOLOGNESE, B. J., LI, Y. H., CARLSON, K., DAVIS, T. G., MELLOR, G. W., EVANS, C. & ROSHAK, A. K. 2005. Attenuation of murine collagen-induced arthritis by a novel, potent, selective small molecule inhibitor of IkappaB Kinase 2, TPCA-1 (2-[(aminocarbonyl)amino]-5-(4-fluorophenyl)-3-thiophenecarboxamide), occurs via reduction of proinflammatory cytokines and antigen-induced T cell Proliferation. *J Pharmacol Exp Ther,* 312**,** 373-81.

PRECIOUS, B., CHILDS, K., FITZPATRICK-SWALLOW, V., GOODBOURN, S. & RANDALL, R. E. 2005. Simian virus 5 V protein acts as an adaptor, linking DDB1 to STAT2, to facilitate the ubiquitination of STAT1. *J Virol,* 79**,** 13434-41.

PROKUNINA-OLSSON, L., MUCHMORE, B., TANG, W., PFEIFFER, R. M., PARK, H., DICKENSHEETS, H., HERGOTT, D., PORTER-GILL, P., MUMY, A., KOHAAR, I., CHEN, S., BRAND, N., TARWAY, M., LIU, L., SHEIKH, F., ASTEMBORSKI, J., BONKOVSKY, H. L., EDLIN, B. R., HOWELL, C. D., MORGAN, T. R., THOMAS, D. L., REHERMANN, B., DONNELLY, R. P. & O'BRIEN, T. R. 2013. A variant upstream of IFNL3 (IL28B) creating a new interferon gene IFNL4 is associated with impaired clearance of hepatitis C virus. *Nat Genet,* 45**,** 164-171.

QUINTAS-CARDAMA, A., VADDI, K., LIU, P., MANSHOURI, T., LI, J., SCHERLE, P. A., CAULDER, E., WEN, X., LI, Y., WAELTZ, P., RUPAR, M., BURN, T., LO, Y., KELLEY, J., COVINGTON, M., SHEPARD, S., RODGERS, J. D., HALEY, P., KANTARJIAN, H., FRIDMAN, J. S. & VERSTOVSEK, S. 2010. Preclinical characterization of the selective JAK1/2 inhibitor INCB018424: therapeutic implications for the treatment of myeloproliferative neoplasms. *Blood,* 115**,** 3109-17.

RAMANAN, P., EDWARDS, M. R., SHABMAN, R. S., LEUNG, D. W., ENDLICH-FRAZIER, A. C., BOREK, D. M., OTWINOWSKI, Z., LIU, G., HUH, J. & BASLER, C. F. 2012. Structural basis for Marburg virus VP35–mediated immune evasion mechanisms. *Proceedings of the National Academy of Sciences,* 109**,** 20661-20666.

RANDALL, R. E. & GOODBOURN, S. 2008. Interferons and viruses: an interplay between induction, signalling, antiviral responses and virus countermeasures. *The Journal of general virology,* 89**,** 1-47.

REICH, N. C. & LIU, L. 2006. Tracking STAT nuclear traffic. *Nat Rev Immunol,* 6**,** 602-12.

RICE, G. I., DEL TORO DUANY, Y., JENKINSON, E. M., FORTE, G. M., ANDERSON, B. H., ARIAUDO, G., BADER-MEUNIER, B., BAILDAM, E. M., BATTINI, R., BERESFORD, M. W., CASARANO, M., CHOUCHANE, M., CIMAZ, R., COLLINS, A. E., CORDEIRO, N. J., DALE, R. C., DAVIDSON, J. E., DE WAELE, L., DESGUERRE, I., FAIVRE, L., FAZZI, E., ISIDOR, B., LAGAE, L., LATCHMAN, A. R., LEBON, P., LI, C., LIVINGSTON, J. H., LOURENCO, C. M., MANCARDI, M. M., MASUREL-PAULET, A.,

MCINNES, I. B., MENEZES, M. P., MIGNOT, C., O'SULLIVAN, J., ORCESI, S., PICCO, P. P., RIVA, E., ROBINSON, R. A., RODRIGUEZ, D., SALVATICI, E., SCOTT, C., SZYBOWSKA, M., TOLMIE, J. L., VANDERVER, A., VANHULLE, C., VIEIRA, J. P., WEBB, K., WHITNEY, R. N., WILLIAMS, S. G., WOLFE, L. A., ZUBERI, S. M., HUR, S. & CROW, Y. J. 2014. Gain-of-function mutations in IFIH1 cause a spectrum of human disease phenotypes associated with upregulated type I interferon signaling. *Nat Genet,* 46**,** 503-9.

RICE, G. I., FORTE, G. M., SZYNKIEWICZ, M., CHASE, D. S., AEBY, A., ABDEL-HAMID, M. S., ACKROYD, S., ALLCOCK, R., BAILEY, K. M. & BALOTTIN, U. 2013. Assessment of interferon-related biomarkers in Aicardi-Goutieres syndrome associated with mutations in TREX1, RNASEH2A, RNASEH2B, RNASEH2C, SAMHD1, and ADAR: a case-control study. *The Lancet Neurology,* 12**,** 1159-1169.

RIEDER, M., BRZOZKA, K., PFALLER, C. K., COX, J. H., STITZ, L. & CONZELMANN, K. K. 2011. Genetic dissection of interferon-antagonistic functions of rabies virus phosphoprotein: inhibition of interferon regulatory factor 3 activation is important for pathogenicity. *J Virol,* 85**,** 842-52.

RODRIGUEZ, J. J., PARISIEN, J. P. & HORVATH, C. M. 2002. Nipah Virus V Protein Evades Alpha and Gamma Interferons by Preventing STAT1 and STAT2 Activation and Nuclear Accumulation. *Journal of Virology,* 76**,** 11476-11483.

RUDIGER, M., HAUPTS, U., MOORE, K. J. & POPE, A. J. 2001. Single-molecule detection technologies in miniaturized high throughput screening: binding assays for G protein-coupled receptors using fluorescence intensity distribution analysis and fluorescence anisotropy. *Journal of biomolecular screening,* 6**,** 29-37.

RUTSCH, F., MACDOUGALL, M., LU, C., BUERS, I., MAMAEVA, O., NITSCHKE, Y., RICE, GILLIAN I., ERLANDSEN, H., KEHL, HANS G., THIELE, H., NÜRNBERG, P., HÖHNE, W., CROW, YANICK J., FEIGENBAUM, A. & HENNEKAM, RAOUL C. 2015. A Specific *IFIH1* Gain-of-Function Mutation Causes Singleton-Merten Syndrome. *The American Journal of Human Genetics,* 96**,** 275-282.

SARKAR, S. N., PETERS, K. L., ELCO, C. P., SAKAMOTO, S., PAL, S. & SEN, G. C. 2004. Novel roles of TLR3 tyrosine phosphorylation and PI3 kinase in double-stranded RNA signaling. *Nat Struct Mol Biol,* 11**,** 1060-7.

SATOH, T., KATO, H., KUMAGAI, Y., YONEYAMA, M., SATO, S., MATSUSHITA, K., TSUJIMURA, T., FUJITA, T., AKIRA, S. & TAKEUCHI, O. 2010. LGP2 is a positive regulator of RIG-I- and MDA5-mediated antiviral responses. *Proc Natl Acad Sci U S A,* 107**,** 1512-7.

SCHLEE, M., ROTH, A., HORNUNG, V., HAGMANN, C. A., WIMMENAUER, V., BARCHET, W., COCH, C., JANKE, M., MIHAILOVIC, A., WARDLE, G., JURANEK, S., KATO, H., KAWAI, T., POECK, H., FITZGERALD, K. A., TAKEUCHI, O., AKIRA, S., TUSCHL, T., LATZ, E., LUDWIG, J. & HARTMANN, G. 2009. Recognition of 5' triphosphate by RIG-I helicase requires short blunt double-stranded RNA as contained in panhandle of negative-strand virus. *Immunity,* 31**,** 25-34.

SCHMOLKE, M., PATEL, J., MILLER, J., APARICIO, M. S., MANICASSAMY, B., MERAD, M. & SASTRE, A. G. 2012. P133 RIG-I mediates recognition of Salmonella RNA in non-phagocytic cells and contributes to early bacterial replication in vivo. *Cytokine,* 59**,** 562.

SCHOGGINS, J. W. & RICE, C. M. 2011. Interferon-stimulated genes and their antiviral effector functions. *Current opinion in virology,* 1**,** 519-525.

SCHOMACKER, H., HEBNER, R. M., BOONYARATANAKORNKIT, J., SURMAN, S., AMARO-CARAMBOT, E., COLLINS, P. L. & SCHMIDT, A. C. 2012. The C proteins of human parainfluenza virus type 1 block IFN signaling by binding and retaining Stat1 in perinuclear aggregates at the late endosome. *PLoS One,* 7**,** e28382.

SCHRODER, K., HERTZOG, P. J., RAVASI, T. & HUME, D. A. 2004. Interferon-γ: an overview of signals, mechanisms and functions. *Journal of leukocyte biology,* 75**,** 163-189.

SCHRODER, K. & TSCHOPP, J. 2010. The inflammasomes. *Cell,* 140**,** 821-32.

SCOTT, D. E., COYNE, A. G., HUDSON, S. A. & ABELL, C. 2012. Fragment-based approaches in drug discovery and chemical biology. *Biochemistry,* 51**,** 4990-5003.

SHARMA, S. V., HABER, D. A. & SETTLEMAN, J. 2010. Cell line-based platforms to evaluate the therapeutic efficacy of candidate anticancer agents. *Nat Rev Cancer,* 10**,** 241-53.

SILVERMAN, R. H. 2007. Viral encounters with 2′, 5′-oligoadenylate synthetase and RNase L during the interferon antiviral response. *Journal of virology,* 81**,** 12720-12729.
SITTAMPALAM, G. S., IVERSEN, P. W., BOADT, J. A., KAHL, S. D., BRIGHT, S., ZOCK, J. M., JANZEN, W. P. & LISTER, M. D. 1997. Design of signal windows in high throughput screening assays for drug discovery. *Journal of Biomolecular Screening,* 2**,** 159-169.
SNELL, L. M. & BROOKS, D. G. 2015. New insights into type I interferon and the immunopathogenesis of persistent viral infections. *Current opinion in immunology,* 34**,** 91-98.
SOMMEREYNS, C., PAUL, S., STAEHELI, P. & MICHIELS, T. 2008. IFN-Lambda (IFN-λ) Is Expressed in a Tissue-Dependent Fashion and Primarily Acts on Epithelial Cells In Vivo. *PLOS Pathogens,* 4**,** e1000017.
SPENGLER, J. R., PATEL, J. R., CHAKRABARTI, A. K., ZIVCEC, M., GARCIA-SASTRE, A., SPIROPOULOU, C. F. & BERGERON, E. 2015. RIG-I Mediates an Antiviral Response to Crimean-Congo Hemorrhagic Fever Virus. *J Virol,* 89**,** 10219-29.
STAHL-HENNIG, C., EISENBLATTER, M., JASNY, E., RZEHAK, T., TENNER-RACZ, K., TRUMPFHELLER, C., SALAZAR, A. M., UBERLA, K., NIETO, K., KLEINSCHMIDT, J., SCHULTE, R., GISSMANN, L., MULLER, M., SACHER, A., RACZ, P., STEINMAN, R. M., UGUCCIONI, M. & IGNATIUS, R. 2009. Synthetic double-stranded RNAs are adjuvants for the induction of T helper 1 and humoral immune responses to human papillomavirus in rhesus macaques. *PLoS Pathog,* 5**,** e1000373.
STANCATO, L. F., DAVID, M., CARTER-SU, C., LARNER, A. C. & PRATT, W. B. 1996. Preassociation of STAT1 with STAT2 and STAT3 in separate signalling complexes prior to cytokine stimulation. *Journal of Biological Chemistry,* 271**,** 4134-4137.
STARK, G. R., KERR, I. M., WILLIAMS, B. R., SILVERMAN, R. H. & SCHREIBER, R. D. 1998. How cells respond to interferons. *Annual review of biochemistry,* 67**,** 227-264.
STEEN, H. C., NOGUSA, S., THAPA, R. J., BASAGOUDANAVAR, S. H., GILL, A. L., MERALI, S., BARRERO, C. A., BALACHANDRAN, S. & GAMERO, A. M. 2013. Identification of STAT2 Serine 287 as a Novel Regulatory Phosphorylation Site in Type I Interferon-induced Cellular Responses. *J Biol Chem,* 288**,** 747-58.
STEWART, C. E., RANDALL, R. E. & ADAMSON, C. S. 2014. Inhibitors of the interferon response enhance virus replication in vitro. *PloS one,* 9**,** e112014.
STREITENFELD, H., BOYD, A., FAZAKERLEY, J. K., BRIDGEN, A., ELLIOTT, R. M. & WEBER, F. 2003. Activation of PKR by Bunyamwera Virus Is Independent of the Viral Interferon Antagonist NSs. *Journal of Virology,* 77**,** 5507-5511.
SUBRAMANIAN, S., TAWAKOL, A., BURDO, T. H., ABBARA, S., WEI, J., VIJAYAKUMAR, J., CORSINI, E., ABDELBAKY, A., ZANNI, M. V. & HOFFMANN, U. 2012. Arterial inflammation in patients with HIV. *Jama,* 308**,** 379-386.
SUN, L., WU, J., DU, F., CHEN, X. & CHEN, Z. J. 2013. Cyclic GMP-AMP synthase is a cytosolic DNA sensor that activates the type I interferon pathway. *Science,* 339**,** 786-791.
SWINNEY, D. C. 2006. Biochemical mechanisms of new molecular entities (NMEs) approved by United States FDA during 2001-2004: mechanisms leading to optimal efficacy and safety. *Current topics in medicinal chemistry,* 6**,** 461-478.
TABETA, K., GEORGEL, P., JANSSEN, E., DU, X., HOEBE, K., CROZAT, K., MUDD, S., SHAMEL, L., SOVATH, S. & GOODE, J. 2004. Toll-like receptors 9 and 3 as essential components of innate immune defense against mouse cytomegalovirus infection. *Proceedings of the National Academy of Sciences of the United States of America,* 101**,** 3516-3521.
TAKAOKA, A. & YANAI, H. 2006. Interferon signalling network in innate defence. *Cellular microbiology,* 8**,** 907-22.
TAKEDA, K. & AKIRA, S. TLR signaling pathways. Seminars in immunology, 2004. Elsevier, 3-9.
TAKEUCHI, O. & AKIRA, S. 2010. Pattern Recognition Receptors and Inflammation. *Cell,* 140**,** 805-820.
TANAKA, Y. & CHEN, Z. J. 2012. STING specifies IRF3 phosphorylation by TBK1 in the cytosolic DNA signaling pathway. *Science signaling,* 5**,** ra20-ra20.

TANG, X., GAO, J.-S., GUAN, Y.-J., MCLANE, K. E., YUAN, Z.-L., RAMRATNAM, B. & CHIN, Y. E. 2007. Acetylation-dependent signal transduction for type I interferon receptor. *Cell,* 131**,** 93-105.

TAWARATSUMIDA, K., PHAN, V., HRINCIUS, E. R., HIGH, A. A., WEBBY, R., REDECKE, V. & HÄCKER, H. 2014. Quantitative proteomic analysis of the influenza A virus nonstructural proteins NS1 and NS2 during natural cell infection identifies PACT as an NS1 target protein and antiviral host factor. *Journal of virology,* 88**,** 9038-9048.

THEOFILOPOULOS, A. N., BACCALA, R., BEUTLER, B. & KONO, D. H. 2005. Type I interferons (alpha/beta) in immunity and autoimmunity. *Annu Rev Immunol,* 23**,** 307-36.

TIAN, D., LUO, Z., ZHOU, M., LI, M., YU, L., WANG, C., YUAN, J., LI, F., TIAN, B., SUI, B., CHEN, H., FU, Z. F. & ZHAO, L. 2016. Critical Role of K1685 and K1829 in the Large Protein of Rabies Virus in Viral Pathogenicity and Immune Evasion. *J Virol,* 90**,** 232-44.

TITOV, D. V. & LIU, J. O. 2012. Identification and validation of protein targets of bioactive small molecules. *Bioorganic & medicinal chemistry,* 20**,** 1902-1909.

UCHIDA, L., ESPADA-MURAO, L. A., TAKAMATSU, Y., OKAMOTO, K., HAYASAKA, D., YU, F., NABESHIMA, T., BUERANO, C. C. & MORITA, K. 2014. The dengue virus conceals double-stranded RNA in the intracellular membrane to escape from an interferon response. *Scientific reports,* 4**,** 7395.

UDDIN, S., SASSANO, A., DEB, D. K., VERMA, A., MAJCHRZAK, B., RAHMAN, A., MALIK, A. B., FISH, E. N. & PLATANIAS, L. C. 2002. Protein kinase C-delta (PKC-delta) is activated by type I interferons and mediates phosphorylation of Stat1 on serine 727. *J Biol Chem,* 277**,** 14408-16.

ULANE, C. M. & HORVATH, C. M. 2002. Paramyxoviruses SV5 and HPIV2 assemble STAT protein ubiquitin ligase complexes from cellular components. *Virology,* 304**,** 160-166.

UNTERHOLZNER, L., KEATING, S. E., BARAN, M., HORAN, K. A., JENSEN, S. B., SHARMA, S., SIROIS, C. M., JIN, T., LATZ, E., XIAO, T. S., FITZGERALD, K. A., PALUDAN, S. R. & BOWIE, A. G. 2010. IFI16 is an innate immune sensor for intracellular DNA. *Nat Immunol,* 11**,** 997-1004.

UNTERHOLZNER, L., SUMNER, R. P., BARAN, M., REN, H., MANSUR, D. S., BOURKE, N. M., RANDOW, F., SMITH, G. L. & BOWIE, A. G. 2011. Vaccinia virus protein C6 is a virulence factor that binds TBK-1 adaptor proteins and inhibits activation of IRF3 and IRF7. *PLoS Pathog,* 7**,** e1002247.

VALLER, M. J. & GREEN, D. 2000. Diversity screening versus focussed screening in drug discovery. *Drug discovery today,* 5**,** 286-293.

VAN EYCK, L., DE SOMER, L., POMBAL, D., BORNSCHEIN, S., FRANS, G., HUMBLET-BARON, S., MOENS, L., DE ZEGHER, F., BOSSUYT, X., WOUTERS, C. & LISTON, A. 2015. Brief Report: IFIH1 Mutation Causes Systemic Lupus Erythematosus With Selective IgA Deficiency. *Arthritis Rheumatol,* 67**,** 1592-7.

VARIN, T., SCHUFFENHAUER, A., ERTL, P. & RENNER, S. 2011. Mining for Bioactive Scaffolds with Scaffold Networks: Improved Compound Set Enrichment from Primary Screening Data. *Journal of Chemical Information and Modeling,* 51**,** 1528-1538.

VARINOU, L., RAMSAUER, K., KARAGHIOSOFF, M., KOLBE, T., PFEFFER, K., MÜLLER, M. & DECKER, T. 2003. Phosphorylation of the Stat1 transactivation domain is required for full-fledged IFN-γ-dependent innate immunity. *Immunity,* 19**,** 793-802.

VERLINDE, C. L. & HOL, W. G. 1994. Structure-based drug design: progress, results and challenges. *Structure,* 2**,** 577-587.

VERSTEEG, G. A. & GARCÍA-SASTRE, A. 2010. Viral tricks to grid-lock the type I interferon system. *Current Opinion in Microbiology,* 13**,** 508-516.

VERSTOVSEK, S., KANTARJIAN, H., MESA, R., PARDANANI, A., CORTES-FRANCO, J., THOMAS, D., ESTROV, Z., FRIDMAN, J., BRADLEY, E., ERICKSON-VIITANEN, S., VADDI, K., LEVY, R. & TEFFERI, A. 2010. Safety and efficacy of INCB018424, a JAK1 and JAK2 inhibitor, in myelofibrosis. *N Engl J Med,* 363**,** 1117-27.

VIATOUR, P., MERVILLE, M.-P., BOURS, V. & CHARIOT, A. 2005. Phosphorylation of NF-κB and IκB proteins: implications in cancer and inflammation. *Trends in Biochemical Sciences,* 30**,** 43-52.

VIDY, A., EL BOUGRINI, J., CHELBI-ALIX, M. K. & BLONDEL, D. 2007. The nucleocytoplasmic rabies virus P protein counteracts interferon signaling by inhibiting both nuclear accumulation and DNA binding of STAT1. *J Virol,* 81**,** 4255-63.

VOTER, A. F., MANTHEI, K. A. & KECK, J. L. 2016. A High-Throughput Screening Strategy to Identify Protein-Protein Interaction Inhibitors That Block the Fanconi Anemia DNA Repair Pathway. *Journal of biomolecular screening*, 1087057116635503.

WACK, A., TERCZYNSKA-DYLA, E. & HARTMANN, R. 2015. Guarding the frontiers: the biology of type III interferons. *Nat Immunol,* 16, 802-9.

WANG, D., FANG, L., LI, P., SUN, L., FAN, J., ZHANG, Q., LUO, R., LIU, X., LI, K. & CHEN, H. 2011a. The leader proteinase of foot-and-mouth disease virus negatively regulates the type I interferon pathway by acting as a viral deubiquitinase. *Journal of virology,* 85, 3758-3766.

WANG, H., VAHERI, A., WEBER, F. & PLYUSNIN, A. 2011b. Old World hantaviruses do not produce detectable amounts of dsRNA in infected cells and the 5′ termini of their genomic RNAs are monophosphorylated. *Journal of General Virology,* 92, 1199-1204.

WEBER, F., BRIDGEN, A., FAZAKERLEY, J. K., STREITENFELD, H., KESSLER, N., RANDALL, R. E. & ELLIOTT, R. M. 2002. Bunyamwera Bunyavirus Nonstructural Protein NSs Counteracts the Induction of Alpha/Beta Interferon. *Journal of Virology,* 76, 7949-7955.

WEBER, M., SEDIRI, H., FELGENHAUER, U., BINZEN, I., BÄNFER, S., JACOB, R., BRUNOTTE, L., GARCÍA-SASTRE, A., SCHMID-BURGK, J. L. & SCHMIDT, T. 2015. Influenza virus adaptation PB2-627K modulates nucleocapsid inhibition by the pathogen sensor RIG-I. *Cell host & microbe,* 17, 309-319.

WEI, C., NI, C., SONG, T., LIU, Y., YANG, X., ZHENG, Z., JIA, Y., YUAN, Y., GUAN, K., XU, Y., CHENG, X., ZHANG, Y., YANG, X., WANG, Y., WEN, C., WU, Q., SHI, W. & ZHONG, H. 2010. The hepatitis B virus X protein disrupts innate immunity by downregulating mitochondrial antiviral signaling protein. *J Immunol,* 185, 1158-68.

WHO 2013. *WHO Expert Consultation on Rabies: second report*, World Health Organization.

WIENER, M. C., SACHS, J. R., DEYANOVA, E. G. & YATES, N. A. 2004. Differential mass spectrometry: a label-free LC-MS method for finding significant differences in complex peptide and protein mixtures. *Analytical chemistry,* 76, 6085-6096.

WIES, E., WANG, M. K., MAHARAJ, N. P., CHEN, K., ZHOU, S., FINBERG, R. W. & GACK, M. U. 2013. Dephosphorylation of the RNA Sensors RIG-I and MDA5 by the Phosphatase PP1 Is Essential for Innate Immune Signaling. *Immunity,* 38, 437-49.

WILDE, H., LUMLERTDACHA, B., MESLIN, F. X., GHAI, S. & HEMACHUDHA, T. 2016. Worldwide rabies deaths prevention—A focus on the current inadequacies in postexposure prophylaxis of animal bite victims. *Vaccine,* 34, 187-189.

WILSON, E. B. & BROOKS, D. G. 2013. Decoding the complexity of type I interferon to treat persistent viral infections. *Trends Microbiol,* 21, 634-40.

WILTZER, L., LARROUS, F., OKSAYAN, S., ITO, N., MARSH, G., WANG, L., BLONDEL, D., BOURHY, H., JANS, D. & MOSELEY, G. 2012. Conservation of a unique mechanism of immune evasion across the Lyssavirus genus. *Journal of virology,* 86, 10194-10199.

WILTZER, L., OKADA, K., YAMAOKA, S., LARROUS, F., KUUSISTO, H. V., SUGIYAMA, M., BLONDEL, D., BOURHY, H., JANS, D. A. & ITO, N. 2014. Interaction of rabies virus P-protein with STAT proteins is critical to lethal rabies disease. *Journal of Infectious Diseases,* 209, 1744-1753.

WRESSNIGG, N., VOSS, D., WOLFF, T., ROMANOVA, J., RUTHSATZ, T., MAYERHOFER, I., REITER, M., NAKOWITSCH, S., HUMER, J. & MOROKUTTI, A. 2009. Development of a live-attenuated influenza B ΔNS1 intranasal vaccine candidate. *Vaccine,* 27, 2851-2857.

WU, B. & HUR, S. 2015. How RIG-I like receptors activate MAVS. *Curr Opin Virol,* 12, 91-8.

WU, C.-J., CONZE, D. B., LI, T., SRINIVASULA, S. M. & ASHWELL, J. D. 2006. Sensing of Lys 63-linked polyubiquitination by NEMO is a key event in NF-κB activation. *Nature cell biology,* 8, 398-406.

YAMAMOTO, M., SATO, S., HEMMI, H., HOSHINO, K., KAISHO, T., SANJO, H., TAKEUCHI, O., SUGIYAMA, M., OKABE, M. & TAKEDA, K. 2003. Role of adaptor TRIF in the MyD88-independent toll-like receptor signaling pathway. *Science,* 301, 640-643.

YAMAMOTO, M., SATO, S., MORI, K., HOSHINO, K., TAKEUCHI, O., TAKEDA, K. & AKIRA, S. 2002. Cutting Edge: A Novel Toll/IL-1 Receptor Domain-Containing Adapter That Preferentially Activates the IFN- Promoter in the Toll-Like Receptor Signaling. *The Journal of Immunology,* 169, 6668-6672.

YAN, H., KRISHNAN, K., GREENLUND, A., GUPTA, S., LIM, J., SCHREIBER, R., SCHINDLER, C. & KROLEWSKI, J. 1996. Phosphorylated interferon-alpha receptor 1 subunit (IFNaR1) acts as a docking site for the latent form of the 113 kDa STAT2 protein. *The EMBO journal,* 15**,** 1064.

YAN, N., REGALADO-MAGDOS, A. D., STIGGELBOUT, B., LEE-KIRSCH, M. A. & LIEBERMAN, J. 2010. The cytosolic exonuclease TREX1 inhibits the innate immune response to human immunodeficiency virus type 1. *Nature immunology,* 11**,** 1005-1013.

YANG, H., MA, G., LIN, C. H., ORR, M. & WATHELET, M. G. 2004. Mechanism for transcriptional synergy between interferon regulatory factor (IRF)-3 and IRF-7 in activation of the interferon-beta gene promoter. *European journal of biochemistry / FEBS,* 271**,** 3693-703.

YANG, Y., ADELSTEIN, S. J. & KASSIS, A. I. 2009. Target discovery from data mining approaches. *Drug Discov Today,* 14**,** 147-54.

YANG, Y., LIANG, Y., QU, L., CHEN, Z., YI, M., LI, K. & LEMON, S. M. 2007. Disruption of innate immunity due to mitochondrial targeting of a picornaviral protease precursor. *Proc Natl Acad Sci U S A,* 104**,** 7253-8.

YAP, T. A., SMITH, A. D., FERRALDESCHI, R., AL-LAZIKANI, B., WORKMAN, P. & DE BONO, J. S. 2016. Drug discovery in advanced prostate cancer: translating biology into therapy. *Nat Rev Drug Discov*.

YARROW, J. C., TOTSUKAWA, G., CHARRAS, G. T. & MITCHISON, T. J. 2005. Screening for cell migration inhibitors via automated microscopy reveals a Rho-kinase inhibitor. *Chemistry & biology,* 12**,** 385-395.

YE, J., CHEN, S. & MANIATIS, T. 2011. Cardiac glycosides are potent inhibitors of interferon-beta gene expression. *Nat Chem Biol,* 7**,** 25-33.

YOSHIZUMI, T., ICHINOHE, T., SASAKI, O., OTERA, H., KAWABATA, S., MIHARA, K. & KOSHIBA, T. 2014. Influenza A virus protein PB1-F2 translocates into mitochondria via Tom40 channels and impairs innate immunity. *Nat Commun,* 5**,** 4713.

ZANDI, E., ROTHWARF, D. M., DELHASE, M., HAYAKAWA, M. & KARIN, M. 1997. The IκB kinase complex (IKK) contains two kinase subunits, IKKα and IKKβ, necessary for IκB phosphorylation and NF-κB activation. *Cell,* 91**,** 243-252.

ZANG, R., LI, D., TANG, I.-C., WANG, J. & YANG, S.-T. 2012. Cell-based assays in high-throughput screening for drug discovery. *International Journal of Biotechnology for Wellness Industries,* 1**,** 31.

ZHANG, J., XU, L. G., HAN, K. J., WEI, X. & SHU, H. B. 2004. PIASy represses TRIF-induced ISRE and NF-kappaB activation but not apoptosis. *FEBS Lett,* 570**,** 97-101.

ZHANG, J. H. 1999. A Simple Statistical Parameter for Use in Evaluation and Validation of High Throughput Screening Assays. *Journal of Biomolecular Screening,* 4**,** 67-73.

ZHANG, Z., GUAN, N., LI, T., MAIS, D. E. & WANG, M. 2012. Quality control of cell-based high-throughput drug screening. *Acta Pharmaceutica Sinica B,* 2**,** 429-438.

ZHANG, Z., YUAN, B., BAO, M., LU, N., KIM, T. & LIU, Y. J. 2011. The helicase DDX41 senses intracellular DNA mediated by the adaptor STING in dendritic cells. *Nat Immunol,* 12**,** 959-65.

ZHENG, W., THORNE, N. & MCKEW, J. C. 2013. Phenotypic screens as a renewed approach for drug discovery. *Drug discovery today,* 18**,** 1067-1073.

ZHU, J. & CAFLISCH, A. 2016. Twenty crystal structures of bromodomain and PHD finger containing protein 1 (BRPF1)/ligand complexes reveal conserved binding motifs and rare interactions. *Journal of medicinal chemistry*.

ZHU, J., SMITH, K., HSIEH, P. N., MBURU, Y. K., CHATTOPADHYAY, S., SEN, G. C. & SARKAR, S. N. 2010. High-throughput screening for TLR3-IFN regulatory factor 3 signaling pathway modulators identifies several antipsychotic drugs as TLR inhibitors. *J Immunol,* 184**,** 5768-76.

ZLITNI, S., BLANCHARD, J. E. & BROWN, E. D. 2009. High-throughput screening of model bacteria. *Cell-Based Assays for High-Throughput Screening: Methods and Protocols***,** 13-27.

ZON, L. I. & PETERSON, R. T. 2005. In vivo drug discovery in the zebrafish. *Nature reviews Drug discovery,* 4**,** 35-44.

ZUFFEREY, R., NAGY, D., MANDEL, R. J., NALDINI, L. & TRONO, D. 1997. Multiply attenuated lentiviral vector achieves efficient gene delivery in vivo. *Nature biotechnology,* 15**,** 871-875.

Appendices

Appendix 1: qPCR data output using MxA and β-Actin primers

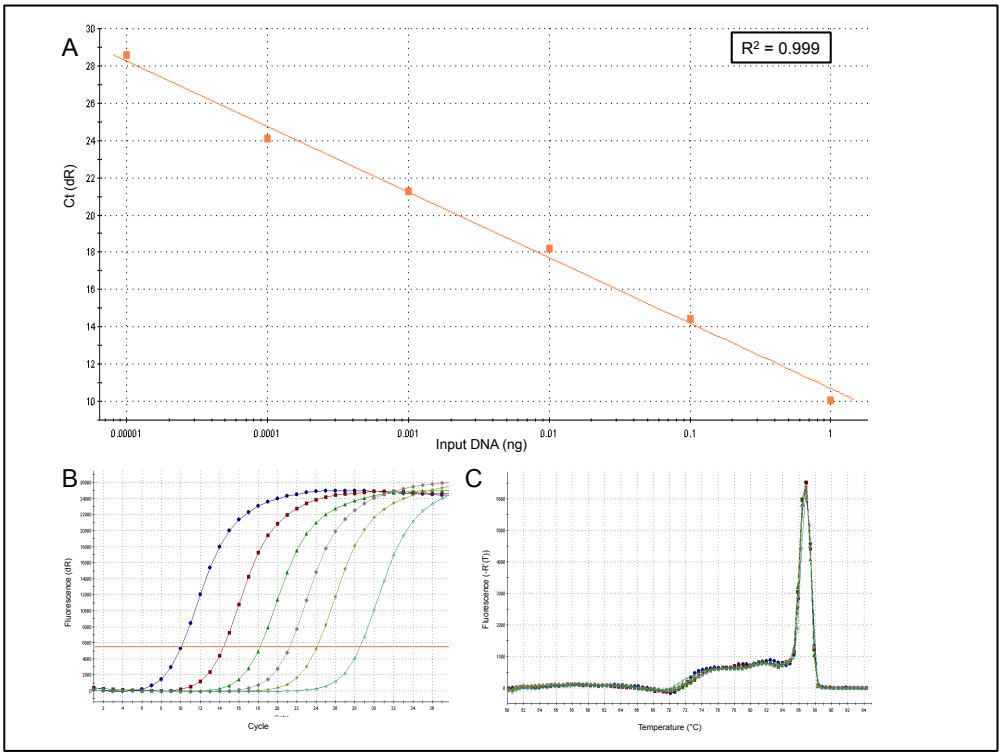

MxA primer set

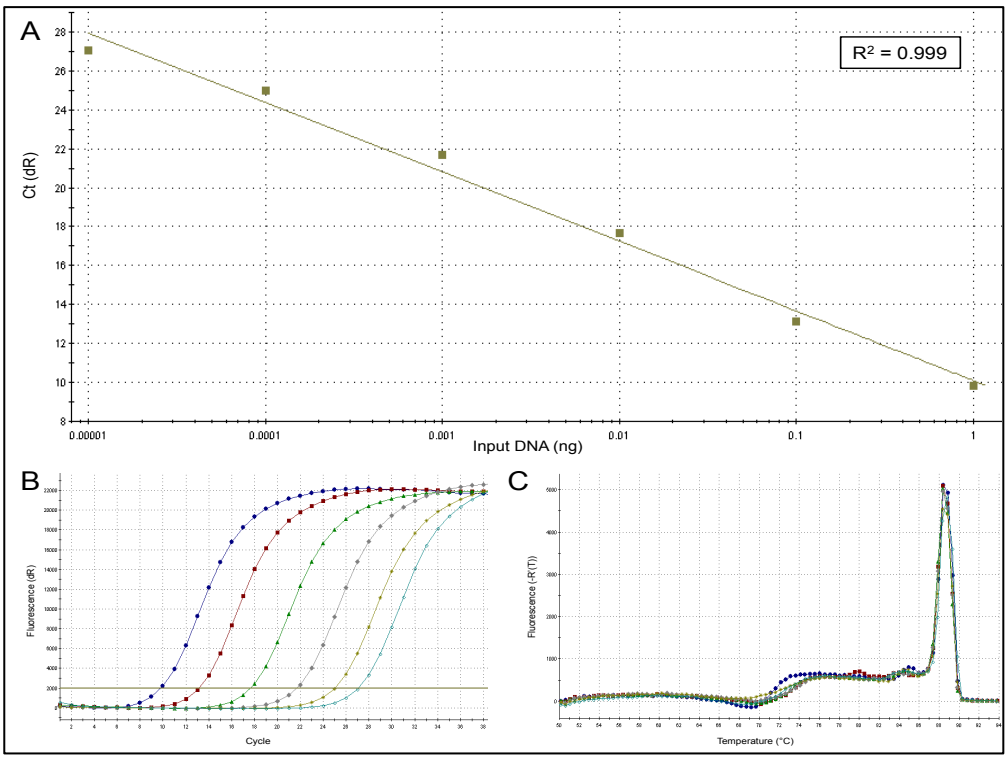

β-Actin primer set

Appendix 2: Published manuscript

Gage, Z.O., Vasou, A., Gray, D.W., Randall, R.E. and Adamson, C.S., 2016. Identification of novel inhibitors of the type I interferon induction pathway using cell-based high-throughput screening. *Journal of Biomolecular Screening*, p.1087057116656314.